The Acyl-ACP Thioesterase FatM from *Lotus japonicus* is involved in lipid transfer during Arbuscular Mycorrhiza Symbiosis

Dissertation

zur

Erlangung des Doktorgrades (Dr. rer. nat.)

der

Mathematisch-Naturwissenschaftlichen Fakultät

der

Rheinischen Friedrich-Wilhelms-Universität Bonn

vorgelegt von

Mathias Brands

Bonn, Juli 2019

Angefertigt mit Genehmigung der Mathematisch-Naturwissenschaftlichen
Fakultät der Rheinischen Friedrich-Wilhelms-Universität Bonn

1. Gutachter: Prof. Dr. Peter Dörmann
2. Gutachter: Prof. Dr. Andreas Meyer
Tag der Promotion: 14.10.2019
Erscheinungsjahr: 2020

Table of Contents

Figures

Tables

Frequently used Abbreviations

ACP	Acyl carrier protein
AMF	Arbuscular mycorrhiza fung(us/i)
ATP	Adenosine triphosphate
A. tumefaciens	*Agrobacterium tumefaciens*
BLAST	Basic local alignment search tool
Ci	Curie
CTAB	Cetyltrimethylammonium bromide
ddH$_2$0	Double deionized water
DAG	Diacylglycerol
DGDG	Digalactosyldiacylglycerol
DNA	Deoxyribonucleic acid
dpi	Days post infection
dpm	Disintegrations per minute
DMDS	Dimehtyldisulfide
DTT	Dithiothreitol
E. coli	*Escherichia coli*
EDTA	Ethylenediaminetetraacetic acid
ERM	Extraradical mycelium
ER	Endoplasmic reticulum
EtBr	Ethidium bromide
FA	Fatty acid
FAME	Fatty acid methyl ester
Fat	Fatty acyl-ACP thioesterase
Fig	Figure
FW	Fresh weight
FS	Free sterol
g	Standard gravity (g = 9.81 m s^{-2})
Gal	Galactose
GC-FID	Gas chromatograph with flame ionization detector
GC-MS	Gas chromatograph with mass spectrometer
G. intraradices/Gi	*Glomus intraradices* (syn. *Rhiozphagus irregularis*)
GPAT	Glycerol-3-phosphate acyltransferase
h	Hour(s)
IS	Internal standard
KAS	3-ketoacyl-ACP synthase
KOH	Potassium hydroxide
LB	Lysogeny broth
LiCl	Lithium chloride
L. japonicus/Lj	*Lotus japonicus*
MAG	Monoacylglycerol
M. truncatula/Mt	*Medicago truncatula*
MES	2-(*N*-morpholino)ethanesulfonic acid
MGDG	Monogalactosyldiacylglycerol
min	Minute(s)
mock	Mock-inoculated
mol%	Molar percentage
myc	Mycorrhiza
MS/MS	Tandem mass spectrometry
m/z	Mass to charge ratio
N. benthamiana	*Nicotiana benthamiana*
OD$_{600/660}$	Optical density at a wavelength of 600/660 nm
OE	Overexpression
OLE1	Oleic acid requiring 1

ON	Over night
PA	Phosphatidic acid
PAM	Periarbuscular membrane
PAS	Periarbuscular space
PBM	Peribacteroid membrane
PC	Phosphatidylcholine
PCR	Polymerase chain reaction
PE	Phosphatidylethanolamine
PIPES	Piperazine-N,N′-bis(2-ethanesulfonic acid)
PS	Phosphatidylserine
ppm	Parts per million
PPA	Pre-penetration apparatus
Q-TOF MS	Quadrupole time-of-flight mass spectrometer
R. irregularis/Ri	*R. irregularis*
RNA	Ribonucleic acid
RT	Room temperature
RT-PCR	Reverse transcriptase polymerase chain reaction
sec	Second
S. cerevisiae	*S. cerevisiae*
sn	Stereospecific numbering
SPE	Solid phase extraction
SQDG	Sulfoquinovosyldiacylglycerol
TBE	Tris-boric acid-EDTA
TE	Tris-EDTA
TY	Tryptone yeast
TAG	Triacylglycerol
TBE	Tris, boric acid, EDTA
TML	Tris, LiCl, $MgCl_2$
UV	Ultra violet
% (v/v)	Percent volume per volume (mL per 100 mL)
WT	Wild type
% (w/v)	Percent weight per volume (g per 100 mL)
WGA	Wheat germ agglutinin
WPI	Weeks post inoculationion
YNB	Yeast nitrogen base

Fatty acids are abbreviated x:Y, where X represents the number of carbon atoms, and Y represents the number of double bonds. β-sitosterol is abbreviated as sitosterol throughout the text.

1 Introduction

1.1 Lipids and Fatty Acids

Lipids are the main components of biological membranes and therefore exert an important function in cellular and organellar compartmentalization in eukaryotic cells. In plants, glycerolipids, sphingolipids and sterols are the major membrane-forming lipids. Non-membrane forming storage lipids (triacylglycerol) are an important source of reducing energy and carbon in cellular metabolism in adipose tissues of animals and seeds of plants. During β-oxidation in the peroxisomes of plants, fatty acids of storage lipids are mobilized and yield the reducing agent NADH as well as the carbon building block acetyl-CoA. Plant lipids can serve in signal transduction (e. g. jasmonic acid, abscisic acid) and provide anchorage via lipid-modification (e. g. acylation, prenylation) of proteins and other macromolecules. Lipids also form apoplastic diffusion barriers in plants. Fatty acids, alcohols, aldehydes and ketones are components of cutin and cuticular waxes on the aerial organs and fatty acids and aclohols are also found as monomers of suberin in the roots of plants. These provide a hydrophobic barrier. Some lipids such as tocopherols (vitamin E) provide antioxidant capacity for protection of membranes against free radicals. Carotenoids serve as photoprotectants of the photosynthetic apparatus. Finally, the pigments chlorophyll and phylloquinone are active in dissipation of light energy and electron transfer during photosynthesis in chloroplasts of plants.

In general, lipids consist of a glycerol (glycerolipids), a ceramide (sphingolipids) or a sterol backbone. Glycerol in gycerolipids has three hydroxyl groups that can be bound to either a polar head group or non-polar fatty acids. Gycerolipids are classified based on the properties of their head group, which can be charged. It can contain phosphate (phosphoglycerolipids) or sugar (glycoglycerolipids). In these lipids, the remaining two glycerol hydroxyl groups are esterified to fatty acids. The carbon atoms of the fatty acids can either be saturated with hydrogen (saturated fatty acids) or contain one (mono) or multiple (poly) unsaturated double bonds formed by dehydrogenation of carbon atoms. The degree of saturation of fatty acids in membrane-lipids influences the membrane fluidity. Next to the polar lipids, lipids without head group modification on the glycerol backbone are uncharged and therefore called neutral lipids.

In membranes, polar glycerolipids form a bilayer by hydrophobic interactions of their fatty acid hydrocarbon tails. Water-soluble molecules from the cytoplasm or the luminal contents of organelles cannot be dissolved in the hydrophobic bilayer of membranes and therefore, membranes prevent unwanted diffusion of polar molecules. Membranes are interspersed with transporter and ion channels for trans-membrane exchanges of compounds between compartments. Other important lipid components are the sterol lipids. Sterol lipids do not contain glycerol and can exist in an unmodified (free sterols), esterified (sterol esters), glycosylated

(sterol glucosides) or esterified and glycosylated form (acylated sterol glucosides). Free sterols in plants are mainly campesterol, stigmasterol and sitosterol (Schaeffer *et al.*, 2001). Campesterol is the precursor for brassinosteroids that are growth hormones and function in biotic stress response while stigmasterol and sigmasterol are integral parts of membranes.

1.1.1 Plant Glycerolipid Synthesis

1.1.1.1 Membrane Glycerolipids

Plant membrane glycerolipid synthesis and metabolism involves the plastid and the ER. Fatty acids are synthesized in the plastid (see 1.1.2) and can be exported to the ER for elongation and desaturation or directly used in glycerolipid synthesis. Two main routes for glycerolipid synthesis exist in plants, termed prokaryotic, occurring in the plastids, and eukaryotic, occurring in the ER membrane (Ohlrogge and Browse, 1995).

In the prokaryotic pathway, acyl-ACP with mainly 18:1Δ9 fatty acid (18:1Δ9-ACP) from type-II fatty acid *de novo* synthesis (see 1.1.2) is esterified to the *sn*-1 position of glycerol-3-phosphate by GLYCEROL-3-PHOSPHATE ACYLTRANSFERASE (GPAT) to give rise to lyso-phosphatidic acid (LPA) that is converted to phosphatidic acid (PA) by LPA-ACYLTRANSFERASE (LPA-AT) via addition of primarily 16:0 fatty acid from 16:0-ACP to the *sn*-2 position. The resulting 18:1-16:0-PA is dephosphorylated to yield diacylglycerol (DAG) that is used as a precursor for the synthesis of the glycoglycerolipids monogalactosyldiacyglycerol (MGDG), digalactosyldiacylglcerol (DGDG) and sulfoquinovosyldiacylgycerol (SQDG) that either contain galactose or sulfoquinovose in their head groups. Alternatively, PA is converted to cytidine diphosphate-DAG (CDP-DAG) that is used for synthesis of the plastidial phosphoglycerolipid phosphatidylglycerol (PG) (Benning and Ohta, 2005).

The eukaryotic pathway also requires fatty acids synthesized in the plastid but involves the ER for lipid synthesis. Fatty acids exported from the plastids are converted by LONG CHAIN ACYL-CoA SYNTHASE (LACS) enzymes into acyl-CoA (Fulda *et al.*, 2004) that is used as substrate at the ER membrane for fatty acid modification and lipid synthesis Fatty acids from acyl-CoA, primarily 16:0-CoA, are transferred to the *sn*-1 position of G-3-P by an ER-membrane associated GPAT enzyme (Gidda *et al.*, 2009; Shockey *et al.*, 2016). Subsequently, desaturated C18 fatty acids from 18:1-CoA, 18:2-CoA or 18:3-CoA are transferred to the *sn*-2 position via LPA-AT to generate 16:0-18:1(18:2/18:3)-PA. Similar to the prokaryotic pathway, DAG and CDP-DAG obtained from PA serve as backbone for membrane glycerolipid synthesis. Afterwards, the phosphoglycerolipids phosphatidylcholine (PC), phosphatidylethanolamine (PE), phosphatidyinositol (PI), phosphati-dylserine (PS) and also some PG are synthesized (Nakamura, 2017).

There is substantial movement of lipids between the ER and plastids (Block and Jouhet, 2015). Therefore, the desaturated 18:2 and 18:3 fatty acids derived from desaturase reactions in

the ER can be relocated to the plastids and incorporated into plastidial lipids MGDG, DGDG and SQDG. The origin of the lipid, however, can be distinguished to be from the prokaryotic or eukaryotic pathway, depending on whether the fatty acid esterified to the *sn*-2 position of glycerol is 16:0 (prokaryotic) or 18:1(18:2/18:3) (eukaryotic).

1.1.1.2 Storage Glycerolipids

Storage glycerolipids in plants are synthesized at the ER. Fatty acids are exported from the plastid and then acylated with CoA. This acyl-CoA pool is used for synthesis of storage glycerolipids. At the ER membrane, GPAT catalyzes the transfer of fatty acids to G-3-P, forming LPA. The LPA is esterified with another fatty acid from the acyl-CoA pool by ACYL-CoA:LYSOPHOSPHATIDATE ACYLTRANSFERASE (LPAT) and dephosphorylated by PHOSPHATIDATE PHOSPHATASE (PAP) to give rise to DAG that is utilized as substrate for synthesis of PC by CDP-CHOLINE:DIACYLGLYCEROL CHOLINEPHOSPHOTRANSFERASE (CPT) which transfers the phosphatidylcholine group from CDP-choline to DAG (Bates *et al.*, 2013). For synthesis of storage glycerolipids, the phosphatidylcholine head group is removed from PC by PHOSPHOLIPASE C to yield DAG that is used as precursor for the synthesis of triacylglycerol (TAG), the main storage glycerolipid. For this purpose, DAG is esterified with a fatty acid from the acyl-CoA pool, catalyzed by ACYL-COA:DIACYLGLYCEROL ACYLTRANSFERASE (DGAT) (Lardizabal *et al.*, 2001; Yen *et al.*, 2005). As an alternative, PC instead of DAG can be used for esterification of diacylglycerol by the enzyme PHOSPHOLIPID:DIACYLGLYCEROL ACYLTRANSFERASE (PDAT) (Kim, 2005). Storage lipids are mainly formed at the rough ER and accumulate in the cell as water-insoluble structures called oil bodies. These bud-off during extensive synthesis of TAG at the ER and are covered by a phospholipid monolayer interspersed with specific protein called oleosins (Shimada *et al.*, 2018).

1.1.2   Fatty acid *de novo* Synthesis in Plants and Fungi

The term FAS refers to all enzymes involved in fatty acid *de novo* synthesis occurring in the plastids of plants and the cytosol of fungi. In plants, multiple proteins are involved in the FAS reactions that collectively form the type-II FAS complex (Brown *et al.*, 2006). In contrast, fungi contain a type-I FAS that compromises a single large enzyme with multiple subunits capable of catalyzing the different reactions necessary for formation of fatty acids (Jenni *et al.*, 2007). While fungal type-I FAS acts like a single large protein complex, the type-II FAS proteins likely form a complex assembled in a supramolecular structure to efficiently channel the substrates and intermediates. The precursor for plant and fungal fatty acids is acetyl-CoA produced in the plastid of plants and cytosol of fungi (Figure 1a).
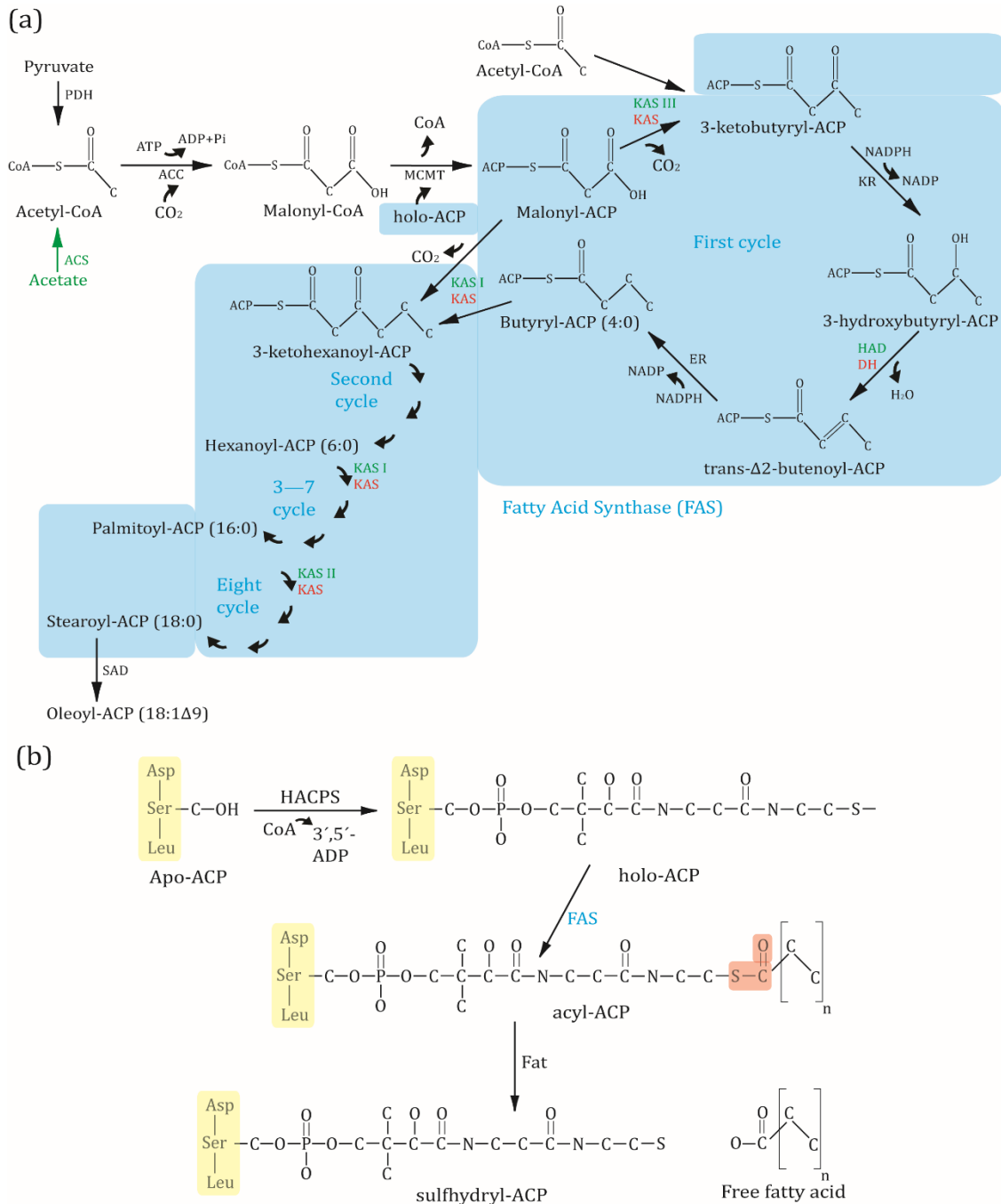
Figure 1: Reactions of Fatty Acid *de novo* Synthesis in Plants and Fungi.
a) Carboxylation of acetyl-CoA to malonyl-CoA by ACC is the commited step during FAS. The growing acyl chain is linked via a thioester to ACP. Successive rounds of FAS consist of four core reactions: condensation, reduction, dehydration and reduction. In plants, three KAS isoforms are present of which KAS III catalyzes only the initial condensation reaction of malonyl-ACP with acetyl-CoA and KAS II only the final FAS cycle to yield stearoyl-ACP. Plant enzymes are green, while red indicates fungal origin.
b) Acyl-ACP Synthesis and Hydrolysis by acyl-ACP Thioesterases.
Inactive apo-ACP is activated by HACPS to generate the active holo-ACP that is used by FAS to generate acyl-ACP. Fatty acid elongation is terminated by hydrolysis of the thioester, releasing sulfhydrdyl-ACP and free fatty acids. The amino acids forming the conserved tripeptide Asp-Ser-Leu are marked in yellow and the thioester on acyl-ACP is indicated in red.
PDH, pyruvate dehydrogenase; CoA, coenzyme A; ACP, acyl-carrier protein; ACS, acetyl-CoA snythase; ACC, acetyl-CoA carboxylase; MCMT, malonyl-CoA:acyl-carrier portein malonyltransferase; KAS, 3-ketoacyl-ACP synthase; KR, 3-ketoacyl-ACP reductase; HAD/DH, 3-hydroxyacyl-ACP dehydratase; ER, enoyl-ACP reductase; SAD, stearoyl-ACP desaturase; HACPS, holo-ACP synthase; Fat, acyl-ACP thioesterase.

In plastids, acetyl-CoA can be generated by pyruvate dehydrogenase (PDH) via oxidative decarboxylation of pyruvate (Johnston *et al.*, 1997) or via plastidial acetyl-CoA synthase (ACS) (Lin and Oliver, 2008). The first committed step in fatty acid synthesis is the carboxylation of acetyl-CoA to yield the C3 compound malonyl-CoA by acetyl-CoA carboxylase (ACC) (Konishi *et al.*, 1996). By regulating ACC activity, organisms control the rate of fatty acid synthesis (Andre *et al.*, 2012). The malonyl group is transferred from CoA to acyl-carrier protein (ACP) via a thioester linkage to yield malonyl-ACP, catalyzed by malonyl-CoA:acyl carrier protein malonyltransferase (MCMT). ACP itself is also regarded as part of the FAS. It is present in two forms: apo-ACP and holo-ACP. Apo-ACP is inactive and can be activated by holo-ACP synthase (HACPS) to generate holo-ACP (Figure 1b), which is the soluble carrier for fatty acids during the FAS reactions (Chan and Vogel, 2010).

In the subsequent FAS reactions, malonyl-ACP is elongated in a series of four reactions, which comprises one cycle of fatty acid *de novo* synthesis. In the first reaction, β-ketoacyl-ACP synthase (KAS) condenses malonyl-ACP with acetyl-CoA, thereby decarboxylating the malonyl-ACP and forming a carbon-carbon bond to yield the C4 compound 3-ketobutyryl-ACP. In plants, this first reaction is catalyzed by a specific isoform, KASIII. Successively, 3-ketoacyl(butyryl)-ACP is reduced by 3-ketoacyl-ACP reductase (KAR) to 3-hydroxyacyl-(butyryl)-ACP using electrons from NADPH. It is further dehydrated by hydroxyacyl(butyryl)-ACP dehydratase (HAD), giving rise to enoyl-ACP. In a final step, electrons from NADPH are again used to reduce enoyl-ACP, catalyzed by enoyl-ACP reductase (ER) to saturate the fatty acid moiety and thereby generate acyl-ACP. The C4 product of this first round of FAS, butyryl-ACP, is subjected to iterative rounds of condensation, reduction, dehydration and reduction until the main products of FAS are synthesized, which are C16—C18 fatty acids. In these successive rounds, no more acetyl-CoA is used in the condensation step, but instead the acyl(butyryl)-ACP is condensed with malonyl-ACP. The first reactions of the second-to-eight rounds of FAS are catalyzed by the KAS I-isoform in plants, generating up to C16 fatty acids. To synthesize C18 fatty acids, a third isoform, KAS II, catalyzes the final condensation reaction, which ultimately leads to production of C18 stearoyl-ACP (Li-Beisson *et al.*, 2013). In summary, 14 molecules of NADPH are consumed to synthesize a C16 fatty acid, which makes fatty acid *de novo* synthesis highly energy demanding.

Fatty acid *de novo* synthesis can be terminated by transfer of the fatty acid to glycerolipids, desaturation of the fatty acid, or hydrolysis of the thioester by acyl-ACP thioesterases (Fat). In plants, stearoyl-ACP is desaturated by stearoyl-ACP desaturase (SAD), synthesizing C18:1Δ9-ACP (Shanklin and Somerville, 1991). Two types of Fat enzymes exist in plants, FatA, preferring C18:1Δ9-ACP and FatB, preferring saturated acyl-ACP with fatty acids of C12—C16 (Jones *et al.*, 1995). Cleavage of the thioester results in a free fatty acid and a sulfhdydryl-ACP. The free fatty acid is exported from the plastid and made available for cytoplasmic transport and e. g.

glycoglycerolipid synthesis at the ER after conversion into acyl-CoA (see 1.1.1) (Fulda *et al.*, 2004; Li *et al.*, 2015).

1.2 Arbuscular Mycorrhiza Symbiosis

Invention of plant-mycorrhiza symbiosis with fungi from the Glomeromycotina is dated back approximately 450 million years, which predates the origin of the root and therefore might have helped early plants to switch to a terrestrial lifestyle (Brundrett, 2002; Brundrett and Tedersoo, 2018). Mycorrhiza associations are diverse and include ecto, ericoid, arbutoid and arbuscular mycorrhiza. In contrast to ecto, ericoid and arbutoid mycorrhiza, the arbuscular mycorrhiza fungi form a monophyletic lineage in the Mucomicotina (Martin *et al.*, 2016; Smith and Read, 2008). The mutual benefit of the symbiosis is foremost, but not limited to, the exchange of photosynthetically fixed carbon supplied by the plant for mineral nutrients, acquired by the fungal mycelium that extends beyond the root depletion zone. It has been estimated that 20% of photosynthates synthesized by the plant shoot are delivered to the fungus (Bago *et al.*, 2000).

Engaging in AM-symbiosis has multiple additional benefits for both partners such as tolerance to abiotic and biotic stresses (Kumar *et al.*, 2017). Multiple studies have confirmed the alleviating effects of AM-inoculation to drought stress (Bárzana *et al.*, 2015; Rapparini and Peñuelas, 2014). In wheat, AMF enhances water use efficiency and causes metabolomic reprogramming for a better tolerance of drought (Bernardo *et al.*, 2019). In a study with tomato, different AMF (*Funneliformis mosseae*, *R. irregularis* and *Claroideoglomus etunicatum*) increased resistance to drought and NaCl stress and the corresponding metabolite profiling revealed increased accumulation of jasmonic acid and intermediates of the carotenoid pathway, such as ABA glucosyl ester, β-ionone and blumenol C glucoside (Rivero *et al.*, 2018). This is consistent with promotion of AM colonization by ABA (Pozo *et al.*, 2015) that is even more eminent under drought stress as shown by increased ABA in tomato and lettuce under drought stress (Ruiz-Lozano *et al.*, 2015). In *Sorghum bicolor*, the AMF *Rhizophagus arabicus*, which is endemic to hyperarid soils, enhanced phosphate and nitrogen supply especially under water-limiting conditions, even to a greater extent than *R. irregualris*, highlighting the importance of fungal diversity on alleviating abiotic stresses (Symanczik *et al.*, 2018). AM fungi counteract biotic stresses, as has been shown for increased resistance towards root-parasitic nematodes (Vos *et al.*, 2012).

AMF reveal a positive effect on soil ecosystems due to phytoremediation, prevention of erosion, increased water retention capacity, decreased nutrient leaching and promotion of other beneficial soil microbes (Calonne *et al.*, 2014; Chen, M. *et al.*, 2018; Debiane *et al.*, 2011). They also act as carbon sinks by providing sequestration of CO_2 via belowground C allocation, accumulating the host-derived carbon in spores and mycelia upon completion of the asexual life-cycle of the fungus (Ho and Trappe, 1973; Lösel and Cooper, 1979; Olsson and Johnson, 2005). AMF therefore help capture excessive CO_2 and to regulate the global carbon cycle. In agriculture, inoculation of crops

with AMF in the field leads to increased grain yield and plant performance (Gibert *et al.*, 2019; Zhang *et al.*, 2019), although the extent depends on the combination of host genotype and fungal strain. This has been shown for maize, where in different genotypes, shoot growth was positively correlated to the amount of extraradical mycelium, promoted differently by the respective maize cultivar (Sawers *et al.*, 2017).

Due to increased usage of fertilizers, agricultural fields often suffer from over-fertilization. This has consequences on the adjacent ecosystems, such as algal blooming due to e. g. elevated phosphate levels caused by leaching of phosphate from the field into the groundwater. Improving phosphate utilization by crop plants can be achieved by increasing phosphate-acquisition-efficiency (PAE), which represents the ability of the roots to take up phosphate from the soil. Inoculation with AMF therefore can contribute to a more efficient usage of available minerals by increasing PAE, even though studies on wheat and barley showed that plant growth promotion depends on the diversity of the plant cultivar and the fungal strain (Campos *et al.*, 2018). In addition, breeding for improved AM symbiosis might proof to be challenging in the future as AM colonization was only mildly affected by genetic diversity in the model plant *Medicago truncatula* (Dreher *et al.*, 2017).

Research on essential genes for the formation of AM symbiosis has mainly been conducted using forward and reverse genetics with plant mutants. Recently, transcriptomic and genomic sequencing of a variety of arbuscular mycorrhiza fungal strains and species at different stages of their life cycle has provided more insights into the fungal molecular components necessary during AM-symbiosis (Chen *et al.*, 2018; Handa *et al.*, 2015; Kamel *et al.*, 2017; Kobayashi *et al.*, 2018; Lin *et al.*, 2014; Mathieu *et al.*, 2018; Salvioli *et al.*, 2016; Sun *et al.*, 2019; Tang *et al.*, 2016; Tisserant *et al.*, 2012; Tisserant *et al.*, 2013; Zeng *et al.*, 2018). In combination with microscopic observations, the underlying genetic regulation and molecular dialogue of the different stages during AM symbiosis has been characterized. The processes that encompass development of the AM symbiosis can be divided into three phases (Figure 2). First, pre-contact signalling of secreted compounds in the rhizosphere by plant and fungus, second, physical contact and root inter- and intracellular colonization and third, extraradical mycelium and daughter spore generation. The last phase can be followed by recolonization. AM symbiosis develops asynchronously and therefore multiple AM life cycle stages are present on different regions of the same root. During the second phase, the colonized root is characterized by the abundance of multiple fully branched arbuscules. These are highly active in nutrient exchange and therefore compromise the central stage during AM symbiosis (see 1.2.4).

1.2.1 Formation and Progression of Root Endosymbiosis with AMF

1.2.1.1 Bidirectional Signalling and Recognition in the Rhizosphere Leads to Root Colonization

Resting spores in the soil are stimulated by a cocktail of host signal compounds for germination and growth towards the root (van Dam and Bouwmeester, 2016). Among them, strigolactones are well characterized components of root exudates that stimulate hyphal branching and metabolism (Akiyama *et al.*, 2005; Besserer *et al.*, 2006; Besserer *et al.*, 2008). Strigolactones are secreted via the ABC transporter PDR1 to create a concentration gradient that guides the growing hyphae toward the root (Kretzschmar *et al.*, 2012). Some plant species, like sunflower and oat, do not exudate strigolactones but carlactones, which also have stimulatory effects on AM hyphae (Mori *et al.*, 2016). Other host-secreted signals are suggested to be N-acetylglucosamines (GlcNAc), which was revealed by the absence of a typical signalling-transcript signature when *R. irregularis* was treated with root exudates from WT and *nope1* (*NO PERCEPTION 1*) transporter mutants (Nadal *et al.*, 2017). Additionally, flavonoids are synthesized by the roots during AM colonization and also function in pre-contact signalling (Harrison, 1993; Larose *et al.*, 2002; Steinkellner *et al.*, 2007). In addition, the hydroxylated fatty acids 2-hydroxytetradecanoic acid and 2-hydroxydodecanoic acid, putatively present in carrot root exudates, were shown to induce multiple lateral branches along the germ tube in germinating spores of *Gigaspora gigantea*, but this response was absent in *R. irregularis* (Nagahashi and Douds, 2011). On the other hand, AM fungi secrete diffusible signals as well that are collectively referred to as myc-factors. The most studied ones are chitooligosaccharides (CO) and lipochitooligosascharides (LCO) (Genre *et al.*, 2013; Maillet *et al.*, 2011) but might also compromise peptides such as the SL-INDUCED PUTATIVE SECRETED PROTEIN 1 (SIS1) (Tsuzuki *et al.*, 2016), SECRETED PROTEIN 7 (Kloppholz *et al.*, 2011) and volatile organic compounds (Sun *et al.*, 2015). Although the full picture has not yet been unraveled, plant cell surface receptor-like kinases (RLKs) containing lysine motifs (LysMs) can bind GlcNAc oligosaccharides and function in perception of signals during AM symbiosis (Zipfel and Oldroyd, 2017).
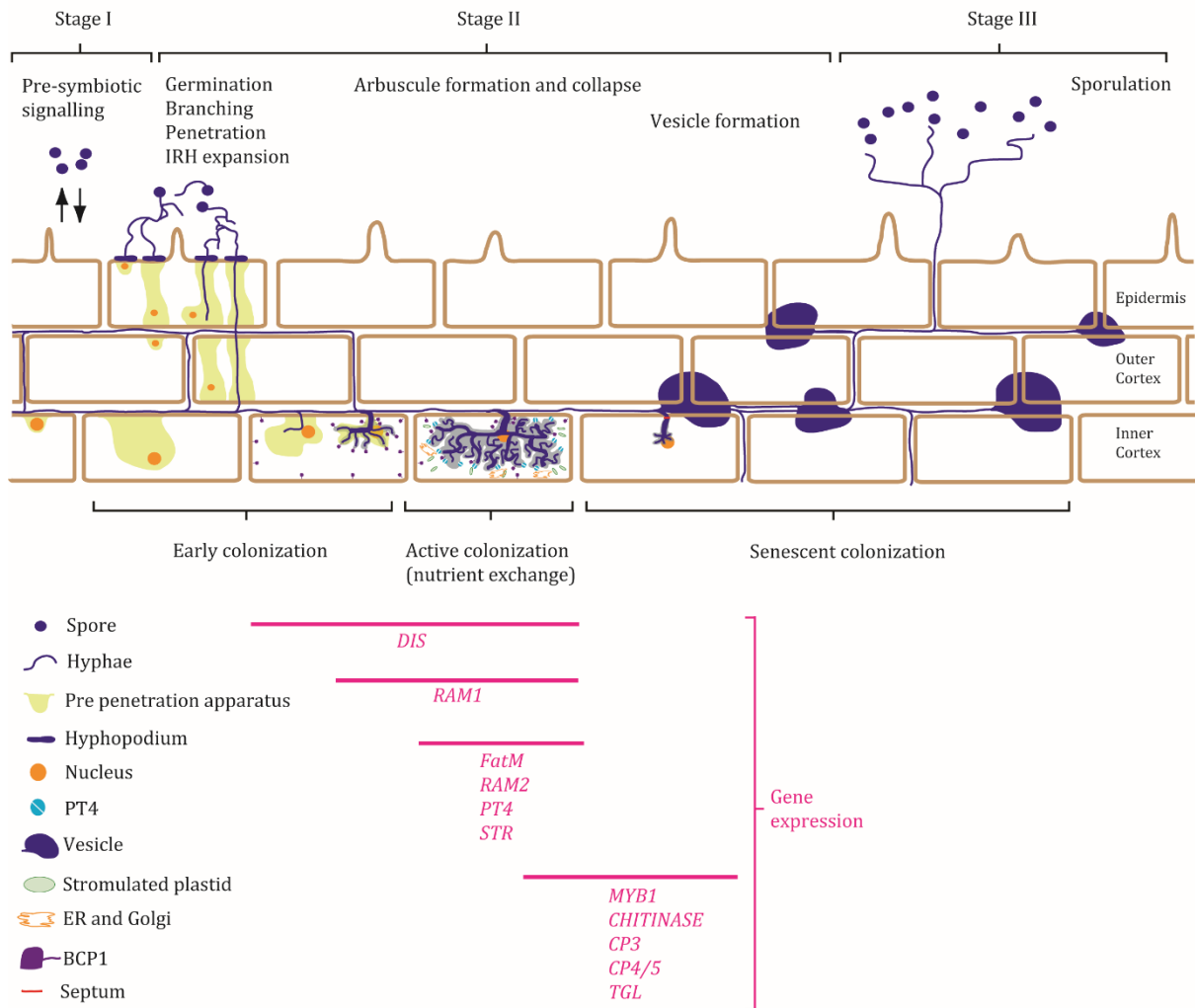
Figure 2: Life Cycle Stages and Progression of AM Root Colonization.
Symbiosis of roots with AM fungi can be divided into three stages: Stage I compromises pre-symbiotic exchange of signalling compounds. Plant roots exudate strigolactones, carlactones, flavonoids and GlcNAcs to stimulate fungal spore germination and branching. The fungus exudes myc-factors, COs, LCOs and the butenolide karrikin for recognition by the plant.

Stage II encompasses physical contact and intercellular hyphae proliferation as well as arbuscule formation. Hyphopdia are formed to support epidermal cell penetration and hyphal transfer through the cells is guided by the PPA. In the inner root cortex, a bigger PPA marks the path for hyphal penetration into cells , where they branch iteratively to form arbuscules. This happens <24h after initial root penetration. The PAM surrounding the arbuscule is synthesized by the plant and equipped with plant nutrient transporters (e. g. PT4) secreted via exocytosis. Therefore, fully branched arbuscules are active in nutrient exchange and are surrounded by cytoplasmic contents such as ER, Golgi and stromulated plastids. The hypha at the point of fungal entry is thickened and is called the arbuscule trunk, forming the trunk domain. Subsequent hyphal branching leads to formation of the branching domain. The BCP1 protein is present in the PAM in the trunk domain and the branching domain and additionally in the host peripheral PM. Arbuscules are transient structures and collapse 1—3 days after their formation by being actively degraded by host-induced hydrolases. The transition zone between intracellular hyphae of the remaining arbuscule and the intercellular hyphae becomes prominent by formation of a septum. As the root colonization proceeds, *R. irregularis* and most other AMF form vesicles. At later stages of root colonization, the root is characterized by the presence of collapsed arbsucules and is enriched in vesicles that contain lipids and glycogen. This is called senescent colonization.

In stage III, fungal hyphae grow out of the root into the soil, where they form daughter spores filled with mainly lipids. Spores are resting structures in the soil until stimulated by host-signals again.

IRH, interradical hyphae; PT4, PHOSPHATE TRANSPORTER 4; BCP1, BLUE COPPER PROTEIN 1; *DIS, DISINTEGRATED ARBUSCULES, RAM1/2; REDUCED ARBUSCULAR MYCORRHIZA; STR, STUNTED ARBUSCULES; CP, CYSTEINE PROTEINASE, TGL; TRIGLYCERIDE LIPASE.*

Consequently, rice mutants of the *LysM-RLK CERK1* (*CHITIN ELICITOR RECEPTOR KINASE 1*) gene were severely impaired in AM development (Miyata *et al.*, 2014). Rice mutants of the *DWARF 14-LIKE* (*d14l*) gene do not engage in AM symbiosis due to the absence of fungus-plant contact sites. *D14L* encodes an α/β-fold hydrolase that forms an intracellular receptor complex for perception of karrikin, a post-wildfire signal in plants. The *d14l* mutant also does not exhibit a transcriptional response to germinating spore extracts from *R. irregularis* and therefore, karrikin probably comprises another chemical signal exuded by AMF (Gutjahr *et al.*, 2015). Perception of fungal signals by root epidermal cells triggers nuclear calcium oscillations similar to signalling in root-nodule symbiosis, which indicates recognition of the fungus (Chiu and Paszkowski, 2019).

Upon contact of the approaching hyphae to the root, the hyphal tip differentiates into a thick supported structure, the hyphopodium, which attaches to the epidermal cell (Figure 2). At root-AMF contact sites, a *LIPID TRANSFER PROTEIN* (*LTP*) gene of unknown function is expressed. The high expression of LTP prompted the hypothesis that fatty acids might act in signalling or are supplied to fungal hyphae upon initial contact to the root (Blilou *et al.*, 2000). At cells destined for fungal penetration, a cytoskeletal rearrangement of the host cytoplasm orchestrated by changed host gene expression takes place and creates a specialized intracellular structure, the pre-penetration apparatus (PPA). The PPA forms an apoplastic tunnel into the cell and is created by an invagination of the plasma membrane supported by an ER-network and cytoskeletal components. It marks the path of fungal entry into the cell (Genre *et al.*, 2005).

Due to similarities in the early events of both root-nodule and AM endosymbiosis, they likely share an evolutionary history. The conserved molecular components that are essential for accommodation of either symbiont are comprised in the Common Symbiosis Pathway (CSP) (Parniske, 2008). At the plasma membrane of the rhizodermal penetration site, integral membrane proteins termed SYMBIOSIS RECEPTOR KINASE (SYMRK) with an intracellular kinase domain and extracellular leucine-rich repeats (LRR) are essential for root-nodule formation and AM-symbiosis alike (Endre *et al.*, 2002; Stracke *et al.*, 2002). The secondary messengers downstream of *SYMRK* that transduce the signal are unknown, but mevalonate might be involved, as demonstrated by the requirement for the *HMGR1 (3-Hydroxy-3-Methylglutaryl CoA REDUCTASE 1)* gene for calcium spiking (Venkateshwaran *et al.*, 2015). *HMGR1* regulates the MVA pathway in plants.

Despite of the unsettled details, it is well documented that the symbiosis-signal is transmitted to the nucleus where it manifests as nuclear and perinuclear calcium spiking again. Calcium spiking is achieved by reiterated influx and efflux of calcium into the nucleoplasm from the nuclear envelope lumen to activate target genes. Molecular requirements for calcium spiking are NUCLEAR PORE COMPLEXES (NUP), the ATP-driven calcium pump MCA8, the potassium efflux channels POLLUX and CASTOR, as well as CYCLIC-NUCLEOTIDE-GATED CHANNEL 15

(CNGC15). Calcium in the nucleoplasm activates calcium and calmodulin-dependent serine/threonine protein kinase (CCamK) that phosphorylates the transcription factor CYCLOPS, which leads to host-gene activation and subsequent accommodation of the endosymbiont (Genre and Russo, 2016).

After penetration of the rhizodermis, the fungal hyphae populate the outer root cortex by growing inter and intracellularly, forming the intraradical mycelium (IRM). Finally, they approach the cells of the inner root cortex, but do not form appressoria again. Instead, the cells destined for fungal hyphae penetration show PPA formation in preparation of accommodation of the symbiont again. This PPA formation preceding inner cortex cell penetration is more complex and different from the preceding initial PPA formation in the rhizodermis or the PPA formation during colonization of the outer root cortex cells, where no arbuscules are formed (Genre *et al.*, 2008). PPA formation in the inner root cortex cells therefore compromises the initial step in arbuscule formation, discussed in the next chapter.

1.2.1.2 Arbuscule Formation

During inner cortical PPA formation and preceding the entry of the hypha, the plant reorganizes its cytoplasmic contents. The nucleus travels opposite of the PPA and polar localization of secretion towards the point of hypha entry takes place. Contrary to PPA formation in the outer cortex and the rhizodermis, in inner cortical cells, the nucleus duplicates prior to fungal penetration. Upon entry of the fungus into the cell, the plant synthesizes the periarbuscular membrane (PAM) that is in-continuum with the plasma membrane and surrounds the expanding hyphae. The PAM delimits the plant cytoplasm from the neighboring periarbuscular space (PAS), an apoplastic continuum that traces the outer surface of the arbuscule membrane. The fungal cell wall encloses the fungal membrane, which confines the fungal cytoplasm (Ivanov *et al.*, 2019).

Eventually, the intracellular hyphae gives rise to the arbuscule, a highly ramified structure created by branched hyphae. Mutants in the transcriptional regulator complex formed by CCaMK-CYCLOPS-DELLA proteins fail to initiate arbuscule branching after cellular penetration due to absence of signal transduction. The CCaMK-CYCLOPS-DELLA complex activates the transcription factor *REDUCED ARBUSCULAR MYCORRHIZA 1* (*RAM1*) that controls arbuscule branching (Floss *et al.*, 2013; Pimprikar *et al.*, 2016). During arbuscule genesis, the invading hypha grows into the PPA and forms a thick trunk at the point of entry, subsequently called the trunk domain. The hypha branches dichotomously and forms the branch domain. The plasma membrane surrounding the trunk domain is characterized by presence of the BLUE COPPER BINDING PROTEIN 1 (BCP 1) that is anchored to the plasma membrane via a predicted glycosylphosphatidylinositol (GPI) anchor and is also present in the host plasma membrane in non-invaded cells (Pumplin and Harrison, 2009). The plant-synthesized PAM causes a 3—4 fold increase of the host plasma membrane (Alexander *et al.*, 1989). The highly-branched

arbuscule-forming hypha increases the surface area of the plant-microbe interface, making exchange of symbiotic metabolites more efficient. The PAM in juxtaposition of the branch domain therefore contains a unique set of proteins with functions in e. g. symbiotic nutrient exchange, such as the phosphate transporter PT4 (Pumplin and Harrison, 2009).

The branch domain of arbuscules is further divided into basal or thick branches that further branch into fine or secondary branches that resemble the canopy of trees. The *ram1* mutants are defective in arbuscular fine branching but still form the thick branches (Park *et al.*, 2015; Rich *et al.*, 2015; Xue *et al.*, 2015). By continuous branching at their growing tips, the arbuscule finally fills almost the entire cavity of the cell. As the PAM surrounding the hyphal branches is actively synthesized during hyphal growth, this requires polarized secretion of membrane material and protein by the host (Choi *et al.*, 2018). This is achieved by focal fusion of exocytotic vesicles, containing e. g. symbiotic nutrient transporters, with the PAM. The vesicle-fusion process is proposed to be mediated by the exocyst complex Exo70i (Pumplin *et al.*, 2012; Zhang *et al.*, 2015), and the SNARE (N-ethylmaleimide-sensitive factor-attachment protein receptors) proteins SYNTAXIN 132a (Huisman *et al.*, 2016; Pan *et al.*, 2016), VTI12 (Lota *et al.*, 2013) and VAMP72d/e (Ivanov *et al.*, 2012).

1.2.1.2.1 Arbuscule Life Cycle Dynamics

Arbuscules are dynamic structures with a lifetime of 1—3 days (Alexander *et al.*, 1989; Kobae and Hata, 2010). Arbuscules are under control of the plant host cell, which can induce expression of a set of genes, termed executor genes. These likely promote arbuscule collapse, probably to prevent underperformance of the fungus in terms of mineral nutrient delivery. The executor genes include a *CHITINASE*, the *CYSTEINE PROTEINASE 3* (*CP3*) and *CP4/5*, and a *TRIGLYCEROL LIPASE* (*TGL*). For activation of these genes, the transcription factor MYB1 has been reported to be central (Floss *et al.*, 2017). It interacts with DELLA and NSP1 transcription factors that then induce the described executor genes and thus induce arbuscule degeneration to enable subsequent recolonization of either the same cell or other cells of the inner root cortex (Gutjahr and Parniske, 2017). Arbuscule maintenance and proper branching is distorted in a variety of plant mutants. These mutants show premature arbuscule collapse, leading to the occurrence of stunted arbuscules. Figure 2 highlights the expression of genes that have functions in arbuscule branching and are either expressed in fully-branched arbuscules (*PT4*, *FatM*, *RAM2*, *STR*), or at the onset of cortical cell penetration and the initial phase of arbuscule generation (*DIS*, *RAM1*), and additionally, genes induced to enforce arbuscule collapse (*MYB1*, *CHITINASE*, *CP3*, *CP4/5, TGL*) that are expressed in mature arbuscules and collapsing ones (Figure 2) (Pimprikar and Gutjahr, 2018). Homologs of *DIS*, *FatM* and *RAM2* are involved in fatty acid biosynthesis and lipid processing at the ER (Gaude *et al.*, 2012; Rich *et al.*, 2017) and *FatM*, *RAM1*, *RAM2* and *STR-STR2* have an AM-specific phylogenomic distribution, i. e. are symbiosis-specific, while *DIS* is also found

in the genomes of some non-host species but also essential for arbuscule branching and AM development (Bravo *et al.*, 2016; Bravo *et al.*, 2017; Keymer *et al.*, 2017).

1.2.1.3 Post-Symbiotic Growth: Generation of Vesicles and Asexual Spores

Upon completion of the asexual life cycle of the fungus, intraradical vesicles and extraradical spores are formed. Intraradically growing hyphae form vesicles at their terminal ends. These are temporary storage structures containing predominantly glycogen and the neutral storage lipid TAG (Jabaji-Hare *et al.*, 1984). Hyphae that extend away from the root are termed extraradical hyphae. They extend in the surrounding rhizosphere, where they form the extraradical mycelium (ERM), and eventually from spores. Spore formation in the ERM is dependent on host carbon delivery (Douds, 1994; Douds and Schenk, 1990) and symbiotic hyphae deliver reduced carbon to the spores predominantly as glycogen (see 1.2.2.2.1) and TAG (see 1.2.2.2.2). Spores predominantly accumulate reduced carbon compounds to provide the energy for hyphal growth in the absence of a host upon germination and exploration of the rhizosphere (Olsson and Johansen, 2000). To date, it is unclear how exactly vesicle and spore formation is organized (Choi *et al.*, 2018). In addition to TAG and glycogen, fungal vesicles are also rich in cations such as potassium, magnesium, sodium and calcium and therefore may function as a reservoir or in sequestration of these ions (Strullu *et al.*, 1983).

1.2.2   Reciprocal Nutrient Exchange

1.2.2.1 Mineral Nutrient Uptake and Transport

Nutrient exchange is the central mechanism of AMF symbiosis. In exchange for carbon, AMF deliver mineral nutrients to the host (Figure 3). Phosphate and nitrogen are the main nutritional factors that influence development of AM symbiosis and plants sustain AM colonization as long as supply of either one is scarce. On the opposite, accumulation of fungal biomass, fungal proliferation and carbon flow to the fungus are impaired by increased availability of either nitrogen or phosphate to the roots (Nouri *et al.*, 2015; Olsson *et al.*, 2005).

In the soil, the fungal ERM acquires orthophosphate (PO_4^-) by high-affinity PHOSPHATE TRANSPORTER (PT) (Harrison and van Buuren, 1995; Maldonado-Mendoza *et al.*, 2001; Olsson *et al.*, 2005; Xie *et al.*, 2016). In the fungus, the imported orthophosphate accumulates in the vacuolar compartment, where it is used to synthesize polyphosphates (poly-P). As the accumulating poly-P is negatively charged, cations are imported along with phosphate to neutralize the negative charges which was demonstrated by increased potassium, calcium and magnesium in fungal ERM as response to Pi uptake and the corresponding cation transporter gene expression (Kikuchi *et al.*, 2014).
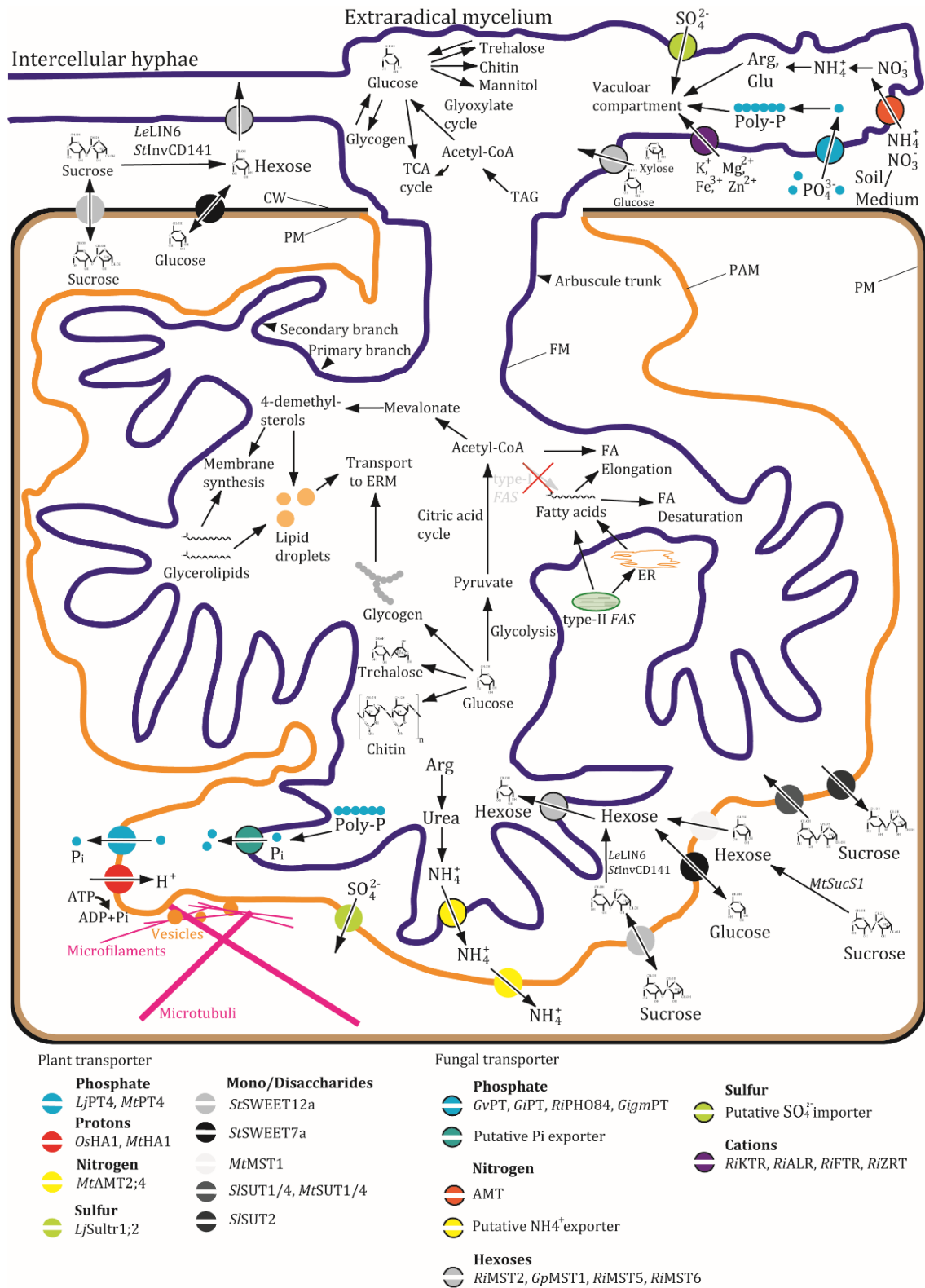
Figure 3: Uptake, Transport, Exchange and Metabolism of Nutrients at the Symbiotic Interface. Mineral nutrients from the soil are harvested by mycorrhizal extraradical hyphae and taken up as inorganic ions but can be made available also from organic compounds in the soil. Both are translocated to arbuscules and into the PAS for import of the plant via symbiotic H+/co-transporter proteins that reside in the PAM. In exchange, AMF obtain carbon from the host in the form of sugars and fatty acids. Sugar export into the PAS and uptake via fungal monosaccharide transporters occurs across the fungal membrane. The exact mechanism of fatty acid transport is not yet understood.

Figure 3: (continued)
In the fungal cytoplasm, glucose is converted into glycogen and trehalose or hydrolyzed in glycolysis to yield energy. Fatty acids in the fungus are used to synthesize membrane and storage lipids and fatty acids are further modified during elongation and desaturation. Fungal storage lipids can be synthesized in the ERM or in the IRM and transported in long-distance transport as lipid droplets to the spores.
The characterized and inferred transporter proteins that engage in nutrient exchange are depicted with their reported names and the organisms in which they were characterized (see text for details).
Arg, arginine; Glu, glutamate; CW, cell wall; PM, plasma membrane; FM, fungal membrane; PAM, periarbuscular membrane; PAS, periarbuscular space; FA, fatty acids; Pi, inorganic phosphate.

To increase phosphate uptake, AMF stimulate soil-borne bacteria that mineralize phosphorous from organic phosphate. This was demonstrated by exudation of fructose by *R. irregularis* that stimulated uptake of inorganic phosphate released from phytate by secreted acid phosphatase from the phosphate-solubilizing bacterium *Rahnella aquatilis* (Zhang *et al.*, 2018). Next to phosphate, nitrogen is acquired from the soil as NH_4^+ or NO_3^- (Johansen *et al.*, 1996) by fungal AMMONIUM TRANSPORTERS (AMT) and converted into glutamate and mainly arginine in the ERM.

Both poly-P and arginine are translocated via the vacuolar compartment from the ERM via intercellular hyphae to the arbuscules. At the arbuscules, arginine is converted via urea to ammonia again that is subsequently released into the PAS (Govindarajulu *et al.*, 2005). From there, ammonia is likely transferred via PAM-resident plant AMT2;3 transporters to the plant cytoplasm (Breuillin-Sessoms *et al.*, 2015). Poly-P at the arbuscules is hydrolyzed and released into the PAS (Solaiman *et al.*, 1999) from where it is acquired by specific plant PHOSPHATE TRANSPORTER termed *Mt*PT4 in Medicago (Harrison *et al.*, 2002; Javot *et al.*, 2007), *Os*PT11 in rice (Kobae and Hata, 2010; Paszkowski *et al.*, 2002), *St*PT3 in potato (Rausch *et al.*, 2001) and *Le*PT1 in tomato (Rosewarne *et al.*, 1999). *Mt*PT4 and *Os*PT11 were shown to reside in the PAM opposite of the extensively branched fungal hyphae that form the fine-branch domain of the arbuscules. They are delivered to the PAM via polarized secretion of exocytotic vesicles via the endomembrane system, which becomes visible by aggregation of cytoplasmic contents such as ER, Golgi and trans-Golgi-network, microfilaments and microtubuli in arbuscocytes (Bonfante, 2018; Kobae and Hata, 2010; Pumplin *et al.*, 2012; Pumplin and Harrison, 2009; Yang *et al.*, 2012).

Besides phosphate and nitrogen, mycorrhizal colonization increases the sulfur content of host roots. Sulfur is likely acquired by fungal transporters and delivered to the host. A candidate transporter, *LjSultr1;2* from *L. japonicus*, was proposed to act on symbiotic sulfur uptake at the PAM (Giovannetti *et al.*, 2014). Host transporters in the PAM likely transport mineral nutrients in a H^+/co-transport manner, as functional characterization of PAM-resident proton pumps (H^+-ATPases *Os*HA1 and *Mt*HA1) have been shown to energize the PAS for subsequent co-transport of mineral nutrients (Krajinski *et al.*, 2014; Wang *et al.*, 2014).

1.2.2.2 Carbon Transfer

Mineral nutrient homeostasis is closely linked to carbon transfer during AM symbiosis. The soil-borne nutrients, especially phosphate, are also precious to the fungus, e. g. for phospholipid synthesis to ensure membrane synthesis and hyphal proliferation, as well as synthesis of nucleic acids for cellular reproduction. *R. irregularis* was shown to stop the transfer of nutrients and instead accumulates mineral nutrients in spores when sucrose in the medium, which served as carbon source for the host, was reduced to 50% (Hammer *et al.*, 2011).

Colonization with AMF leads to an increased source strength of mycorrhizal roots and therefore induces photosynthetic CO_2 fixation, sucrose synthesis and translocation to the root to compensate for the carbon drain by the colonizing fungus (Lanfranco *et al.*, 2018). The available carbon sources for AMF are sugars and fatty acids, both of which are obtained from the host (Luginbuehl *et al.*, 2017). The transfer of these two carbon compounds is discussed in the next chapters.

1.2.2.2.1 Mono-, Di- and Polysaccharides

For carbon translocation in the form of sugars, transporter proteins are found in the fungal membrane that import monosaccharides, but not disaccharides into the fungal cytosol (Solaiman and Saito, 1997). The MONOSACCHARIDE TRANSPORTER (MST), *Gp*MST1 from *Geosiphon pyriformis*, has substrate transport preferences in the following order: glucose > mannose > galactose > fructose, as revealed by sugar uptake experiments after expression in yeast (Schüssler *et al.*, 2006; Schüßler *et al.*, 2007). Similarly, *Ri*MST2 from *R. irregularis* showed the highest activity with glucose, but it can also transport xylose, mannose and fructose. *Ri*MST2 is mainly expressed in the arbuscules but also in intercellular hyphae and its expression is strongly induced by the cell wall sugar xylose. In addition, the ERM of *R. irregularis* growing out of *D. carota* roots was shown to actively take up ^{14}C-glucose and ^{14}C-xylose via H^{+} co-transport (Helber *et al.*, 2011). In another experiment, *R. irregularis* germinating spores were able to take up ^{14}C-glucose from the medium as well (Bücking *et al.*, 2008).

R. irregularis expresses two additional *MONOSACCHARIDE TRANSPORTER* genes in the ERM and spores: *RiMST5* and *RiMST6*. Both have been functionally characterized as glucose importers after expression in yeast (Ait Lahmidi *et al.*, 2016). Therefore, expression patterns and substrate properties of *RiMST2*, *RiMST5* and *RiMST6* show that hexose uptake is not restricted to the arbuscules, but can also happen from the rhizosphere.

Glucose, once taken up by the fungus, can be converted into glycogen by GLYCOGEN SYNTHASE in the IRM and ERM of *R. irregularis* (Bago *et al.*, 2003) or used for synthesis of trehalose via trehalose-6-phosphate (Ocón *et al.*, 2007). Under oxidative stress and heat stress, trehalose synthesis is furthermore induced to enhance stress recovery (Lenoir *et al.*, 2016).

Labeling of leek roots colonized with *Glomus etunicatum* using $^{13}C_1$-glucose showed that glycogen and trehalose can be synthesized from host-derived carbon in the IRM. Furthermore, in germinating spores of *G. etunicatum*, mannitol synthesis was observed to occur at even higher rates than trehalose synthesis (Shachar-Hill *et al.*, 1995).

Glycogen can also be used for long-distance transport to the ERM where it can be hydrolyzed to glucose for the synthesis of other carbohydrates or stored (Bago *et al.*, 2003). Glucose is used for trehalose synthesis, which mainly takes place in the ERM via acetate that enters the glyoxylate cycle and subsequently gluconeogenesis. This was revealed by expression of the glyoxylate cycle genes *ISOCITRATE LYASE* (*ICL*) and *MALATE SYNTHASE* (*MS*) as well as positional labeling of carbon atoms in trehalose with $^{13}C_2$-acetate in ERM and germinating spores of *R. irregularis* (Bago *et al.*, 1999; Bago *et al.*, 2000; Lammers *et al.*, 2001).

Isotopic labeling of colonized roots with $^{13}C_1$-glucose followed by NMR spectroscopy in isolated ERM suggests that in addition to trehalose, chitin synthesis takes places in the ERM (Bago *et al.*, 2003). The precursor for chitin synthesis is glucose, which can be obtained from trehalose or hydrolyzed glycogen. Glucose is converted into N-acetylglucosamine (GlcNAc) that polymerizes to yield the long-chain polymer chitin, catalyzed by CHITIN SYNTHASE (Flores and Gancedo, 2015). Chitin is a major component of the cell wall of AMF and upon arbuscule collapse, the GlcNAc monomers are taken up and recycled via the fungal transporter *Ri*NGT (Kobae *et al.*, 2015).

If not incorporated into glycogen or chitin (after conversion into GlcNAc), glucose can be broken down via glycolysis to yield ATP and the reducing agent NADH as well as pyruvate that is converted into acetyl-CoA by pyruvate dehydrogenase. Acetyl-CoA can be employed for fatty acid elongation (see 1.2.4.2.2).

On the plant side, glucose and sucrose are hypothesized to be exported into the PAS via PAM-localized transporters. The genes belonging to the SWEET family (*SUGARS WILL EVENTUALLY BE EXPORTED TRANSPORTERS*) *StSWEET7a* and *StSWEET12a* from potato show mycorrhiza-induced gene expression (Manck-Götzenberger and Requena, 2016). Transporters of the SWEET family were characterized to export and import carbohydrates from the extracellular space and cellular compartments in Arabidopsis and rice, and are also the targets of manipulation by pathogens to increase sugar efflux from the infected cells (Chen *et al.*, 2010). *StSWEET7a* and *StSWEET12a* promoters are induced in arbuscocytes, even though the *StSWEET7a* promoter is also active in cortex cells of non-inoculated roots. There are four clades of SWEET proteins and *St*SWEET7a belongs to clade II of hexose transporters and *St*SWEET12a to clade III of sucrose transporters. Therefore, these two candidate transporters likely function in sucrose and glucose transport across the PAM and the PM in arbuscule-containing cells (Manck-Götzenberger and Requena, 2016).

The *SUCROSE TRANSPORTER* genes 1 and 4 from *M. truncatula* (*MtSUT1/4*) are induced by low phosphate and AM colonization and the recombinant proteins are active in transport of

sucrose and maltose in yeast, which they transport in a H^+/disaccharide co-transport manner (Doidy *et al.*, 2012). *Mt*SUT1 and *Mt*SUT4 do not transport monosaccharides. Instead, the MONOSACHARIDE TRANSPORTER 1 from *M. truncatula* (*Mt*ST1) was shown to transport glucose and fructose alike, but not sucrose (Harrison, 1996). Thus, plants likely secrete monosaccharides and disaccharides into the PAS.

Plant PAM-localized SUT proteins function directly and indirectly in AM symbiosis. In tomato, *SlSUT2* RNAi-plants had increased arbuscule colonization (Bitterlich *et al.*, 2014), and *Sl*SUT2 interacts with brassinosteroid signalling components. *Sl*SUT2 therefore negatively regulates AM development, either by competing for sucrose in the PAS by re-import into the plant cytoplasm or by regulating the activity of other competitive sucrose importers (Roth and Paszkowski, 2017). Consistent with an indirect signalling function rather than direct transport by *Sl*SUT2, the Medicago *Mt*SUT2 transporter was unable to transport sugars in yeast (Doidy *et al.*, 2012). AM colonization induced the genes *SlSUT1* and *SlSUT4* and root sucrose and fructose were increased, while glucose remained constant. As AM colonization also elevates CO_2 assimilation rates and therefore increases the sink strength of the mycorrhizal root, this is consistent with the idea of increased sucrose transport to the root sink and eventually the fungal interface, while only glucose is taken up by the fungus (Boldt *et al.*, 2011). This as has also been demonstrated by the increased usage of glucose but not sucrose by mycorrhizal onion roots (Solaiman and Saito, 1997).

Therefore, plant apoplastic invertases (*Le*LIN6, *St*InvCD141) and cytoplasmic invertase (*SUCROSE SYNTHASE*; *Mt*SucS1) potentially convert sucrose to fructose and glucose for subsequent re-import by the plant or uptake by the fungus (Baier *et al.*, 2010; Blee and Anderson, 2002; Hohnjec *et al.*, 2003; Manck-Götzenberger and Requena, 2016; Schaarschmidt *et al.*, 2006). Over-expression of different yeast invertases located either to the apoplast, the cytoplasm or the vacuole in Medicago increased hexose-to-sucrose ratios but did not lead to increased mycorrhiza biomass in the roots, indicating that the AM symbiosis operates at optimum hexose-import conditions under normal circumstances. However, inhibitions of root apoplastic invertase or vacuolar invertase in tobacco roots decreased hexose contents and also led to reduction in AM colonization (Schaarschmidt *et al.*, 2007), suggesting that a certain concentration of hexose in the periarbuscular space is required for regular AM colonization.

1.2.2.2.2 Fatty Acids and Lipids

As stated above, pyruvate obtained via glycolysis is converted into acetyl-CoA by pyruvate dehydrogenase. Acetyl-CoA in turn can be used to elongate fatty acids at the ER. In most organisms, acetyl-CoA can additionally serve as primer for fatty acid *de novo* synthesis (see 1.1.2) to provide fatty acids for acyl-lipid synthesis (see 1.1.1). AMF are a remarkable exception as they lack the genes encoding type-I *FAS* (Wewer *et al.*, 2014). It is therefore likely that they do not synthesize fatty acids *de novo* and rely on their hosts for fatty acid supply. This was demonstrated

by labeling experiments on split-compartment petri dishes with carrot roots and *R. irregularis*. 16:0 and 16:1 fatty acids (typical products of fungal *de novo* fatty acid synthesis and desaturation) were only labeled with ^{14}C-acetate when it was supplied to the root compartment containing IRM and not the ERM compartment. Nevertheless, *R. irregularis* ERM was still capable of elongating fatty acid with the supplied ^{14}C-acetate (Trepanier *et al.*, 2005). Previously, in *R. irregularis-D. carota* split-petri dish experiments, fungal neutral lipids and mycorrhiza-signature fatty acids could be labeled with $^{13}C_1$-glucose only when the label was supplied to the root compartment, which shows that the ERM was unable to synthesize fatty acids from glucose (Bago *et al.*, 2002; Pfeffer *et al.*, 1999).

Lipid transfer was visualized 1d after labeling of symbiotic carrot roots with ^{13}C-glucose by measuring an ^{13}C enrichment in fungal fatty acids in ERM which increased to >2% of total carbon after 7 days (Olsson *et al.*, 2005). Similar to monosaccharide-transfer, the translocation of lipids also depends on the nutritional status of the host root and consequently, symbiotic carrot roots that were supplemented with high amount of nitrogen did transfer less lipids to the fungal IRM and ERM. This was visualized by decreased ^{13}C content in mycorrhiza-signature fatty acids after labeling of ^{13}C-glucose to the root compartment in a split-petri dish system (Olsson *et al.*, 2005).

Two recent studies have expanded the knowledge on transfer of fatty acids from host to AMF. In *M. truncatula*, expression of the *UcFatB* thioesterase that preferably hydrolyzes 12:0-ACP led to accumulation of 12:0 in the spores of the connected *R. irregularis*. Besides, the radiolabel from ^{14}C-acetate but not ^{14}C-sucrose, which was applied to the host roots, failed to accumulate in TAG from spores feeding on *M. truncatula acetyl-CoA synthase* (*acs*) mutant. This proved that sugars are still transferred, but not fatty acids as the *acs* mutant is unable to synthesize fatty acids from exogenously applied ^{14}C-acetate (Luginbuehl *et al.*, 2017). In a second approach, ^{13}C-glucose was applied to *L. japonicus str*, *ram2* and *dis* mutant roots supporting the growth of *R. irregularis*. By comparing the fatty acid isotopolog ^{13}C-labeling patterns with WT roots, it could be demonstrated that a mutation in either of these genes led to uncoupling of ^{13}C-patterns in mycorrhiza fatty acids (Keymer *et al.*, 2017).

1.2.3 Lipid Metabolism during AMF Symbiosis

Despite their apparent disability to synthesize fatty acids *de novo*, AMF fungi contain a variety of lipids. The abundance and distribution of lipids and fatty acids in AMF depend on the mycorrhizal structure (interradical hyphae, vesicles, extraradical hyphae or spores), the environmental stimulus (e. g. stress or nutrient availability), the host response and nutritional status as well as the fungal strain. For example, AMF belonging to the Gigasporaceae do not form interradical vesicles and therefore do accumulate less lipids than Glomeraceae (Dalpé *et al.*, 2012).

1.2.3.1 Distribution and Changes of Lipids in AMF

In *R. irregularis* extraradical mycelium (hyphea and spores), the most abundant lipid by far is TAG, followed by DAG and phospholipids, free sterols and sterol esters. Only minor amounts of sterol glucosides and acylated sterol glucosides as well as glycosylceramides are present (Wewer *et al.*, 2014). Measurements of lipids in spores of *G. versiforme* showed that 38% of the spore fresh weight consists of TAG (Gaspar *et al.*, 1994). The amount of total lipids based on spore weight in non-germinated spores of *Glomus caledonius* varied between 45.2%—70.0% and was mostly TAG (25% DW) (Beilby and Kidby, 1980). A comparable distribution was found in spores of *R. irregularis* containing 78% TAG and 11% phospholipids (Jabaji-Hare, 1988). In homogenized ERM (hyphae and spores) of *G. mossae*, TAG synthesis rates increased with age of the mycelium as did incorporation of ^{14}C-palmitic acid into palmitoyl-CoA (Gaspar *et al.*, 2001). In another experiment, *R. irregularis* and *G. margarita* germ tubes and the ERM growing from symbiotic carrot roots showed high abundance of lipid droplets (syn. oleosomes, lipid globules). AMF lipid droplets consist of a phospholipid monolayer interspersed with protein and are filled with TAG and sterol esters as storage lipid. The highest density was observed for *G. margarita* hyphae, where 47.2% of the hyphal volume was occupied by lipid droplets, which was 23.9% for *R. irregularis* hyphae. It was estimated that in *R. irregularis*, 0.26 µg TAG are moved per hour to the ERM. Thus, throughout the entire symbiotic growth stage of *R. irregularis*, massive amounts of TAG, synthesized from host-derived fatty acids, are moved from the IRM to the ERM to accumulate in spores (Figure 3). Even though the general direction is from IRM to ERM, some circulation in the opposite direction was also observed (Bago *et al.*, 2002a; Bago *et al.*, 2002b).

Upon spore germination, the relative proportion of neutral lipids decreased while phospholipids increased, indicative of TAG hydrolysis and membrane lipid synthesis in the germ tube (Beilby and Kidby, 1980). In *G. versiforme* spores, TAG content decreased by four-fold ten days post germination (Gaspar *et al.*, 1994). TAG hydrolysis in germinating spores was shown to be catalyzed by a fungal lipase in *G. versiforme* (Gaspar *et al.*, 1997), producing DAGs, MAGs and free fatty acids (Gaspar *et al.*, 2001). In addition to providing energy and a glycerol-backbone for membrane lipid synthesis, TAG hydrolysis in germinating spores serves to provide acetyl-CoA that enters the glyoxylate cycle to yield succinate which is fed into gluconeogenesis for synthesis of hexose that is used to synthesize chitin and trehalose (see 1.2.2.2.1). The metabolic activity of germinating spores from *R. irregularis* was also demonstrated by rapid ^{14}C-acetate uptake from the growth medium (Bücking *et al.*, 2008). When supplied with ^{13}C$_2$-acetate, trehalose in germinating spores of *R. irregularis* was shown to be rapidly labeled (79.1% above natural abundance in carbon position 6), which is consistent with lipolysis of TAG and usage of acetyl-CoA in gluconeogenesis upon spore germination (Bago *et al.*, 1999). Consistently, a gene coding for *Acyl-CoA DEHYDROGENASE*, involved in β-oxidation of fatty acids, was shown to be expressed in

R. irregularis germ tubes and the ERM at later stages after sporulation. Lipid droplets in *R. irregularis* and *G. margarita* accumulated more frequently in hyphae in close distance to germinating spores or symbiotic host roots, indicating that TAG hydrolysis increases towards the growing hyphal tip (Bago *et al.*, 2002a).

Separation of hyphae and spores of ERM from *R. irregularis* and *Glomus calroideum* and subsequent lipid quantification showed that 20% of spore biomass consists of neutral lipids. In two-month old spores of *G. calroideum*, neutral lipids were 53-times more abundant than phospholipids, while this increased to 146 in three-month-old *R. irregularis* spores. In contrast, extraradical hyphae contained more phospholipids than spores, but here also neutral lipids were more abundant. Even though this accounted only for a 24-times increase in *G. claroideum* hyphae and a 5.8-times in *R. irregularis* hyphae, respectively (Olsson and Johansen, 2000). This exemplifies that even though TAG accumulates in external spores, it is also synthesized in the interradical hyphae. This is in agreement with increased neutral and phospholipids with increased root colonization rate (Gaspar *et al.*, 1997; Stumpe *et al.*, 2005).

In interradical vesicles of *R. irregularis*, lipids make up 58.2% of IRM dry mass and the proportion of neutral lipids (putatively predominantly TAG) is 16.77% (Jabaji-Hare *et al.*, 1984). The amount of TAG in vesicles of *Glomus versiforme* and *Glomus vesiculiferum* was 65% and 83% of total lipids, respectively, while phospholipids made up only 2% and 7%, respectively (Jabaji-Hare, 1988).

The main phospholipid in *R. irregularis* ERM (hyphae and spores) is phosphatidylcholine that accounts to ~58 mol% of total phospholipids. Phosphatidylethanolamine (20 mol%), phosphatidylinositol (13 mol%), phosphatidic acid (0.7 mol%) and phosphatidylserine (7.3 mol%) are also present while the plastidial phospholipid phosphatidylglycerol is absent. During symbiotic growth, the fatty acid composition of PC, PE, PI and PS is altered. Di-16:1 and 24:1 containing phospholipids are not found in root tissue colonized by *R. irregularis* but in ERM and these fatty acids are still found in TAG from colonized roots. This phospholipid acyl editing by the fungus might, on the one hand, provide a mechanism for AMF to avoid host-induced defense reactions when growing symbiotically, while on the other hand these fatty acids provide protection in the asymbiotic ERM membranes against unfavorable environmental conditions (Wewer *et al.*, 2014).

Sterol lipids compromise a major constituent of membranes of the fungal hyphae. In *R. irregularis* ERM, free sterols accumulate to 64.3 mol%, while sterol esters make up 33.5 mol% and sterol glucosides and acylated sterol glucosides are only minor components that account for 1.2 mol% and 0.8 mol%, respectively (Wewer *et al.*, 2014). In contrast to ectomycorrhiza fungi, AMF do not contain ergosterol, which might attribute to their recognition as being non-pathogenic by the host (Klemptner *et al.*, 2014). The major sterol lipids in AMF are 4-demethylsterols synthesized *de novo* from acetate via mevalonate (Figure 3) (Fontaine *et al.*, 2001a). The most

abundant sterols are 24-methylcholesterol, 24-ethylcholesterols and to a lesser extent lanosterol, 24-ethylcholesta-5,22-dien-3β-ol and cholesterol (Campagnac *et al.*, 2009; Fontaine *et al.*, 2001b; Wewer *et al.*, 2014).

AMF can populate even polluted or saline soils. The adjustment of their lipid metabolism comprises one mechanism to grow under these adverse conditions. *R. irregularis* induce TAG hydrolysis to provide energy and a glycerol-backbone for membrane lipid (mainly PC) regeneration and stress-induced lipid signalling (via PA) in the presence of the polycyclic aromatic hydrocarbon (PAH), benzo[a]pyrene (Calonne *et al.*, 2014; Debiane *et al.*, 2011).

1.2.3.2 Fatty Acids of AMF

Mycorrhiza fungi contain a multitude of unsaturated fatty acids. The major fatty acids in AMF are C16 and C18 (Bentivenga and Morton, 1996). The most abundant one, C16:1n-5 (syn. *cis*-palmitvaccenic acid; C16:1ω5) is found almost exclusively in AMF and can therefore be employed as lipid biomarker (Dalpé *et al.*, 2012). It accounts for 46.5—78 mol% of total fatty acids in spores of AMF of the order Glomales including the families Acaulosporaceae, Glomaceae and Gigasporaceae, albeit some Glomaceae (*G. leptotichum*, *G. occultum*) and *Gigaspora spp.* from the Gigasporacea (*G. albida*, *G. gigantea, G. margarita, G. rosea*) contain none only low amounts (<1% total FA). In addition to C16:1ω5, *R. irregularis*, *G. claroideum* and *G. roseae* spores and hyphae contain 0.2—3.3 mol% of C16:1n-7 (syn. palmitoleic acid; C16:1Δ9) and the Glomaceae that do not accumulate C16:1ω5 (*G. leptotichum*, *G. occultum*) contain considerable amounts (11—55%) of palmitoleic acid instead. In addition, in the *Gigaspora spp.* spores, where C16:1ω5 is low or absent, higher amounts (38—48%) of C18:1n-9 (syn. *cis*-oleic acid; C18:1Δ9) and 8—15% C20:1n-9 (syn. *cis*-gondoic acid; C20:1ω9) are found (Graham *et al.*, 1995). Oleic acid is present in lower amounts (~1—5%) in spores of *R. irregualris* and other Glomaceae as well, while gondoic acid was reported as being absent (Graham *et al.*, 1995), or comprising only minute amounts (0.06 mol%) in *R. irregularis* spores (Trepanier *et al.*, 2005). Palmitoleic acid, oleic acid, and gondoic acid are present in plant roots also in the absence of a mycorrhiza fungus (Olsson and Johansen, 2000; Trepanier *et al.*, 2005).

AMF additionally contain C20, C22 and C24 fatty acids. Of these, the predominant one is 20:3 that can be detected in *R. irregularis* extraradical hyphae, spores and IRM where it comprises 0.2—1.5 mol% of total fatty acids (Olsson and Johansen, 2000; Trepanier *et al.*, 2005).

1.2.3.3 Changes in Plant Lipids and Fatty Acids due to AMF

The fatty acids and lipids that are present in AMF extraradical tissues (see 1.2.3.1 and 1.2.3.2) can also be detected in colonized roots, albeit mostly in lower amounts. Therefore, colonized roots contain a mixture of plant lipids and lipids found in inter and intraradically growing mycelium. Various studies reported the accumulation of mycorrhiza-signature fatty acids

(mostly hexadecenoic acid) neutral storage lipids (mostly TAG) and 24-methylcholesterol and 24-ethylcholesterol in colonized roots (Cooper and Lösel, 1978; Dalpé *et al.*, 2012; Gaspar, L. *et al.*, 1997; Schliemann *et al.*, 2008; Stumpe *et al.*, 2005; Trepanier *et al.*, 2005; Wewer *et al.*, 2014). As described above, AMF contain various fatty acids and lipids that are also present in non-colonized plant roots (e. g. oleic acid) and are therefore indistinguishable in lipid measurements of colonized roots.

In *R. irregularis*-colonized roots of Medicago and barley, the amount of jasmonic acid (JA) is elevated. JA levels increased even more after longer colonization periods and JA-biosynthesis genes were expressed in arbuscule-containing cells. JA is typically involved in biotic stress interactions, and elevated JA levels therefore might contribute to enhanced stress tolerance of mycorrhizal plants (Hause *et al.*, 2002; Stumpe *et al.*, 2005).

Plants react to phosphate-limiting conditions by replacing phospholipids from their extraplastidial membranes with galactolipids, mainly DGDG, and by replacing PG in plastids with SQDG (Tjellström *et al.*, 2008). By increasing phosphate supply in shoots and roots, mycorrhiza-colonization can reverse this effect and therefore has an indirect effect on plant lipid content by changing the root lipid composition in a way that it resembles the one in phosphate-supplied plants (Bravo *et al.*, 2017; Wewer *et al.*, 2014).

In well-colonized AM symbiotic roots, certain apocarotenoids accumulate that are apparent by orange-yellow coloring of mycorrhized roots. Apocarotenoids are derived from C40 carotenoids via cleavage catalyzed by *CAROTENOID CLEAVAGE DIOXYGENASES* (*CCD*) (Siebers *et al.*, 2016). Two apocarotenoids, the C13 cyclohexenone (α-Ionol-glycoside) and the C14 polyene (mycorradicin) are synthesized by the mycorrhiza-specific CCD1a enzyme and therefore accumulate in the cytoplasm of arbuscule-containing cells at later stages of the symbiosis (Fester, 2002; López-Ráez *et al.*, 2015). As strigolactones are synthesized from the same precursor, the induction of CCD1a might fulfill the purpose of channeling isoprenoid synthesis towards α-Ionol-glycoside and mycorradicin instead of strigolactones in order to prevent over-promotion of AMF and induce the arbuscule-degeneration-generation cycle (Walter 2013).

1.3 Research Objectives and Approach

The focus of this project is the analysis of the fatty acid transfer from root cortex cells of *L. japonicus* to the fatty acid auxotrophic arbuscular mycorrhiza fungus *R. irregularis*. The genomes of arbuscular mycorrhiza fungi are devoid of type-I cytosolic fatty acid synthase genes. Therefore, *R. irregularis* cannot synthesize fatty acids *de novo* from acetyl-CoA obtained by glycolysis, as other heterotrophic fungi do. To investigate the symbiotic lipid transfer, this project took advantage of the expanding knowledge on the co-evolution of host and fungal genomes as the AMF-host genomes contain genes specifically evolved for AMF-symbiosis. One of these genes codes for an ortholog of the *acyl-ACP Thioesterase B* (*FatB*) from Arabidopsis, called *FatM*. Acyl-ACP

Thioesterases catalyze the termination of fatty acid *de novo* synthesis by release of free fatty acids. Five main approaches were developed to study the function of *FatM* fom *L. japonicus* for mycorrhizal fatty acid supply and to investigate fatty acid and lipid metabolism in *R. irregularis*. First, reverse genetics with two independent *FatM* transposon insertional mutants to study the effect on *R. irregularis* root colonization and specifically lipid accumulation in the fungus. Second, quantification and identification of lipids and lipid intermediates in *R. irregerularis* extraradical and intraradical growth. Third, stable ^{13}C-isotope labeling of fatty acids during symbiosis in *fatm* and WT. Fourth, biochemical analysis of the recombinant FatM enzyme *in vitro*. Fifth, functional characterization of candidate desaturase genes from *R. irregularis* by heterologous expression in yeast and *N. benthamiana*.

The outcome of these experiments was intended to provide knowledge about the question whether the fungus receives fatty acids from the host and, if so, how it metabolizes and stores these fatty acids. It was furthermore intended to investigate how a defect in a host gene involved in *de novo* fatty acid synthesis might affect the fungal morphology or metabolic capacity. Another aim was to elucidate the nature of the transferred lipid and to provide an estimation on the importance of lipid supply in relation to the supply of carbon in the form of carbohydrates.

2 Materials and Methods

2.1 Materials

2.1.1 Equipment

Autoclave	Tuttnauer Systec, Kirchseeon-Buch (D)
Balance 770	Kern, Balingen-Frommern (D)
Balance PG503-S Delta Range	Mettler Toledo, Gießen (D)
BalancexS205 DualRange	Mettler Toledo, Gießen (D)
Binocular microscope SZX16	Olympus, Hamburg (D)
Büchner funnel (porcelain, 800 mL volume, 125mm ID)	Hartenstein Laborbedarf, Würzburg (D)
Rubber seal GUKO	Hartenstein Laborbedarf, Würzburg (D)
Block heater SBH130D/3	Stuart, Bibby Scientific, Staffordshire (USA)
Camera DP7Z for microscope	Olympus, Hamburg (D)
Centrifuge 5810 R	Eppendorf, Hamburg (D)
Centrifuge 5417R	Eppendorf, Hamburg (D)
Centrifuge 5430	Eppendorf, Hamburg (DE)
Centrifuge Sorvall RC 5C PLUS	Thermo Fisher Scientific, Braunschweig (D)
Dual fluorescent protein flashlight	NightSea, Bedford (US)
Gel caster, Mighty small II GE	Healthcare Europe, Freiburg (D)
Growing cabinet, Rumed	Rubarth Apparate GmbH (D)
Heating block	Bioer, Hangzhow (CHN)
Homogeniser Precellys®24	PeQlab, Erlangen (D)
Homogeniser HO 4/A	Edmund Bühler, Hechingen (D)
Horizontal electrophoresis chamber	Cti, Idstein (D)
Incubator, Kelvitron®	Thermo Scientific Heraeus®, Waltham (USA)
Incubation shaker, Multitron 28570	INFORS, Einsbach (D)
Light microscope BH-2	Olympus, Hamburg (D)
Magnetic stirrer MR30001	Heidolph Instruments, Schwabach (D)
Micro pulser electroporator	BioRad Laboratories, München (D)
Mini vertical Gel Electrophoresis unit	Amersham Bioscience
Mixer mill MM400	Retsch, Haan (D)
Multiple Gel Caster	Amersham Bioscience
PowerPac Basic electrophoresis power supply	Bio-Rad Laboratories, München (D)
pH meter inoLab pH Level 1	WTW, Weilheim (D)
Photometer, Specord 205	Analytik Jena, Jena (D)
Phytochamber SIMATiC OP17	York International, York (USA)
Reverse-Phase Liquid Chromatography Column Eurosphere-II RP8	Knauer
Reverse-Phase Liquid Chromatography Column Nucleoshell Bluebird RP18	Macherey-Nagel, Düren (D)
Running chamber for gel electrophoresis	Cti, Idstein (D)
Sample concentrator for organic solvents	Techne (Bibby Scientific), Stone (UK)
Semi-dry transfer cell Trans-BLOT SD	Bio-Rad Laboratories, München (D)
Spectrophotometer Nanodrop 1000	PeQlab, Erlangen (D)
SpeedVac® Vacuum Concentrator SPD121 P	Thermo Fisher Scientific, Braunschweig (D)
Sterile bench model 1.8	Holten Lamin Air, Allerød (DK)
Thermocycler TPersonel 48	Biometra, Göttingen (D)

Thermocycler TProfessional 96	Biometra, Göttingen (D)
Ultracentrifuge Optima L 90K equipped with swing-out rotor SW 28	Beckman Coulter, Krefeld (D)
UV-transilluminator DP-001 T1A	Vilber Lourmat, Eberhardzell (D)
6530 Accurate-mass quadrupole time-of-flight (Q-TOF) LC/MS	Agilent, Böblingen (D)
7890 Gas chromatograph (GC) with flame ionization detector (FID)	Agilent, Böblingen (D)
7890 Gas chromatograph (GC) with mass spectrometer (MS)	Agilent, Böblingen (D)
Tri-Carb Liquid Scintillation Counter 2900 TR	Packard BioScience, Meriden (USA)

2.1.2 Consumables

Blotting membrane, nitrocellulose (0.45 µm)	GE Healthcare
Blotting paper, pure cellulose	Sigma-Aldrich, Taufkirchen (D)
Centrifuge tubes, polypropylene (PP) 1.5 mL, 2 mL	Sarstedt, Nümbrecht (D)
Centrifuge tubes, polypropylene (PP) 15 mL, 50 mL	Greiner bio-One, Frickenhausen (D)
Coverslips, 24 mmx 60 mm	Marienfeld, Lauda Königshofen (D)
DEAE-cellulose (pre-swollen)	Whatman
	GE Healthcare
Dialysis membrane Spectra/Pore®	Spectrum® Laboratories/VWR, Darmstadt (D)
dNTP-Mix (10 mM)	DNA Cloning Service (D)
Electroporation Cuvettes (1mm gap)	Bio-Budget, Krefeld (D)
Round Filter paper Ø 150 mm (Ref. 10334512)	Schleicher & Schüll
Glass Pasteur pipettes	Brand, Wertheim (D)
Glass tubes with screw cap, GL 14tThread, 12x100 mm, 6 mL (DURAN®)	DWK Life Science, Mainz (D)
Glass tubes with screw cap, 24-400 thread, 28x95 mm, 40 mL (VOA-Vials)	Schmidling Labor + Service SA, Neuheim (CH)
Glass vials for autosampler	Agilent, Böblingen (D)
Glass beads, acid-washed (≤106 µm)	Sigma-Aldrich, Taufkirchen (D)
Inlets for autosampler vials (Conical and flat-bottom)	Agilent, Böblingen (D)
Liquid Scintillation vial (Polyethylene)	PerkinElmer, Solingen (D)
Merck™ MF-Millipore Mixed Cellulose Ester Membranes (0.025µm Pore Size)	Fisher Scientific, Schwerte (D)
Microliter pipette tips type 3 series 1700	Labomedic, Bonn (D)
Microscope slides, 76x 26x 1 mm	Labomedic, Bonn (D
Miracloth filtration material (22—25 µm)	Merck, Darmstadt (D)
PCR tubes (BRAND® 781332), Polypropylen	
Petri dishes (polystyrene) 35x 10 mm	Greiner bio-One, Frickenhausen (D)
Petri dishes (polystyrene) 94x 16 mm	Greiner bio-One, Frickenhausen (D)
Petri dishes (polystyrene) 145x 20 mm	Greiner bio-One, Frickenhausen (D)
PolyPrep® chromatography column (10 mL reservoir)	Bio-Rad Laboratories, München (D)
Pots for plant cultivation, (10 cm h, 7.5 cm ⌀)	Pöppelmann, Lohne (D)
Salmon Sperm DNA	Sigma-Aldrich, Taufkirchen (D)
Silica sand, grain size 1.4 – 2.3 mm	Quarzwerke Witterschlick GmbH, Alfter (D)
Soil, type „Einheitserde Classic"	Klemens Rolfs Gärter Einkauf, Siegburg (D)
SPE columns, type Strata® Silica SI-1 (55 µm, 70 Å), 100 mg / 1 mL	Phenomenex, Aschaffenburg (D)
SPE columns, type Strata® Silica SI-1 (55 µm, 70 Å), 500 mg / 6 mL	Phenomenex, Aschaffenburg (D)

Sterile filters, 0.2 µm pore size   Schleicher und Schuell, Dassel (D)
PTFE (Teflon) septa for GL 14 screw caps   Schmidlin, Neuheim (CH)
Trays for plant cultivation   Pöppelmann, Lohne (D)

2.1.3 Chemicals

Acetic acid   AppliChem, Darmstadt (D)
Acetone   Prolabo VWR, Darmstadt (D)
Acetonitrile   Roth, Karlsruhe (D)
Acrylamide   Roth, Karlsruhe (D)
Agarose   PeQlab, Erlangen (D)
Ammonium acetate   Sigma-Aldrich, Taufkirchen (D)
Ammonium sulfate   Sigma-Aldrich, Taufkirchen (D)
Ammonium molybdate heptahydrate   Sigma-Aldrich, Taufkirchen (D
Ammoniumpersulfate (APS)   AppliChem, Darmstadt (D)
Bacto agar   Duchefa Biochemie, Haarlem (NL)
Bacto peptone   Duchefa Biochemie, Haarlem (NL
Barium hydroxide   Riedel-de Haën (Honeywell),
                                                         Seelze (D)
Boric acid   Grüssing, Filsum (D)
Bovine Serum Albumin (BSA), fatty acid free   Sigma-Aldrich, Taufkirchen (D)
Bovine Serum Albumin (BSA), fraction V   Sigma-Aldrich, Taufkirchen (D)
Cadmium carbonate   Sigma-Aldrich, Taufkirchen (D)
Calcium chloride   Merck, Darmstadt (D)
Chloroform   Merck, Darmstadt (D)
Coomassie R250   AppliChem, Darmstadt (D)
Diethylether   Prolabo VWR, Darmstadt (D)
Dimethyldisulfide (DMDS)   Sigma-Aldrich, Taufkirchen (D)
Dipotassiumhydrogenphosphate   AppliChem, Darmstadt (D)
Ethanol 99%, technical grade with 1% MEK   Hofmann
Ethanol, p.A.   Merck, Darmstadt (D)
Ethidium bromide   Serva, Heidelberg (D)
EDTA-Na$_2$ Sigma-Aldrich, Taufkirchen (D)
Formaldehyde   AppliChem, Darmstadt (D)
Formic Acid   VWR, Darmstadt (D)
Gelrite   Duchefa Biochemie, Haarlem (NL)
Glucose   Formedium, Norfolk (UK)
Glycerol   AppliChem, Darmstadt (D)
Glycine   AppliChem, Darmstadt (D)
Hexane   Merck, Darmstadt (D)
Ink (dark blue)   Pelican, supplied by Dr. Caroline
                                                         Gutjahr
Isopropyl ß-D-1-thiogalactopyranoside (IPTG)   Formedium, Norfolk (UK)
Iodine   AppliChem, Darmstadt (D)
Iron-Ethylenediaminetetraacetic acid   Sigma-Aldrich, Taufkirchen (D)
(Fe-EDTA)
Isopropanol (2-propanol)   AppliChem, Darmstadt (D)
Lithium acetate   AppliChem, Darmstadt (D)
Magnesium chloride   AppliChem, Darmstadt (D)
Magnesium sulfate   Duchefa Biochemie, Haarlem (NL)
Malachite green, oxalate salt   Acros Organics, Geel (BEL)
β-Mercaptoethanol   Sigma-Aldrich, Taufkirchen (D)
Methanol   J.T. Baker, Phillipsburg (USA)

Methanolic hydrochloric acid (3N)	Sigma-Aldrich, Taufkirchen (D)
Molybdenumtrioxide ammoniumtetrahydrate	Sigma-Aldrich, Taufkirchen (D)
Sodiumthiosulfate	Sigma-Aldrich, Taufkirchen (D)
N-methyl-N-(trimethylsilyl)-trifluoroacetamide (MSTFA)	AppliChem, Darmstadt (D)
3-(N-morpholino) propanesulfonic acid (MOPS)	AppliChem, Darmstadt (D)
Peptone	Formedium, Norfolk (UK)
Polyethylenglycerol (PEG) 4000	Roth, Karlsruhe (D)
Phosphoric acid	AppliChem, Darmstadt (D)
Piperazine-N,N′-bis(2-ethanesulfonic acid (PIPES)	AppliChem, Darmstadt (D)
Potassium chloride	Merck, Darmstadt (D)
Potassium dihydrogenphosphate	Merck, Darmstadt (D)
Potassium hydroxide	Merck, Darmstadt (D)
Potassium nitrate	Grüssing, Filsum (D)
Pyridine	AppliChem, Darmstadt (D)
Skimmed-milk powder, blotting-grade	Roth, Karlsruhe (D)
Sodium chloride	Duchefa Biochemie, Haarlem (NL)
Sodium citrate	AppliChem, Darmstadt (D)
Sodium dodecyl sulfate (SDS)	AppliChem, Darmstadt (D)
Sodium hypochlorite	Roth, Karlsruhe (D)
Sorbitol	Duchefa Biochemie, Haarlem (NL)
Sucrose	Duchefa Biochemie, Haarlem (NL)
Talcum	Flora Apotheke, Bonn (D)
Tetramethylethylenediamine (TEMED)	Bio-Rad Laboratories, München (D)
Trichloracetic acid (TCA)	Roth, Karlsruhe (D)
Toluene	Prolabo VWR, Darmstadt (D)
Tritonx-100	Sigma-Aldrich, Taufkirchen (D)
Tricine	Sigma-Aldrich, Taufkirchen (D)
Tris-(hydroxymethyl)-aminomethane (Tris)	Duchefa Biochemie, Haarlem (NL)
Tween-20	Sigma-Aldrich, Taufkirchen (D)
Tryptone	AppliChem, Darmstadt (D)
Ultima Gold Scintillation Cocktail	PerkinElmer, Solingen (D)
Wheat germ agglutinin (WGA) alexa fluor 488	Life Technologies (Invitrogen),
Yeast Extract	Duchefa Biochemie, Haarlem (NL)
Yeast Nitrogen Base (YNB)	Formedium, Norfolk (UK)
$^{13}C_2$-Sodium Acetate	Sigma-Aldrich, Taufkirchen (D)
$^{13}C_6$-Glucose	Sigma-Aldrich, Taufkirchen (D)
$^{13}C_4$-Palmitic acid	Sigma-Aldrich, Taufkirchen (D)

2.1.4 Antibiotics

Ampicillin	Duchefa Biochemie, Haarlem (NL)
Carbenicillin	Duchefa Biochemie, Haarlem (NL)
Gentamycin	Duchefa Biochemie, Haarlem (NL)
Kanamycin	Duchefa Biochemie, Haarlem (NL)
Rifampicin	Duchefa Biochemie, Haarlem (NL)
Spectinomycin	Duchefa Biochemie, Haarlem (NL)
Streptomycin	Duchefa Biochemie, Haarlem (NL)

2.1.5 Commercial Kits and Enzymes

CloneJET PCR Cloning Kit	Thermo Fi. Sci.,, Karlsruhe (D)
Color Prestained Protein Standard, Broad Range (11–245 kDa)	NEB, Frankfurt a. M (D)
DCS DNA Polymerase (10 U/µL)	DNA Cloning Service, Hamburg (D)

DNaseI (A3778)	AppliChem, Darmstadt (D)
Endoproteinase Asp-N Sequencing Grade (2µg 50µL⁻¹)	Promega
GeneRuler 1kb DNA ladder	Thermo Fi. Sci., Braunschweig (D)
First Strand cDNA Synthesis Kit	Thermo Fi. Sci., Karlsruhe (D)
HisDetector Nickel-HRP Conjugate	Kirkegaard & Perry Laboratories, Wedel (D)
Ni-NTA Agarose	Qiagen, Hilden (D)
NucleoSpin® Gel and PCR Clean-up Kit	Macherey-Nagel, Düren (D)
NucleoSpin® Plasmid DNA Miniprep Kit	Macherey-Nagel, Düren (D)
NucleoSpin® RNA Plant Kit	Macherey-Nagel, Düren (D)
Plant Total RNA Mini Kit	DNA Cloning Service, Hamburg (D)
Restriction endonucleases and buffers	NEB, Frankfurt a. M (D)
SuperSignal West Pico Chemiluminescence Substrate	Thermo Fi. Sci., Braunschweig (D)
T4 DNA Ligase M0202S (400 U/µL)	NEB, Frankfurt a. M (D)
TURBO DNA-*free* Kit	Thermo Fi. Sci., Karlsruhe (D)
Q5® High-Fidelity DNA polymerase (M0491)	NEB, Frankfurt a. M (D)
Quick Start™ Bradford Protein Assay	Bio-Rad Laboratories, München (D)

2.1.6 Internal Standards for Lipid Quantification and Identification

Pentadecanoic acid (15:0)	Sigma-Aldrich, Taufkirchen (D)
Arachidonic acid (20:4$^{\Delta 5,8,11,14cis}$)	Larodan, Malmö (S)
Cholesterol	Sigma-Aldrich, Taufkirchen (D)
Cholestanol	Sigma-Aldrich, Taufkirchen (D)
Stigmasterol	Sigma-Aldrich, Taufkirchen (D)
Stigmastanol	Sigma-Aldrich, Taufkirchen (D)
di14:0-PC	Avanti Polar Lipids, Alabaster AL (USA)
di20:0-PC	Avanti Polar Lipids, Alabaster AL (USA)
di14:0-PE	Avanti Polar Lipids, Alabaster AL (USA)
di20:0-PE	Avanti Polar Lipids, Alabaster AL (USA)
di14:0-PG	Avanti Polar Lipids, Alabaster AL (USA)
di20:0-PG	Avanti Polar Lipids, Alabaster AL (USA)
di14:0-PA	Avanti Polar Lipids, Alabaster AL (USA)
di20:0-PA	Avanti Polar Lipids, Alabaster AL (USA)
di14:0-PS	Avanti Polar Lipids, Alabaster AL (USA)
di20:0-PS	Avanti Polar Lipids, Alabaster AL (USA)
PI Mix, from soybean	Larodan, Malmö (S)
MGDG mix	Larodan, Malmö (S)
DGDG mix	Larodan, Malmö (S)
SQDG mix	Larodan, Malmö (S)
Monopentadecanoin (MAG-15:0)	Larodan, Malmö (S)
Monopalmitine (MAG-16:0)	Larodan, Malmö (S)
Monooleoine $^{\Delta 9cis}$ (MAG-18:1)	Larodan, Malmö (S)
Monolinoleine $^{\Delta 9,12cis}$ (MAG-18:2)	Larodan, Malmö (S)
Monolinolenine $^{\Delta 9,12,15cis}$ (MAG-18:3)	Larodan, Malmö (S)
Monoarachidone $^{\Delta 5,8,11,14cis}$ (MAG-20:4)	Larodan, Malmö (S)
di-14:0-DAG	Larodan, Malmö (S)
di-14:1$^{\Delta 9cis}$-DAG	Larodan, Malmö (S)
di-20:0-DAG	Larodan, Malmö (S)
di-20:1$^{\Delta 14cis}$-DAG	Larodan, Malmö (S)
tri-10:0-TAG	Larodan, Malmö (S)
tri-11:1$^{\Delta 10cis}$-TAG	synthesized by Helga Peisker (IMBIO)

tri-17:0-TAG	Larodan, Malmö (S)
tri-17:1-TAG	Larodan, Malmö (S)
tri-20:0-TAG	Larodan, Malmö (S)
tri-22:1$^{\Delta 13cis}$-TAG	Larodan, Malmö (S)
Palmitoyl-CoA (16:0-CoA)	Larodan, Malmö (S)
Heptadecanoyl-CoA (17:0-CoA)	Sigma-Aldrich, Taufkirchen (D)
Heptadecanoyl-CoA (17:0-CoA)	Avanti Polar Lipids, Alabaster AL (USA)
Stearoyl-CoA (18:0-CoA)	Sigma-Aldrich, Taufkirchen (D)
Octadecenoyl-CoA (18:1$^{\Delta 9}$-CoA)	Sigma-Aldrich, Taufkirchen (D)
Linoleoyl-CoA (18:2$^{\Delta 9,12cis}$-CoA)	Sigma-Aldrich, Taufkirchen (D)
Linolenoyl-CoA (18:3$^{\Delta 9,12,15cis}$-CoA)	Sigma-Aldrich, Taufkirchen (D)

2.1.7 Plants, Bacteria and Fungi

L. japonicus wild type, ecotype Gifu	Jens Stougaard, University of Aarhus (DK)
L. japonicus LORE1 retrotransposon insertion mutant (*FatM*-1/G63)—Lotus BASE Plant ID: 30003218 (MG20 Genome v2.5 +LjSGA)	(Malolepszy *et al.*, 2016)
L. japonicus LORE1 retrotransposon insertion mutant (*FatM*-2/D20)—Lotus BASE Plant ID: 30052489 (MG20 Genome v2.5 +LjSGA)	(Malolepszy *et al.*, 2016)
N. benthamiana WT	
A. tumefaciens strain GV3101-pMP90	(Koncz and Schell, 1986)
E. coli ElectroSHOX	Bioline, Luckenwalde (D)
E. coli fadD mutant	(Dörmann *et al.*, 1995)
R. irregularis inoculum with attapuglite clay powder or diatomite as carrier (1 Million spores 100 g^{-1}), corresponding to voucher number DAOM197198, DAOM181602 and MUCL43194	Symplanta GmbH, München (D)
R. irregularis in axenic root culture with *Agrobacterium rhizogenes*-transformed carrot roots	Department of Genetics, Arthur Schüßler, LMU München (D)
S. cerevisiae WT, Genotype: BY4741	EUROSCARF, Johann Wolfgang Goethe Universität, Frankfurt a. M. (D)
S. cerevisiae ole1 mutant (ORF: YGL055W, Acc. No.: Y40963, Strain: TSA506 Genotype: BY4741)	EUROSCARF, Johann Wolfgang Goethe Universität, Frankfurt a. M. (D) (Stukey *et al.*, 1989)

Table 1: Cloning and Expression Vectors

Vector	Description, Selection Marker	Reference
pDR196	Vector for expression in *S. cerevisiae*, Amp^R, URA3	(Rentsch *et al.*, 1995)
pYES2	Vector for expression in *S. cerevisiae*, Amp^R, URA3	Invitrogen
pJET1.2	Vector for subcloning in *E. coli* , Amp^R	Thermo Fisher Scientific
pQE-80L	Vector for expression in *E. coli*, Amp^R	Qiagen
pBin35S[1]	Vector for expression in plants with 35S promoter, Kan^R	pBinGlyRed3 (Zhang *et al.*, 2013)

[1]*Bam*HI and *Mlu*I were used to exchange the Glycinin Promoter by 35S Promoter, then eGFP was added with *Mlu*I and X*ho*I (Georg Hölzl, IMBIO). *eGFP* was replaced by *AtWSD1* with *Mlu*I and X*ho*I (Andreas Ahrens, IMBIO).

Table 1: (continued)

Vector	Description, Selection Marker	Reference
917p9RFPUBQ Expr	Vector for expression in plants with Ubiquitin promoter, Strep[R], Spec[R]	pVS1-backbone (Vodala *et al.*, 2008), modified plasmid obtained by Nicole Gaude, MPI Golm
pUC57	Level 0 sublconing of PCR fragments for Golden Gate Cloning[R], Amp[R]	Thermo Fisher Scientific, (Binder *et al.*, 2014)
pUC57+*Bpi*I	Level 1 sublconing for Golden Gate Cloning[R], Gent[R]	Thermo Fisher Scientific, (Binder *et al.*, 2014)

Table 2: Recombinant Expression Vectors

Construct	Insert with Restriction Sites or PCR	Vector	Organism of Destination	Glycostock (*E. coli*)
pQE-*LjFatA[Δtp]*	*LjFatA* cDNA, *BamH*I-*Hin*dIII (989 bp)	pQE-80L	*E. coli*	bn 1160, bn 1161
pQE-*LjFatB[Δtp]*	*LjFatB* cDNA, *BamH*I-*Hin*dIII (1101 bp)	pQE-80L	*E. coli*	bn 1162, bn 1163
pQE-*LjFatM[Δtp]*	*LjFatM* cDNA, *BamH*I-*Hin*dIII (1070 bp)	pQE-80L	*E. coli*	bn 881
pDR196-*RiOLE1*	*RiOLE1*cDNA, *Sma*I-*Xho*I (1226 bp)	pDR196	*S. cerevisiae*	bn 1215
pDR196-*RiOLE1-LIKE*	*RiOLE1-LIKE* cDNA, *Sma*I-*Xho*I (1262 bp)	pDR196	*S. cerevisiae*	bn 1216
pYES2-*RiOLE1-LIKE*	*RiOLE1-LIKE* cDNA, *Hin*dIII-*Sac*I (1262 bp)	pYES2	*S. cerevisiae*	bn 1217
p917UBQ3-*RiOLE1*	*RiOLE1*cDNA, *BamH*I-*Hin*dIII (1226 bp)	p917RFP UBQ Expr	*N. benthamiana*	bn 1250
pBin35S-*RiOLE1-LIKE*	*RiOLE1*cDNA, *Mlu*I-*Xho*I (1262 bp)	pBin35S	*N. benthamiana*	bn 1246

2.1.8 Software and Online Resources

Resource	Reference
Clone Manager Professional Suite, ver. 8.0	Sci-Ed Software, 2005
Molecular Evolutionary Genetic Analysis (MEGA), ver.6.0	Sci-Ed Software, 2005 (Tamura *et al.*, 2013)
ChloroP 1.1 Server, ver.1.1	(Emanuelsson *et al.*, 1999)
L. japonicus Gene Expression Atlas (LjGEA), ver. 2 (2012)	(Verdier *et al.*, 2013) https://ljgea.noble.org/v2/
Medicago truncatula Gene Expression Atlas (MtGEA), ver. 3	(Benedito *et al.*, 2008; He *et al.*, 2009)
Lotus BASE; Genomic, Proteomic & Expression Resources for *L. japonicus* (LORE1), ver.2.5	(Malolepszy *et al.*, 2016)

Phytozome; Plants Comparative Genomics Portal, ver.7	(Goodstein *et al.*, 2012)
MassHunter Workstation Software Qualitative Analysis, ver. B.06.00	Agilent Technologies, Inc. 2012
MassHunter Workstation Software Quantitative Analysis for Q-TOF, ver. B.07.00	Agilent Technologies, Inc. 2008
Multiple Sequence Alignment (MultiAlin)	(Corpet, 1988)
MycoCosm; *R. irregularis* Genome (DAOM 181602), ver. 1.0	(Tisserant *et al.*, 2013)
EnsemblFungi; Ensembl Genome Browser, ver. Release 40	(Kersey *et al.*, 2018)
ImageJ 1.52a, Java 1.8.0_77 (64-Bit)	Wayne Rasband, National Institutes of Health, USA (https://imagej.net/ImageJ)
Isotope Distribution Calculator and Mass Spectrum Plotter	John J. Manura, David J. Manura, Scientific Instrument Service, USA (https://www.sisweb.com/mstools/isotope.htm)
Cyberlipid Center	Cyberlipid.org
Saccharomyces Genome Database (SGD), ver. January 2017	(Engel *et al.*, 2014)

2.2 Methods

2.2.1 Minimal Statistics

Statistical analysis of raw data was done with Microsoft Excel 2013. If possible, a minimum number of five biologically independent replicas was used. To test for significant differences in the mean value between more than two groups, one-way ANOVA was conducted. Significant differences between the mean value of a given measurement between two independent groups (e. g. WT and mutant) were tested with two-tailed students t-test assuming equal variance. When $p < 0.05$ (α, level of significance), the null hypothesis was rejected and differences between mean values were defined significant. For multiple pairwise comparisons (e. g. WT, mutant A and mutant B), post-hoc tukey or bonferroni-corrected t-test was done to correct for the increase in family-wise error rate.

2.2.2 Identification and Isolation of Homozygous Insertional Mutants in *L. japonicus* Acyl-ACP Thioesterases

L. japonicus FatM and *FatB* gene sequence were identified previously based on sequence homology to Arabidopsis *FatB* (Gomez *et al.*, 2009; Wewer *et al.*, 2014). Using the transcript sequences, the *L. japonicus* Gene Expression Atlas (LjGEA) and the *M. truncatula* Gene Expression Atlas (MtGEA) were searched to identify expression patterns under various treatments and to identify other *FatB* homologs. The LjGEA transcript sequences of the acyl-ACP thioesterase homologoues identified (LjGEA Gene ID´s: *LjFatM*: chr5.CM0328.70.r2.d, *LjFatB:* Ljwgs_013315.1_at, *LjFatA*: chr1.CM0316.110.r2 and *LjFatC*: LJwgs_022305.1_at) were employed

in a BLAST search against the *L. japonicus* genome database ver. 2.5 (Lotus BASE). The resulting BLAST header of the most similar hit was then used to identify LORE1 retrotransposon insertion mutants with the LORE1-lines search option from Lotus BASE and R3 seeds were obtained for these lines. Plants were cultivated, leaf DNA extracted and touchdown PCR performed for genotyping of homozygous LORE1 insertions as described below (see 2.2.2.2, 2.2.3.1, 2.2.3.2 and appendix 7.1). To confirm the exact position of the LORE1 insertion, PCR products were gel-purified and sequenced using the respective genotyping primers.

2.2.2.1 Phylogenetic Tree of Plant Acyl-ACP Thioesterases

To compare protein sequences of acyl-ACP thioesterases from various plant species, a BLASTp search against all translated genomes in the Phytozome database (Plant Comparative Genomics portal, ver. 7) was conducted using the *Lj*FatM translated amino acid sequence as query. Sequences from *Umbellularia californica UcFatB1* (Voelker *et al.*, 1992) and *Cuphea hookeriana ChFatB*2 (Dehesh *et al.*, 1996) were added manually. Multiple sequence alignment was done automatically using the MUSCLE algorithm implemented in MEGA ver. 6.0 with the UPGMB clustering method with pre-set parameters. The alignment was exported and a phylogenetic tree reconstructed by use of maximum likelihood (ML) with amino acid substitution model WAG (+F), Gamma distributed rates among sites with invariant sites (G+I) and subtree pruning and regrafting was done as heuristic method for tree reconstruction. The initial tree was created by Neighbor-joining and the resulting ML tree was tested for validity by performing 1000 pseudo-iterations (Bootstraps) of the initial amino acid sequence alignment followed by reconstruction of the ML tree.

2.2.2.2 Amino Acid Sequence Comparison of Yeast and *R. irregularis* Desaturases

To identify *R. irregularis* desaturases, the protein sequence of *S. cerevisiae* acyl-CoA desaturase OLE1 (OLEIC ACID DEPENDENT 1, systemic name YGL055W) was used for a BLAST search against *S. cerevisiae* (R64-1-1) and *R. irregularis* (DAOM 181602=DAOM 197198 GCA_000439145) proteins, accessed at EnsemblFungi (www.fungi.ensembl.org). All hits with an E-value >0.05 (20 sequences) were retrieved and used subsequently for multiple sequence alignment with MEGA ver. 6.0 using the MUSCLE algorithm. To visualize sequence similarities with regard to *Sc*OLE1, a neighbor joining tree was constructed with all retrieved *R. irregularis* sequences using the JTT model, gamma distributed rates among sites and pairwise deletions of gaps. Robustness of the resulting branches was tested by 1000 pseudo-iterations (Bootstraps).

2.2.2.3 Cultivation of *N. benthamiana*

N. benthamiana was cultivated on soil:vermiculite (3:1 v/v) under long day conditions (16 h light, 8 h dark) at 25°C, 60% humidity, light intensity of 250 mmol s^{-1} m^{-2} and watered with tap water except for the first irrigation, which contained 0.186% (w/v) boric acid and 0.15% (v/v) Proplant (Dr. Stähler). Seedlings were seperated into single pots after two weeks and used at 4 weeks after sowing for infiltration experiments.

2.2.2.4 Cultivation of *L. japonicus*

Seeds from *L. japonicus* were stored in seed bags for 1—3 month after harvest at RT. Afterwards, they were transferred to HPLC-vials without inlet and dried in a vacuum desiccator for three days. For sterilization and pre-germination treatment, seeds were transferred to 2 mL Eppendorf tubes (50—200 seeds per tube). To break dormancy, the tubes were incubated for 10 sec in liquid nitrogen. Afterwards, the seeds were incubated in 1 mL 96% (v/v) ethanol for 10 sec and dried thoroughly. Then, they were soaked for 20 min in 2 mL sterilization solution (2% (v/v) sodium hypochlorite and 0.0001% (v/v) Tween 20) while shaking to ensure equal treatment of every seed with the solution. The solution was discarded and the seeds rinsed at least five times with sterile water and finally left in the final wash in the dark ON at RT for swelling. The next day, they were placed on water-agar medium (tap water solidified with 0.6% (w/v) agar) and transferred to a 16 h light/8 h dark cycle with 60% relative humidity, 21°C and a light intensity of 120 µmol m^{-2} s^{-1}. After 5—14 days, seedlings were transferred to pots (7.5 cm height, 10 cm diameter) filled with soil:vermiculite (1:3) or silica sand for seed propagation or used for inoculation with *R. irregularis* (see 2.2.2.5).

1L Nutrient Solution (+P)	1L Nutrient Solution (-P)	Trace Elements Stock Solution
1.25 mM K_2HPO_4	0.025 mM K_2HPO_4	9.2 mM $MnCl_2$
1.25 mM KH_2PO_4	0.025 mM KH_2PO_4	46.3 mM H_3BO_3
0.5 mM KNO_3	0.5 mM KNO_3	0.81 mM $ZnCl_2$
0.5 mM $MgSO_4$	0.5 mM $MgSO_4$	0.11 mM $NaMoO_4$
0.25 mM KCl	0.25 mM KCl	0.29 mM $CuCl_2$
0.25 mM $CaCl_2$	0.25 mM $CaCl_2$	
0.025 mM Fe-EDTA	0.025 mM Fe-EDTA	
0.25 mL trace Elements	0.25 mL trace Elements	

2.2.2.5 Inoculation of *L. japonicus* with *R. irregularis*

Germinated seedlings were transferred to pots filled by three quarters with a substrate of sand:vermiculite (1:1) containing *R. irregularis* in diatomite or clay as spore carrier material (1 million spores per g material). The sand was previously washed thoroughly with tap water and finally with deionized water to eliminate all traces of phosphate, then mixed with vermiculite and autoclaved in small bags. The pots were filled, and per pot, 0.3—1 g carrier material containing 3000-10000 spores was added and mixed to a homogenous substrate with a small spoon. The amount of spores differed between experiments, but was the same for all pots of a particular experiment, so that mutant and WT plants were inoculated with the same density of spores. Per pot, 3—4 seedlings were embedded into the upper 1 cm layer. As non-inoculated control, carrier material devoid of AMF spores was utilized. Inoculated plants were incubated at standard phytochamber conditions (see 2.2.2.4), covered by plastic hoods for the first 1—2 weeks and watered three times per week directly into the pots, two times with tap water (30 mL per pot) and once with 50 mL nutrient (–P) solution to enhance colonization with AMF. Samples of inoculated and mock-inoculated plants were taken 4 or 7 weeks after inoculation. For harvest of roots, whole pots were emptied, the substrate brushed off gently and the plants disentangled in a beaker with water to avoid damage to the roots.

2.2.2.5.1 Staining of Fungal Structures in Colonized Roots and Microscopy

Roots were washed gently under tap water, cut at the root-shoot junction and transferred to Eppendorf tubes (2 mL) pre-filled with 10% (w/v) KOH. In case roots were stored prior to staining, they were put in 50% (v/v) ethanol at 4°C until transfer to KOH and staining. *R. irregularis* structures were either stained with ink:vinegar for light microscopy or Alexa-Fluor Wheat-Germ Agglutinin (WGA) (Panchuk-Voloshina *et al.*, 1999) for confocal laser scanning microscopy.

For ink:vinegar staining, the method of Vierheilig *et al.* (1998) was employed. The roots were incubated at 95°C for 15 min, then the liquid was carefully discarded, and the roots rinsed once with tap water and once with 10% (v/v) acetic acid prior to 5 min incubation at 95°C in staining solution (5% (v/v) Ink (Pelican), 5% (v/v) acetic acid). The roots were carefully removed with forceps, rinsed under tap water for 10 sec and incubated in 5% (v/v) acetic acid at 4°C for 20 min or long-term storage.

WGA-staining and confocal microscopy was done together with Andreas Keymer in the laboratory of Caroline Gutjahr at the Ludwig-Maximilian University (LMU) in München. The method described by Pimprikar *et al.* (2016) was used. Roots were incubated in KOH as described above but only for 5 min. Afterwards, they were rinsed three times with tap water and incubated for 1—2 h in 0.1 M HCl, then rinsed once with tap water and 1x PBS, pH 7.4. For staining, WGA

staining solution (0.2 µg in 1 mL 1x PBS, pH 7.4) was added and the roots incubated in the dark for at least 6 h and stored at 4°C. Roots were mounted on microscope slides and images taken with a confocal laser scanning microscope Leica SP5 along the Z-axis. Z-stacks were superimposed with the ImageJ software and merged into a single picture for three-dimensional visualization of fungal arbuscules.

2.2.2.5.2 Quantification of Colonization Parameters

Different colonization parameters were quantified in *R. irregularis* colonized WT and *fatm* mutant roots. Ink-stained colonized roots were investigated at 10-fold magnification with a bright-field microscope (BH-2, Olympus).

Root length colonization (%) was quantified based on the grid-line intersection method (Brundrett, 1996; McGonigle *et al.*, 1990). Root systems were placed in a petri dish with tap water and dissected with forceps and scalpel into 1 cm root segments. Ten of these segments were placed on a microscope slide, covered with water and a cover slip and monitored for the occurrence of fungal structures. To this end, a thread was placed in the middle of the eyepiece (the intersect) and every root segment was assessed ten times at different, randomly chosen spots whether the intersect traverses a vesicle, an arbuscule, an intraradical hypha, or no mycorrhizal structure. Multiple fungal structures could be scored by the intersect at one spot. The percentages of arbuscule, vesicle and hyphae were expressed as percentage of total spots counted, which were generally 100 spots per root system.

Measurements of vesicle size was done in the same roots that were used for root length colonization quantification. All vesicles were measured with the CellLens software (Olympus) in the ten root segments (1 cm) and averaged per root system.

To visualize premature arbuscule degeneration in the *FatM* mutant, four categories of arbuscules were counted similarly to the root length colonization parameters described above. The ten root segments (1 cm) were randomly investigated at 10 spots per segment and the intersect used for evaluation of the arbuscule type. Four types of arbuscules were considered: a normal arbuscule that fills the entire cavity of the cell, a stunted arbuscule that appears shriveled and small, both types together, or no arbscule at all in the cell. Examples of the arbuscule types stained with WGA and captured with a confocal microscope are shown in Figure 6.

2.2.2.6 Root Axenic Culture of *D. carota* with *R. irregularis*

In-vitro cultivation of *R. irregularis* was done in axenic root culture in symbiosis with *D. carota* roots (Cranenbrouck *et al.*, 2005). The culture was originally obtained by Arthur Schüßler (LMU, München). To amplify *R. irregularis* extraradical mycelium on plates, a section of MSR medium containing colonized roots and ERM was excised with a sterile scalpel. The piece of MSR medium with roots and ERM was placed on freshly prepared MSR medium (see below) in an

one-compartment petri dish (145x 20 mm), or onto one side of a two-compartment petri dish (94x 16 mm), and incubated at 28°C in the dark for 1—4 month. Hyphal and spore densities of the ERM in the medium were calculated from a 1 cm^2 square with a light microscope and extrapolated for the whole plate.

Stock 1 (Macroelements)
73.9 g MgSO$_4 \cdot$7H$_2$O
7.6 g KNO$_3$
6.5 g KCl
0.4 g KH$_2$PO$_4$
Add ddH$_2$O to 1 L. Store at 4°C.

Stock 2 (Calcium Citrate)
35.9 g Ca(NO$_3$)$_2 \cdot$4H$_2$O
Add ddH$_2$O to 1 L. Store at 4°C.

Stock 3 (Vitamins)
0.09 g calcium panthotenate
0.0001 g biotin
0.1 g nicotinic acid
0.09 g pyridoxine
0.1 g thiamine
0.04 g cyanocobalamine
Add ddH$_2$O to 500 mL. Store as 5 mL aliquots at -20°C.

Stock 4 (NaFeEDTA)
0.16 g NaFeEDTA
Add ddH$_2$O to 500 mL. Store as 5 mL aliquots at -20°C.

Stock 5 (Microelements)
I) 1.225 g MnSO$_4 \cdot$4H$_2$O add ddH$_2$O to 100 mL
II) 0.14 g ZnSO$_4 \cdot$7H$_2$O add ddH$_2$O to 100 mL
III) 0.925 g H$_3$BO$_3$ add ddH$_2$O to 100 mL
IV) 1.1 g CuSO$_4 \cdot$5H$_2$O add ddH$_2$O to 50 mL
V) 0.12 g Na$_2$MoO$_4 \cdot$2H$_2$O add ddH$_2$O to 100 mL
VI) 1.7 g (NH4)$_6$Mo$_7$O$_{24} \cdot$4H$_2$O add ddH$_2$O to 100 mL
Mix solution I, II and III, add 5 mL of solution IV, 1 mL of solution V and VI, add ddH$_2$O to 500 mL. Store at 4°C.

MSR Medium
10 mL Stock 1
10 mL Stock 2
5 mL Stock 3
5 mL Stock 4
1 mL Stock 5
10 g Sucrose
3 g Gelrite.
Dissolve all components. Add ddH$_2$O to 1L. Adjust pH to 5.5 with NaOH 1M.

2.2.2.6.1 Extraction of *R. irregularis* ERM from Culture

For harvest of ERM, roots were removed manually with forceps, leaving only hyphae and spores (ERM) in the medium. The medium was mashed with a spoon and then transferred to approximately 10 volumes (200 mL for 145x 20 mm petri dish) of sodium citrate solution (20 mM) pre-heated to 40°C, and mixed vigorously by shaking. After 5—20 min incubation at 40°C, the gelrite was completely dissolved in the sodium citrate buffer and the ERM floated freely in the liquid. The solubilization of the medium took substantially longer when older (>50 days) plates were used, due to loss of water from the medium.

In the liquid buffer, hyphae and spores formed an aggregate that was retained after passing the dissolved medium through miracloth (22—25 µm pore size) mounted on a plastic funnel. The ERM was transferred with forceps to a fresh miracloth piece on a funnel and washed with 1 L ddH$_2$O to remove residual medium and external contaminants. Fresh weight was determined and ERM stored at -80°C until RNA or lipid extraction (Wewer *et al.*, 2014) (see 2.2.3.7.1 and 2.2.8.2).

2.2.2.7 Measurement of Shoot Inorganic Phosphate

The inorganic phosphate content was measured in shoots of colonized and non-colonized plants. The method from Itaya and Ui (1966) was used. Either, a shoot section containing 1—3 trifoliate leaves with the stem portion was harvested or total shoots including the leaves. For every treatment, similar shoots sections with the same amount of leaves were chosen and dried for 110°C for 2h, homogenized in a ball mill with ceramic beads (Precellys®) and soluble compounds were dissolved with 1 mL extraction buffer, centrifuged at 4000 g for 5 min. Next, 20 µL of the supernatant were mixed with 480 µL color reagent (molybdate and malachite green), 480 µL 1N HCl and 20 µL Tween 20 and the color was allowed to developed for 30 min. Then, the absorpiton was measured photometrically at an OD of 660 nm. At acidic pH, the organic dye malachite green forms a complex with phosphomolybdate that causes a shift in the absorption maximum, allowing quantification of soluble, inorganic phosphate at 660 nm. A calibration curve was set up with 0, 10, 75, 100, 200 and 500 µmol KH$_2$PO$_4$ for phosphate quantification.

Extraction Buffer
0.33 M Sorbitol
2 mM MgCl$_2$
1 mM EDTA
50 mM Tricine

Color Reagent
One volume 4.2% w/v ammonium molybdate in 5 N HCl
Three volumes 0.2% w/v Malachite Green

2.2.3 Methods for Working with Nucleic Acids

2.2.3.1 Isolation of Genomic DNA from Plant Tissue

For DNA isolation, 10—100 mg of leaf tissue was frozen in liquid nitrogen and ground with a ball mill (Precellys). One mL of CTAB (cetyltrimethylammonium bromide) buffer was added and the mixture was incubated at 65°C for 10 min under continuous shaking. Phase separation was then achieved by centrifugation for 5 min at 3000 rpm. The aqueous phase was transferred to a fresh tube, and incubated on ice for 10 min after mixing with 0.7 mL of isopropanol to precipitate DNA. DNA was pelleted by centrifugation (10000 g, 5 min), the supernatant discarded and the pellet rinsed with cold 70% (v/v) ethanol, which was discarded after an additional centrifugation step (10000 g, 5 min). The remaining pellet was dried and re-dissolved in 50 µL ddH$_2$O and DNA

concentration determined by measuring the absorption at a wavelength of 260 nm with the Nanodrop 1000 photometer.

CTAB Buffer
0.1 M Tris, pH 8.0
20 mM EDTA, pH 8.0
280 mM NaCl
20% (w/v) CTAB
The pH for Tris was adjusted with HCl, the pH for EDTA was adjusted with NaOH.

2.2.3.2 Polymerase Chain Reaction

The polymerase chain reaction (PCR) conditions for primer pairs are listed in appendix 7.1. DNA fragments from DNA or cDNA were amplified by PCR with DNA-polymerases from *Thermus aquaticus* (*Taq*) for genotyping and RT-PCR or with Q5 High-Fidelity Polymerase (NEB) with proofreading ability if sequences were amplified for cloning and recombinant expression.

PCR Reaction-Mix (*Taq*)
0.5 μL *Taq*-polymerase (1 U/μL)
1—3 μL template DNA
1 μL primer forward (10 pmol/μL)
1 μL primer reverse (10 pmol/μL)
2.5 μL 10x buffer
2 μL dNTPs (2.5 mM per nucleotide)
1.5 μL MgCl$_2$ (25 mM)
Add nuclease-free ddH$_2$O to a final volume of 25 μL.

Q5 Reaction-Mix
0.25 μL Q5 High-Fidelity Polymerase[a]
1—3 μL template DNA
1 μL primer forward (10 pmol/μL)
1 μL primer reverse (10 pmol/μL)
5 μL 5x Q5 reaction buffer
0.5 μL dNTPs (2.5 mM per nucleotide)
Add nuclease-free ddH$_2$O to a final volume of 25 μL.

[a] Q5 polymerase was added after the reactions were heated to 98°C to avoid exouclease activity

2.2.3.3 Restriction Digestion

High-fidelity restriction endonucleases from New England Biolabs were used with the CutSmart buffer system and incubated at the appropriate temperature for 15 min for up to 2 h. Cleaved fragments were then seperated by gel electrophoresis. Restriction of plasmid DNA after extraction of plasmids from recombinant *E. coli* was done to produce recombinant plasmids for expression, or to verify correct insertions of insert DNA into the plasmid.

Restriction Reaction
5—10 µL plasmid DNA (up to 1 µg)
0.5—1 µL restriction enzyme 1 (10 U µL^{-1})
0.5-1 µL restriction enzyme 2 (10 U µL^{-1})
5 µL 10x CutSmart buffer
Add nuclease-free ddH$_2$O to a final volume
of 50 µL.

The restriction reaction was scaled down to 25 µL if only a test restriction for proper insertion into the plasmid was required.

2.2.3.4 Ligation

After preparation of plasmid DNA and restriction digestion or PCR, gel-purified plasmids and inserts were used in a ligation reaction. Amplification of cDNA by Q5-PCR yields blunt-end PCR products that were cloned into blunt-end sublconing vector pJET 1.2 from the CloneJET PCR Cloning Kit (Thermo Fisher Scientific) in a blunt-end ligation with T4 DNA Ligase (New England Biolabs). For ligation, a 3:1 molar ratio of insert-to-vector was used. The relative intensities of insert and vector DNA fragments were estimated by loading 1 µL of each fragment on a thin agarose gel that was developed for 5 minutes at 120 V. The estimated intensities were used to calculate the amount of insert and vector that were needed to achieve a 3:1 molar ratio in the ligation reaction.

Blunt-end Ligation	**Cohesive-end Ligation**
1—10 µL gel-purified PCR product	1—10 µL gel-purified insert
0.5—1 µL linear, blunt-end pJET 1.2 (1 ng.µL^{-1})	0.5—3 µL gel-purified linear expression vector (50—400 ng µL^{-1})
2 µL 10x T4 DNA Ligase buffer	2 µL 10x T4 DNA Ligase buffer
0.25—0.5 µL T4 DNA Ligase M0202S (400.000 U mL^{-1})	0.25—0.5 µL T4 DNA Ligase M0202S (400.000 U mL^{-1})
add nuclease-free ddH$_2$O to a final volume of 20 µL	Add nuclease-free ddH$_2$O to a final volume of 20 µL.
The reaction was incubated at RT for 2 h and stopped at 65°C for 5 min.	The reaction was incubated at RT for 30 min and stopped at 65°C for 5 min.

After heat-inactivation of the ligation reaction, the whole reaction mixture was spotted on a mixed cellulose ester membrane (0.025 µm pore size) floating on 20 mL ddH$_2$O in a small petri dish (35x 10 mm) and incubated at RT for 30—60 min to desalt the ligation mix.

2.2.3.5 Preparation of Plasmid DNA

Plasmid DNA was purified from *E. coli* cells with the NuceloSpin® Plasmid DNA Miniprep Kit (Macherey & Nagel) according to standard procedures from pelleted ON cultures (5 mL) prepared from single colonies grown on selective agar.

2.2.3.6 Elution of Nucleic Acids from Agarose Gels

DNA Fragments from restriction digestions or PCR amplification were eluted from DNA agarose gels with the NuceloSpin® Gel and PCR Clean-up Kit (Macherey & Nagel).

2.2.3.7 Amplification of Expressed Genes by RT-PCR

Expressed genes from *L. japonicus* roots or *R. irregularis* ERM were amplified after cDNA synthesis from mRNA either for cloning into expression vectors (see appendix 7.4, 7.5, 7.6) or to compare gene expression (see 2.2.3.7.3).

2.2.3.7.1 Isolation of RNA from *L. japonicus* and *R. irregularis*

To avoid RNAse degradation, the samples were kept on ice and RNAse-free equipment was used. Freshly harvested *L. japonicus* roots and *R. irregularis* ERM prepared from MSR plates (see 2.2.2.6) were immediately frozen in liquid N_2 and homogenized with pre-cooled mortar and pestle. Approximately 50—100 mg of material was weighed into pre-cooled Eppendorf tubes and total RNA was extracted with the Plant Total RNA Mini Kit (DNA Cloning Service). Contaminating DNA was digested with the TURBO DNA-*free*™ Kit (Thermo Scientific). The DNAse-digested RNA was measured on a Nanodrop photometer to ensure good quality RNA with a $A260_{nm}/A280_{nm}$ ratio of 1.8—2.0 and to quantify the exact concentration of total RNA. RNA gel electrophoresis was done afterwards to ensure that no degradation of RNA took place and that equal amounts of RNA were used for subsequent cDNA synthesis.

2.2.3.7.2 RNA Formaldehyde Gel Electrophoresis

Extracted total RNA from plant and fungal tissues was investigated by formaldehyde gel electrophoresis prior to first strand cDNA synthesis to ensure good quality RNA. Agarose was melted in the microwave oven and mixed with MOPS buffer, pH 8.0. After cooling, formaldehyde was added and the gel was immediately poured. 100—1000 ng total RNA dissolved in water was diluted to a volume of 10 μL with RNAse-free ddH_2O and mixed with 2x RNA sample loading buffer. Prior to loading, the samples were incubated at 65°C for 10 min to denature the RNA. Electrophoresis was conducted at 90 V for 30 min. The RNA-Ethidium bromide complexes were visualized under UV light at a wavelength of 312 nm.

10x MOPS Buffer
0.2 M MOPS
50 mM Sodium acetate
10 mM Na-EDTA
Adjusted to pH 7 or pH 8 with NaOH.

2x RNA Sample Loading Buffer
65% v/v Formamide
8% v/v Formaldehyde
1.3% w/v 1x MOPS, pH 8
54 µg mL^{-1} Ethidium bromide

Formaldehyde Agarose Gel
1.5% (w/v) Agarose
6% v/v Formaldehyde
in 1x MOPS, pH 8

RNA Running Buffer
10% (w/v) Formaldehyde
in 1x MOPS, pH 7

2.2.3.7.3 First Strand cDNA Synthesis and Reverse Transcription PCR (RT-PCR)

Gene expression was determined with semi-quantitative RT-PCR in mock-inoculated and AMF-inoculated roots and in fungal ERM. To this end, total RNA was isolated from *L. japonicus* roots and fungal ERM harvested from *D. carota* roots. The mRNA was transcribed into cDNA using a first strand cDNA synthesis kit (Thermo Fisher Scientific) with oligo (dT)-primers.

Generally 50—200 ng of DNAse-digested, total RNA was diluted with RNAse-free water to a final volume of 11 µL and added to 1 µL of oligo dT$_{18}$ primers. A master mix of 4 µL 5x Reaction Buffer, 1 µL RiboLock RNase inhibitor (20 U/µL), 2 µL 10 mM dNTP mix and 1 µL RevertAid M-MuLV RT (200 U/µL) Reverse Transcriptase for each sample was prepared and 8 µL added to each sample. The mixture was incubated at 42°C for 60 min and was stopped by an incubation step at 70°C for 5 min. Transcribed cDNA was diluted 1:10, stored at -20°C or used as a template for subsequent RT-PCR reactions with gene specific primers.

RT-PCR was carried out with a *Taq* DNA polymerase for amplification of selected plant and fungal genes (see appendix 7.1). The housekeeping genes *UBIQUITIN (UBI) and ACTIN2 (ACT2)* served as RNA loading controls for *L .japonicus* and *α-TUBULIN* (*α-TUB*) for *R. irregularis*. Except for *UBI*, primers were designed that span intron-exon borders to distinguish cDNA from residual genomic DNA. The *UBI* gene from *L. japonicus* does not contain introns. Amplification was done by 25—30 PCR cycles and the products loaded onto agarose gels and stained with ethidium bromide. The signal intensities of the PCR products from different samples were compared for an estimation of gene expression, and dilution series were conducted to ensure that the product-to-signal ratio was linear.

PCR Reaction-Mix (*Taq*)
0.5 µL DCS-*Taq*-polymerase (1 U µL^{-1})
1-3 µL cDNA
1 µL primer forward (10 pmol µL^{-1})
1 µL primer reverse (10 pmol µL^{-1})
2.5 µL 10x buffer

0.3 µL dNTPs (2.5 mM per nucleotide)
1.5 µL MgCl$_2$ (25 mM)
Add ddH$_2$O to a final volume of 25 µL.

For PCR conditions and oligonucleotide sequences, see appendix 7.1.

2.2.3.7.4 DNA Gel Electrophoresis

Samples for DNA gel electrophoresis were mixed 6x DNA loading dye to obtain a 1x concentration and then loaded onto 1% (w/v) agarose gels. The DNA was seperated at 90 V for 20-30 min in 1x TBE running buffer and fluorescence of DNA was visualized with UV light (λ=302 nm) caused by intercalation of the DNA with ethidium bromide. The size of PCR products was compared to a DNA standard of known size (Gene Ruler 1 kb DNA ladder, Thermo Fisher Scientific).

10x TBE Buffer
890 mM Tris-base
890 mM Boric acid
20 mM Na$_2$-EDTA (pH 8.0)
pH 8.3

TBE Agarose Gel
1% (w/v) Agarose
0.01% (v/v) Ethidium bromide
(Ethidium bromide stock solution: 1 mg mL^{-1}
ethidium bromide in ddH$_2$O)
in 1x TBE buffer

6x DNA Loading Dye
10 mM Tris-HCl (pH 7.6)
0.03% (w/v) Bromophenol blue
0.03% (w/v) Xylene cyanol FF
60% /v/v) Glycerol

2.2.4 Heterologous Expression of Coding Sequences in Microorganisms and Plants

To study the function of enzymes from *L. japonicus* and *R. irregularis*, they were heterologously expressed in either *N. benthamiana* (see 2.2.4.1.2), *E. coli* (2.2.4.2) or *S. cerevisae* (see 2.2.4.3). Heterologous expression enables to study the products of enzyme-catalyzed reactions in a foreign background, allowing a distinction between endogenous, redundant enzyme products and those that are catalyzed by the studied enzyme. This was done either directly upon heterologous expression with the living cells (feeding experiment) or after cell rupture and extraction of the recombinant enzyme from *E. coli*.

2.2.4.1 Procedures for working with *A. tumefaciens*

For heterologous expression of the *R. irregularis* genes *RiOLE1* and *RiOLE1-LIKE*, the coding sequences were ligated into plant expression vectors (see appendix 7.5) and transferred

into *A. tumefaciens* (see 2.2.6.1.1), which were then used for transient transformation of *N. benthamiana* by leaf infiltration (see 2.2.6.1.2).

2.2.4.1.1 Transformation of *A. tumefaciens* by Electroporation

Agrobacterium tumefaciens, strain GV3101 (pMP90) was grown at 28°C and 200 rpm in selective YEP medium with rifampicin (80 µg mL^{-1}). 100 mL cultures were grown ON until an OD$_{600}$ of 0.5—0.7 and cooled for 15 min on ice. Bacteria were pelleted at 2500 g for 20 min at 4°C by centrifugation. The pellet was resuspended in 200 mL sterile ddH$_2$O and incubated on ice for 15 min. The centrifugation and the following wash step were repeated twice and the cells were resuspended in 1 mL of sterile 10% (v/v) glycerol. 40 µL aliquots were shock frozen in liquid nitrogen and then stored at -80°C.

YEP Medium
0.5% (w/v) Beef extract
0.1% (w/v) Yeast extract
0.5% (w/v) Peptone
0.5% (w/v) Sucrose
2 mM MgSO$_4$

An aliquot of electrocompetent *A. tumefaciens* strain GV3101 (pMP90) was thawed on ice, and 1—2 µL of a 100x dilution of purified plasmid DNA was added and the mixture incubated on ice for 30 min. The cells were transferred to pre-cooled electroporation cuvettes and transformed by application of an electric pulse of 12.5 kV/cm. 0.5—1 mL of pre-warmed 28°C YEP medium was added to the cuvettes to dilute the cells, they were pipetted to Eppendorf tubes and incubated at 28°C for 4 h while rotating and subsequently plated on selective YEP-Agar with rifampicin (80 µg mL^{-1}) as genetic resistance marker for the *A. tumefaciens* GV3101 (pMP90) strain and the appropriate selective antibiotic for the expression vector and incubated at 28°C for 2 days.

2.2.4.1.2 Leaf Infiltration for transient Transformation of *N. benthamiana*

Transient expression of coding sequences by infiltration of *N. benthamiana* leaves was conducted according to Wood et al. (2009) with slight modifications. To this end, *A. tumefaciens* GV3101 (pMP90) containing expression vectors p917UBQ3-*RiOLE1* or pBin35S-*RiOLE1-LIKE* were used. *A. tumefaciens* pre-cultures were inoculated from single colonies in 10 mL YEP medium with rifampicin (80 µg mL^{-1}) and kanamycin (50 µg mL^{-1}) for pBin35S-*RiOLE1-LIKE* or rifampicin (80 µg mL^{-1}) and streptomycin (300 µg mL^{-1}) + spectinomycin (100 µg mL^{-1}) for p917UBQ3-*RiOLE1* and grown at 28°C while shaking at 180 rpm for 20 h. To induce virulence genes, 100 mM acetosyringone dissolved in dimethyl sulfoxide (DMSO) was added and incubated for another 2—3 h. Prior to transformation, plants were transferred to sufficient light and watered to stimulate stomata opening. *A. tumefaciens* were harvested from the cultures by centrifugation

for 10 min at 4000 g and resuspended by adding 0.5 volumes of infiltration medium, pipetted with a cut tip to avoid damge to the bacteria. For infiltration, *A. tumefaciens* strains containing different constructs were mixed to a final OD_{600}=0.2 for each construct. Each mixture contained two *A. tumefaciens* strains, one expressing the P19 protein of tomato bushy stunt virus to suppress gene silencing (Garabagi *et al.*, 2012) and the expression construct for the gene of interest. The construct pBin35S-*AtWSD1* was used as positive control for expression of the *dsRed* fluorescence marker. The mixture of *A. tumefaciens* strains was drawn up in a 2 mL syringe without a needle and infiltrated into the bottom side of leaves (Sparkes *et al.*, 2006). Comparable leaves on different plants were used to ensure comparability of the results. Fluorescent marker gene expression was detected after 4—11 days with a fluorescent lamp (NightSea, Bedford, USA). Leaf areas that displayed a dsRed signal were used for lipid extraction (see 2.2.8.2).

Infiltration Medium
5 mM $MgCl_2$
5 mM MES pH 5.7
100 mM Acetosyringone (dissolved in DMSO)

2.2.4.2 Procedures for working with *E. coli*

E. coli was used as heterologous expression system for truncated *L. japonicus* thioesterases *LjFatA^{Δtp}, LjFat^{Δtp} and LjFatM^{Δtp}* without N-terminal signal peptides and for multiplication of cloning vectors and expression vectors for plant and yeast transformation.

2.2.4.2.1 Transformation of *E. coli* by Electroporation

For generation of electrocompetent *E. coli* ElectroSHOX or *fadD* cells, a 5 mL culture of *E coli* was grown from a single colony overnight at 37°C and 200 rpm in LB medium without antibiotics. The total culture volume was used for the inoculation of 250 mL LB medium that was grown to an OD_{600} of 0.4, harvested by centrifugation (4000 g, 5 min, 4°C) and resuspended in 125 mL of ice cold 50 mM $CaCl_2$ and incubated at 4°C for 20 min. The bacteria were pelleted and resuspended in 20 ml of 50 mM $CaCl_2$ and kept on ice for 4 h. Then, the suspension was mixed with 7 mL of ice cold 50% (v/v) glycerol and 50 μL aliquots were shock-frozen in liquid nitrogen and stored at -80°C. For transformation, an aliquot of cells was thawed on ice and mixed with 1— 2 μL of 100x diluted plasmid DNA or 5—10 μL of desalted ligation reaction (see 2.2.3.4) and incubated for 5 min on ice. The transformation mix was transferred to pre-cooled electroporation cuvettes and transformed by application of an electric pulse of 12.5 kV/cm. In the next step, 0.5— 1 mL of pre-warmed 37°C LB medium was added to the cuvettes to dilute the cells. Then, they were pipetted to Eppendorf tubes and incubated at 37°C for 1 h while rotating and subsequently

plated on selective LB-Agar with the appropriate selective antibiotic for the expression vector and incubated at 37°C ON.

LB Medium
 1% (w/v) tryptone
0.5% (w/v) yeast extract
0.5% (w/v) NaCl

For LB-agar bacto agar was used at 1.5% (w/v).

2.2.4.3 Procedures for working with *S. cerevisiae*

S. cerevisiae was employed as heterologous expression system for *R. irregularis RiOLE1* and *RiOLE1-LIKE.* Both WT yeast (BY4741) and the *Δole1* mutant were used to this end. The *Δole1* (Stukey *et al.*, 1989) is deficient in the gene which encodes a STEAROYL-CoA Δ9 DESATURASE and is fatty-acid auxotroph but can be grown by supplementation of oleic acid to the growth medium (Ogasawara *et al.*, 2017).

2.2.4.3.1 Generation of competent *S. cerevisiae* and Transformation

Chemically competent yeast cells were generated and transformed via heat-shock according to Gietz *et al.* (1995) with modifications by Gabriel Schaaf and Dominique Loqué. Competent cells were not stored but prepared fresh for transformation. For preparation, yeast was cultivated on YPD plates. For generation of competent cells, 5 mL liquid YPD medium was inoculated with single colonies for growth ON at 28°C on a rotary shaker. 200—400 µL of the ON culture was added to 4 mL of fresh YPD medium and the cells grown until an $OD_{600nm}=0.8\text{-}1.0$ was reached (approximately 4—6 h). Cells were harvested at 1500g in 15 mL Falcon tubes, the supernatant was discarded and the pellet resuspended in 500 µL TE/LiAc buffer at RT and transferred to an 2 mL Eppendorf tube and centrifuged at 1700 g. The supernatant was discarded and the pellet resuspended again in the same volume, centrifuged again and the step was repeated one more time. Finally, the pellet was resuspended in 150—300 µL TE/LiAc buffer and placed on ice. The mixture was sufficient for ~five transformations.

For heat-shock transformation, a mixture was set up in PCR tubes containing 3.5 µL salmon sperm carrier DNA (8 mg mL^{-1}) which was warmed up and denatured for 3 min at 95°C prior to use. The tube was cooled on ice for 2 min. Then, 0.5-4 µL of purified plasmid DNA (200—500 ng DNA) and 50 µL of chemical competent cells were added. Next, 300 µL of PEG/LiAc buffer was added and incubated at 30-40 min at RT while shaking at 500 rpm. The mixture was heat-shocked at 42°C for 20 min, 800 µL sterile ddH$_2$O added and cells gently resuspended. The mixture was centrifuged at 1700 g for 1 min and the pellet recovered in 60 µL sterile ddH$_2$O and plated on selective media (see 2.2.4.3.2).

YPD Medium
1% (w/v) Yeast extract
2% (w/v) Bacto-peptone
2% (w/v) Glucose

Solidified medium contained 2% (w/v) bacto agar.

PEG 4000 [50% (w/v)]
4 g PEG
Add ddH$_2$O to 7 mL. Dissolve by heating, autoclave, add ddH$_2$O to final volume of 8 mL.

PEG/LiAc buffer
10 mL 1 M LiAc
10 mL 10x TE (100 mM Tris-HCl, 10 mM EDTA, pH=7.5)
Add to 80 mL 50% (w/v) PEG 4000 solution.

TE/LiAc Buffer
5 mL 10x TE (100 mM Tris-HCL, 10 mM EDTA, pH=7.5)
5 mL 1 M LiAc
Add 40 mL ddH$_2$O to final volume of 50 mL.

Salmon Sperm Carrier DNA
400 mg Salmon Sperm DNA (Sigma #D6898)
Add TE/LiAc buffer to a final volume of 50 mL.
Incubate at 4°C for 24-48 h while rotating. Aliquot (2 mL) and stor at -20°C.

2.2.4.3.2 Selection of recombinant *S. cerevisiae*

For selection of successfully transformed yeast cells, transformation mixtures were plated on Selective Yeast medium (-uracil). Recombinant plasmids for yeast transformation encode URA3 (orotidine 5'-phosphate decarboxylase), allowing only recombinant yeast to grow on medium lacking uracil. The whole transformation mix was plated out and grown for at least 2 d at 28°C until the development of colonies was visible. For liquid cultures, single colonies were used.

Glucose (20% (w/v))
20 g Glucose
Add sterile ddH$_2$O to a final volume of 100 mL.
Filter sterilize.

Dropout powder
2.5 g Adenine (hemisulfate)
1.2 g L-arginine
6 g L-aspartate
6 g L-glutamate (sodium-salt)
1.8 g L-lysine (HCl)
1.2 g L-methionine
3 g L-phenylalanine
22.5 g L-serine
12 g L-threonine
1.8 g L-tyrosine
9 g L-valine
(fine ground powder)

Histidine, leucine, tryptophan stock
Prepare three seperate solutions.
0.755 g Histidine per 50 mL ddH$_2$O (100 mM).
0.658 g Leucine per 50 mL ddH$_2$O (100 mM).
1.021 g Tryptophan[a] per 50 mL ddH$_2$O (40 mM).
Filter sterilize.
[a]For solubilization, traces of NaOH (5M) were added.

Selective yeast medium (-Uracil) (1L)
1.16 g dropout powder
2 g bacto agar[a]
6.7 g Yeast Nitrogen Base (with ammonium sulfate, without amino acids).
Adjust volume to 780 mL with ddH$_2$O, adjust pH to 5.9 with NaOH and autoclave. Cool to 55°C.
Add 100 mL glucose (20% (w/v)).
Add 8 mL of each histidine, leucine and trypotphan stock.
[a]For liquid cultures, bacto agar was omitted.

2.2.4.3.3 Growth Parameters and feeding of Fatty Acids to *S. cerevisiae*

Singe colonies of WT and Δ*ole1* expressing *RiOLE1* and *RiOLE1-LIKE* were used to inoculate ON cultures in 5 mL Selective Yeast medium (-uracil) with and without 1% (v/v) Tritonx-100 and 1 mM oleic acid. For dilution series, the OD$_{660}$ was determined in 1:10 dilutions and the culture diluted to an OD$_{660}$=0.2 in 1 mL ddH$_2$O and two more dilutions (1:10 and 1:100) were made. Five µL of every dilution was spotted on solid Selective Yeast medium (-uracil) with and without 1% (v/v) Tritonx-100 and 1 mM oleic acid and incubated for 6 days at 28°C.

For extraction of lipids and fatty acid feeding of yeast cultures, ON cultures from single colonies were diluted to an OD$_{660}$=0.02 in 5 mL liquid selective yeast medium (-uracil) containing 1% (v/v) Tritonx-100 and 1 mM fatty acid. This was done to complement the Δ*ole1* mutant or to label the products of fatty acid desaturation in the yeast cultures. As fatty acids, oleic acid (18:1Δ9) or pentadecanoic acid (15:0) were added. As an additional control, fatty acids were omitted from the medium. To increase solubility of the fatty acids in the aqueous medium, a concentrated solution of fatty acids was heated to 60°C in 50% (v/v) Tritonx-100, and added to the pre-heated medium and shaken ON at RT until no clumps were visible and the solution was homogenous. When Tritonx-100 and oleic acid were added, the solution remained cloudy.

2.2.5 General Procedures for working with Protein

Investigation of the total protein composition from *E. coli* heterologously expressing His-tagged *L. japonicus* acyl-ACP thioesterases was done by SDS-PAGE (see 2.2.5.1). For detection of his-tagged protein, the proteins were blotted and immunodetected using chemiluminescence (see 2.2.5.2).

2.2.5.1 SDS-PAGE and Coomassie Staining

Sodium dodecyl phosphate-polyacrylamide gel electrophoresis (SDS-PAGE) was employed to seperate proteins according to their electrophoretic mobility after denaturation (Laemmli, 1970). SDS is a detergent which binds to polypeptides and masks their charges, which results in an overall negative charge, allowing a separation according to approximate protein size by migration through the polyacrylamide pores. The separating acrylamide gel was prepared by mixing all components, but ammonium persulfate (APS) and tetramethylethylenediamine (TEMED), which were added at last to induce polymerization. After this, the stacking gel was immediately poured between a glass plate and an alumina plate in a gel caster. To ensure an even edge of the gel, it was covered with isopropanol (1 mL per gel). After 30 min polymerization, isopropanol was removed and the stacking gel was poured on top. Immediately prior to pouring the stacking gel, polymerization was initiated by addition of TEMED and APS. After the stacking gel was poured, combs were inserted. After another 30 min, the gels were ready for use and stored at 4°C until use.

For loading, protein samples were mixed with one-third volume of 4x sample loading buffer and incubated for 5 min at 95°C to denature all proteins. Per gel slot, 10-30 μL protein solution was loaded along with the Color Pre-stained Protein Standard, Broard Range (NEB) as a reference for protein size. Electrophoresis was conducted initially at 25 mA and 200 V per 64cm^2 gel until the running front approached the separating gel. Then the current was increased to 35 mA until the electrophoresis was stopped.

5x Loading Buffer
500 mM Tris
10% (w/v) SDS
50% (w/v) Glycerol
0.025% (w/v) Bromophenol Blue
5 mM EDTA
adjust pH to 6.9 with HCl
Stored as aliquots (400 μL) at -20°C.

4x Loading Buffer
50 μL ddH$_2$O
50 μL ß-mercaptoethanol
400 μL 5x Stock Loading Buffer

Separating Gel (10%)
6.25 mL 40% Acrylamide/Bis-acrylamide stock (29:1 v/v)
6.25 mL 1.5 M Tris-HCl, pH=8.8
250 μL 10% (w/v) SDS
12.1 mL ddH$_2$O
Mix until dissolved.
10 μL TEMED
150 μL 10% (w/v) APS
TEMED and APS were added only immediately prior to pouring of the gel

Stacking Gel (4%)
1 mL 40% Acrylamide/Bis-acrylamide stock (29:1 v/v)
2.5 mL 1.5 M Tris-HCl, pH=8.8
100 μL 10% (w/v) SDS
6.3 mL ddH$_2$O
Mix until dissolved.
5 μL TEMED
100 μL 10% (w/v) APS
TEMED and APS were added only immediately prior to pouring of the gel.

Tank Buffer
125 mM Tris
960 mM Glycine
0.5% (w/v) SDS

Seperated proteins were stained in the SDS-PAGE gel using coomassie R-250 (Diezel *et al.*, 1972). The stacking gel was removed and the separating gel placed in a glass Weck jar and covered with coomassie staining solution and heated in the microwave oven until the solution started to boil. The gel was shaken on a rotary platform at RT for 5 min, rinsed with ddH$_2$O and destained with destaining solution, and heated until the solution started to boil and subsequently shaken at RT for 5—15 min. The procedure was repeated until the gel was destained sufficiently for individual protein bands to appear.

Staining Solution	**Destaining Solution**
50% (v/v) Ethanol	5% (v/v) Glycerol
7% (v/v) Acetic Acid	7.5% (v/v) Acetic Acid
0.252% (w/V) Coomassie R-250	

2.2.5.2 Western Blot and Immunodetection

To detect heterologously expressed His-tagged Fat proteins in *E. coli*, immunodetection with His-Detector Nickel-HRP immunodetection was performed. Prior to this, total proteins were transferred from the SDS-PAGE gel to a nitrocellulose membrane by semi-dry blotting. A blotting sandwich was assembled by stacking three blotting papers, one nitrocellulose membrane (both cut to the size of the protein gel), the protein gel and three more blotting paper. Everything was soaked for 5 min in Towbin transfer buffer (Towbin *et al.*, 1979) prior to assembly of the sandwich. The sandwich was placed on the anode of the semi-dry transfer cell and the kathode was placed on top. Total proteins were transferred to the nitrocellulose membrane by blotting at 15 V and 70 mA per 64 cm² gel for 60 min.

Towbin Transfer Buffer
25 mM Tris
192 mM Glycine
20% (v/v) Methanol
0.1% (w/v) SDS

The blotted membrane was incubated in blocking solution ON at 4°C with gentle shaking, to block remaining protein binding sites. For binding of His-tagged proteins, the HisDetector Nickel-HRP conjugate was diluted 1:20000 in blocking solution and the blocked membrane incubated with gentle shaking for 1 h at RT. Subsequently, the membrane was washed for total

20 min at RT with gentle shaking in TBST buffer with refreshing the buffer seven times to remove excess milk protein and His-detector Nickel-HRP conjugate. Histidine residues in the His-Tags of protein are bound by nickel, and the conjugated horseradish peroxidase (HRP) was used to detect proteins using the SuperSignal West Pico Chemiluminescence (Thermo Fisher Scientific) substrate according to the supplier's instructions. HRP oxidizes luminol in the presence of peroxide, which produces a chemiluminescence that was captured onx-ray film.

TBST buffer
20 mM Tris, pH to 8.0 with HCl
0.05% (v/v) Tween 20
150 mM NaCl

Blocking Solution
5% (w/v) skimmed-milk powder in TBST buffer

2.2.5.3 Determination of Protein Concentration

For quantification of total protein in crude soluble protein extract or purified recombinant protein (see 2.2.7.1 and 2.2.7.2), the Quick Start™ Bradford Protein Assay (Bio-Rad) was used. The method uses colorimetric protein determination with Coomassie Blue G-250 (Bradford, 1976). Under acidic conditions, Coomassie G-250 binds to the protein, which results in the occurrence of blue color. The absorbance shift is detected photometrically at OD_{595nm}. For the assay, 100 µL of sample (either crude protein, purified protein fraction from Ni-NTA column or BSA standard) were mixed with 900 µL of Bradford color reagent, incubated for 5 min at RT and the OD recorded. For blank measurements, either protein extraction buffer or dialysis buffer (see 2.2.7.1 and 2.2.7.2) were used. A calibration curve with 0, 0.75, 2.25, 3, 4.5, 22.5 and 45 µg mL^{-1} BSA Fraction V in the respective buffer was set up for quantification.

2.2.6   Synthesis of Acyl-ACP Substrates

Acyl-ACPs are constituents of the multisubunit enzyme complex of fatty acid synthase (FAS). Acyl carrier proteins (ACP) carry fatty acids during *de novo* synthesis. A conserved serine residue of the ACPs is post-translationally modified by the addition of a 4'-phosphopantetheine prosthetic group onto the serine. The terminal thiol group of 4'-phosphopantetheine is linked via a thioester bond to the fatty acid (Campopiano, 2014). Acyl-ACPs can be synthesized chemically by imidazole-catalyzed S-acylation with N-acylimidazole (Cronan and Klages, 1981) or enzymatically (Lauciello *et al.*, 2016; Rock and Garwin, 1979). Here, recombinant acyl-ACP synthetase (Aas) from *E. coli* was used (see 2.2.6.1) together with *E. coli* ACP (see 2.2.6.2) to enzymatically synthesize acyl-ACPs (see 2.2.6.3).

2.2.6.1 Purification of Acyl-ACP Synthase

The inner membrane acyl-ACP synthase (Aas) was purified from recombinant *E. coli* cell line C41(DE3) containing the *E. coli* Aas open reading frame fused to an N-terminal His-tag in pET28 plasmid (pAasH) (Shanklin, 2000). To this end, a total volume of 18 L *E. coli* C41 AasH pET28a cells were cultured in LB medium with kanamycin (50 µg mL^{-1}) in several 2 L Erlenmeyer flasks each containing 500 mL medium. The cells were harvested by centrifugation and combined in falcon tubes (50 mL) and stored at -80°C until extraction of Aas. The extraction and subsequent column purification and dialysis were done at 4°C, and equipment, centrifuges and solutions were pre-cooled to 4°C. The bacterial pellet of 18 L culture was thawed on ice, weighed (~50 g), resuspended in 75 mL of 1x extraction buffer and flakes (several mg) DNAseI (AppliChem) were added. To disrupt cells, 1.5 mL of resuspended pellet was pipetted to 2 mL Eppendorf tubes containing approximately 200 µL volume of glass beads (≤106 µm diameter) and homogenized on a Precellys homogenizer for 1 min at 6000 rpm. The supernatants (~1 mL per tube) were combined in centrifuge tubes (Centrifuge Sorvall RC 5C PLUS) and the volume adjusted to 200 mL with 1x extraction buffer. The solution was centrifuged at 18000 rpm for 10 min and the supernatant (~140 mL) was transferred to centrifuge tubes (4 mL per tube) for ultra centrifugation at 49 000 rpm for 90 min (Optima L-90K, swing-out rotor SW 28). The supernatant was discarded and the pellet, containing the membrane fraction, resuspended in 250 µL 1x extraction buffer via ultrasonification and pipetting up and down. As the swing-out rotor could only hold 6 ultra centrifuge tubes at once, this process was repeated 5 more times, the resuspended pellets from ultracentrifugation were combined and the volume adjusted to 10 mL. Next, 100 mL 2x extraction buffer was added and ddH$_2$O to 200 mL and the solution stirred for 10 min, transferred to Sorval centrifuge tubes and centrifuged for 10 min at 18 000 rpm and the supernatant, containing the membrane fraction (~180 mL) taken for subsequent Ni^{2+} affinity chromatography.

For binding of His-tagged Aas to nickel, 33 mL of Ni-NTA Agarose (Qiagen; supplied in ethanol) were transferred to a 50 mL Falcon tube. The Ni-NTA Agarose-Ethanol mix was centrifuged at 4000 rpm, the supernatant (ethanol) discarded and the Ni-NTA pellet resuspended in 16.5 mL extraction buffer. This step was repeated two times to equilibrate the Ni-NTA matrix with the resuspension buffer. To the final 33 mL, 17 mL of the *E. coli* C41 AasH pET28a membrane fraction from the previous step was added and the tube gently shaken on a rotary platform for 30 min to ensure homogenous binding of nickel to the histidine-tagged Aas protein. The mixture (50 mL) was applied to a protein chromatography column, allowed to settle and the solution passed through the Nickel-NTA Agarose matrix with a flow rate of 1-2 mL min^{-1}. Subsequently, the remaining *E. coli* C41 AasH pET28a membrane fraction (~160 mL) was added and allowed to pass through the column matrix. The column was washed with 100 mL 1x extraction buffer and then

100 mL 1x extraction buffer with 25 mM imidazole. For elution of bound Aas protein, 100 mL 1x extraction buffer with 100 mM EDTA was used and 6 elution fractions collected (15 mL each). EDTA is a chelator that also removed nickel from the matrix. An aliquot of each elution fraction was taken for SDS-PAGE (see 2.2.5.1) to check for purity of the Aas preparation.

Elution fractions containing the 80.6-kDa Aas protein were combined, pipetted into a dialysis membrane with a cutoff of 6000-8000 Da (Spectrum® Laboratories) and dialyzed against 100 volumes of 1x extraction buffer for 4 h with gentle shaking. The dialysis buffer was replaced after 4h and dialysis was continued for another 4h. This step allows EDTA and nickel to pass through the dialysis membrane thereby removing them from the protein preparation. It was necessary to restrict dialysis to 2x 4 h as otherwise, increasing amounts of Aas precipitate from the solution and would be lost. Dialyzed elution fractions were centrifuged at 18000 rpm for 5 min. The clear supernatant (~40 mL) was transferred to a fresh tube and ATP added from the stock to a final concentration of 5 mM (~2 mL). Glycerol was added from a 70% (v/v) stock to obtain 10% (v/v) final concentration. Addition of ATP stabilizes Aas upon freezing and is also necessary for the subsequent acyl-ACP synthesis reaction (see 2.2.6.3). For determination of protein concentration, an aliquot was quantified with the Bradford Protein Assay (Bio-Rad) (see 2.2.5.3) and Aas protein preparations were stored as 1 mL aliquots (88 µg mL^{-1}) under N_2 atmosphere at -80°C.

1x Extraction Buffer
50 mM Tris
20 mM $MgCl_2$
2% (v/v) Tritonx-100
Adjust pH to 8.0 with HCl.

2x Extraction Buffer
100 mM Tris
40 mM $MgCl_2$
4% (v/v) Tritionx-100
Adjust pH to 8.0 with HCl.

ATP Stock
0.1 M ATP
in 50 mM Tris-HCl
Adjust pH to 7.0 with HCl.

2.2.6.2 Purification of ACP from *E. coli*

ACP from *E. coli* was extracted from electroSHOX cells (Bioline) via anion-exchange chromatography using diethylaminoethyl (DEAE)-cellulose (Majerus *et al.*, 1965). Bacterial pellets were harvested consecutively from 500 mL LB cultures grown in 2 L Erlenmeyer flasks and stored at -80°C. The bacterial pellets (3 times 50 mL falcon tubes =~150 g) were thawed on ice and resuspended in one-tenth volume (~15 mL) extraction buffer at RT. The resuspended cell pellet was homogenized by pipetting 1 mL to 2 mL Eppendorf tubes containing approximately 200 µL volume glass beads (≤106 µm diameter) and homogenized on a Precellys homogenizer for

1 min at 6000 rpm. The supernatants were combined and a few drops of lysozyme added and the solution stirred for 2h at RT. The resulting cell paste became very viscous. One volume (~165 mL) of 0.5% (v/v) Tritonx-100 was added and the solution stirred for 1 h at RT. For further homogenization, again 1 mL of the viscous cell paste was pipetted with blue Eppendorf pipette tips, which were cut at the top, to 2 mL Eppendorf tubes containing approximately 200 µL volume glass beads (≤106 µm diameter) and homogenized on a Precellys homogenizer for 1 min at 6000 rpm. From here on, extraction and purification of ACP was done at 4°C, equipment, centrifuges and solutions were pre-cooled to 4°C, except otherwise stated. To precipitate DNA and most protein, but not ACP, one volume (~330 mL) of isopropanol was added slowly over the course of 30 min (one-thirtieth volume added every 2 min) while gently stirring the solution and then stirred further for 1 h. The mixture was centrifuged for 30 min at 5000 rpm (Sorvall, GS-3 rotor), the supernatant brought to pH 6.1 with acetic acid and incubated with 20 g (70 g/400 g *E. coli* pellet) equilibrated DEAE-cellulose (see below) ON while stirring. At pH 6.1, only ACP and a few other proteins bind to the DEAE-cellulose.

The mixture was applied via a clean glass funnel and a clean spoon to a round filter paper (Ø150 mm, Schleicher & Schüll, Ref. 10334512) that was placed in a Büchner funnel (800 mL volume, 125 mm ID, Hartenstein Laborbedarf) placed on a glass bottle, sealed with a rubber seal (GUKO, Hartenstein Laborbedarf) and sucked through the filter paper by vacuum applied via a water jet pump. The remaining slurry was washed with approximately five volumes of the wet cellulose (~100 mL) of PIPES wash buffer 1 and the same volume PIPES wash buffer 2. The washed cellulose-slurry with bound ACP was taken from the filter paper with a clean spoon and poured into a glass chromatography-column with frit for subsequent anion-exchange column purification. The column matrix was allowed to settle after addition of a small volume of PIPES wash buffer 2, with a flow rate of 2–3 mL.min^{-1}. For elution, ~150 mL of PIPES elution buffer were added and fractions collected. The fractions that had an amber, brownish color, derived from a protein co-eluting with ACP, were pooled (~75 mL) and one-tenth volume (~7.5 mL) of 50% (v/v) TCA was added so that the final concentration of TCA was 5% (v/v), which precipitates ACP. The solution was incubated ON and centrifuged at 8000 g for 20 min, and the ACP pellet resuspended in a minimal volume (3 mL) of resuspension buffer. The pH was adjusted to ~7.0–7.5 by adding small amounts of 1M Tris base. For precipitation of contaminating proteins (but not ACP), four volumes of saturated ammonium sulfate (pH~6.8—7.5) were added and the solution incubated for 1 h at RT and centrifuged at 8000 g for 20 min. To the ACP-containing supernatant, one-tenth volume of 50% (v/v) TCA was added and ACP precipitated for 1—2 h. The ACP pellet was harvested by centrifugation at 8000 g for 20 min and resuspended in minimal volume (~0.5 mL) of 1M Tris and the pH adjusted to 7—7.5 with Tris base. The resuspended ACP was centrifuged for 20 min at 1000 g and the ACP-containing supernatant transferred to a fresh tube. An aliquot

of ACP was used for protein quantification with the Bradford Protein Assay (Bio-Rad) (see 2.2.5.3), and frozen as 0.5 mL aliquots diluted to 0.75 mg mL^{-1}.

Extraction Buffer
1M Tris, pH=8.0 with HCl
0.1 M Glycine
0.25 M EDTA-Na$_2$

Equilibrated DEAE-cellulose
20 g DEAE-cellulose (pre-swollen)
Mix with PIPES binding buffer, centrifuge, discard supernatant, use equilibrated cellulose for chromatography

PIPES Binding Buffer
10 mM PIPES
Adjust to pH 6.1 with acetic acid.

PIPES Wash Buffer 1
10 mM PIPES
0.2 M LiCl
0.1% (v/v) Tritonx-100
Adjust to pH 6.1 with acetic acid.

PIPES Wash Buffer 2
10 mM PIPES
0.2 M LiCl
Adjust to pH 6.1 with acetic acid.

PIPES Elution Nuffer
10 mM PIPES
0.6 M LiCl
Adjust pH=6.1 with acetic acid.

50% (v/v) TCA
5 mL 50% (v/v) TCA
5 mL ddH$_2$O

100% (v/v) TCA (Sambrook and Russell, 2001)
5 g TCA
2.27 mL ddH$_2$O. The density of the solution is approximately 1.45 mg.mL^{-1}.

Resuspension Buffer
0.1 M Tris
10 mM DTT

2.2.6.3 Acyl-ACP Synthesis and Ion-Exchange Purification

ACP was acylated enzymatically with recombinant *E. coli* Aas (see 2.2.6.1) according to Salas and Ohlrogge (2002). Test reactions contained 100 µL total volume. To investigate acylation over-time, a time-course series was pipetted, as well as a series of reactions with increasing ACP and fatty acid concentrations, to identify optimal conditions for acylation. For large-scale acylation prior to purification, 1000 µL reactions were set up and incubated ON at 37°C. Aliquots of all acylation reactions were applied to urea PAGE (see 2.2.6.4) to investigate the reaction products and the efficiency of the acylation reaction. For synthesis of radioactive acyl-ACPs, [1-^{14}C]fatty acids were used in 400 µL acylation reactions for 4 h at 37°C.

Test Acylation of ACP (100 µL)
10 µL 10x TML buffer
5 µL 0.1 M ATP (pH 7.0)[a]
1 µL 0.4 M DTT
10—40 µL *E. coli* ACP (0.75 mg mL^{-1})
10 µL 10 mM Fatty Acid in 10% (v/v) Triton X- 100[b]
Adjust volume to 100 µL with purified *E. coli* Aas (88 µg mL^{-1}) (see 2.2.6.1).
[a]Prepared fresh and stored as aliquots at -20°C
[b]18:0 and 20:0 fatty acid needed to be heated to 80°C prior to pipetting

Acylation of ACP (1000 µL)
100 µL 10x TML buffer
50 µL 0.1 M ATP (pH 7.0)[a]
10 µL 0.4 M DTT
400 µL *E. coli* ACP (0.75 mg mL^{-1})
30 µL 10 mM Fatty Acid in 10% (v/v) Tritonx-100[b]
Adjust volume to 1000 µL with purified *E. coli* Aas (88 µg.mL^{-1}) (see 2.2.6.1)
[a]Prepared fresh and stored as aliquots at -20°C
[b]18:0 and 20:0 fatty acid needed to be heated to 80°C prior to pipetting

Acylation of ACP with [1-^{14}C]Fatty Acids (400 µL)
40 µL 10x TML buffer
20 µL 0.1 M ATP (pH=7.0)[a]
8 µL 0.2 M DTT
120 µL *E. coli* ACP (0.75 mg mL^{-1})
10.81 µL [1-^{14}C]Fatty Acid (250 µCi in 2.5 mL ethanol)[b]
Adjust volume to 400 µL with purified *E. coli* Aas (see 2.2.6.1).
[a]Prepared fresh and stored as aliquots at -20°C
[b]Pipetted as first component from stock in EtOH, evaporated and added 10.81 µL 10% (v/v) Tritonx-100.

10x TML Buffer
1 M Tris-HCl, pH 8.0
40 mM LiCl
100 mM MgCl$_2$

The acyl-ACP products were purified by ion-exchange chromatography using DEAE-cellulose (Rock and Garwin, 1979). Per 1000 µL acylation reaction, 300 mg pre-swollen DEAE-cellulose (1000 mg per 1000 µg ACP) were mixed with 5 mL MES-KOH binding buffer in a 15 mL falcon tube, centrifuged at 1500 rpm for 5 min and the supernatant discarded to remove particles that later might clog the column. The equilibrated DEAE-cellulose was mixed with the acylation reaction and 7 mL MES-KOH binding buffer were added. The mixture incubated while shaking for 1 h at RT to ensure binding of acyl-ACPs. At pH 6.1, only acyl-ACPs bind, while remaining fatty acids and *E. coli* Aas do not. The mixture was applied to a PolyPrep® chromatography column (Bio-Rad), allowed to settle and the liquid (MES-KOH binding buffer with unbound molecules) allowed to flow-through. Next, the column was washed with 8 mL MES-KOH wash buffer and again with 8 mL MES-KOH binding buffer. For elution, 10 mL MES-KOH elution buffer were used and fractions of 0.5–1 mL collected. Aliquots of all wash steps and elution fractions were applied to urea PAGE (see 2.2.8.4) and those elution fractions containing the eluted acyl-ACPs were combined and dialyzed for 2 h against 100 volumes MES-KOH binding buffer using a dialysis membrane (see 2.2.6.1) to remove the LiCl from the acyl-ACP fraction that otherwise would interfere with subsequent thioesterase assays. Dialysis led to an increase of the volumes of

the acyl-ACP elution fractions by approximately five volumes. Non-radioactive acyl-ACP elution fractions were concentrated with the SpeedVac® Vacuum Concentrator without heating. To concentrate [^{14}C]acyl-ACPs, they were incubated in a water bath at 40°C for 6 h to reduce volumes to ~1.5–2 mL. Care was taken not to completely dry the acyl-ACPs and a minimal volume was left in the tubes. For the non-radioactive, purified, dialyzed acyl-ACPs, aliquots were used for protein determination with the Bradford Protein Assay (Bio-Rad) (see 2.2.5.3), urea PAGE (see 2.2.6.4) and they were divided into 200 µL aliquots, overlaid with N$_2$ gas and stored at -20°C. Radioactivity of [1-^{14}C]-labeled acyl-ACPs was determined with liquid scintillation counting (see 2.2.7.4) and 100 µL aliquots (~300 dpm µL^{-1}) frozen at -20°C.

MES-KOH Binding Buffer
10 mM MES
Adjust pH to 6.1 with KOH

MES-KOH Wash Buffer
1 volume 10 mM MES-KOH binding buffer
4 volumes isopropanol

MES-KOH Elution Buffer
0.5 M LiCl prepared in MES-KOH binding buffer

2.2.6.4 Urea PAGE

The purity and identity of acyl-ACPs was investigated with polyacrylamide gel electrophoresis (PAGE) using urea as denaturing agent (Post-Beittenmiller *et al.*, 1992). The stacking and separating gels were prepared similar to the SDS-PAGE gels (see 2.2.5.1) but with urea (5M) instead of SDS and with a 20% acrylamide separating gel. Similar to SDS-PAGE, the samples were diluted with 4x sample buffer containing urea (5M) instead of SDS and incubated at 95°C for 5 min prior to loading of 10-30 µL on the gel, which were developed at 25—35 mA and 200 V per 8 cm^2 gel.

2.2.7   *L. japonicus* Acyl-ACP Thioesterase Activity and Enzyme Assay

Enzyme activity of acyl-ACP thioesterases was examined using either recombinant, purified thioesterases or crude total protein after induction of thioesterases in *E. coli* cultures. The latter was done with *L. japonicus* FatB and the former with Lotus FatA and FatM.

2.2.7.1 Heterologous Expression of *L. japonicus* Thioesterases in *E. coli*

Proteins were heterologously expressed to purify recombinant thioesterases from *E. coli* electroSHOX and to test for thioesterase activity in the *E. coli fadD* 88 mutant (Overath *et al.*, 1969). Glycostocks of recombinant *E. coli* expressing acyl-ACP thioestereases in the pQE-80L vector were streaked out on selective LB media with agar containing carbenicillin (100 µg mL^{-1}), grown ON at 37°C and single colonies used for inoculation of 5 mL selective medium, grown at 37°C ON at 180

rpm and used for inoculation of a main culture of 50—200 mL at a starting OD_{600}=0.1 and incubated until OD_{600}=0.5. IPTG was added at a concentration of 1 mM; IPTG binds and releases inhibition by the *lac* repressor, thereby achieving induction of the *lac* operon and transcription of the recombinant Fat mRNA. After induction, the cells were transferred to 16°C to optimize expression and folding of recombinant protein. Growth curves for *E. coli fadD* 88 were recorded by monitoring the OD_{600} at regular intervals, and 5 mL of the culture was used 16 h after induction for extraction of free fatty acids by solid-phase extraction (see 2.2.8.3 and 2.2.8.5) and quantification by GC-FID (see 2.2.8.9). *E. coli fadD* 88 lacks acyl-CoA synthetase activity. Therefore, free fatty acids that are hydrolyzed by recombinantly expressed thioesterases cannot be incorporated into lipids via acyl-CoA. Instead they accumulate and cause growth retardation (Dörmann *et al.*, 1995;xu *et al.*, 2013).

2.2.7.2 Recombinant Protein Purification of Plant Acyl-ACP Thioesterases from *E. coli*

The cells of induced *E. coli* ElectroSHOX cultures grown ON at 16°C were harvested by centrifugation and the cell pellet suspended in lysis buffer either directly or after storage at -20°C. All equipment and buffers subsequently used were pre-cooled and the work was done at 4°C. Per 0.35 g pellet FW (obtained from a 50 mL culture), 2.25 mL lysis buffer was used. The resuspended cells were divided into 2 mL Eppendorf tubes (750 µL each) filled with ~200 µL glass beads (≤106 µm diameter) and mechanically homogenized using the Precellys homogenizer three times at 6500 rpm for 20 seconds. In between, the samples were cooled on ice. The lysed cells were centrifuged at 13500 rpm for 30 min at 4°C to pellet cell debris and insoluble, membrane-bound protein and the supernatant, containing soluble protein, combined in a 15 mL Falcon tube. The total soluble protein was mixed with 1 mL equilibrated Ni-NTA Agarose/lysis buffer 50:50 (v/v). The Ni-NTA Agarose is supplied and stored in 50:50 (v/v) ethanol. For equilibration, the agarose-ethanol was mixed, 1 mL taken out and centrifuged, the supernatant (~0.5 mL ethanol) discarded and 0.5 mL lysis buffer added, resuspended, and the equilibration repeated two more times.

The Ni-NTA Agarose-protein mix was incubated on a rotary platform for 1 h to ensure efficient binding of the immobilized Ni^{2+} to the histidine tag of recombinant thioesterases. The mixture was poured into a PolyPrep® chromatography column (Bio-Rad), capped and the particles were allowed to settle to the bottom of the column. All column eluates were collected at a flow-rate of 1 mL min^{-1}. Aliquots of all fractions were collected for subsequent SDS-PAGE analysis. After the flow-through, which contained unspecifically bound protein and excessive His-tagged recombinant proteins, was allowed to pass through the matrix, two times 5 mL wash buffer were added to the column. To ensure efficient washing, the matrix was resuspended each time by gently pipetting up and down and was allowed to settle again prior to opening of the tubing for collection of the liquid. For elution, 5 mL elution buffer was added, the matrix suspended, allowed to settle

and nine 0.5 mL fractions were collected in 2 mL Eppendorf tubes. This was done to minimize the volume of the fractions of the recombinant protein, to ensure high protein concentration.

After analysis of all fractions by SDS-PAGE (see 2.2.5.1), elution fractions containing the thioesterases FatM or FatA were combined and dialyzed to remove imidazole. The combined fractions were pipetted into a dialysis membrane tubing with a cutoff of 6000—8000 Da (Spectrum® Laboratories) and dialyzed against 100 volumes of Tris-HCl (50 mM, pH 8.0) for 2 h with gentle shaking. The dialysis buffer was replaced after 4h and dialysis was continued for 4h. The dialyzed elution fractions were diluted with 80% (v/v) glycerol to a final concentration of 10% (v/v) glycerol and stored as aliquots of 125 µL at –80°C. Protein concentration was determined with the Bradford Protein Assay (see 2.2.5.3).

Lysis Buffer
50 mM NaH_2PO_4
300 mM NaCl
10 mM Imidazole
Adjust pH to 8.0 with NaOH.

Wash Buffer
50 mM NaH_2PO_4
300 mM NaCl
20 mM Imidazole
Adjust pH to 8.0 with NaOH.

Elution Buffer
50 mM NaH_2PO_4
300 mM NaCl
20 mM Imidazole
Adjust pH to 8.0 with NaOH.

2.2.7.3 Enzyme Assay with recombinant *L. japonicus* Acyl-ACP Thioesterases

Acyl-ACP thioesterase activity was determined according to Ecclestone and Ohlrogge (1998). The assays were conducted with 5000 dpm (40.95 pmol) [1-^{14}C]acyl-ACPs as substrates, which was approximately 15-25 µL per [1-^{14}C]acyl-ACP preparation (see 2.2.6.3). For *Lj*FatM, 2.2 ng recombinant enzyme was used in the assay and 5.7 ng for *Lj*FatA. For *Lj*FatB, the soluble protein fraction after *LjFatB* induction contained 200 ng total protein. The assay was started with the addition of the purified enzyme or the soluble protein fraction, respectively, and incubated at RT until ~40% of the initial substrate (5000 dpm) was hydrolyzed. For LjFatM, the assay was incubated for 30 min and for LjFatA 5 min. The reaction was terminated by addition of 50 µL 1 M acetic acid containing 1 mM non-labeled oleic acid as carrier fatty acid. The hydrolyzed free fatty acids were extracted three times with 300 µL hexane each, and the hexane supernatants collected in scintillation vials. The solvent was evaporated at 40°C in a water bath and the vials used for liquid scintillation counting of the remaining free fatty acids (see 2.2.7.4.).

Acyl-ACP Thioesterase Assay
5000 dpm [1-^{14}C]Acyl-ACP
1 µL 1 M Tricine-KOH, pH 8.5
2.5 µL 10 mM DTT
2-5 ng recombinant Fat enzyme (~20 µL)
Add ddH$_2$O to 50 µL.

2.2.7.4 Liquid Scintillation Counting

For determination of radioactivity by liquid scintillation counting, 20 mL of Ultima Gold Liquid Scintillation cocktail (PerkinElmer) were added to the scintillation vials after evaporation of hexane. Hexane was evaporated to ensure uniform distribution of the [1-^{14}C]fatty acids in the scintillation cocktail. After addition of the scintillation cocktail, the vials were shaken vigorously and incubated for 24 h prior to counting, to ensure that all air bubbles were evolved.

In liquid scintillation counting, the kinetic energy of nuclear emissions from the decaying ^{14}C are converted into light energy. In detail, β-particles emitted from ^{14}C excite solvent molecules in the scintillation cocktail, which in turn excite more solvent molecules and fluor solutes that release photons. Finally, the fluor molecules emit flashes of blue light upon return to the ground state. The total photons emitted as blue light from excited fluor molecules constitutes the scintillation and the light energy intensity corresponds to the initial energy of the β-particle.

Counting was done on a Tri-Carb Liquid Scintillation Counter (Packard BioScience) for 10—30 min per sample with the QuantaSmart software using standard ^{14}C-nuclide settings. The desintregrations per minute (dpm), which represent nuclear decays per minute, were normalized to pmol [1-^{14}C]acyl-ACP hydrolyzed per minute per µg recombinant protein or soluble protein extract using the specific radioactivity (122.1 dpm pmol^{-1}) of the commercial fatty acid used for the synthesis of the [1-^{14}C]acyl-ACP.

2.2.8   Quantification and Identification of Lipids and Fatty Acids

2.2.8.1 Internal Standards for Lipid and Fatty Acid Analysis

For lipid quantification, concentrations were calculated in correlation to internal standards of known quantity. Commercially available standards were purchased from Sigma, Avanti Polar Lipids, Matreya LLC and Larodan (see 2.1.6).

For the quantification of internal standards for phospholipids and galactolipids, DAGs, TAGs, fatty acids, MAGs, acyl-CoAs and acyl-ACPs, the lipids were trans methylated and measured on GC-FID as fatty acid methyl esters (see 2.2.8.9). Peak areas were quantified relative to 5 µg pentadecanoic acid methyl ester (15:0) or myristic acid methyl ester (14:0) in the case for the IS 15:0.

Fatty acid and Monoacylglycerol Internal Standards

For fatty acid quantification either by GC-FID, GC-MS or QTOF LC-MS, 100 µL IS containing 5 µg of pentadecanoic acid (0.05 µg µL^{-1}) in methanol were added to the sample prior to lipid extraction. For monoacylglycerol (MAG) measurements, 15 µg monopentadecanoin (15:0-MAG) in chloroform were added to the sample prior to lipid extraction. The 15:0-MAG IS was a racemic mixture of 12.3% β-MAG and 87.7% α-MAG. The ratio was experimentally verified by replicate measurement of the 15:0-MAG IS by GC-MS which is capable to seperate these two MAG forms.

Phospholipid, Galactolipid and Sulfolipid Standard Mix

The phospholipid, galactolipid and sulfolipid standard mix was quantified and prepared by Helga Peisker (IMBIO Institute, Bonn) (Gasulla *et al.*, 2013; Wewer *et al.*, 2014). For each sample, 10 µL of phospholipid and galactolipid standard mix in chloroform/methanol (2:1) contained 10.35 nmol of di14:0-PC and 13.25 nmol di20:0-PC, 9.33 nmol of di14:0-PE and 12.1 nmol di20:0-PE PE, 9.92 nmol of di14:0-PG and 11.25 nmol di20:0-PG, 6.96 nmol of di14:0-PA and 7.145 nmol di20:0-PA, 1.41 nmol di14:0-PS, 15.9 nmol 34:0-PI, 7.278 nmol 34:0-MGDG and 6.75 nmol 36:0 MGDG, 10.134 nmol 34:0-DGDG and 22.2 nmol 36:0-DGDG and 21.2 nmol 34:0-SQDG. Per sample, 10 µL of phospholipid, galactolipid and sulfolipid standard mix were added to 10 µL sample from a 1 mL crude lipid extract in chloroform. 80 µL Q-TOF running buffer were added to the sample to ensure that NH$_4$OAc was present for the formation of ammonium adducts during nanospray ionization.

DAG and TAG Standard Mix

DAG and TAG standards were prepared by Katharina Gutbrod (IMBIO Institute, Bonn) (Gasulla *et al.*, 2013; vom Dorp *et al.*, 2013). The standards were added to the samples as internal standards prior to lipid extraction. Two different versions of TAG internal standard were used; the first version contained 10 µL DAG and TAG standard mix in chloroform/methanol (2:1) which included 1 nmol each of di14:0, di14:1, di20:0 and di21:0 or tri10:0, tri11:1, tri20:0 and tri22:1, respectively. The second version contained 0.02 nmol µL^{-1} tri17:0, tri 17:1, of which 50 µL (1 nmol) were used per sample.

Free Sterols Internal Standard

For the measurement of free sterols with GC-MS, 10 µL of cholestenol internal standard (0.1 nmol µL^{-1}) dissolved in chloroform was added prior to lipid extraction of the sample as described previously for plant samples (Wewer *et al.*, 2011).

Acyl-CoA Internal Standard

The internal standard for acyl-CoA quantification was 17:0-CoA. The dried acyl-CoA powder (5 mg) was dissolved in 500 μL MES-KOH buffer (100 mM, pH 6.0) and stored at -20°C as a super stock. For quantification, a 1000-fold dilution was prepared as working stock and 5 μL added to the dissolved lipid sample as internal standard after homogenization of the tissue. The concentration of the 17:0-CoA super stock and the working stock was quantified against 15:0 using GC-FID.

2.2.8.2 Extraction of Lipids from Plants and fungal ERM

Lipids from were extracted from plant and fungal tissue according to the two-phase separation method by Bligh and Dyer (1959). In order to minimize contamination during Q-TOF MS analysis, non-autoclaved plastic tips were used, and glass ware, especially glass pasteur pipettes, were rinsed with chloroform prior to use. In the first step of lipid extraction, formic acid was added to the solvent, to inhibit lipase-induced degradation of lipids (Browse *et al.*, 1986). Typically, 10—100 mg tissue was harvested and the fresh weight (FW) determined quickly to minimize the risk of lipid degradation. The tissue was harvested in 2 mL Eppendorf tubes, which were then quickly frozen in liquid nitrogen and immediately processed or stored at -80°C. For most lipid extractions, the tissue was homogenized with a ball mill directly in the 2 mL reaction tubes. For homogenization, ceramic beads were added to the frozen tissue and homogenized using a ball mill (Precellys) at 6000 Hz for 20 sec. To ensure complete extraction of lipids, the samples were ground a second time for 60 sec in the presence of two volumes (1 mL) of the extraction solvent (chloroform/methanol/formic acid, 1:1:0.1). For acyl-CoA extraction and extraction of lipids from *R. irregularis* ERM, the tissue was transferred to a pre-cooled mortar, homogenized in the presence of liquid N_2, scraped into 2 mL Eppendorf tubes and the extraction solvent added to the samples.

After the extraction solvent (together with the IS) was added, lipid degradation is inhibited and the samples can be processed at RT. Phase separation was induced by addition of 1 volume (0.5 mL) of 1 M KCl/0.2 M H_3PO_4. After vortexing and centrifugation at 5000 g for 5 min, the lower organic phase was collected and the remaining aqueous phase re-extracted twice with 2 volumes (1 mL) chloroform. The organic phases were combined in a fresh glass tube and dried under N_2 and stored at -20°C until solid-phase extraction (see 2.2.8.5) or measurement of lipids (see 2.2.8.7—2.2.8.10).

2.2.8.3 Extraction of Lipids from *E. coli* and *S. cerevisiae*

After expression of plant thioesterases in *E. coli,* 5 mL of induced ON-culture (16 h) was transferred into glass vials and heated at 95°C for 5 min. Lipids were extracted with 8 mL

chloroform/methanol 6:1 (v/v), the vial centrifuged at 2000 rpm for 5 min and the bottom organic phase transferred to a fresh glass vial. This step was repeated two times to ensure complete extraction of lipids. The lipid extract was stored at -20°C until solid phase extraction of free fatty acids (see 2.2.8.5).

S. cerevisiae lipids were extracted from 1—50 mL pelleted yeast cells obtained from 5— 50 mL ON cultures. Cell pellets were resuspended in 1—10 mL ddH$_2$O, heated in glass tubes at 95°C for 20 min and three volumes of chloroform/methanol 2:1 (v/v) were added. After vortexing and centrifugation for 5 min at 2000 rpm, the organic phase was harvested and the sample re-extracted twice with two volumes chloroform. Yeast total lipids were transmethylated to obtain total lipid fatty acid methyl esters, which were analyzed by GC-FID directly (see 2.2.8.9) or used to determine the position of the double bonds in unsaturated fatty acids (see 2.2.8.4).

2.2.8.4 Determination of the Double Bond Position in unsaturated Fatty Acids

For determination of the double bond position, unsaturated fatty acids were methylthiolated. During this reaction dimethyl disulfide is added to the carbon atoms of the double bond, catalyzed by iodine (Francis, 1981)(Cahoon *et al.*, 1994). The solvent from total fatty acid methyl esters from 1 mL yeast culture was evaporated. Methyl esters were dissolved in 100 µL iodine solution (60 mg mL^{-1} in diethylether) and 350 µL dimethyldisulfide and incubated for 3 h at 37°C. Next, 1 mL hexane/diethylether 1:1 (v/v) was added while gently vortexing the mixture. To neutralize the iodine, drops of 10% (w/v) Na$_2$S$_2$O$_3$ were added while strongly vortexing the mixture until it appeared colorless. The upper phase containing the methylthio-derivatives was harvested and analyzed by GC-MS (see 2.2.8.10).

2.2.8.5 Solid Phase Extraction of Lipid Extracts

Solid phase extraction was done to seperate lipid classes or individual lipids from complex lipid extracts according to their polarity. Strata® Silica SI-1 columns with unmodified silica (SiOH) as stationary phase was used.
A crude lipid extract dissolved in chloroform (see 2.2.10.2 and 2.2.10.3) was applied to a silica column previously equilibrated three times with one mL of chloroform (three times one mL for 100 mg silica and three times five mL for 500 mg silica). After application of the crude lipid extract dissolved in chloroform, the flow-through was collected and two more times one mL or 5 mL (for a 100 mg or 500 mg column, respectively) of chloroform were passed through the column. The resulting chloroform eluate contains neutral lipids, such as MAGs, DAGs, TAGs and free sterols. The less polar galactolipids were eluted with three mL acetone/isopropanol 1:1 (v/v) and the more polar phospholipids in methanol.

Individual lipid classes were seperated from complex lipids by applying a crude lipid extract dissolved in hexane to the hexane-equilibrated silica column and eluted with a hexane/diethylether gradient. The elution solvent increases in polarity due to increased proportions of diethylether (Gasulla *et al.*, 2013; vom Dorp *et al.*, 2013). Hexane is unpolar, and therefore most lipids bind to the silica column. As first fraction, TAGs were eluted with 95:5 hexane/diethylether (v/v) from the column, free fatty acids with 92:8, free sterols and DAGs with 85:15 and MAGs with 0/100.

The eluted SPE-fractions were evaporated to dryness and used for lipid measurement by Q-TOF MS/MS directly (phospholipids, galactolipids, DAGs and TAGs; see 2.2.8.7) or after derivatization with GC-FID/MS (free fatty acids, free sterols and MAGs; see 2.2.8.9 and 2.2.8.10).

2.2.8.6 Extraction of Acyl-CoA from Plants and Yeast

Acyl-CoA were extracted from plant tissue according to (Domergue *et al.*, 2005; Larson *et al.*, 2002; Larson and Graham, 2001). For *N. benthamiana* leaves and *L. japonicus* roots, the tissue was harvested, immediately frozen in liquid nitrogen in a porcelain mortar, ground with a pre-cooled pestle and 20 mg of ground tissues used per replicate for acyl-CoA extraction. The plant tissue was resuspended in 200 µL freshly prepared, pre-cooled extraction buffer. For extraction from yeast, cell pellets from 1 mL culture were frozen at –20°C, thawed on ice in 200 µL extraction buffer and cells mechanically disrupted in a Precellys homogenizer twice at 6000 rpm for 20 sec in the presence of ~50 µL glass beads (≤106 µm diameter). The samples were centrifuged at 13 500 rpm for 5 min at 4°C and the supernatant used for acyl-CoA extraction.

For quantification, 5 µL 17:0-CoA working stock was added at this point as internal standard. Lipids were removed with 200 µL hexane that was saturated with isopropanol/ddH$_2$O (20 mL hexane with 80 mL isopropanol/ddH$_2$O 1:1 v/v), the sample vortexed for several sec, centrifuged at 2000 rpm for 3 min and the upper organic phase discarded. Care was taken to not disrupt the interface and to not take out the entire organic phase, to minimize loss of acyl-CoAs that are dissolved in the lower, aqueous phase. To ensure complete removal of contaminating lipids, the extraction was repeated three more times. Five µL saturated (NH$_4$)$_2$SO$_4$ and 600 µL methanol/chloroform 2:1 (v/v) were added, the samples incubated at RT for 20 min and centrifuged at 13500 rpm for 2 min. The (NH$_4$)$_2$SO$_4$ precipitates contaminating protein and salts, while the acyl-CoAs are soluble in the organic solvent mixture and are harvested in the supernatant. The supernatants were transferred to conical glass inlets for autosampler vials (300 µL volume at once), which were placed in 2 mL Eppendorf tubes that were placed with opened lids into the SpeedVac® Vacuum Concentrator without heating to evaporate the water/methanol/chloroform. Care was taken not to over-dry the samples. Samples were overlayed with N$_2$-gas and stored at –80°C. Prior to measurement with Q-TOF LC-MS/MS (see

2.2.8.8.1) samples were dissolved in a minimal volume (~70 µL) of ddH$_2$O/acetonitrile 9:1 (v/v) containing 15 mM ammonium hydroxide, with pipetting up and down and ultrasonification.

Acyl-CoA extraction buffer	**KH$_2$PO$_4$ (50 mM, pH 7.2)**
1 mL Isopropanol	30.75 mL K$_2$HPO$_4$ (1 M)
1 mL KH$_2$PO$_4$ (50 mM, pH 7.2)	19.25 mL KH$_2$PO$_4$ (1 M)
25 µL Acetic Acid	Mix and dilute to 100 mM.
40 µL Fatty Acid-Free BSA (50 mg.mL^{-1})[b]	Dilute 100 mM K$_2$HPO$_4$/KH$_2$PO$_4$ stock to 50
b=50 mg. mL^{-1} stocks were prepared and stored as aliquots of 250 µL at –20°C.	mM, adjust pH to 7.2 with K$_2$HPO$_4$ (1 M).

2.2.8.7 Measurement of Lipids by Q-TOF MS/MS

Lipids were analyzed with a 6530 Accurate-Mass Quadrupole Time-of-Flight (Q-TOF) LC/MS (Agilent) mass spectrometer using either nanoflow direct infusion Chip Cube technology (see 2.2.8.7.1) or liquid chromatography coupled to electrospray ionization (ESI), Q-TOF LC-MS/MS (see 2.2.8.8). The dissolved lipid samples were injected into the ion source for ionization. The mass-over-charge ratios of positively or negatively ionized lipids or lipid adducts were scanned for in the ion selecting cell (Q1). These were collided with nitrogen collision gas in the collision cell (Q2) to achieve collision-induced dissociation with the generation of fragments, which were detected in the mass analyzer after separation in the flight-tube. The amount of lipids was calculated in relation to internal standards (see 2.2.8.1). Exact molecular masses of ions were calculated using the Agilent Mass Hunter Calculator and the distribution of isotopes was calculated with the Isotope Distribution Calculator and Mass Spectrum Plotter from Scientific Instrument Services.

2.2.8.7.1   Measurement of Lipids by Q-TOF MS/MS with Nanoflow Direct Infusion

Phospholipids, galactolipids, DAGs and TAGs were measured by Q-TOF MS/MS direct infusion with positive ionization using methods developed by Helga Peisker, Vera Wewer and Katharina Gutbrod (IMBIO Institute, Bonn). Lipids were dried, dissolved in chloroform/methanol/300 mM ammonium acetate (300:665:35), and 5–22 µL of the sample injected, depending on the type of analysis. In the ion selecting cell, targeted lists of molecular species of the respective ionized lipids were scanned and mass spectra of fragmented ions recorded at a rate of 1 spectrum per second. Table 19 in Appendix 7.8 shows the targeted lists for all lipid classes analyzed by Q-TOF MS/MS with nanoflow direct infusion and table 3 summarizes the Q-TOF MS/MS instrument settings for this configuration.

Table 3: Instrument Settings for Q-TOF MS/MS Nanoflow Direct Infusion

Part	Properties/Settings
Infusion chip	FIA Chip II flow injection and infusion
Solvent	chloroform/methanol/300 mM ammonium acetate 300:665:35 (v/v/v)
Flow rate	0.5—1 µL min^{-1}
Drying gas	Nitrogen: 8 mL min^{-1}
Ionization mode	Positive
Fragmentor voltage	200 V
Gas temperature	300°C
Injection volume per sample	5—22 µL
Chip V_{cap}	1700 V
Spectrum scan rate	1 spectrum sec^{-1}

The abundance of a charged daughter ion was used to identify the lipid after fragmentation. MGDG, DGDG, SQDG, PA, PS, PI, PE, PG, DAG and TAG were quantified based on the abundance of the product ion after subtraction of a specific neutral loss from the precursor ion (Table 4). PC was identified and quantified based on precursor ion scanning for the ion with m/z 184.0739.

Table 4: Parameters of Lipid classes for Quantification with Q-TOF MS/MS Nanoflow Direct Infusion

Lipid Class	Collision Energy (V)	Neutral loss (m/z)	Product Ion (m/z)
MGDG	12	179.0556	
DGDG	17	341.1084	
SQDG	19	261.0518	
PA	20	115.0034	
PS	22	185.0089	
PI	20	277.0563	
PE	20	141.0190	
PG	20	189.0402	
PC	35		184.0739
DAG	20	NL of the FA	
TAG	20	NL of the FA	

2.2.8.7.2 Data Analysis for Quantification of Lipids by Q-TOF MS/MS with Nanoflow Direct Infusion

Mass spectrums and chromatograms were visualized with the Agilent Mass Hunter Qualitative Analysis Software (Version B.06.00). To calculate molar quantities, ion counts of product ions of endogenous lipids and lipid standards were exported to Microsoft Excel 2013. The counts from four iterations of mass selection, fragmentation and detection were averaged per molecular species. Lipids that differ from each other only in the occurrence of a single double bond in their fatty acids differ in their m/z values by two hydrogen atoms (m/z =2), and therefore the presence of naturally occurring $^{13}C_2$ isotopes can lead to isotopic overlap (Ejsing *et al.*, 2006). To account for isotopic overlap, the probability of a fragment ion containing two ^{13}C atoms was

calculated and subtracted from the respective lipid molecular species. For most glycolipid analyses, two different internal standards (see 2.2.8.1) were used. Their detector signal response can vary due to differences in their m/z values. In general, smaller molecules are better ionized and their abundance might be overestimated. To correct for this inaccuracy, a trend function of m/z against ion counts was calculated for the two internal standards and this value used to divide the ion counts of the molecular species from the tissue to be analyzed. The isotope-and trend-corrected ion counts were then used to calculate molar concentrations of lipids in relation to internal standard signal and tissue weight.

2.2.8.8 Measurement of Lipids by Q-TOF LC-MS/MS

For measurement of fatty acids, acyl-CoA and acyl-ACP, the Q-TOF was operated with electrospray ionization (ESI) with normal flow. Table 5 summarizes the instrument settings for Q-TOF LC-MS/MS. To achieve separation of analytes, a reverse-phase column (C8 or C18) for liquid chromatography (LC) was installed. The sample was injected onto the column in a polar solvent and lipids retained on the unpolar stationary phase. Elution was achieved with a gradient of an unpolar solvent.

Table 5: Instrument Settings for Q-TOF LC-MS/MS

Flow rate	$0.2—0.5$ mL min^{-1}
Drying gas	Nitrogen: 8 mL min^{-1}
Fragmentor voltage	200 V
Gas temperature	300°C
Injection volume per sample	$20—35$ µL
Chip V_{cap}	1700 V
Spectrum scan rate	1 spectrum sec^{-1}

For acyl-CoAs and acyl-ACPs, the mass spectrometer was utilized in MS/MS mode with positive ionization. Upon ionization, different adducts of ions are formed that differ in their suitability for subsequent fragmentation and detection. For acyl-CoAs, H$^+$-adducts were selected and for acyl-ACPs, NH$_4^+$-adducts (see appendix 7.8, Table 19). Selected ions (Q1) were fragmented in Q2 and the fragment ions seperated in the ToF and quantified, similar to glycerolipid analysis (see 2.2.8.7). Table 6 shows the optimized collision energies and neutral losses.

Table 6: Parameters of Lipid Classes for Quantification with Q-TOF LC MS/MS

Lipid Class	Collision Energy (V)	Neutral Loss (m/z)
Acyl-CoA	35	506.9960[a]
Acyl-ACP	45	413.1432, 315.1663[b]

[a]=Neutral loss of 506.9960 (m/z) corresponds to adenosine-3'-phosphate-5'-diphosphate.
[b]=Neutral loss of 413.1432 (m/z) corresponds to aspartic acid-serine-leucine with 4'-phosphopantetheine(DSLp), 315.1663 corresponds to aspartic acid-serine-leucine (DSL) with phosphate from the 4´-phosphopantetheine

2.2.8.8.1 Acyl-CoA

Extracted Acyl-CoAs (see 2.2.8.6) were seperated with reverse-phase chromatography using silica modified with C8 alkyl chains as stationary phase with an unpolar solvent gradient (Domergue *et al.*, 2005; Larson *et al.*, 2002; Larson and Graham, 2001), see table 7 and table 8.

Table 7: Parameters for Acyl-CoA Analysis with Q-TOF LC-MS

Flow rate	0.5 mL min^{-1}
LC Column	Knauer Eurospher-II RP8 (150x 3 mm)
Solvent A	Acetonitrile + 15 mM NH$_4$OH
Solvent B	ddH$_2$O/Acetonitrile 9:1 (v/v) + 15 mM NH$_4$OH (final concentration)
Solvent C	ddH$_2$O/Acetonitrile 3:7 (v/v) + 0.1% Formic Acid (final concentration)
Ionization	Positive
MS mode	MS/MS

Table 8: Liquid Chromatography Gradient for Acyl-CoA

Time (min)	Solvent A (%)	Solvent B (%)	Solvent C (%)
0	0	100	0
5	25	75	0
11	100	0	0
13	100	0	0
15	0	0	100
18	0	0	100
20	0	100	0
20.1	0	100	0

2.2.8.8.2 Acyl-ACP

After enzymatic synthesis of acyl-ACPs (see 2.2.6.3), their purity and identity was confirmed by Q-TOF LC-MS/MS. To prepare acyl-ACPs as standards for chromatography and mass spectrometry, they were digested with endoproteinase Asp-N as described previously (Bates *et al.*, 2014; Kim *et al.*, 2015). 50 μL of acyl-ACP (dissolved in 10 mM MES pH=6.1) were mixed with 50 μL MOPS 50 mM pH=7.6 to ensure that the pH was above 7.0 for optimal Asp-N activity. Two μL (80 ng) of Asp-N endoproteinase (Promega) were added, incubated at 37°C for 2 h and the reaction stopped by addition of 70 μL methanol. The Asp-N endoproteinase specifically hydrolyses the peptide bonds at the N-terminal side of aspartic acid and leucine residues. In acyl-ACPs of Arabidopsis and many other organisms (e. g. *E. coli*), aspartic acid and leucine flank the serine group where the 4'-phosphopantetheine arm is attached to the fatty-acyl chain, thereby releasing acyl-4'-phosphopantetheine-aspartic acid-serine-leucine from the mature acyl-ACP upon endoproteinase digestion. The resulting acyl-phosphopanthteine-tripeptide limb is small

enough for mass spectrometry. Per sample, 30 µL of digested acyl-ACP was injected onto the instrument prior to separation on a reverse phase (C18) column (Macherey & Nagel Nucleoshell Bluebird RP18). For details, see tables 9 and 10.

Table 9: Parameters for Acyl-ACP Analysis with Q-TOF LC-MS

Flow rate	0.2 mL min^{-1}
LC-Column	Macherey & Nagel Nucleoshell Bluebird RP18 with pre-column
Solvent A	Acetonitrile/10 mM Ammonium Formate + 10 mM Formic Acid 1:9 (v/v)
Solvent B	Acetonitrile/10 mM Ammonium Formate + 10 mM Formic Acid 9:1 (v/v)
Ionization	Positive
MS mode	MS/MS

Table 10: Liquid Chromatography Gradient for Acyl-ACP

Time (min)	Solvent A (%)	Solvent B (%)
0	100	0
3	100	0
3.1	85	15
12	0	100
17	0	100
19	100	0
30	100	0

2.2.8.8.3 Fatty Acids

The method for ^{13}C-quantification in fatty acids with Q-TOF LC-MS was initially developed by Katharina Gutbrod (IMBIO Institute, Bonn). Prior to the measurement, esterified fatty acids were saponified by alkaline hydrolysis to obtain free fatty acids following an protocol adopted from the Cyberlipid Center (www.cyberlipid.org). Crude lipid extracts (see 2.2.8.2) were evaporated, dissolved in 3 mL methanol/KOH (3 M) 9:1 (v/v) and incubated for 1 h at 80°C. After cooling, the reaction was neutralized by addition of 300 µL concentrated HCl and fatty acids extracted after addition of 500 µL hexane. The hexane was evaporated and the free fatty acids dissolved in acetonitrile prior to injection.

Free fatty acids were ionized in the negative mode, generating [M-H]$^-$ ions due to their carboxyl groups. Their fragmentation pattern is of little use for identification and quantification and therefore, the ion counts for fatty acids were extracted from a full ion scan (m/z 100=1300) without fragmentation (Q-TOF LC-MS as only the first quadrupole is utilized without fragmentation). The sample was dissolved in 300 µL acetonitrile, 30 µL injected and the flow rate set to 0.2 mL min^{-1}. A previously published chromatography gradient was used for separation of free fatty acids by liquid chromatography (Kortz *et al.*, 2013). For details see table 11 table 12.

Table 11: Parameters for Fatty Acid Analysis with Q-TOF LC-MS

Flow rate	0.2 mL min^{-1}
LC-Column	Knauer Eurospher-II RP8 (150x 3 mm)
Solvent A	ddH$_2$O/Acetonitrile/Formic Acid 63:37:0.02 (v/v/v)
Solvent B	Isopropanol/Acetonitrile 1:1 (v/v)
Ionization	Negative
MS mode	MS only

Table 12: Liquid Chromatography Gradient for Fatty Acids

Time (min)	Solvent A (%)	Solvent B (%)
0	100	0
18	0	100
22	0	100
22.2	100	0
30	100	0

2.2.8.8.4 Data Analysis for Quantification of Lipids by Q-TOF LC-MS/MS

Chromatograms from acyl-CoA and acyl-ACP chromatography were analyzed with Agilent Mass Hunter Qualitative Analysis Software (Version B.06.00). Peak areas (ion counts) were integrated and the results exported to Microsoft Excel 2013. The ion count for each analyte was recorded as the main product ion after fragmentation (for LC-MS/MS) or without fragmentation (LC-MS). Molar quantities were calculated in relation to internal standard peak areas, and normalized to tissue weight or optical density of a culture in the case of yeast.

Evaluation of ^{13}C-labeled fatty acid isotopologs was done with Agilent MassHunter Quantitative Analysis for Q-TOF (Version B.07.00). Fatty acid ion abundancies were extracted from the total ion chromatogram by scanning for the molecular ions [M-H]$^-$ without fragmentation. The peaks in the resulting extracted ion chromatogram (EIC) were manually integrated for every fatty acid isotopolog, exported to Microsoft Excel 2013 and used for quantification of unlabeled ^{12}C fatty acid and ^{13}C-labeled fatty acid isotpologues after subtraction of naturally occurring ^{13}C (see 2.2.9.2), in relation to internal standard and tissue weight.

2.2.8.9 Analysis of Fatty Acids Methyl Esters by Gas Chromatography Flame Ionization Detection

Non-labeled fatty acid quantification was performed by analysis of fatty acid methyl esters (FAME) on a gas chromatograph (GC) with flame ionization detection (FID). Esterified fatty acids were transmethylated from lipids by acidic catalysis, which transfers the ester bound fatty acid to a methyl group, generating fatty acid methyl esters. Dried lipid extracts were dissolved in 1 mL 1 N methanolic HCl and incubated for 30 min at 80°C. 1 mL 0.9% (w/v) NaCl and 1 mL hexane were added, samples mixed and phases seperated by centrifugation (3 min, 2000 g). The upper

hexane phase containing the unpolar, volatile FAMEs was harvested and directly applied to the GC or concentrated by evaporation under N_2 gas. The FAMEs were eluted from the GC column (Supelco SP-2380) with a temperature gradient starting with 100°C, increased to 160°C by 25°C/min, then to 220°C by 10°C/min and finally decreased to 100°C by 25°C/min. Table 13 summarizes the instrument settings for FAME analysis by GC-FID. Peaks in the GC-FID chromatograms were identified by their retention times compared to a rapeseed standard mixture (Supelco).

Table 13: Parameters for Gas Chromatography Flame Ionization (GC-FID)

Part	Properties/Settings
Column	Supelco SP-2380
Length	25 m
Inner diameter	0.53 mm
Film thickness	0.2 μm
Carrier gas	Helium
Flow rate	1.2 mL min $^{-1}$
Injection volume per sample	1—4 μL
H_2 flow	30 mL min $^{-1}$
Synthetic air flow	440 mL min

2.2.8.10 Analysis of Lipids by Gas Chromatography Mass Spectrometry (GC-MS)

GC-MS was used for identification of lipids based on their mass spectra. Mass spectra were compared with the National Institute of Standards and Technology (NIST) mass spectral library or by comparison to the mass spectra of in-house synthesized or purchased standards. The method was used for FAMEs, free sterols and MAGs. The analysis was conducted on a gas chromatograph (Agilent 7890) coupled to mass spectrometer 5975C inertxL MSD (Agilent). For fatty acid analysis, FAMEs were prepared as described above (see 2.2.8.9).

For free sterols and MAGs, the respective SPE fractions (see 2.2.8.5) were evaporated. Lipids were dissolved and free OH-groups silylated with 100 μL of N-methyl-N-(trimethylsilyl)-trifluoroacetamide (MSTFA) at 80°C for 30 min. MSTFA was then evaporated under N_2 gas and the samples were dissolved in hexane for injection onto the GC. Silylated compounds or FAMEs were seperated on a HP-5MS column (Agilent) using a temperature gradient starting at 150°C, increased to 280°C at 10°C/min, held for 10.5 min, and decreased to 150°C at 20°C/min (Table 14).

Upon elution from the column, compounds enter the ion source and are ionized by electron impact (EI) ionization with 69 electron volt (eV), which causes also fragmentation. The he product ion is subsequently guided by the quadrupole mass-filter analyzer to the detector. The mass filter selects ions in the range of 50-550 (m/z). One full ion scan was recorded per 2.91 seconds.

Table 14: Gas Chromatograph Parameters for GC-MS

Part	Properties/Settings
Column	Agilent HP-5MS
Length	30 m
Inner diameter	0.25 mm
Film thickness	0.25 μm
Carrier gas	Helium
Flow rate	2 mL min $^{-1}$
Injection volume per sample	1—4 μL

MAGs were present in the analyzed tissues as two regio-isomers, α and β, depending on the position of the acyl chain on the glycerol backbone. In the α-MAG isomer, the acyl chain is esterified to *sn*-1 or *sn*-3 of *sn*-glycerol, while in β-MAG, it is attached to *sn*-2. On the GC-column, the syliated regio-isomers were seperated and identified based on characteristic fragment ions (Destaillats *et al.*, 2010; Li *et al.*, 2007; Yang *et al.*, 2010). As the GC-MS was operated in scan-mode, the ion abundancies for MAG-isomers were extracted from total ion chromatograms (Table 20). Free sterols were also quantified based on characteristic fragment ions (see table 21) extracted from the total ion chromatogram (Wewer and Dörmann, 2014).

2.2.9 Stable ^{13}C-Isotope Labeling

2.2.9.1 Labeling with ^{13}C-Acetate

Colonized roots of *L. japonicus* with *R. irregularis* were retrieved from the substrate of the pots, washed with water and the roots submerged in 10 mL labeling buffer (20 mMMES-KOH, 0.2 (v/v) Tween 20, pH=5.6) in 50 mL falcon tubes. [[13]C$_2$]sodium acetate was added to the buffer directly at a concentration of 4 mM. The bottom half of the tube was covered with aluminum foil and the shoots exposed to continuous light for the 24 h labeling period.

2.2.9.2 Quantification of [13]C Over-Excess Label in Fatty Acid Isotopologs

Upon labeling with ^{13}C, the incorporated label from exogenously applied compounds enters the metabolism and changes the ^{13}C-pattern that now deviates from the naturally occurring ^{13}C-isotope pattern. The percentage distribution of naturally occurring ^{13}C in every fatty acid was retrieved with the Isotope Distribution Calculator and Mass Spectrum Plotter (www.sisweb.com) and subtracted from the molar quantity of the respective fatty acid isotopolog quantified with Q-TOF LC-MS. The resulting amount was designated the over-excess (OE) amount as it exceeds the threshold for natural ^{13}C abundance and therefore must have originated from the ^{13}C labeling (Keymer *et al.*, 2017). To verify this approach, a negative control without ^{13}C label was analyzed. This control showed the expected ^{13}C distribution identical to the naturally occurring ^{13}C distribution.

3   Results

3.1   The Function of *FatM* in Arbuscular Mycorrhiza Symbiosis

3.1.1   The phylogenetic Relationship of Acyl-ACP Thioesterases in Mycorrhiza Host and non-Host Plant Species reveals mycorrhiza-specific Clades

To conduct a survey of the gene repertoire of acyl-ACP thioesterases, translated coding sequences from nine plant species were aligned and used to establish an unrooted maximum-likelihood phylogenetic tree showing the relationship among mycotrophic and non-mycotrophic plants, based on the differences in amino acid sequence (Figure 4). The phylogenetic analysis returned two major clades, named FatA-type and non-FatA-type, according to their respective orthologs in *A. thaliana* FatA1/FatA2 (FatA-type) and FatB (non-FatA-type) (Jing *et al.*, 2018). The non-FatA-clade was divided into three sub-clades, FatB, FatC and FatM, named according to the *L. japonicus* sequences that were grouped there. FatA and FatB were present in AMF-host and non-host species, while FatC and FatM sub-clades were found only in AMF-hosts. In all mycotrophic plants, Fat sequences were seperated between the monocotyledons *Z. mays*, *S. bicolor* (Poaceae) and the dicotyledons *M. truncatula*, *G. max* and *L. japonicus* (Fabaceae) that were included in the phylogenic analysis.

Acyl-ACP thioesterases from different plant species differ in their substrate specificities. In general, FatA-type thioesterases prefer mostly 18:1-ACP as substrate and FatB-type act preferentially on saturated acyl-ACP with chain lengths of C8—C18 (Jing *et al.*, 2011). The acyl-ACP thioesterases specific for medium chain acyl-ACP from *Cuphea hookeriana* (*Ch*FatB2) and *Umbellaria californica* (*Uc*FatB1) were grouped to the FatB sub-clade. FatC sequences from mycorrhiza hosts were more closely related to the FatB sub-clade than to the FatM sub-clade, which is the most distant of the three non-FatA-type sub-clades. This reveals that mycorrhiza hosts have probably acquired two more copies of non-FatA-type acyl-ACP thioesterases during their co-evolution with AMF. Of these two (*FatC* and *FatM*), only *FatM* exhibited a mycorrhiza-specific gene expression pattern (see appendix 7.3) and was therefore selected as candidate to investigate symbiotic lipid transfer.

3.1.2   Isolation of *fatm* mutant Plants and Analysis of Mycorrhiza-dependent Gene Expression

To study the function of *FatM*, a reverse genetic approach was conducted using mutant alleles that contain transposon insertions upstream of the *FatM* start codon. The Lotus *FatM* nucleotide sequence (chr5.CM0328.70.nd) was blasted against the flanking sequences of the Lotus Retrotransposon (LORE1) mutant database to identify transposon insertions in the *FatM* gene.
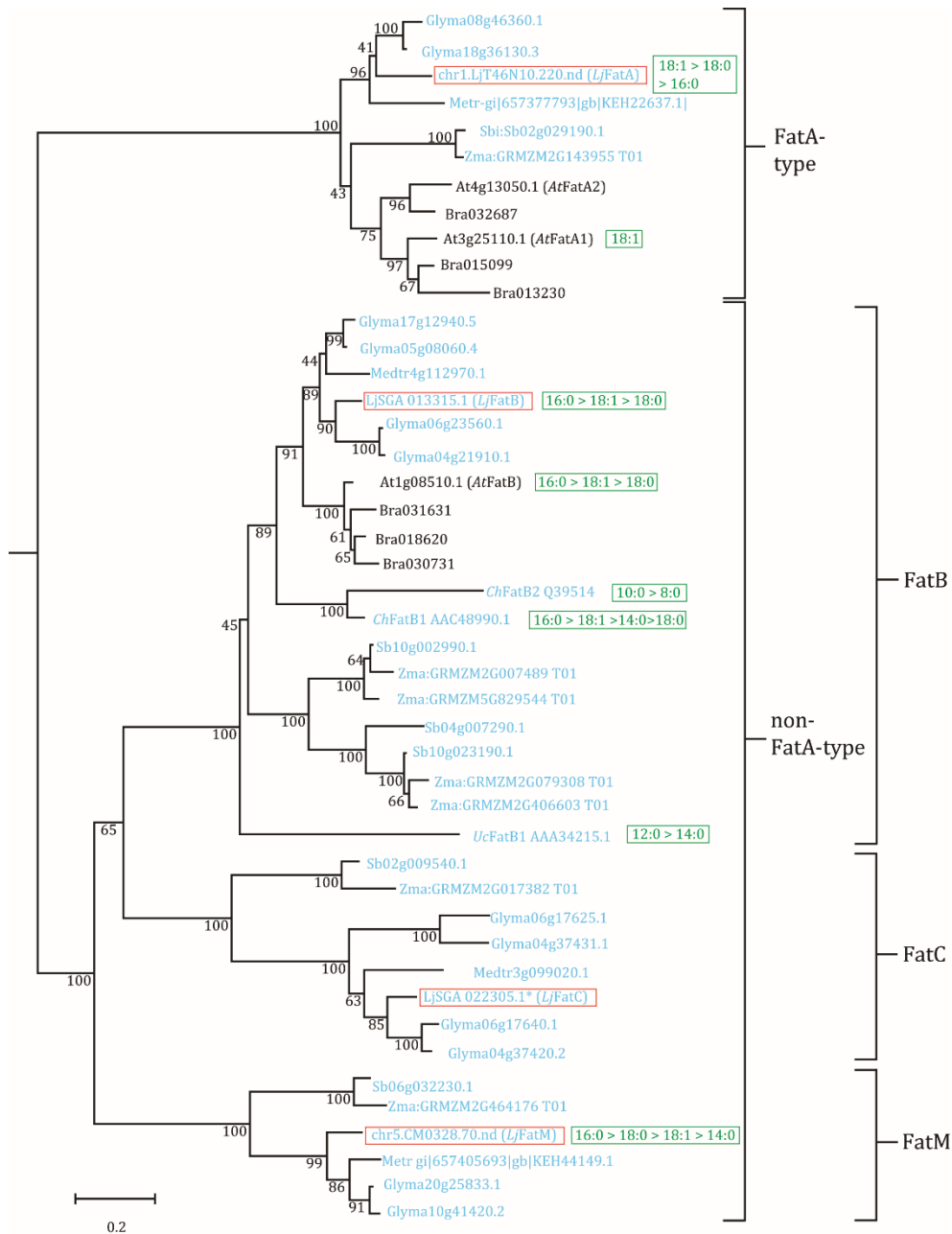
Figure 4: Phylogenetic Tree of acyl-ACP Thioesterases from AM Host and Non-Host Plants.
Amino acids sequences were aligned with ClustalX using MEGA v 6.0, and a maximum-likelihood tree
was constructed. The numbers on the branches indicate boot-strap values (1000 iterations). At,
Arabidopsis thaliana; Bra, *Brassica rapa*; Ch, *Cuphea hookeriana*; Glyma, *Glycine max*; Lj, *L. japonicus*;
Medtr, *Medicago truncatula*; Sb, *Sorghum bicolor*; Uc, *Umbellularia californica*; Zma, *Zea mays. Lotus*
sequences are highlighted with red boxes. Mycotrophic plants are highlighted in blue, non-mycotrphic
plants are depicted in black. The experimentally verified preferences for different acyl-ACPs of the
thioesterases are indicated in green boxes next to the protein name in the order of substrate
preference. *Ch*FatB1 (Jones et al. 1995); *Ch*FatB2 (Dehesh et al. 1996); *Uc*FatB1 (Voelker et al. 1992);
*At*FatA1, *At*FatB (Salas and Ohlrogge 2002); *Lj*FatA, *Lj*FatB, *Lj*FatM (this work).

T3 seeds of plants containing insertions were obtained, plants grown and genomic leaf DNA used for genotyping of the insertion. Two independent *fatm* mutant alleles, designated *fatm*-1 ("G63", LORE1 Plant ID: 30003218) and *fatm*-2 ("D20", LORE1 Plant ID: 30052489), carrying LORE1-insertions 218 bp and 248 bp upstream of the start codon (Figure 5a) were selected for mycorrhiza-colonization experiments. The mutant plants were confirmed to be by PCR (Figure 5b).

The two independent alleles of the homozygous insertion lines showed decreased *FatM* gene expression upon colonization with *R. irregularis* at 4 wpi and 7 wpi (Figure 5c, d). In *fatm*-1 and *fatm*-2, at 4 wpi, no gene expression was observed and at 7 wpi, it was reduced in relation to the WT control. This shows that although the two lines do not represent null mutations, *FatM* expression is strongly affected. Expression of *FatA*, *FatB* and *FatC* remained unchanged upon colonization, either at 4 wpi or 7 wpi in both *fatm* mutant alleles. In the colonized *fatm* mutant lines, expression of the plant mycorrhiza-marker *PHSOPHATE TRANSPORTER 4* (*PT4*), was strongly reduced in *fatm*-1 and absent from *fatm*-2 at 4 wpi, while expression was recovered at 7 wpi to a level similar to WT. The same expression pattern was detected for the fungal housekeeping gene *α-TUBULIN* that was reduced at 4 wpi, but similar to WT at 7 wpi. These data indicate that colonization is strongly reduced at 4 wpi but can be recovered at to some degree at 7 wpi.

3.1.3 The *fatm* Mutation affects Root Colonization and Lipid Storage in *R. irregularis* and symbiotic Phosphate Transfer to the Plant

To quantify root colonization parameters in *fatm* mutant plants, fungal cell walls were stained in colonized roots and investigated under a bright-field microscope (Figure 6a—d). Using the modified grid-line intersection method, the relative frequency of fungal structures was quantified in the samples harvested at 4 and 7 wpi (Figure 6a). The percentage of hyphae, arbuscules, vesicles and total colonization (either one of the preceding) was decreased in colonized *fatm*-1 and *fatm*-2 root systems at 4 wpi. Arbuscule and hyphae frequency was recovered to WT levels in *fatm*-2 at 7 wpi, but remained decreased in *fatm*-1. In the WT and the two *fatm* mutant lines, the frequency of fungal structures was increased at 7 wpi relative to 4 wpi. Vesicles frequency was consistently decreased in the two mutant alleles at 4 wpi and 7 wpi, but to a greater extend in *fatm*-1, especially at 7 wpi.

Fungal arbuscules are dynamic structures that undergo programmed degeneration and generation cycles, dependent on the host plant (Gutjahr and Parniske, 2013). Mutations of plant genes essential for AMF symbiosis can lead to the premature degeneration of arbuscules, causing the occurrence of stunted arbuscules (Breuillin-Sessoms *et al.*, 2015; Floss *et al.*, 2017). Therefore, it was investigated whether stunted arbuscules are also found in the Lotus *fatm* mutant roots.
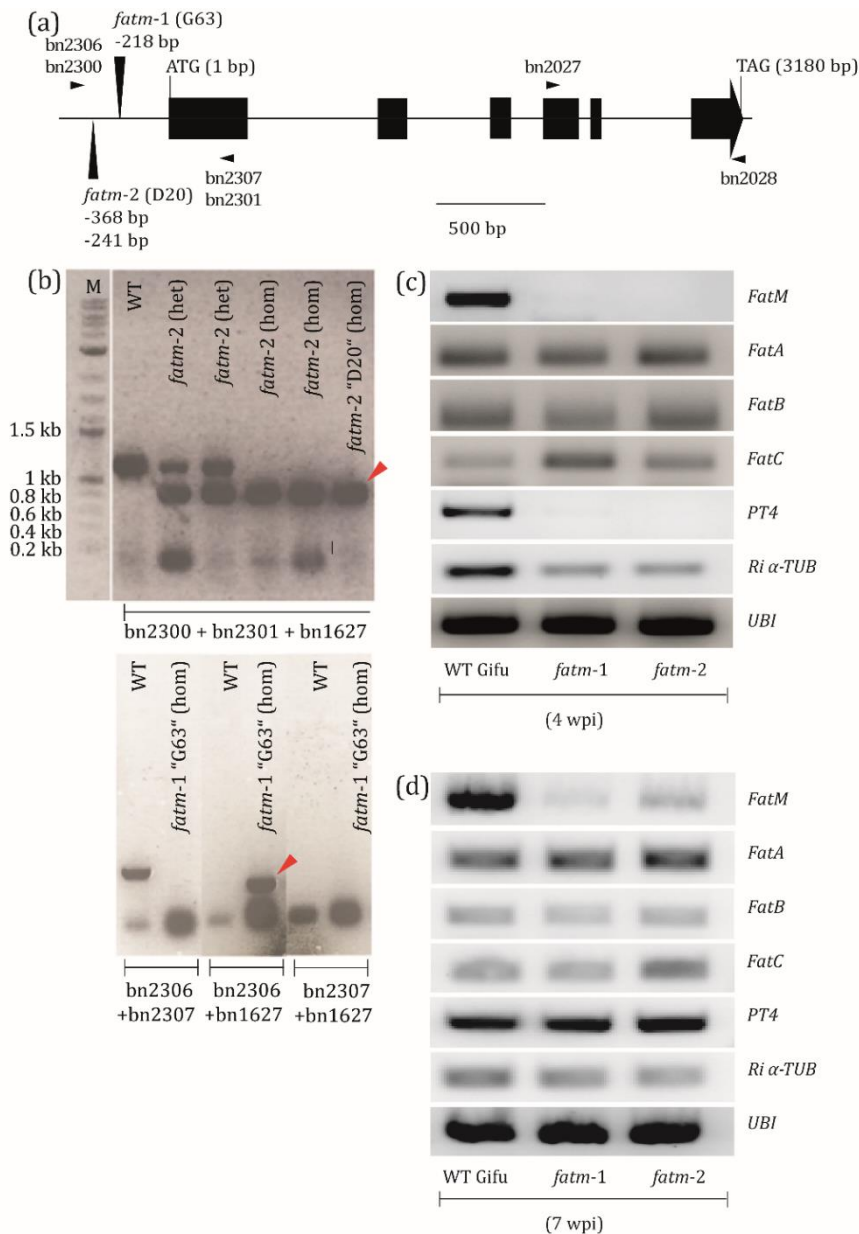
Figure 5: Isolation of *FatM* Insertional Mutants and Mycorrhiza-induced Marker Gene Expression.

a) Scheme for the *L. japonicus FatM* gene depicting exons (black boxes), introns (solid line), the position of the LORE1 transposon insertions in *fatm*-1 and *fatm*-2 (black triangles), start codon (ATG), stop codon (TAG) and the position of primers (black arrowheads). The exact position of the insertion was determined by sequencing the PCR product of *fatm*-1 genomic DNA (using the primers bn2306+bn1627) with bn2306, and by sequencing the PCR product of *fatm*-2 genomic DNA (using bn2300+bn1627) with bn2300. The primers bn2027+bn2028 were used for RT-PCR.

b) PCR products of touchdown-PCR with the primers for genotyping. The PCR reaction for *fatm*-2 was pipetted in a single reaction containing the transposon-specific primer bn1627 and the gene primers bn2300 and bn2301. In *fatm*-1, three seperate reactions were performed with bn2306/bn 2307, bn2306/bn1627 and bn2307/bn1627. Homozygous insertion lines show a PCR product with the forward gene primer and bn1627 (red arrowheads). Plant lines that were kept for seed propagation for use in the subsequent experiments are indicated as "D20" and G63". M, Marker; Het, heterozygous; Hom, homozygous.

c, d) Semi-quantitative RT-PCR using primer bn2027+ bn2028 with cDNA synthesized from total root RNA of WT, *fatm*-1 and *fatm*-2 after colonization with *R. irregularis* for 4 and 7 weeks. Thioesterases and mycorrhiza marker genes were amplified in 30 PCR cycles. As control for RNA loading, *UBIQUITIN* was amplified. *Fat*, Acyl-*ACP thioesterase*; *PT4, PHOSPHATE TRANSPORTER 4*; *Ri α-TUB, R. irregularis alpha-TUBULIN, UBI, UBIQUITIN*.
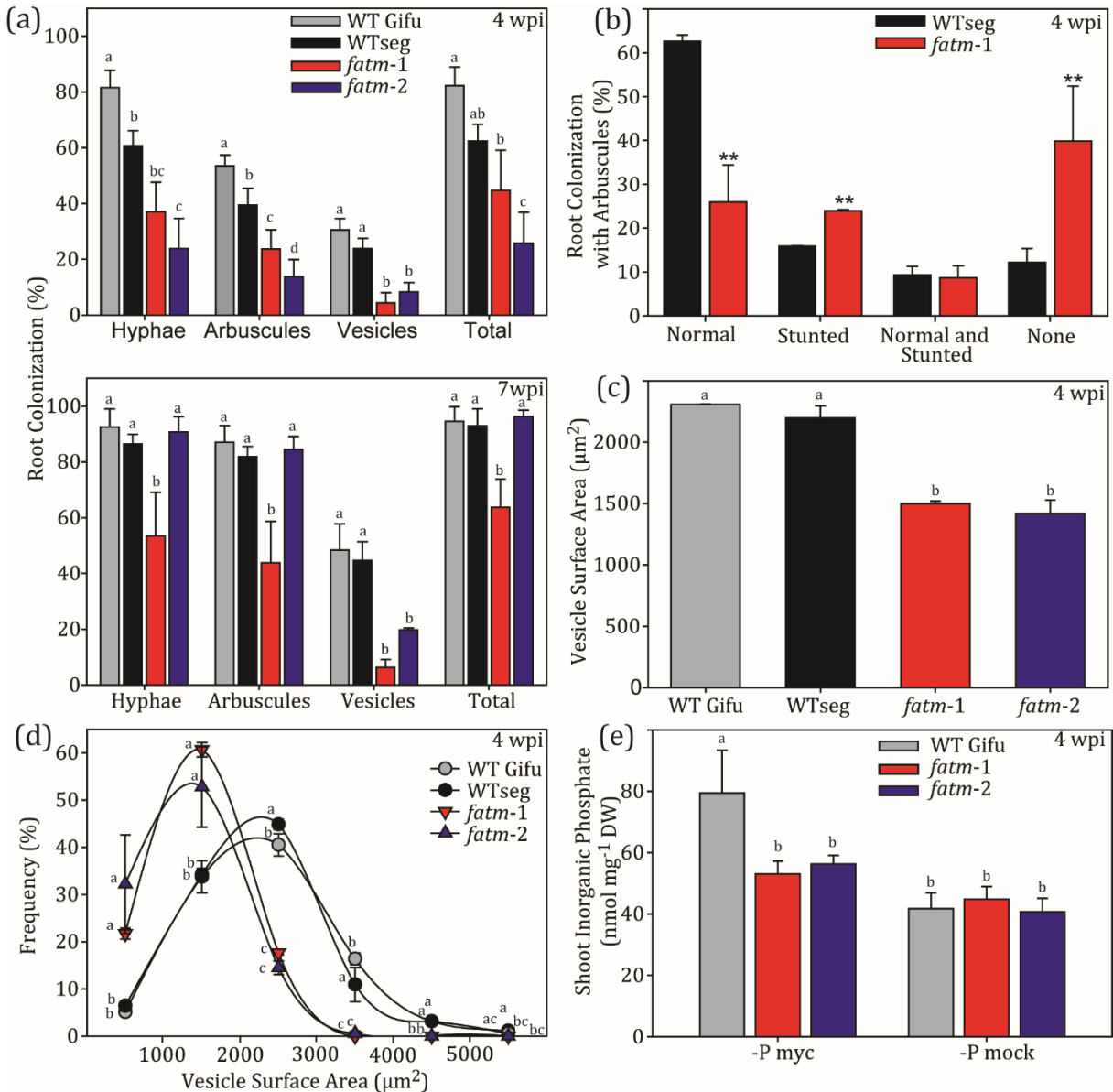
Figure 6: Colonization Parameters and symbiotic Phosphate Uptake in colonized *fatm* and WT Roots.

a) Colonized roots were stained with ink-vinegar, fungal structures (hyphae, arbuscules, vesicles) counted and expressed as % of total spots counted. This was done with five independent root systems harvested at 4 and 7 wpi (n=5).

b) At 4 wpi, roots were used for quantification of the distribution of different types of arbuscules in the arbuscule population in *fatm*-1 and WT. n= four independent root systems.

c) Vesicle surface area was measured in the same root systems that were used in **a)**.

d) The frequency of the measured vesicles in **c)** in the root systems. Vesicles were placed in categories according to their size: 0—1000 μm^2, 1000—2000 μm^2, 2000—3000 μm^2, 3000—4000 μm^2 and 4000—5000 μm^2, counted and divided by the total number of vesicles.

For **c)** and **d)**, five independent root systems were counted (n=5).

e) Inorganic shoot phosphate was quantified photometrically in shoots harvested from mycorrhiza-inoculated plants. Results –P myc are from at least eight independent leaf samples from three different pots and –P mock are from at least three individual leaf samples from single pots. –P myc, infected with *R. irregularis*; –P mock, inoculated with carrier material.

WT Gifu, Wild type ecotype Gifu; WT seg, LORE1 segregating wild type allele of *fatm*-1. All graphs represent average values, error bars depict standard deviation. In **a,c—e** one-way ANOVA with post-hoc Tukey, different letters indicate significant differences (P < 0.05). In **b)**, students t-test (**P < 0.01).

To do so, the frequency of different types of arbuscules was scored in the entire arbuscule population (Figure 6b). On the one hand, WT-like arbuscules, which appear in the bright-field microscope as densely packed, fully branched squares that fill the entire cavity of the cortex cell, were very abundant in WT and to a lesser extent in *fatm*-1. On the other hand, small, shriveled mutant arbuscules were enriched in *fatm*-1.

The latter were called "stunted" to differentiate them from arbuscules that were regularly degenerated after reaching the end of their lifespan. Such degenerated arbuscules can also be observed in colonized WT roots, albeit these were most often found in the vicinity of vesicles, indicating a progression in the mycorrhiza life cycle. Vesicles in mycorrhiza symbiosis are storage organs for mainly triacylglycerol and glycogen (Smith and Read, 2008). Vesicles were formed in both WT and *fatm* mutants, but less frequently in the latter. Vesicles in *fatm*-1 and *fatm*-2 were also smaller (Figure 6c). To visualize these changes in detail, the vesicles were organized in categories according to their size. The two *fatm* alleles showed an accumulation of small-sized vesicle of categories from 0—1000 μm, 1000—2000 μm and a decrease in vesicle size categories 2000—3000 μm and 3000—4000 μm while very large ones of 4000—5000 and > 5000 μm were absent (Figure 6d).

AMF deliver phosphate to the plant. As AMF colonization and symbiotic phosphate transporter (*PT4*) gene expression were affected in *fatm* mutant roots, the efficiency of symbiotic phosphate transfer was investigated. Upon colonization with mycorrhiza fungi, *PT4* is expressed in the periarbuscular membrane responsible for phosphate transport to the plant cytoplasm (Harrison *et al.*, 2002). Free inorganic phosphate serves as a measure of plant phosphate nutritional status (Chapin and Bieleski, 1982). Free inorganic phosphate was measured and compared between shoots of mycorrhiza-inoculated WT and *fatm* mutant plants (Figure 6e). The colonized mutant plants contained the same amounts of inorganic phosphate as the mock-inoculated WT and mutants. Mycorrhiza colonization elevated phosphate content in colonized WT shoots to 79.4 μmol mg^{-1} DW, which represents an increase by ~33% relative to colonized *fatm*-1. This result demonstrates that the deficiency in mycorrhiza colonization in *fatm* has a negative impact on the host nutrient status and also likely on plant performance.

3.1.4 Arbuscule Branching is distorted in *fatm*-1

To study fungal arbuscule morphology in *fatm* mutants in detail, the fungal cell wall was stained with a WGA-conjugated fluorophore (WGA-Alexa Fluor 488) and stained roots inspected with a confocal laser scanning microscope (Figure 7). The colonized root cortex exhibited regions where the arbuscules had stunted appearances. These arbuscules were shrunken and less abundant, compared to healthy, WT arbuscules. The stunted arbuscules stopped their development and therefore exhibited less extensive hyphal fine branching that led to their shriveled appearances. Besides stunted arbuscules, normal arbuscules were also identified in the

two mutant alleles. Stunted arbuscules in *fatm*-1 and *fatm*-2 generally occurred in the neighborhood of other stunted arbuscules, despite of the root being extensively colonized with intraradical hyphae. This led to the occurrence of root regions where exclusively stunted arbuscules appeared (see Figure 7 for examples in *fatm*-1 and *fatm*-2). These are likely the result of abortion of the whole infection unit. Arbuscule degeneration is a regular feature of mycorrhiza intracellular growth that is also observed, although with lower frequency, in WT.
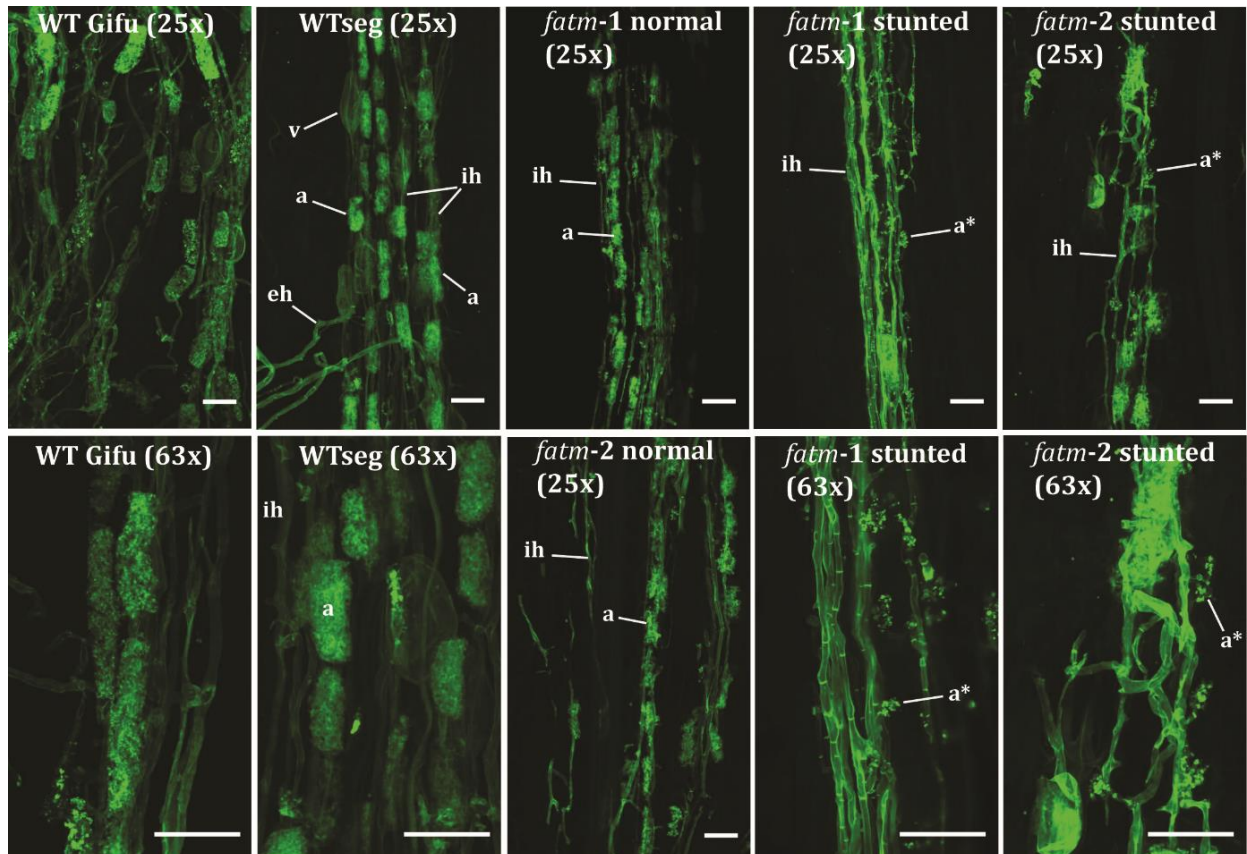
Figure 7: Stunted Arbuscules appear in colonized *fatm* Mutants.
Roots of colonized WT Gifu, WT seg and both *fatm* mutant alleles were colonized for 4 weeks with *R. irregularis*. The fungus was stained with WGA Alexa Fluor 488, and stained roots investigated with Confocal Laser Scanning Microscopy with excitation at 488 nm and emission at 500—550 nm. Two types of maginifcations were used, 25-fold (25x) and 63-fold (63x). In WT, arbuscules are formed by extensive branching of the invading hyphae, the resulting arbuscules appear as squares filling the entire cavity of the cortex cell. In *fatm*-1 and *fatm*-2 mutants, arbuscules branching was arrested, giving rise to stunted arbuscules that remaining small in comparison. Besides stunted arbuscules, normal, fully branches arbuscules were occasionally present in both *fatm*-1 and *fatm*-2. Fungal structures are indicated by letters and lines; v, vesicles; a, fully-branched WT arbuscule; eh, extraradical hyphae; ih, intraradical hyphae; a*, stunted arbuscule with arrested development. Bars, 50 µm.

Arbuscule degeneration is the result of programmed arbuscule senescence controlled by the plant to ensure arbuscule productivity (Floss *et al.*, 2017; Toth and Miller, 1984). It is associated with the generation of fungal vesicles and therefore indicates a general progression in the symbiosis. Contrary to degenerated arbuscules in WT, regions in the mutant roots where

stunted arbuscules occurred were generally not associated with vesicles. The hyphae in the two mutant roots exhibited regular morphology which was not affected by the *fatm* mutation. Thus, the *fatm* mutation leads to distortion of hyphal fine-branching in the later stage of arbuscule formation, causing the occurrence of stunted, immature, non-functional arbuscules. These are not associated with the progression in fungal life cycle but indicate premature abortion of a functional symbiosis.

3.1.5 Arbuscule Branching and Root Colonization is restored by genetic Complementation of *fatm*-1

To confirm that arbuscule fine-branching is distorted due to the *fatm* mutation, genetic complementation was done. To this purpose, the 2 kb promoter region upstream of *FatM* was used to express the *FatM* gene sequence. The construct was introduced into *A. rhizogenes* and employed for transient transformation of *fatm*-1 and WT *L. japonicus.* Transiently transformed *L. japonicus* roots were then inoculated with *R. irregularis* (Figure 8). To inspect AMF performance, colonization parameters were quantified and arbuscule morphology inspected. Infection sites with exclusively stunted arbuscules were still observed in *fatm*-1 containing the empty vector control. In the complemented line, arbuscles were fully developing after expression of the *FatM* gene (Figure 8a). Consistent with the restoration of arbuscule branching, the root colonization rate returned to levels almost equal to WT. This was observed with regard to total colonization and the frequency of intraradical hyphae and arbuscules (Figure 8b). Only the percentage of vesicles in the colonized roots was not complemented completely, but still increased compared to *fatm*-1 (EV). These results confirm that the *fatm* mutation caused the reduced AMF colonization and, more specifically, the arbuscule fine-branching defect.

3.1.6 Lipid with Mycorrhiza-desaturation Signature are decreased in colonized *fatm* Mutants

Mycorrhiza-colonized and non-colonized plant roots differ in their lipidome. When colonized with *R. irregularis*, the plant lipid composition is changed and in addition, lipids from the mycorrhiza fungus can be detected in colonized roots (Wewer *et al.*, 2014). To study changes in plant and mycorrhiza lipid composition, lipids were measured in colonized roots and mock-inoculated roots of WT and *fatm*-1 mutants. Colonized roots compromise a mixed sample with plant and fungal lipids, and in addition, the plant lipid composition can be changed in response to colonization with AMF.
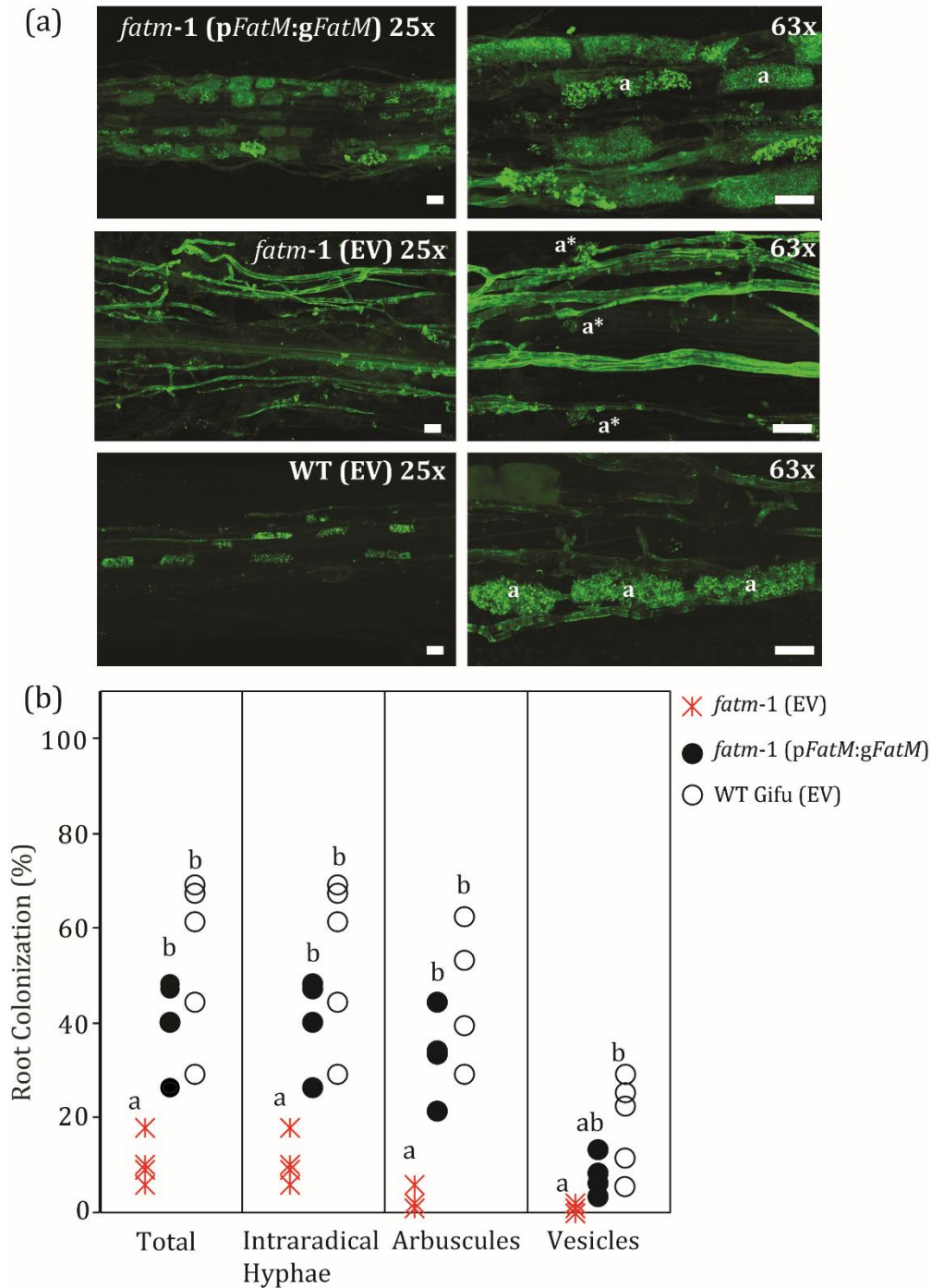
Figure 8: Genetic Complementation of defective Arbuscule Morphology in the *fatm*-1 mutant.
a) Hairy roots of *fatm*-1 were transformed with *Agrobacterium rhizogenes* carrying an empty vector (EV) or a construct with the *FatM* promoter and gene (p*FatM*:g*FatM*). After infection with *R. irregularis*, fungal structures in the roots were stained with WGA Alexa Fluor 488 and observed under a confocal microscope at 25-fold and 63-fold magnification. Stunted arbuscules were observed in *fatm*-1 (EV), but arbuscule branching was restored in *fatm*-1 complemented with *pFatM:gFatM*.
a, fully branched WT arbuscules; a*, mutant arbuscules with stunted appearance. Bars, 25 μm.
b) Quantification of colonization parameters in the same lines shown in **a)**. Fungal structures were counted with the grid-line intersection method. Different letters indicate significant differences (ANOVA; post-hoc Tukey; n = 14; $p < 0.001$) among genotypes for each fungal structure (Total, Intraradical Hyphae, Arbuscules, Vesicles). Total and intraradical hyphae, n= 14, $p \leq 0.01$; arbuscules, $p \leq 0.005$; vesicles, $p \leq 0.01$.

3.1.6.1 Glycerolipids and Fatty Acids

The membrane-forming phospholipids and galactolipids as well as non-membrane forming neutral lipids (triacylglycerol) were measured in colonized WT, *fatm*-1 and *fatm*-2. The most abundant mycorrhiza-signature fatty acid is palmitvaccenic acid (16:1ω5) (Olsson and Johansen, 2000). Additional to this marker fatty acid, the highly desaturated fatty acids 20:3, 20:4 and 20:5 are found in *R. irregularis* and not in the plant root. Another abundant fatty acid in the fungal tissue is 16:0, but this fatty acid also is a major fatty acid in the plant. Membrane forming phospholipids and galactolipids acylated with 16:1, 16:0 and 20:3/4/5 did not accumulate to the same extent in colonized *fatm* mutants as they did after colonization with mycorrhiza in the WT (Appendix 7.8).

The most abundant lipid in the fungal cytoplasm is triacylglycerol (TAG) (Olsson *et al.*, 2003). The TAG molecular species that contain mycorrhiza specific fatty acids were substantially decreased in colonized *fatm*, especially the triacylglycerols tri-16:1 (48:3), di-16:1-16:0 (48:2) and 16:1-di-16:0 (48:1) (Appendix 7.8). They are the main triacylglycerol forms in *R. irregularis* and very prominently accumulate in vesicles and spores. Diacylgycerol (DAG) molecular species with 16:0 and 16:1 were as well decreased in colonized *fatm* mutants. DAG is a precursor for TAG synthesis.

Concordantly, the reduction in membrane forming and neutral glycerolipids containing mycorrhiza-signature fatty acids in *fatm* mutant plants was also reflected in the composition of total fatty acids (Figure 9). Palmitvaccenic acid occurs only in colonized roots and was the most abundant fatty acid in WT colonized roots at 7 wpi. The degree of root colonization is reflected in the amount of 16:1ω5, as it increases during colonization (Schliemann *et al.*, 2008). At 7 wpi, 16:0, and to a lesser extent, other mycorrhiza-marker fatty acids (18:1ω7 and 20:3) accumulation in colonized *fatm* mutants. Noteworthy, the minor fatty acids 14:0, 22:0 and 24:0 accumulated in WT at 7 wpi, while they remained less abundant in *fatm*-1 and *fatm*-2, even though these fatty acids are not typical signature fatty acids for mycorrhiza fungi. The decreased amounts of mycorrhiza-signature lipids and fatty acids reflect the decrease in fungal biomass in colonized *fatm* roots, in agreement with the results obtained after root staining and microscopy (see 3.1.3). However, detailed lipid and fatty acid analysis showed in addition that the most prominent decrease is observed for 16:1/16:0-containing TAG, even after 7 wpi in *fatm*-2 (Figure 9c), which showed a similar total colonization as WT (Figure 9a). This is consistent with the decreased vesicle frequency and smaller vesicle size in the two *fatm* mutant roots (Figure 9c, d). Hence, the deficiency in storage lipid accumulation correlates with decreased vesicle frequency and occurrence of smaller vesicles.
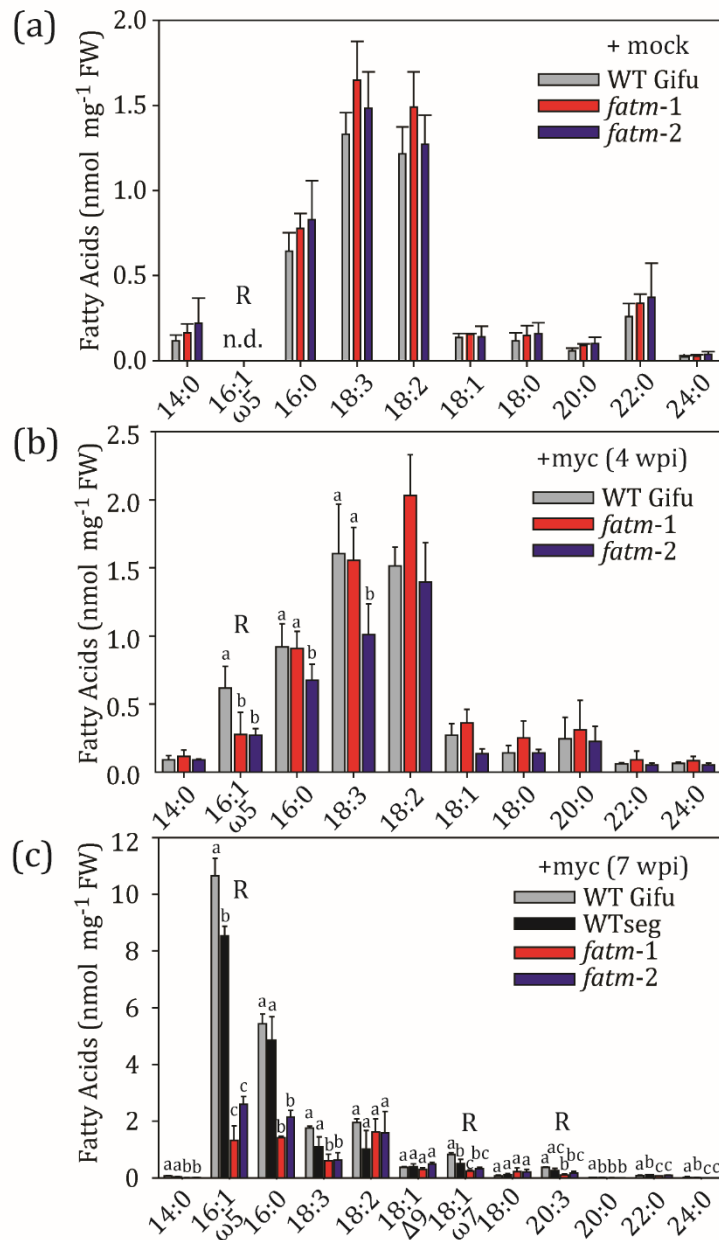
Figure 9: Comparison of Mycorrhiza-Signature Fatty Acids in total Fatty Acids from *L. japonicus* WT and *fatm* mutant Roots.

a) Total fatty acids from whole root systems of myc-inoculated WT Gifu or *fatm* mutant roots at 4 wpi (n=4).
b) Total fatty acids from whole root systems infected with *R. irregularis* at 4 wpi.
c) Total fatty acids from whole root system infected with *R. irregularis* at 7 wpi. (n=3).
Total fatty acids were hydrolyzed from crude lipid extracts via transmethylation, generating fatty acid methyl esters that were quantified by GC-FID and identified by GC-MS. Mycorrhiza signature fatty acids accumulate upon colonization with *R. irregularis*, but to a lesser extent in *fatm* mutants than in WT at 4 wpi and 7wpi.
R, Fatty acids originating from *R. irregularis*; n.d., not detected; +myc, inoculated with *R. irregularis*; +mock, inoculated with mycorrhiza carrier material; WT Gifu, Wild type ecotype Gifu; WT seg, LORE1 segregating wild type allele of *fatm*-1. All graphs represent average values, error bars depict standard deviation. One-way ANOVA with post-hoc Tukey, different letters indicate significant differences (P < 0.05).

3.1.6.2 Comparison between Neutral Lipid Fatty Acids and Polar Lipid Fatty Acids

To investigate changes in storage and membrane lipid fatty acids more closely, total lipids were seperated into two fractions: neutral lipids (storage lipids) and polar lipids (membrane lipids). Fatty acid methyl esters were then generated and quantified by GC-FID (Figure 10). In WT and *fatm* 1, the amounts of mycorrhiza-specific neutral lipid fatty acids (NLFA) were higher (7.04 nmol mg FW^{-1} for WT and 0.89 nmol mg FW^{-1} for *fatm*-1) than mycorrhiza-specific polar lipid fatty acids (PLFA) (0.66 nmol mg FW^{-1} in WT and 0.14 nmol mg FW^{-1} in *fatm* -1) (Figure 10a). In both fractions, mycorrhiza-signature fatty acids were decreased in colonized *fatm*-1, as shown before. To visualize the differential decrease between 16:1ω5 and 20:3, the fold change (WTseg/*fatm*-1) was plotted (Figure 10b).

Here, a 11-fold decrease in 16:1ω5-NLFA and a 9.7-fold decrease in mycorrhiza-specific PLFA was obtained (Figure 10a). This shows that even though 16:1ω5-NLFA is more abundant, the ratio of reduction due to the *fatm* mutation is nearly the same as for 16:1ω5-PLFA. This was also true for 20:3 fatty acid, but with an overall less ratio of reduction of 2.9 in NLFA and 2.3 in PLFA. Theseanalyses show that the main deficit of *R. irregularis* growing in *fatm*-1 is the synthesis of 16:1ω5, regardless of the lipid fraction, and 20:3 synthesis is less affected. It has previously been proposed that a 16:0 containing lipid might be the substrate for transfer to the fungus from the plant, in addition to carbohydrates (possibly glucose) (Bravo *et al.*, 2017; Keymer *et al.*, 2017). Furthermore, 16:0 is the substrate for 16:1ω5 synthesis by desaturation in the fungus (see 3.2). The deficit in accumulation of 16:1ω5 is therefore consistent with these findings and likely represents decreased 16:0 fatty acid transfer in *fatm*.

3.1.6.3 Free Sterols

The distribution of sterols in roots changes after mycorrhiza colonization, especially the free sterol and sterol ester contents increase with extended colonization (Fontaine 2001; Olsson *et al.*, 2003; Wewer *et al.*, 2014). Mycorrhiza fungi are exceptional as they do not accumulate ergosterol as most fungi, but instead contain high amounts of 24-methylcholesterol and 24-ethylcholesterol (Fontaine *et al.*, 2004; Grandmougin-Ferjani *et al.*, 1999; Olsson *et al.*, 2003) (Figure 11). 24-methylcholesterol is structurally related to the phytosterol campesterol and 24-ethylcholesterol to the phytosterol sitosterol. They could not be differentiated by GC-MS analysis. Sterol quantification in *R. irregularis* extraradical mycelium confirmed that 24-methylcholesterol and 24-ethylcholesterol make up the bulk amount of free sterols in mycorrhiza tissue (59.1 mol% and 33.0 mol%, respectively), while cholesterol, 24-ethylcholesta-5,22-dienol (structurally related to stigmasterol) and lanosterol are only minor components (Figure 11b).
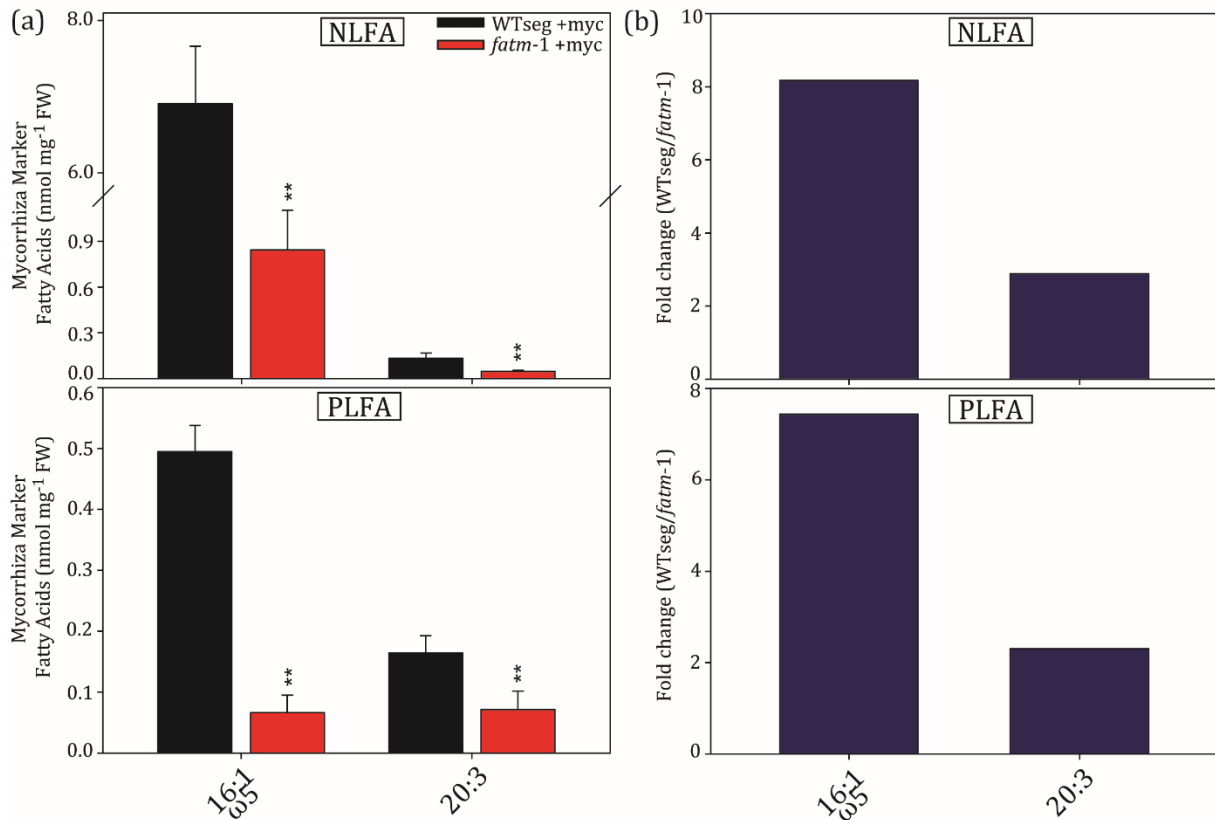
Figure 10: Mycorrhiza-Signature Fatty Acids are differentially reduced in colonized *fatm*-1 Mutants.

a) Colonized roots after seven weeks of inoculation where used to extract total lipids, which were divided by solid-phase extraction into neutral lipids and polar lipids. Fatty acids were transmethylated from lipids and measured as fatty acid methyl esters on GC-FID (n=4).

b) The amount of mycorrhiza signature fatty acids 16:1ω5 and 20:3 in the WT were divided by the amounts in *fatm*-1 to obtain the fold-change reduction in NLFA and PLFA. Albeit both fatty acids are biomarkers for mycorrhiza colonization, 20:3 shows a less severe decrease in accumulation upon mycorrhiza proliferation.

NLFA, Neutral Lipid Fatty Acids; PLFA, Polar Lipid Fatty Acids; WT seg, LORE1 segregating wild type allele of *fatm*-1. All graphs represent average values, error bars depict standard deviation. Student's t-test (**P < 0.01).

The 24-methylcholesterol content can serve as biomarker for successful colonization and interaction of the mycorrhiza fungus with the plant host (Fontaine *et al.*, 2004). Here, it was used as non-fatty acid, lipid-biomarker for mycorrhiza in the colonized *fatm*-1 and WT Lotus roots (Figure 11c, d). 24-methylcholesterol accumulated due to colonization with *R. irregularis* in the WT control to 0.347 nmol mg FW^{-1} (35.45 mol%) and remained decreased in *fatm*-1 (0.243 nmol mg FW-1; 27.32 mol%). Consequently, 24-ethylchole-sta-5,22-dienol (stigmasterol) showed a relative and absolute increase in *fatm*-1 with mycorrhiza (44.51 mol% in *fatm*-1 to 32.36 mol% in WT and 0.40 nmol mg FW^{-1} over 0.32 nmol mg FW^{-1}), possibly indicating that stigmasterol synthesis is depressed in colonized WT, but to a lesser extent depressed in colonized *fatm*-1. 24-methylcholesterol could not be distinguished from campesterol, which was detected in plant roots without mycorrhiza, although it only accounts for ~5 mol% of total free plant sterols

(Wewer *et al.*, 2014) and can therefore be neglected when using 24-methylcholesterol as mycorrhiza lipid biomarker. Free sterols are typical membrane constituents in eukaryotes (Schaeffer *et al.*, 2001) and 24-methylcholesterol therefore serves as a measure of fungal membranes in colonized roots. The decrease in 24-methylcholesterol in *fatm*-1 therefore confirms a decrease in fungal biomass as shown earlier with staining and fatty acid measurements (see 3.1.3 and 3.1.6.1).
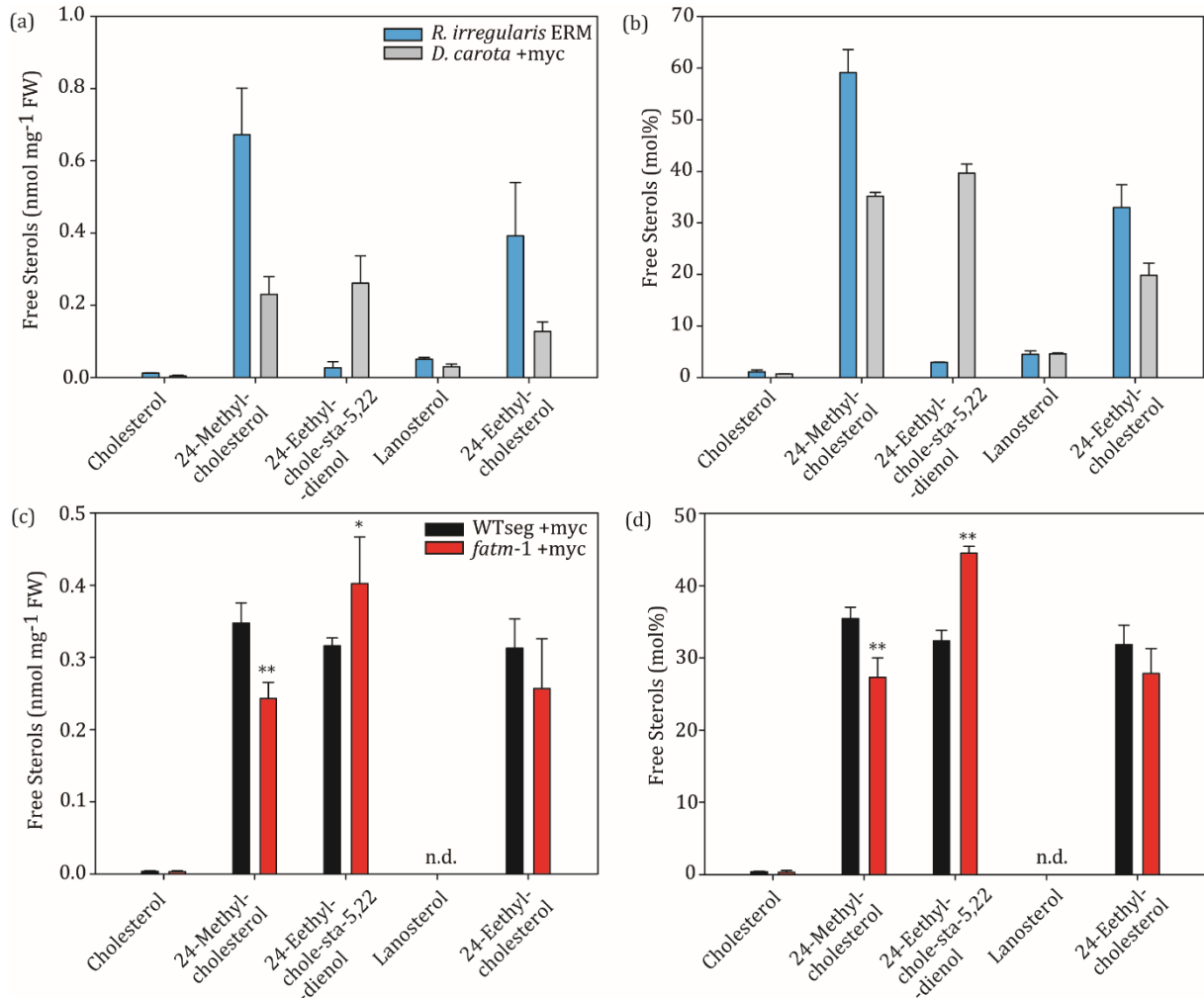
Figure 11: Membrane Sterol Lipid Quantification in *R. irregularis* extraradical Mycelium and colonized *L. japonicus* WT and *fatm*-1 Mutant Roots.
a,b) Free sterols were extracted from *R. irregularis* ERM and *D. carota* colonized roots grown in axenic root culture after 86 d. (n=6).
c,d) Free sterols were measured in colonized roots of *L. japonicus* in a WT control and *fatm*-1 mutant at 7 wpi (n=4).
Free sterols were obtained from crude lipid extracts by solid-phase extraction and measured on GC-MS as trimethylsilyl ethers. The most abundant membrane-forming sterol in *R. irregularis* is 24-methylcholesterol that is used as non-fatty acid lipid biomarker. In *fatm*-1, it fails to accumulate to the same amount as in WT, reflecting decreased amount of fungal membranes.
ERM, Extraradical mycelium; WT seg, LORE1 segregating wild type allele of f*atm*-1; +myc, inoculated with *R. irregularis*. All graphs represent average values, error bars depict standard deviation. Student's t-test (*P < 0.05; **P < 0.01).

3.1.7 β-Monoacylglycerol has a Mycorrhiza-signature and is decreased in Colonized *fatm* Mutants

Monoacylglycerol (MAG) with 16:0 fatty acid attached to the *sn*-2 position of *sn*-glycerol (ß-MAG) is the main product of the GLYCEROL-3-PHOSPHATE ACYLTRANSFERASE (GPAT) REDUCED ARBUSCULAR MYCORRHIZA 2 (RAM2) that has acyltransferase and phosphatase activity (Luginbuehl *et al.*, 2017). The *RAM2* gene is highly expressed in roots colonized with mycorrhiza, similar to *FatM* (Gomez *et al.*, 2009; Wang *et al.*, 2012). In plants, β-MAGs are precursors for the polyesters suberin and cutin that are suggested to be secreted to the apoplast (Beisson *et al.*, 2012; Yadav *et al.*, 2014). Therefore, 16:0 β-MAG could play a role in lipid secretion to the fungus. To detect MAGs with a mycorrhiza-signature, the same approach was used as described for other glycerolipids and free sterols. This approach utilizes the information from isolated extraradical mycelium (ERM) of *R. irregularis* from monoxenic root culture with *D. carota* to identify lipids specific for *R. irregularis*. These accumulate to high abundance in the ERM and to a lesser extent in the colonized roots. For a detailed investigation of MAG accumulation during spore formation, ERM was harvested from the root compartment (RC) and the fungal compartment (FC) of a *D. carota/R. irregularis* culture. ERM from the RC contained less spores than ERM from the FC, due to the space restrictions in the RC. The *sn*-1/3-acylated MAGs (α-MAG) were seperated from β-MAGs in GC-MS analysis of SPE-lipid fractions. The positional isomers of α-MAG (*sn*-1 MAG, *sn*-3 MAG) could not be seperated by GC-MS and were therefore quantified together.

Several α-MAGs were detected that accumulate in the ERM and are therefore fungal specific (Figure 12a). The most prominent one was α-MAG acylated with the signature fatty acid 16:1ω5. It accumulated to 71.96 mol% of all α-MAGs in ERM extracted from the FC, to 34.42 mol% in ERM from the RC and to 4.26 mol% in the colonized roots (Figure 12b). The same signature was observed for 20:5, 20:4 and 20:3 α-MAGs, albeit these were under the detection limit for the samples from the root compartment and the colonized roots and accumulated to a smaller degree in the ERM from the FC (20:3 to 0.23 mol%). In ERM from the FC, the number of spores is greatly increased. Thus, with increasing spore number, the amount of 16:1ω5 α-MAG also increased. This was also true for the absolute amount of 16:0 α-MAG, which is a MAG species that occurs in the plant and the fungus. However, when plotted in mol% of all α-MAGs (Figure 12b), the increase in 16:1ω5 α-MAG in fungal tissue was accompanied by a relative decrease of 16:0 α-MAG. The relative proportion (mol%) was reduced from 60.63 mol% in colonized roots to 49.82 mol% in ERM (RC) and to 22.41 mol% in ERM (FC). Most MAG molecular species were also detected in the β configuration, but their overall concentration was less than α-MAGs (Figure 12c,d). The distribution of mycorrhiza-marker β-MAGs was the same as for α-MAGs. 16:1ω5 β-MAG was the most abundant marker and the absolute amount also decreased when less fungal biomass was present in the sample (FC>RC>colonized roots).
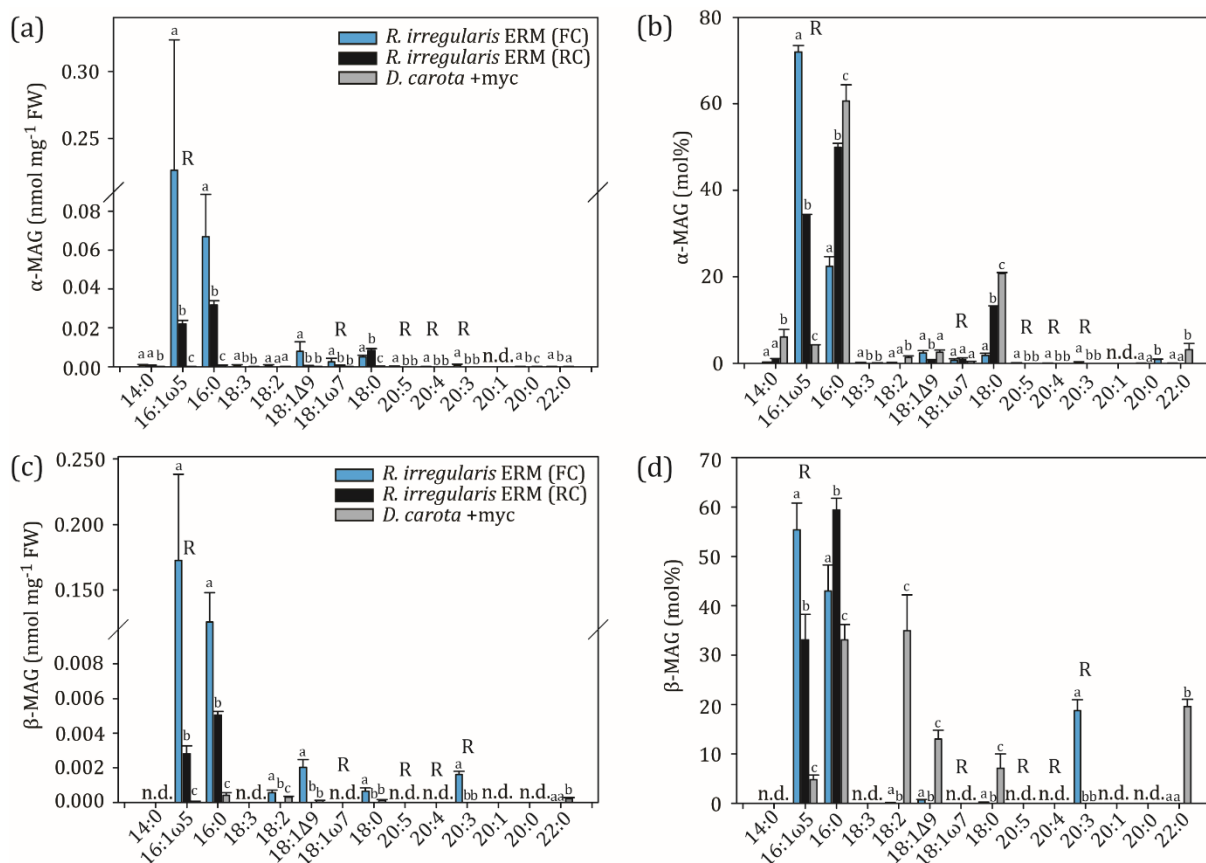
Figure 12: Identification of Monoacylglycerol molecular Species with a Mycorrhiza-Signature.
a,b) Absolute (nmol mg FW^{-1}) and relative (mol%) quantification of *sn*-1/3-acylated α-MAGs in *R. irregularis* ERM and *D. carota* colonized with *R. irregularis*.
c,d) Absolute (nmol mg FW^{-1}) and relative (mol%) quantification of *sn*-2-acylated β-MAGs in *R. irregularis* ERM and *D. carota* colonized with *R. irregularis*.
R. irregularis was grown in monoxenic root culture in symbiosis with *A. rhizogenes*-transformed, hairy roots of *D. carota* as host in a petri dish system with two compartments. The root compartment (RC) contained colonized roots and extraradical mycelium growing into the medium, where the fungal compartment (FC) contained only extraradical mycelium (spores and hyphae). The number of spores and hyphae is larger in the fungal compartment. After extraction of tissue from the medium, MAGs were seperated, detected and quantified by GC-MS (n=3).
FC, Fungal compartments; RC, Root compartment; ERM, Extraradical mycelium; R, Fatty acids originating from *R. irregularis*; n.d., not detected; +myc, infected with *R. irregularis*. All graphs represent average values, error bars depict standard deviation. One-way ANOVA with post-hoc Tukey, different letters indicate significant differences (P < 0.05).

The same was observed for 16:0 β-MAG. Noteworthy, 16:1ω5 β-MAG was present in the mixed tissue of the colonized *D. carota* roots as well, which likely reflects the high amount of fungal biomass in these roots that have a colonization rate of ~100%. Interestingly, 20:3 β-MAG was the third most abundant β-MAG in FC-ERM (18.78 mol%) and was under the detection limit in RC-ERM and colonized roots. These findings reveal that β-MAGs, even though they are likely produced by the plant via RAM2, accumulate to a large degree in fungal mycelium, prominently in spores. They therefore could represent intermediates in TAG synthesis in IRM and ERM.

In addition to axenic root cultures, MAGs were also measured and compared between colonized and mock-inoculated *L. japonicus* roots at 7 wpi (Figure 13a, b). The previously

identified mycorrhiza-marker MAGs 16:1ω5 α-MAG and 18:1ω7 α-MAG were detected only in colonized roots (Figure 13a). As in the previous *D. carota* experiment, the α-MAGs were more abundant than β-MAGs. β-MAG mycorrhiza-marker could not be detected (Figure 13b), probably due to relatively low amount of fungal tissue in *L. japonicus* roots compared to *D. carota* colonized roots. From the β-MAG species that were detected, only 16:0 β-MAG showed a mycorrhiza-response, i. e. it accumulated by six-fold in colonized roots compared to non-colonized roots of the same age, while all other β-MAGs were unchanged (Figure 13b).
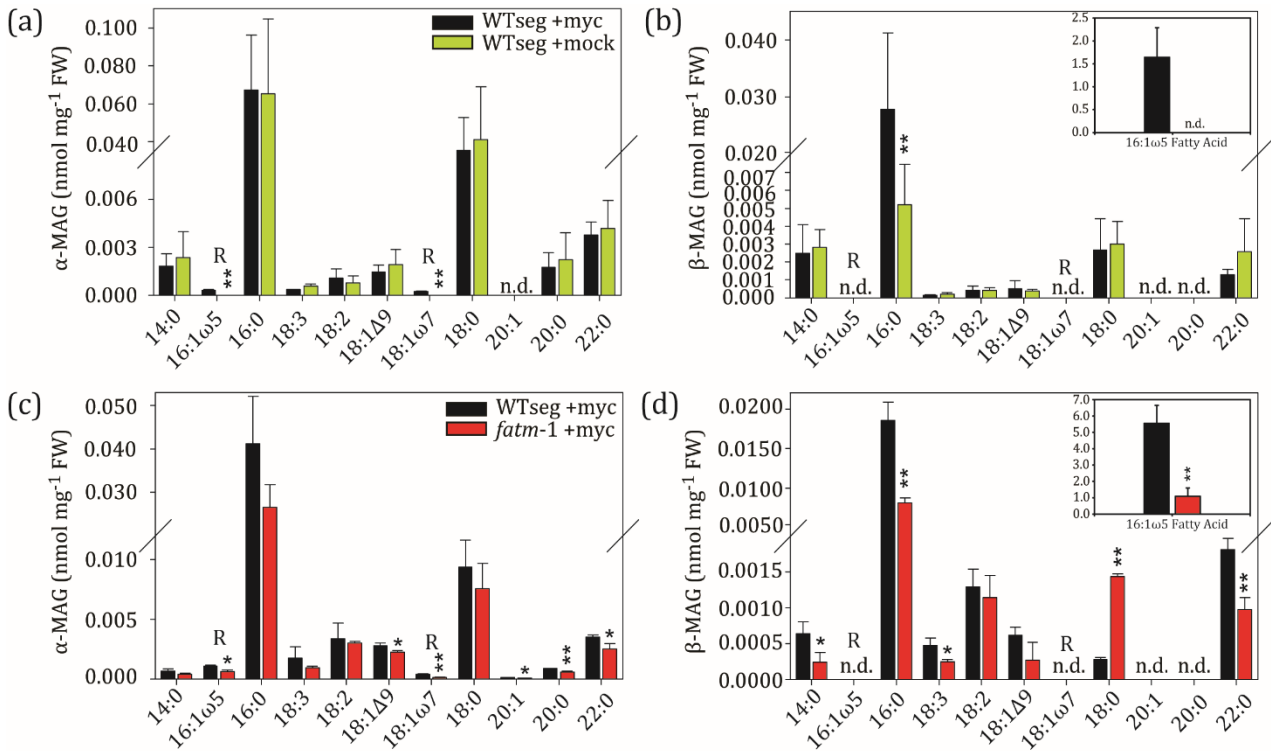
Figure 13: Monoacylglycerol Composition in mock-inoculated and colonized *L. japonicus* Roots of WT and *fatm*-1.

a,b) Amounts of *sn*-1/3-acylated α-MAGs and *sn*-2-acylated β-MAGs in Lotus roots with and without mycorrhiza. **Inset**: mycorrhiza marker fatty acid 16:1 ω5 (nmol mg FW^{-1}) measured in the same samples (n=3).

c,d) Comparison of α-MAGs and β-MAGs between colonized WT control and *fatm*-1 mutant **Inset**: mycorrhiza marker fatty acid 16:1 ω5 (nmol mg FW^{-1}) measured in the same samples (n=3).

MAGs were seperated, detected and quantified via GC-MS in lipid extracts from samples taken at 7 wpi. Some MAG species were previously shown to exist, but could not be detected in this experiment. Of the β-MAGs, only 16:0 β-MAG shows responsiveness to mycorrhiza colonization and is the major β-MAG reduced in colonized *fatm*-1.

R, Fatty acids originating from *R. irregularis*; n.d., not detected;+myc, infected with *R. irregularis*; +mock, inoculated with mycorrhiza carrier material; WT seg, LORE1 segregating wild type allele of *fatm*-1. All graphs represent average values, error bars depict standard deviation. Student's t-test (*P < 0.05; **P < 0.01).

16:1ω5 α-MAG and 18:1ω7 α-MAG were lower in the *fatm*-1 samples (Figure 13c). This is in agreement with the colonization phenotype in *fatm*-1 mutant roots shown by microscopy and fatty acid analysis described previously (see 3.1.3 and 3.1.6.1). The most abundant β-MAG species in colonized roots was 16:0 β-MAG, which exhibited a decrease in *fatm*-1 (0.0186 nmol mg FW^{-1}

in WT to 0.0083 nmol mg FW^{-1} in *fatm*-1, figure 13d). In addition, 14:0 β-MAG was reduced as well, albeit the total amount was less than 16:0 β-MAG. 16:0 β-MAG is the preferred product of the mycorrhiza-specific RAM2 enzyme and the second most abundant product is 14:0 β-MAG (Luginbuehl *et al.*, 2017). Thus, the decrease in 16:0 β-MAG and 14:0 β-MAG in *fatm*-1 could reflect decreased RAM2 activity in these mutants. The content of 18:0 β-MAG was five-fold increased in *fatm*-1 (Figure 13d). Even though RAM2 prefers 16:0-CoA and 14:0-CoA as fatty acid donor, it can also act on 18:0-CoA. Therefore, accumulation of 18:0 β-MAG in *fatm*-1 might reflect alternative substrate activity by RAM2 and thus could also represent a shift from 14:0/16:0-symbiotic fatty acid transfer to 18:0 fatty acids. Alternatively, the 18:0 β-MAG in colonized *fatm*-1 could accumulate in in the plant, because 18:0 β-MAG is a less accepted substrate for secretion to the fungus. As a control of the degree of fungal colonization and lipid accumulation in *L. japonicus* roots used for MAG analysis, 16:1ω5 total fatty acid was measured (Figure 13b,d, insets). A ~30% total root colonization is reflected by 0.5—1 nmol mg FW^{-1} 16:1ω5, and 8—12 nmol mg FW-1 is equivalent to 90—100% root colonization. This was done to ensure comparability between the different measurements and as the control of the degree of colonization with *R. irregularis*. Thus, both sample sets were shown to be well-colonized and accumulated considerable amounts of fungal lipids (1.64 and 5.55 nmol mg FW-1 for WTseg +myc, see figure 13b inset and figure 13d inset, respectively).

3.1.8   The Mycorrhiza-specific *Lj*FatM Acyl-ACP Thioesterase preferentially hydrolyses Palmitoyl-ACP

The *L. japonicus* acyl-ACP thioesterases *LjFatM* was heterologously expressed in *E. coli* (Figure 14). The cloned coding sequence encodes a truncated protein that was cloned without the predicted N-terminal transit peptide (*Lj*FatM^{Δtp}), resulting in the expression of a recombinant protein with the predicted size of 40.52 kDa (Figure 14a). Thioesterase activity for *Lj*FatM^{Δtp} was investigated by expression in the *E. coli fadD* mutant, which lacks acyl-CoA synthethase activity and therefore accumulates free fatty acids upon over-expression of thioesterases. The accumulation of free fatty acids can serve as indicator for thioestease activity (Jing *et al.*, 2011). A large fraction of the free fatty acids are secreted to the medium. Therefore, free fatty acids were measured in entire cultures (including liquid medium) of *E. coli* fadD cells harboring an empty vector or the *LjFatM^{Δtp}* construct.

LjFatM^{Δtp}-expressing *E. coli fadD* mutants accumulated 14:0, 16:0, 16:1Δ9, and 18:1Δ9 free fatty acids, resulting in a total five-fold accumulation of free fatty acids, compared to EV *fadD* control (Figure 14b). Here, the acyl-ACP substrate availability depends on the acyl-ACP pattern of *E. coli* and is therefore different from plant plastids. To study the substrate preferences in detail, recombinant enzyme assays with equal substrate amounts were conducted.
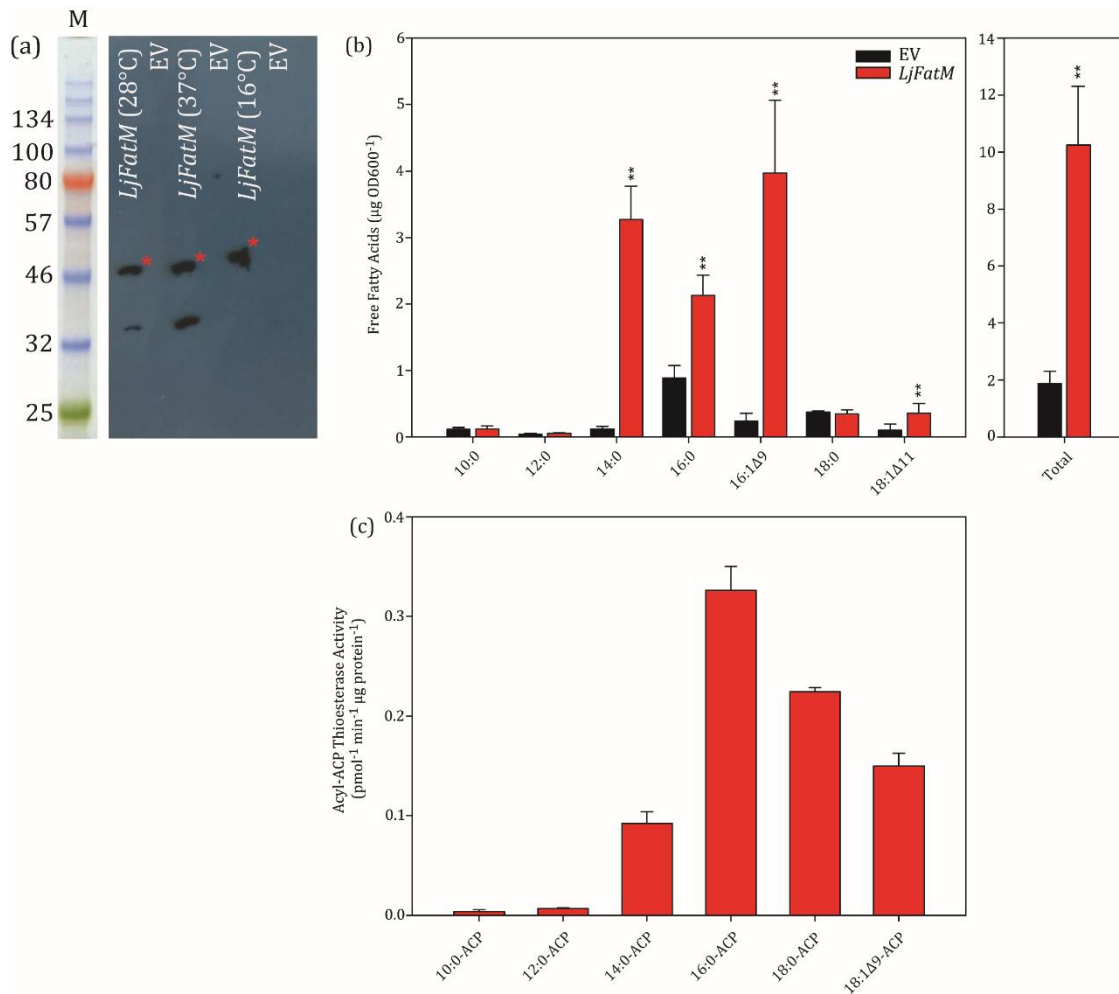
Figure 14: Expression of *L. Japonicus* acyl-ACP Thioesterase FatM in *E. coli* and *in vitro* Enzyme Assay with recombinant FatM.

a) Western blot from *E. coli fadD* cultures expressing *LjatM*. Cultures were inoculated from ON cultures and induced with 1 mM IPTG at OD_{600}=0.5 and incubated at 28°C, 37°C or 16°C ON. The calculated size of the recombinant protein without transit peptide and including the N-terminal His-Tag is 40.51 kDa (red asterisk). Incubation at 28°C and 37°C resulted in the presence of an unspecific band slightly above the 32 kDa marker. For subsequent determination of thioestease activity **(b)** and protein purification **(c)**, cultures were incubated at 16°C after induction with IPTG.

b) Free Fatty Acid Quantification with GC-FID from cell pellets of *E. coli fadD* expresising *LjFatM* at 16°C ON after induction with IPTG (n=3).

c) *In vitro* enzyme assay of *LjFatM*. Recombinant *FatM* was His-Tag purified and incubated with various ^{14}C-marked acyl-ACP substrates in seperate reactions. The radioactivity of the extracted free fatty acids from the thioesterase reaction indicated the enzyme substrate preferences (n=3).

M, Protein size marker; *LjatM, L. japonicus acyl-ACP thioesterase M*; EV, Empty vector control. All graphs represent average values, error bars depict standard deviation. Student's t-test (*P < 0.05; **P < 0.01).

Recombinant *Lj*FatM was purified from *E. coli* via affinity-chromatography on nickel columns using the N-terminal His-tag. Purified, recombinant *Lj*FatM was incubated in seperate reactions with a range of ^{14}C-acyl-ACP substrates at the same concentrations. The radioactivity of the hydrolyzed free fatty acids served as measure of thioesterase activity (Figure 14c). The reactions containing 16:0-ACP were hydrolyzed with the highest rate by *Lj*FatM, while 18:0-ACP was the second preferred substrate. The substrates 18:1Δ9-ACP and 14:0-ACP were also hydrolyzed to some degree, while 10:0-ACP and 12:0-ACP, representing very uncommon fatty

acids in *L. japonicus*, were not hydrolyzed. Thus, *Lj*FatM prefers palmitoyl-ACP as substrate, which coincides with its homology to Arabidopsis *At*FatB and is consistent with the proposed role in feeding palmitic acid to the mycorrhiza fungus.

3.1.9 Substrate Specificities of the non-Mycorrhiza-specific Acyl-ACP Thioesterases *Lj*FatA and *Lj*FatB

Upon mycorrhiza colonization, plants must ensure that acyl-lipid synthesis for plant metabolism is seperated from acyl-lipids destined for secretion to the fungus. As plants also depend on plastidial fatty acid supply, the acyl-ACP thioesterases that are not engaged in mycorrhiza colonization, LjFatA and LjFatB, where characterized biochemically. Similar to *LjFatM*, truncated coding sequences of *LjFatA* and *LjFatB* were expressed in *E. coli* and purified for an *in vitro* enzyme assay (Figure 15). The calculated sizes of the recombinant proteins without predicted N-terminal transit peptides are 37.26 kDA (*LjFatAΔtp*) and 41.76 kDa (*LjFatBΔtp*). The western blot from induced *E. coli fadD* cultures showed specific His-tag signals for the two proteins close to the 46 kDa marker (Figure 15a). Consistent with the predicted sizes, the band for *Lj*FatBΔtp was slightly bigger than for *Lj*FatAΔtp. The blot signals also indicated that *LjFatA* expression was stronger than *LjFatB*, which might explain why purification of *Lj*FatB was unsuccessful.

The amounts of the monounsaturated free fatty acids 16:1Δ9 and 18:1Δ11, which accumulated in *E. coli fadD*, where higher when *LjFatA* was expressed compared to expression of *LjFatB*. Although in both cultures, these fatty acids accumulated stronger than in the EV control (Figure 15b). While 16:0 free fatty acid only comprised a small proportion of the accumulating free fatty acids in both cultures, 14:0 free fatty acid was additionally increased in the cultures expressing *LjFatB*. This coincides with the preference of *FatB*-type thioesterases for saturated acyl-ACPs, while the FatA-types prefer monounsaturated acyl-ACPs. However, as described bevore (see 3.1.8), the accumulation of free fatty acids in *E. coli fadD* is also influenced by the endogenous concentrations of acyl-ACPs and not only by acyl-ACP thioesterase substrate specificities. Therefore, *in vitro* enzyme assays were conducted for *Lj*FatA and *Lj*FatB as well (Figure 15c,d). *LjFatA* revealed acyl-ACP substrate preference for 18:1Δ9-ACP>18:0-ACP> 16:0-ACP>14:0-ACP>12:0-ACP and 10:0-ACP (Figure 15c). Recombinant LjFatB enzyme could not unequivocally be purified from *E. coli*, probably due to weaker expression than *LjFatA* (see above). Therefore, the crude soluble protein extracted from *E. coli* ElectroSHOX cells subsequent to IPTG-induction were incubated with the ^{14}C-Acyl-ACPs, and thioesterase activity calculated compared to a control using total soluble protein from induced EV cultures (Figure 15d). Acyl-ACP thioesterase activity in *E. coli* EV ElectroSHOX resembled the pattern of free fatty acids shown before for *E. coli* EV *fadD* (Figure 15b): 16:0>14:0>18:1Δ11>12:0>18:0 and 10:0.
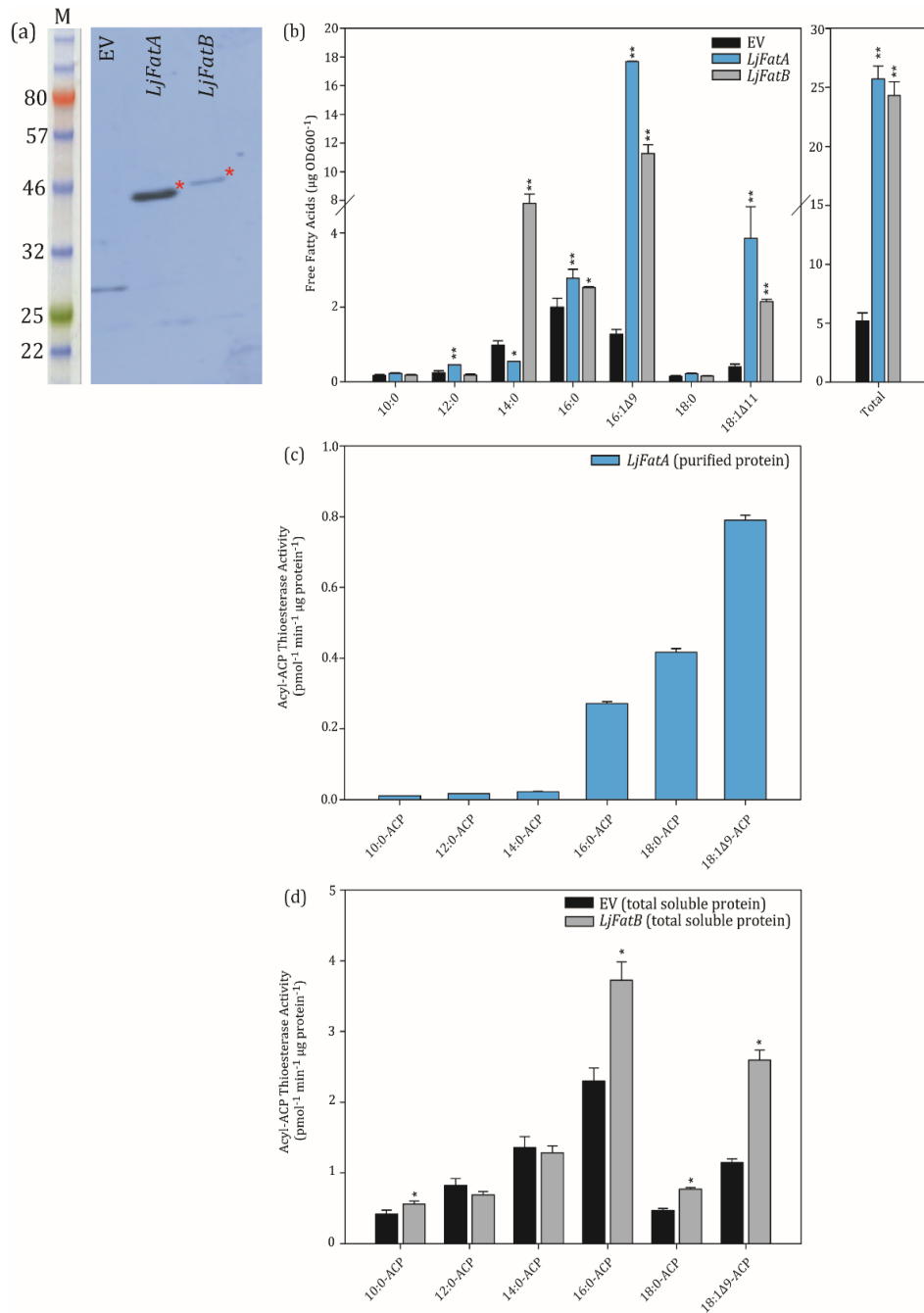
Figure 15: Expression of *L. Japonicus* Acyl-ACP Thioesterases FatA and FatB not involved in AM Symbiosis in *E. coli* and *in vitro* Enzyme Assay with Recombinant Protein.
a) Western blot from *E. coli fadD* cultures expressing *LjFatA* or *LjFatB*. Cultures were inoculated from ON cultures and induced with 1 mM IPTG at OD_{600}=0.5 and incubated at 16°C ON. The calculated sizes of the recombinant proteins without transit peptides and including the N-terminal His-Tags are 37.26 kDa for LjFATA and 41.76 kDa for LjFATB (red asterisks).
b) Free Fatty Acid Quantification with GC-FID from cell pellets of *E. coli fadD* expresising *LjFatA* and *LjFatB* at 16°C ON after induction with IPTG (n=3).
c,d) Acyl-ACP thiosterase enzyme assays. His-Tag purified *LjFatA* or total soluble protein from *induced E. coli* ElectroSHOX expressing *LjFatB* and an EV control were incubated with various ^{14}C-labeled acyl-ACP substrates in seperate reactions. The radioactivity of the extracted free fatty acids from the thioesterase reaction indicated the enzyme substrate preferences (n=3).
M, Protein size marker; *LjFatA, B*, *L. japonicus acyl-ACP thioesterase A,B*; EV, Empty vector control. All graphs represent average values, error bars depict standard deviation. Student's t-test (*P < 0.05; **P < 0.01).

The thioesterase activity in *E. coli* electroSHOX expressing *LjFatB* deviates from that pattern as 16:0-ACP was hydrolyzed at a higher rate than in the EV control and furthermore, 18:1Δ9 was the second most preferred substrate, next to 18:0-ACP and a small portion of 10:0-ACP, which both are minor substrates for *LjFatB*. Thioesterase activity for 12:0-ACP and 14:0-ACP were similar to EV control, even though *E. coli fadD* expressing *LjFatB* showed 14:0 free fatty acid accumulation (Figure 15b).

3.1.10 Labeling of *de novo* synthesized Fatty Acids with ^{13}C-Acetate reveals a Flux of Fatty Acids from the Plant to the Fungus via FatM

To monitor fatty acid *de novo* synthesis and symbiotic lipid transfer to the fungus, a labeling experiment with ^{13}C-acetate was set up. When presenting roots with acetate, it is taken up by the root into the apoplast and enters the root cytoplasm where it is imported into the plastid and converted into acetyl-CoA by acetyl-CoA synthethase (Lin and Oliver, 2008). Acetyl-CoA is subsequently utilized for *de novo* synthesis of fatty acids. Due to the absence of FAS from *R. irregularis*, acetate is likely not incorporated into 16:0 fatty acids, one of the main products of *de novo* fatty acid synthesis (see Figure 1), but can be taken up by hyphae of *R. irregularis* and used for elongation of C16 fatty acids to C18, C20 and C22 fatty acids. The profile of ^{13}C-labeled fatty acids was compared for mock-inoculated and mycorrhiza-colonized WT and *fatm*-1 plants. Colonized roots were submerged in buffer with ^{13}C$_2$-acetate and incubated ON for labeling of fatty acids and symbiotic lipid transfer to the fungus. Finally, total fatty acids were hydrolyzed from total lipid extracts and the amount of ^{13}C-label quantified with Q-TOF LC-MS/MS and GC-MS (Figure 16).

The utilization of ^{13}C$_2$-acetate for *de novo* synthesis of fatty acids led to the occurrence of fatty acids containing 1—16 ^{13}C atoms, called isotopologs. When successfully labeled with exogenously applied ^{13}C$_2$acetate, the abundance of the fatty acid ^{13}C-isotopologs differs from the naturally occurring isotpologs. The percentage of natural ^{13}C isotopologs was predicted (Isotope Distribution Calculator; www.sisweb.com) and experimentally verified by measuring fatty acids from non-labeled plants. Substraction of the natural isotopologs from the ^{13}C-isotopologs in the acetate-labeled samples gave rise to the ^{13}C over-excess value that represents the absolute amount of incorporated ^{13}C in ^{13}C$_2$-acetate labeling. Even chain isotoplogs (^{13}C$_2$, ^{13}C$_4$, ^{13}C$_6$ e.t.c) were typically more abundant than uneven ones, which is characteristic for direct incorporation of ^{13}C$_2$-acetate as ^{13}C$_2$-acetyl-CoA in *de novo* synthesis (see Figure 1).

The ^{13}C over-excess label was present in all major fatty acids (Figure 16a). For all labeled fatty acids, the highest peak was the ^{13}C$_2$-isotopolog and the amount of label incorporated into fatty acids was decreased with increasing number of ^{13}C atoms present. In the fatty acid isotpologs of 16:1ω5 fatty acid, ^{13}C$_6$—^{13}C$_{16}$ were not detected, in 20:3 fatty acid, ^{13}C$_{11}$—^{13}C$_{20}$ could not be detected, ^{13}C$_{17}$—^{13}C$_{18}$ could not be detected in 16:0 and 18:2 fatty acid and ^{13}C$_{14}$—^{13}C$_{18}$ were

absent from 18:0 fatty acid. The sum of all ^{13}C over-excess isotopologs were compared per fatty acid (Figure 16b). In WT, colonization with *R. irregularis* led to increased abundance of ^{13}C over-excess label in all fatty acids compared to mock-inoculated roots. The highest sum of over-excess label was obtained for the mycorrhiza-signature fatty acid 16:1ω5. The fatty acids 16:0, 18:2 and 18:1 were also abundantly labeled and some over-excess label was still detectable in 18:0 and 20:3. In colonized *fatm*-1, the ^{13}C over-excess label did not accumulate in mycorrhiza-signature fatty acids 16:1ω5 and 20:3. In 16:1ω5, it was decreased six-fold from 0.12 nmol mg FW^{-1} OE to 0.02 nmol mg FW^{-1} OE and three-fold in 20:3 from 0.013 nmol mg FW^{-1} OE in WT to 0.0039 nmol mg FW^{-1} OE in *fatm*-1. Furthermore, the ^{13}C over-excess label was increased in all other fatty acids, noticeably in 18:2 and 18:0 (two-fold increases), but also in 16:0 and 18:1, albeit to a lesser extent. This shows a redirection of ^{13}C$_2$-acetate into synthesis of typical plant fatty acids when symbiotic fatty acid transfer is hindered.

To investigate whether the incorporation of ^{13}C from ^{13}C$_2$-acetate into fungal fatty acids was influenced by the differences in fungal biomass in *fatm*-1 and WT (see 3.1.3 and 3.1.6), the sum of over-excess ^{13}C was divided by the amount of total fatty acid isotopologs (^{12}C+^{13}C) measured by GC-FID (Figure 17a). The labeling pattern was the same as shown for absolute amounts before (Figure 16), except for 18:1 fatty acid, where the relative ^{13}C over-excess label was higher for mock-inoculated than for colonized roots (Figure 17b and Figure 17c). Importantly, the relative incorporation of ^{13}C over-excess label in mycorrhiza-signature fatty acids 16:1ω5 and 20:3 in was consistently decreased in colonized *fatm*-1 compared to WT (Figure 17c). Thus, reduced ^{13}C over-excess label in mycorrhiza-fatty acids in colonized *fatm*-1 is not due to decrease in total fungal biomass, but due to a specific effect caused by the *fatm* mutation, i. e. a block in symbiotic fatty acid transfer.

To compare the symbiotic fatty acid transfer at different symbiotic stages (i. e. 4 and 9 wpi), the percentage distribution of the ^{13}C over-excess fatty acids was calculated (Figure 18). To this end, the total amount of ^{13}C over-excess fatty acids was defined as 100% and the relative proportion of ^{13}C over-excess of every individual fatty acid calculated. The proportion of ^{13}C over-excess in the mycorrhiza-signature fatty acids 16:1ω5 and 20:3 was highest (43.5%) in colonized WT (Figure 18a). It was prominently high in 16:1ω5 (38.5%) compared to 20:3 (4.9%). The ^{13}C over-excess label in 16:0 cannot clearly be assigned to the plant or fungus, although the fungus likely cannot utilize ^{13}C$_2$-acetate for 16:0 synthesis. Therefore, as a conservative estimation, at least 38.5% (% of total ^{13}C over-excess label in 16:1ω5 at 4 wpi in WT) of *de novo* synthesized fatty acids are transferred in the ~12 h (ON) labeling period, from the plant to the fungus at the 4 wpi growth stage in the functional symbiosis with WT *L. japonicus*. The fraction of ^{13}C over-excess label in mycorrhiza-signature fatty acids is reduced with progression of the symbiosis, so that at 9 wpi, 19.5% (% ^{13}C over-exces of 16:1ω5 + 20:3) of these are labeled in colonized WT.
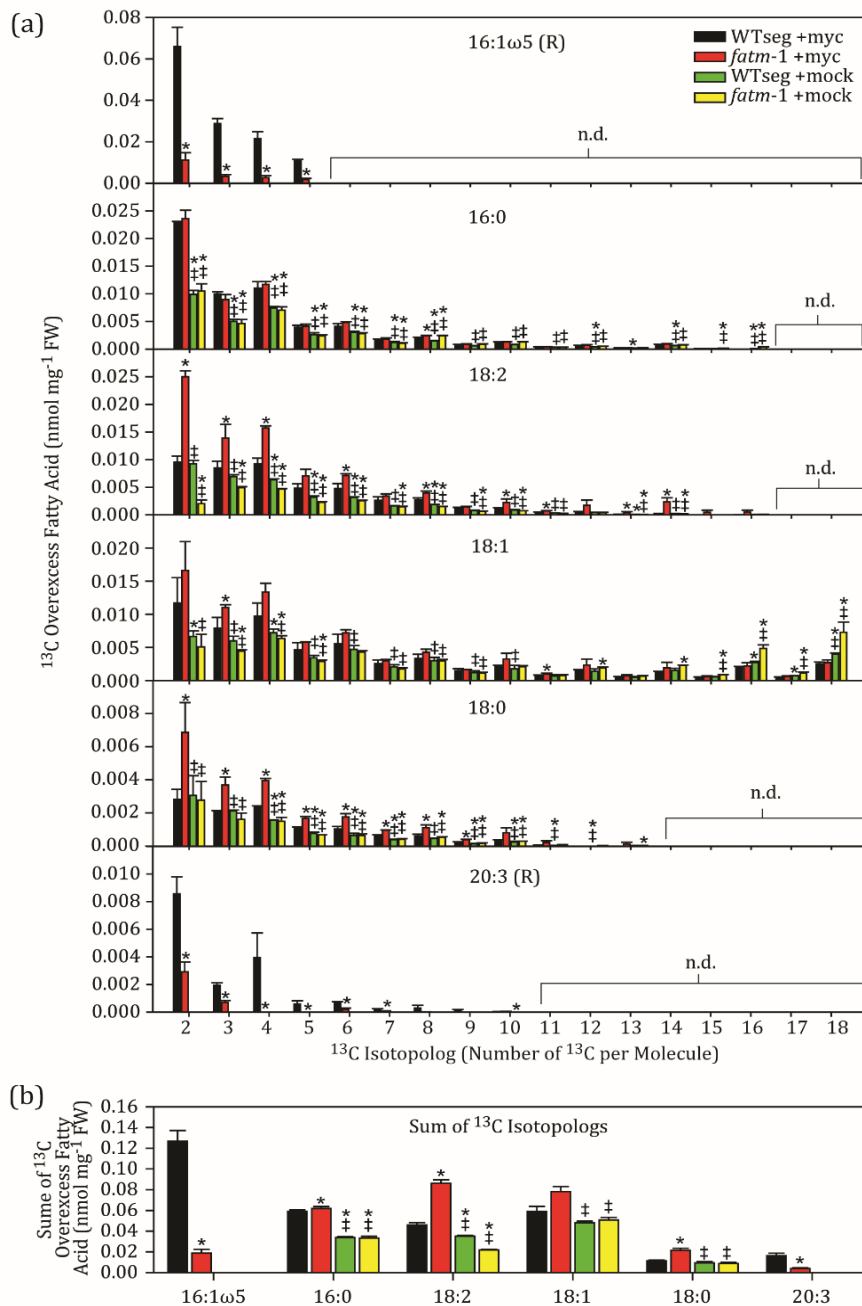
Figure 16: ¹³C-Acetate Labeling of Fatty Acids during Symbiosis in WT and *fatm*-1 Roots at 4wpi.
The absolute amoutns of ¹³C over-excess fatty acids were quantified.
a) Roots of WT and *fatm*-1 mutant plants were submerged in ¹³C-acetate buffer for labeling of fatty acids ON. Lipids were extracted and hydrolyzed and ¹³C-fatty acid isotopologs quantified with Q-TOF LC-MS/MS, except for 16:1ω5, which was measured with GC-MS. The amount of naturally-occurring ¹³C was subtracted, yielding ¹³C-over excess values. The number on thex-axis indicates the isotopologs, i. e. the respective fatty acid containing an increasing number of ¹³C-carbons originating from ¹³C-acetate (n=3).
b) Sum of the individual ¹³C-isotopologs depicted in **a)** (n=3).
The ¹³C-acetate is used for plastidial fatty acid *de novo* synthesis, and in *fatm*-1 colonized with *R. irregularis*, the total amount of label in mycorrhiza-signature fatty acids 16:1ω5 and 20:3 was lower than in WT, showing that FatM controls symbiotic fatty acid transfer.
R, Fatty acids originating from *R. irregularis*; n.d., not detected; +myc, infected with *R. irregularis*; +mock, inoculated with mycorrhiza carrier material; WT seg, LORE1 segregating wild type allele of *fatm*-1. All graphs represent average values, error bars depict standard deviation. Student's t-test with Bonferroni correction for multiple pairwise comparisons (*, significantly different from WTseg +myc; ‡, significantly different from *fatm*-1 +myc; P < 0.0125).

Decreased labeling at later stages of the symbiosis likely is indicative of decreased symbiotic fatty acid transfer. This fits with the observation that at later growth stages, when the AMF extensively generates spores, the colonized root is saturated with hyphae and vesicles, but arbuscules are less abundant. In root regions with this senescent colonization, also symbiotic phosphate transfer is hampered (Kobae, 2019). Thus, at later growth stages (>9 wpi), the bulk transfer of symbiotic fatty acids is mostly complete and therefore decreased at 9 wpi. Additionally, there is a relative increase in the label into 20:3 fatty acid from 4.9% at 4 wpi to 11.4% at 9 wpi. As $^{13}C_2$-acetate can be scavenged by the fungus to elongate fatty acids to 20:3, this might indicate increased usage of $^{13}C_2$-acetate by the fungus for fatty acid elongation. This could be a result of increased fungal tissue at 9 wpi that in turn can scavenge more $^{13}C_2$-acetate than at 4 wpi.

In colonized *fatm*-1, the ^{13}C over-excess label in mycorrhiza-fatty acids was consistently low with 11.7% at 4 wpi and 12.3% at 9 wpi. It was distributed nearly evenly between 16:1ω5 and 20:3. Thus, symbiotic fatty acid transfer remained inefficient and low in *fatm*-1 even when the root was heavily colonized at 9 wpi. An additional isomer of 16:1 fatty acid was found in *L. japonicus* roots. This fatty acid was seperated from 16:1ω5 by GC-MS and was present also in mock-inoculated samples but only at 9 wpi (Figure 18a and b). The retention time and mass spectra are identical to 16:1Δ9 fatty acid from *S. cerevisiae* (see Figure 22) and this nomenclature is therefore used, although no positional analysis of the double bond was performed. This fatty acid is likely of plant origin, but a fraction could also be derived from *R. irregularis*, as the fungus also contains 18:1Δ9, but to a lower amount than plant roots. In a mock sample from 9 wpi, 16:1Δ9 was abundantly labeled (16.7% in WT and 11.2% in *fatm*-1) (Figure 18b). Noteworthy, ^{13}C over-excess label in 16:1Δ9 accumulated in 9 wpi colonized *fatm*-1 to 16.5%, while being only 6.9% in WT of the same age. Therefore, most of the ^{13}C over-excess labeled 16:1Δ9 is of plant origin and confirms the induction of plant fatty acid *de novo* synthesis by AMF colonization. This observation is similar to the redirection of ^{13}C over-excess label into other plant fatty acids, i. e. 18:0, 18:2 and partially 16:0 and 18:1 in colonized *fatm*-1 at 4 wpi, as discussed above (Figure 16, Figure 17 and Figure 18a).
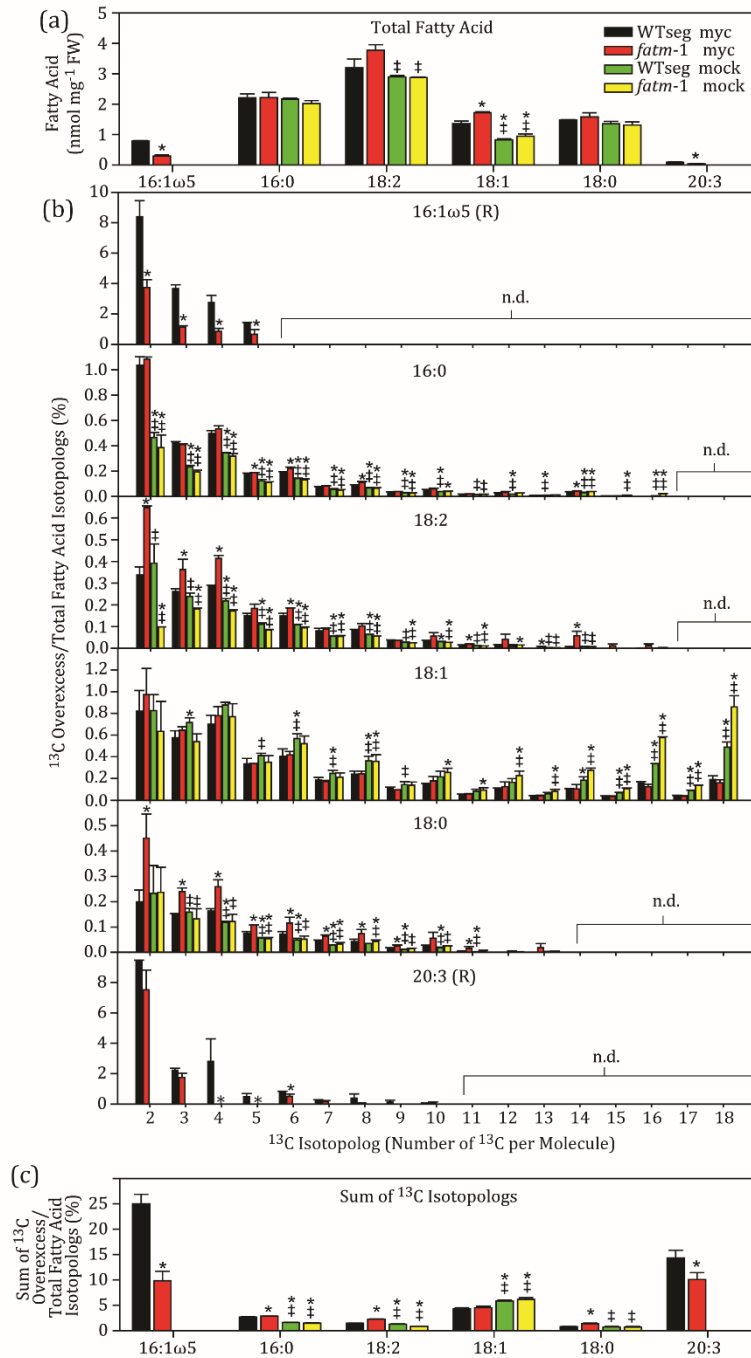
Figure 17: Relative Proportion of ¹³C-Acetate Labeling of Fatty Acids during Symbiosis.
a) Measurement of total fatty acids (all isotopologs, ¹²C+¹³C) with GC-FID in the ¹³C-labeled, colonized roots**.**
b,c) The absolute amounts of ¹³C-over excess fatty acids (Figure 16) were divided by the amounts of total fatty acids (¹²C+¹³C, see **a**) and expressed as% of these. The number on thex-axis indicates the isotopolog (increasing number of ¹³C-carbons originating from ¹³C-acetate) (n=3).

In *fatm*, the reduced fungal biomass leads to a decrease in mycorrhiza signature fatty acids. The relative incorporation of ¹³C (%¹³C over-excess relative to total fatty acid) into mycorrhiza-signature fatty acids is decreased in colonized *fatm* compared to WT, as shown before for absolute amounts (Figure 16). This confirms that the reduction of ¹³C-incorporation is not due to decrease in total fungal biomass.

R, Fatty acids originating from *R. irregularis*; n.d., not detected;+myc, infected with *R. irregularis*; +mock, inoculated with mycorrhiza carrier material; WT seg, LORE1 segregating wild type allele of *fatm*-1. All graphs represent average values, error bars depict standard deviation. Student's t-test with Bonferroni correction for multiple pairwise comparisons (*, significantly different from WTseg +myc; ‡, significantly different from *fatm*-1 +myc; P < 0.0125).
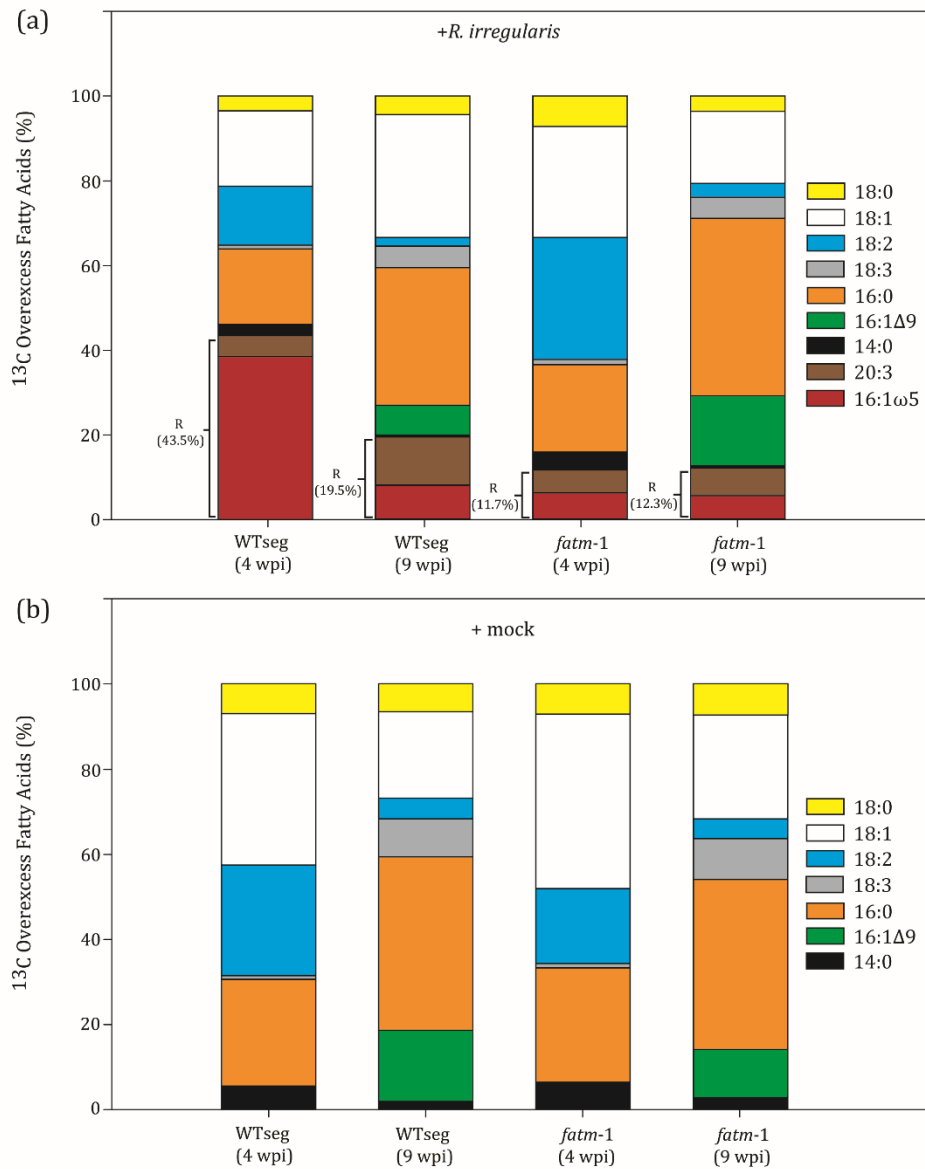
Figure 18: Distribution of ^{13}C-Label in Fatty Acids during AMF-Symbiosis and mock-Treatment.
The sum of all ^{13}C over-excess fatty acids was set to 100% and the relative proportion of the indivudal ^{13}C over-excess fatty acids was calculated.
a) ^{13}C-label in the major fatty acids during inoculation with *R. irregularis* for 4 and 9 weeks in WTseg or *fatm*-1 mutant.
b) ^{13}C-label in the major fatty acids in mock-inoculated roots incubated for 4 and 9 weeks in WTseg or *fatm*-1 mutant.
Every colored segment represents the average of three (4 wpi) or five (9 wpi) independent biological samples. The detailed isotopolog labeling for the 4 wpi samples is depicted in Figures 16 and 17. The highest proportion of ^{13}C over-excess label derived from acetate is found in mycorrhiza fatty acids at 4 wpi in the WT and is lower at 9 wpi, while being decreased consistently in colonized *fatm*-1. 16:1-isomers 16:1Δ9 and 16:1ω5 were measured via GC-MS. 16:1Δ9 was only labeled in older roots (9 wpi). Number on the brackets denote the sum of ^{13}C over-excess label in mycorrhiza signature fatty acids.
R, Fatty acids originating from *R. irregularis*;+ *R. irregularis*, infected with mycorrhiza; +mock, inoculated with mycorrhiza carrier material; WT seg, LORE1 segregating wild type allele of *fatm*-1

3.2 Fatty Acid Desaturation in *R. irregularis*

3.2.1 The acyl-CoA Pool Composition in Host Roots is changed by AMF Colonization

Because fatty acids released by acyl-ACP thioesterases from plastidial *de novo* synthesis enter the acyl-CoA pool at the ER, acyl-CoAs were quantified in mock-inoculated and AMF-colonized WT and *fatm*-1 roots. This measurement revealed the *R. irregualris*-dependent alteration of the acyl-CoA pool (Figure 19). The main acyl-CoA molecular species in AMF-inoculated roots was 16:0-CoA, while in mock-inoculated roots, 18:2-CoA had the same abundance as 16:0-CoA. 16:1-CoA accumulated in colonized roots, but could not be detected in non-colonized roots. In colonized *fatm*-1, 16:1-CoA was decreased, compared to colonized WT. Additionally, 20:1-CoA showed very little abundance in colonized *fatm*-1 and mock-inoculated WT, and only traces were identified. 20:0-CoA, which was the second most abundant CoA-species in mycorrhiza-colonized roots of WT, was less abundant in *fatm*-1 +myc and mock-inoculated WT. The changes in acyl-CoAs carrying mycorrhiza-signature fatty acids 16:1 and 20:1 are consistent with the results obtained from total fatty acid, lipid and MAG analysis (see 3.1.6 and 3.1.7). The changes in acyl-CoA pool in colonized roots were accompanied by an increase in acyl-CoAs with typical plant fatty acids (i. e. 18:3 and 18:2) in mock-inoculated roots.
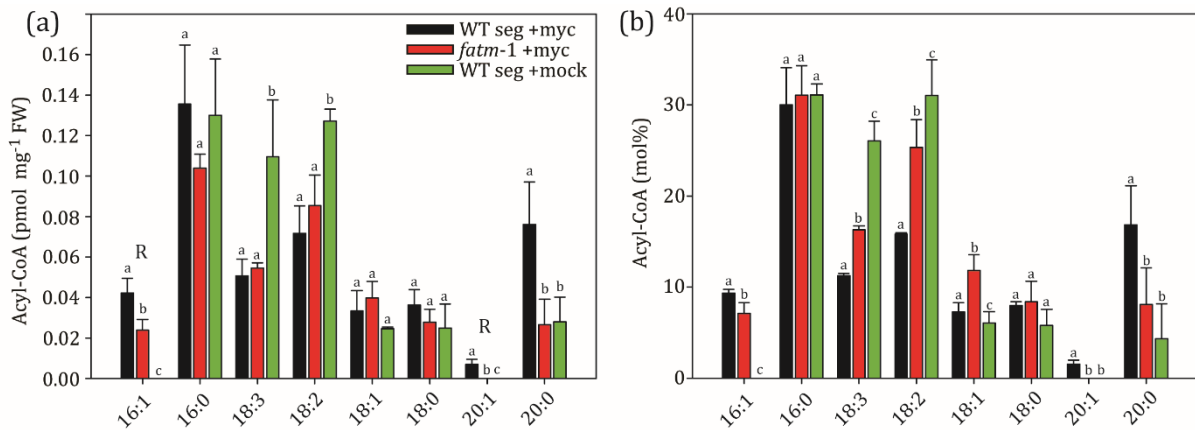
Figure 19: Alteration of the acyl-CoA Pool during AMF Symbiosis.
a,b) Absolute **(a)** and relative **(b)** quantification of acyl-CoAs in colonized and mock-inoculated WT and *fatm* mutants. Plants were inoculated for seven weeks with *R. irregularis* or mock-treated before extraction of acyl-CoAs. AMF colonization causes the occurrence of 16:1 and 20:1-CoAs as well as the increase of 20:0-CoA.
+myc, infected with *R. irregularis*; +mock, inoculated with mycorrhiza carrier material; WT seg, LORE1 segregating wild type allele of *fatm*-1. All graphs represent average values, error bars depict standard deviation. One-way ANOVA with post-hoc Tukey, different letters indicate significant differences ($P < 0.05$).

The origin of mycorrhiza-signature fatty acids 16:1 and 20:3 in colonized roots were not yet experimentally verified. However, these fatty acids are likely derived from desaturases in the mycorrhiza symbiont, because the ERM accumulates considerable amounts of 16:1 and 20:3 esterified to TAG and phospholipids. To study symbiotic fatty acid transfer and lipid biosynthesis in *R. irregularis,* the genes involved in fatty acid desaturation in *R. irregularis* were investigated using *S. cerevisiae* as a model system (see 3.2.2).

3.2.2 *R. irregularis* contains Desaturases with Homology to Yeast Acyl-CoA Desaturase OLE1

In the model fungus *S. cerevisiae*, fatty acid desaturation depends on the acyl-CoA desaturase OLEIC ACID REQUIRING 1 (*Sc*OLE1) that desaturases stearoyl-CoA and hexadecanoyl-CoA to produce oleoyl-CoA and palmitoyl-CoA, respectively (Smet *et al.*, 2012). The *Sc*OLE1 amino acid sequences was used in a BLASTp search against the *R. irregularis* translated genome (DAOM 181602=DAOM 197198 GCA_000439145) accessed at EnsemblFungi (www.fungi.ensembl.org).
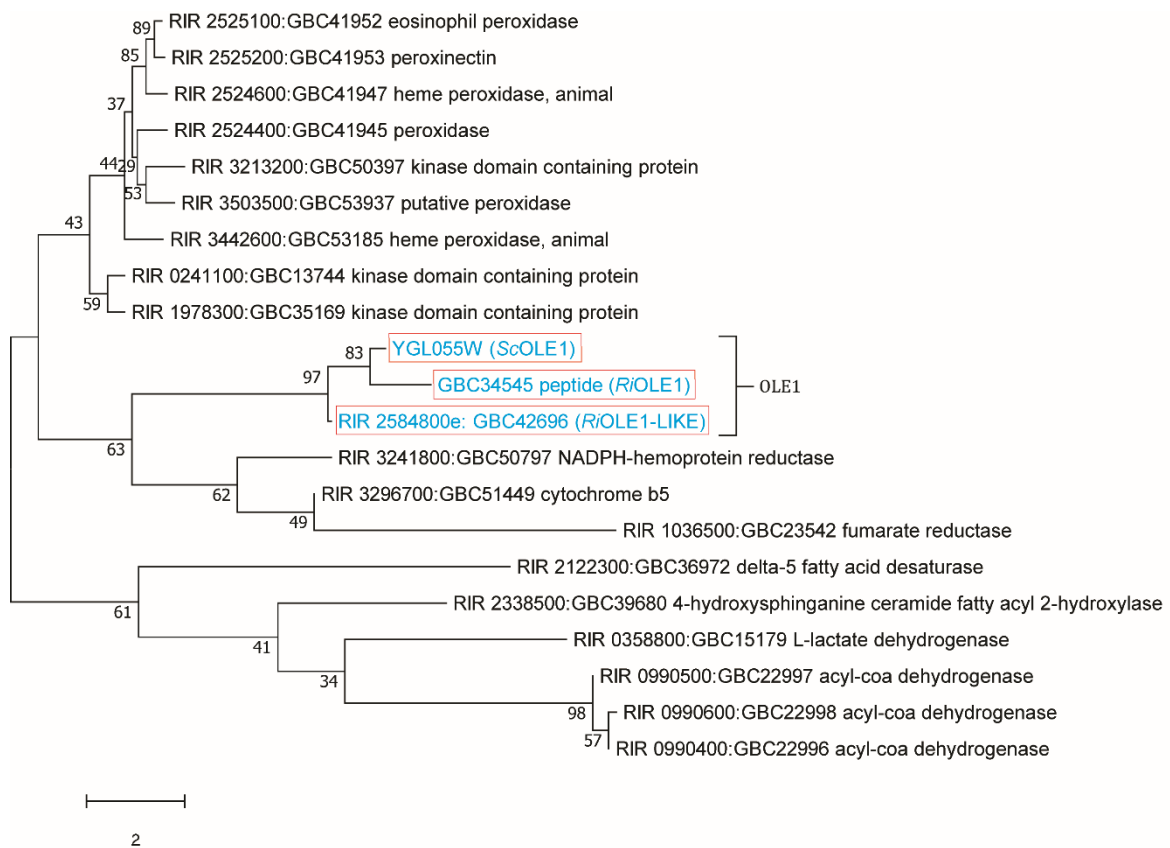
Figure 20: Protein Sequences of *R. irregularis* similar to *S. cerevisiae* acyl-CoA Desaturase OLE1. BLASTp with *Sc*OLE1 was done against the *R. irregularis* translated nucleotide genome and all significant hits were used in a multiple sequence alignment of protein sequences using ClustalX with MEGA v 6.0. A neighbor-joining (NJ) tree was constructed. Two sequences are highly similar to *Sc*OLE1, termed *Ri*OLE1 and *Ri*OLE1-LIKE, indicated by red boxes. The numbers on the branches indicate boot-strap values (1000 iterations). *Sc*, *S. cerevisiae; Ri, R. irregularis.*

Twenty three non-redundant, significant hits (E-value < 0.05) were retrieved of which two protein sequences were highly similar to *Sc*OLE1 and were therefore termed *Ri*OLE1 and *Ri*OLE1-LIKE (Figure 20). *Ri*OLE1 was more similar to *Sc*OLE1 than *Ri*OLE1-LIKE. Subsequently, their coding sequences were amplified from *R. irregularis* cDNA and expressed in yeast and *N. benthamiana* (see 3.2.3—3.25) to study their enzymatic activity.

3.2.3 The Auxotrophy for Oleic Acid of the Yeast *Δole1* Mutant is complemented by Expression of *R. irregularis RiOLE1* and *RiOLE1-LIKE*

RiOLE1 and *RiOLE1-LIKE* were used to rescue the *Δole1* yeast mutant that exhibits a growth deficiency when no unsaturated fatty acids are supplemented to the medium (Stukey *et al.*, 1989). Constitutive expression of *RiOLE1* and *RiOLE1-LIKE* allowed *ScΔole1* mutants to grow on medium free of monounsaturated fatty acids and did not affect growth in the WT background (Figure 21).
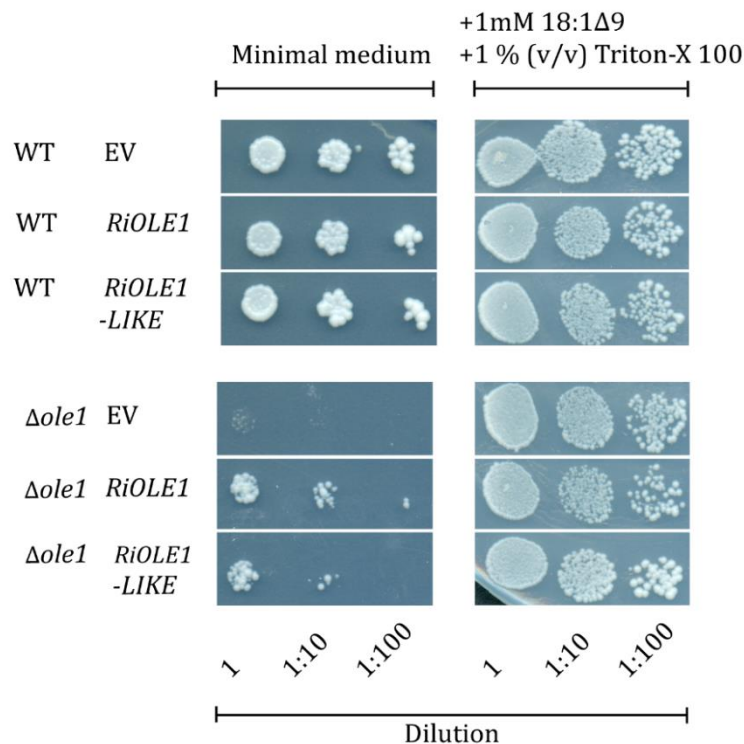
Figure 21: Growth Complementation of *S. cerevisiae Δole1* by Expression of *R. irregularis RiOLE1* and *RiOLE1-LIKE*.
The coding sequences of *Rhiozphagus* OLE1 and OLE1-LIKE were constitutively expressed in yeast WT or *ScΔole1* background. A dilution series was plated out on minimal medium without fatty acids and, as a positive control, minimal medium containing 1mM oleic acid (18:1Δ9). The plates were incubated at 28°C for 5 days. When grown without supplementation of unsaturated fatty acids, expression of *RiOLE1* and *RiOLE1-LIKE* partially rescued the growth phenotype of the yeast *Δole1* mutant, similar to supplementation of 18:1Δ9.
WT, wild-type; EV, Empty vector control; Ole1, Oleic acid dependent 1; Ri, *R. irregularis.*

Supplementation of oleic acid to the medium rescued growth of the Sc*Δole1* mutant. Growth of yeast on the oleic acid-supplemented medium expressing *RiOLE1* or *RiOLE1-LIKE* did not differ between the Sc*Δole1* or WT background. However, Sc*Δole1* cells expressing *RiOLE1* grew slightly better than those expressing *RiOLE1-LIKE.* This might be explained by the higher sequence similarity between *Sc*OLE1 and *Ri*OLE1 which might indicate a higher functional relationship, in contrast to *Ri*OLE1-LIKE (Figure 20).

3.2.4 Mycorrhiza-Signature Fatty Acids are synthesized by *Ri*OLE1-LIKE

The most abundant fatty acid *in R. irregularis* ERM is palmitvaccenic acid (16:1ω5). In colonized plant roots, 16:1ω5 accumulates and it is absent from mock-treated roots (Figure 9). Additionally, 18:1ω7 can be detected in colonized roots (Stumpe *et al.*, 2005). Fatty acids with similar retention times and mass spectra as 16:1ω5 and 18:1ω7 were exclusively found in yeast cells expressing *RiOLE1-LIKE* but not *RiOLE1* or the EV control (Figure 22a and b). 16:1ω5 and 18:1ω7 were eluted prior to palmitic acid and stearic acid, but after palmitoleic and oleic acid, respectively. The composition of fatty acids was additionally analyzed in *N. benthamiana* leaves transiently expressing *RiOLE1* or *RiOLE1-LIKE* coding sequences (Figure 22c and d). In *N. benthamiana* expressing *RiOLE1-LIKE*, 16:1ω5 and 18:1ω7 fatty acids are present (Figure 22d) that were absent from *N. benthamiana* leaves transiently expressing *RiOLE1* and the EV negative control (Figure 22c).

In addition to the WT, expression of *RiOLE1-LIKE* in the yeast Sc*Δole1* mutant also caused the accumulation of 16:1ω5 fatty acids (Figure 22e and f). Quantification of total fatty acids revealed a shift towards 16:1ω5 fatty acids with an accompanying decrease in 16:1Δ9 and18:1Δ9 in *RiOLE1-LIKE*-expressing Sc*Δole1* that was not observed in *RiOLE1-LIKE*-expressing WT. Both, WT and Sc*Δole1* exhibited a relative reduction in 16:0 fatty acid (in mol%) when *RiOLE1-LIKE* was expressed (Figure 22f). On the other hand, 18:1Δ9 accumulated in yeast WT and Sc*Δole1* when *RiOLE1* was expressed (Figure 22e and Figure 22f) and the relative amount of 18:0 decreased (Figure 22f). In the same samples, the amount of of 16:1Δ9 in WT and Sc*Δole1* decreased as well, but in absolute amounts, this was only observed in the Sc*Δole1* background. Thus, *Ri*OLE1-LIKE is responsible for the synthesis of 16:1ω5 and 18:1ω7 in *R. irregularis* IRM and ERM and *Ri*OLE1 synthesises Δ9-fatty acids, consistent with the higher sequence similarity to *Sc*OLE1 which is a 16:0-CoA and 18:0-CoA delta9 desaturase (Figure 20).

To evaluate whether fatty acid desaturation by *R. irregularis* desaturases is influenced by exogenous application of fatty acids, the culture medium was supplemented with 15:0 fatty acid and the yeast total fatty acid composition investigated (Figure 23). Fatty acids with odd carbon atoms are absent from yeast.
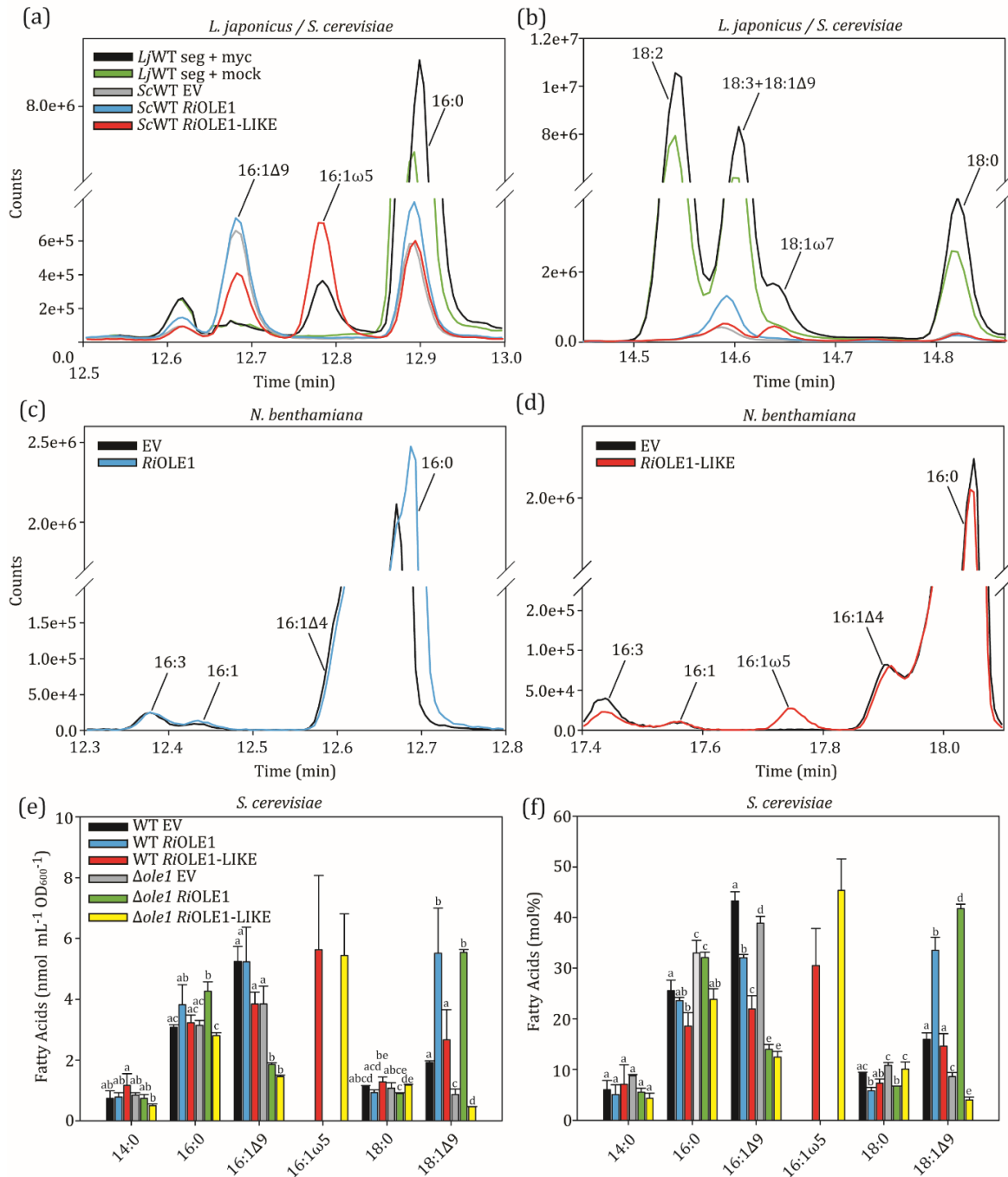
Figure 22: Identification and Quantification of Mycorrhiza-Signature Fatty Acids in *N. benthamiana* and *S. cerevisiae* expressing *R. irregularis* OLE1 orthologs.

a,b) GC-MS total ion chromatograms of fatty acid methyl esters synthesized from total lipid extracts obtained from 1 mL yeast culture or approximately 100 mg *L. japonicus* root inoculated with or without mycorrhiza for 4 weeks.

c,d) GC-MS total ion chromatograms of fatty acid methyl esters synthesized from the methanol-fraction after solid-phase extraction of lipid extracts obtained from *N. benthamiana* leaves transiently expressing *Ri*OLE1 **(c)** and *Ri*OLE1-LIKE **(d)**. Leaves were harvested 5 days **(c)** or 4 days **(d)** after leaf infiltration with Agrobacterium.

Yeast and *N. benthamiana* expressing *Ri*OLE1-LIKE contain the mycorrhzia signature fatty acid 16:1ω5 that is otherwise only found in mycorrhiza-containing tissue.

e,f) Quantification of total fatty acids by GC-FID of 1 mL yeast culture expressing *Ri*OLE1 or *Ri*OLE1-LIKE in the WT or *Δole1* mutant background.

+myc, infected with *R. irregularis*; +mock, inoculated with mycorrhiza carrier materia; Lj, *L. japonicus*; WT, wild-type; EV, Emtpy vector control; Ole1, Oleic acid dependent 1; Ri, *R. irregularis.* All graphs represent average values, error bars depict standard deviation. One-way ANOVA with post-hoc Tukey, different letters indicate significant differences (P < 0.05).

In all six yeast cultures that were fed with 15:0, fatty acids with retention times similar to Δ9-*cis* monounsaturated fatty acids were detected. These comprised 15:1Δ9, 16:1Δ9, 17:1Δ9 and 18:1Δ9. In WT and Sc*Δole1* expressing *RiOLE1-LIKE*, additional monounsaturated fatty acids were distinguished that were absent from the other samples. These were identified as 15:1ω4, 16:1ω5 and 18:1ω7, due to their retention times and mass spectra. In the WT background, a 17:1 fatty acid was detected, regardless of the expression constructs (Figure 23a) and this was absent from Sc*Δole1* EV and Sc*Δole1RiOLE1*. Instead, a 17:1 peak (17:1ω6) was only found when *RiOLE1-LIKE* was expressed in Sc*Δole1* (Figure 23b). Thus, 17:1ω6 in *ScΔole1* expressing *RiOLE1-LIKE* co-elutes with a 17:1 fatty acid that is also synthesized in yeast WT after feeding with 15:0 fatty acid. The ω-denoted fatty acids eluted between the Δ9-cis and the saturated fatty acids of similar chain lengths, identical to the mycorrhiza-signature monounsaturated fatty acids detected in other tissues (Figure 22a—d). Therefore, *Ri*OLE1-LIKE has a broad substrate specificity and can introduce the double bond at position delta11 ('mycorrhiza-signature') into the fatty acids 15:0, 16:0, 17:0 and 18:0.
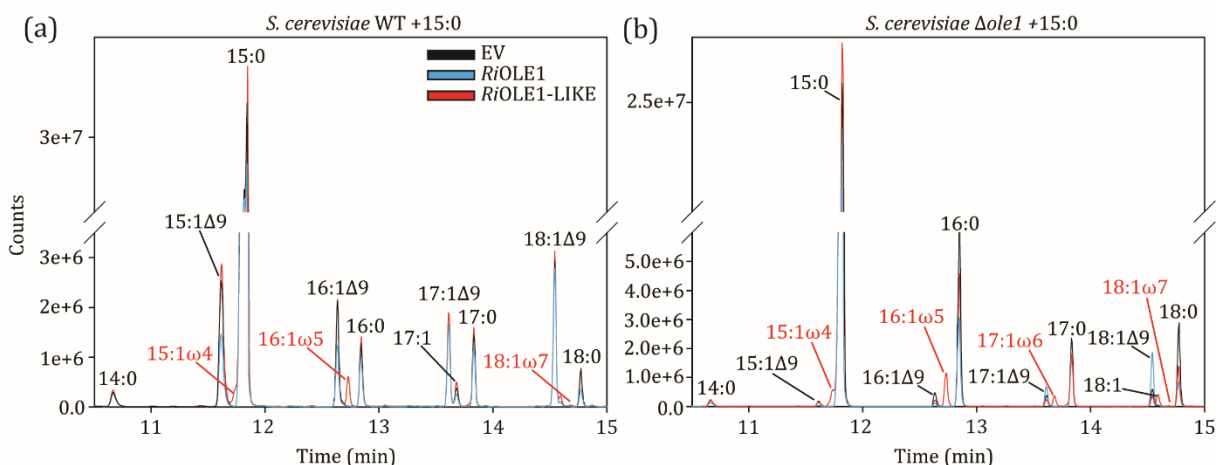
Figure 23: Fatty Acid Composition of Fatty Acid-supplemented Yeast Cultures Expressing *R. irregularis* Desaturases.
a,b) GC-MS total ion chromatograms of total fatty acids obtained from yeast WT **(a)** or Sc*Δole1* **(b)** expressing Rhiozphagus *OLE1* and *OLE1-LIKE* coding sequences. The culture media were supplemented with 1 mM 15:0 fatty acid that is normally absent from yeast. Upon supplementation with 15:0, novel monounsaturated fatty acids can be detected. These have either retention times similar to Δ9-cis fatty acids or, when *RiOLE1-LIKE* is expressed, to mycorrhiza-signature fatty acids that are denoted as ω-fatty acids here.
WT, wild-type; EV, Empty vector control; Ole1, Oleic acid dependent 1; Ri, *R. irregularis*.

3.2.5 *Ri*OLE1 and *Ri*OLE1-LIKE are Front-End Desaturases producing Δ9 or Δ11 Double Bonds

For determination of the double bond position in monoeonic fatty acids, fatty acid methyl esters from yeast cultures expressing *RiOLE1* and *RiOLE1-LIKE* were derivatized with dimethyl disulfide (DMDS) and subsequently analyzed by GC-MS. DMDS reacts with the double bonds of

unsaturated fatty acids and thus generates dimethyl disulfide adducts, causing a shift in retention time during GC-MS analysis (Yamamoto *et al.*, 1991) (Figure 24). When analyzed with the same temperature program described for underivatized fatty acid methyl esters in Figure 22a, DMDS derivatization caused a retention time shift of approximately 6 min for monounsaturated fatty acids. Figure 24 shows that $16:1\omega5$ and $18:1\omega7$ were found as DMDS adducts only in yeast expressing *RiOLE1-LIKE*.
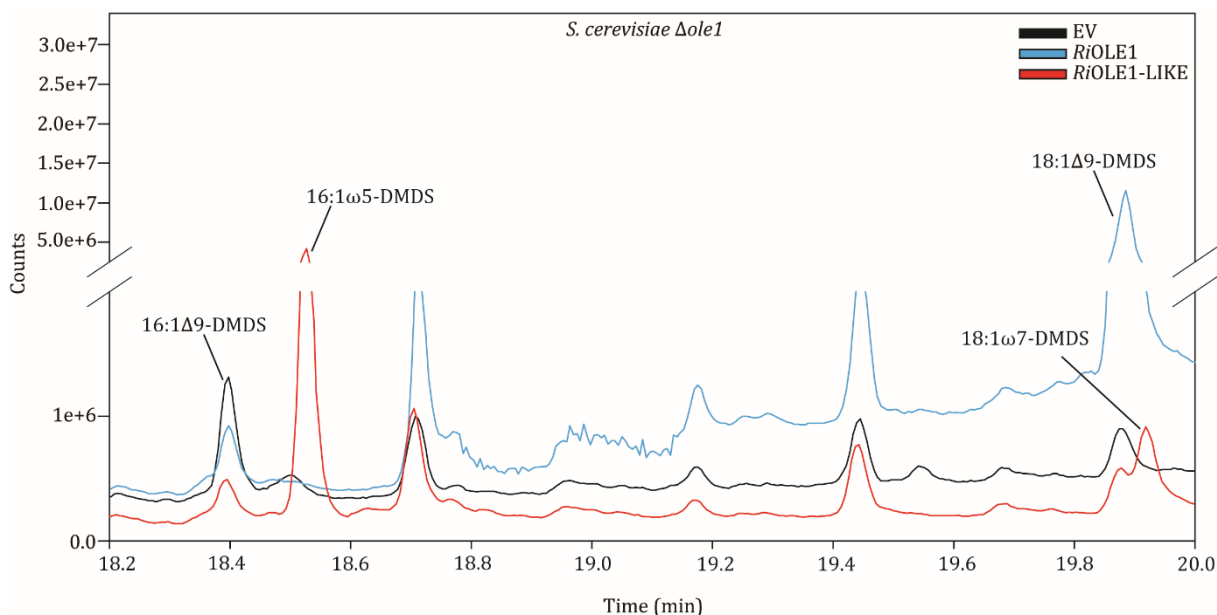
Figure 24: Fatty Acid Methyl Ester DMDS-adducts from Yeast Cultures Expressing *R. irregularis* Desaturases.
GC-MS total ion chromatograms of fatty acid methyl esters after DMDS derivatization, obtained from total lipids of yeast Sc*Δole1* expressing Rhiozphagus *OLE1* and *OLE1-LIKE* coding sequences. DMDS-adduct formation causes delayed elution from the column by approximately 6 minutes, compared to non-derivatized fatty acid methyl esters. Next to Δ9-cis fatty acids, when *RiOLE1-LIKE* is expressed, mycorrhiza-signature fatty acids (denoted as ω-fatty acids) occur.
WT, wild-type; EV, Empty vector control; Ole1, Oleic acid dependent 1; Ri, *R. irregularis*; DMDS, Dimethyldisulfide.

The mass spectra of the moneonic fatty acids revealed two major fragments that resulted from disruption of the bond between the methylthio-substituted carbon atoms (Figure 25). These fragments allowed the identification of the original double bond position. Fragmentation of 16:1Δ9-DMDS yielded a 145 m/z fragment containing the seven carbon atoms from the methyl-end with the additional methylthio-group (Fragment A in Figure 25a) and a second fragment of 217 m/z that included the remaining nine carbon atoms with the carboxyl group and the other methylthio-group at the carbon atom that formed the double bond in the original fatty acid (Fragment B in Figure 25a). The 217 m/z fragment also underwent secondary fragmentation, resulting in the loss of methanol (32 m/z) from the ester moeiety, which yields the fragment 185 m/z (Fragment A – 32 m/z), confirming the identity as a methyl ester. In $16:1\omega5$ fatty acid, the position of the double was verified to be located between carbon atoms 11 and 12, because

fragments of 117 m/z and 245 m/z were obtained in the mass spectrum (Figure 25b). The mass spectra for 18:1Δ9-DMDS adducts confirmed the position of the double bond in oleic acid between carbon atoms 9 and 10, because fragments of 173 m/z and 217 m/z were prominent (Figure 25c). In 18:1ω7, two major fragments of 145 m/z and 245 m/z were present in the mass spectrum of the DMDS adduct that confirmed the position of the double bond between carbon atoms 11 and 12. Therefore, 18:1ω7 is the second product of *Ri*OLE1-LIKE and resulted from the desaturation of 18:0, not from elongation of 16:1ω5, as the double bond would have been at 18:1ω5 in that case, because fatty acids are elongated by addition of two carbons at the carboxyl end (Tehlivets *et al.*, 2007). The mass spectra of DMDS adducts thus indicate that *Ri*OLE1-LIKE introduces double bonds on 16:0 and 18:0 fatty acids eleven carbon atoms counting from the carboxyl (delta) end. Accordingly, *Ri*OLE1-LIKE is a front-end desaturase that produces Δ11-monoeonic fatty acids.

3.2.6 Expression of *RiOLE1* and *RiOLE1-LIKE* influences Desaturation of the acyl-CoA Pool

As *Ri*OLE1 and *Ri*OLE1-LIKE are highly similar to the *Sc*OLE1 acyl-CoA desaturase, the impact *of RiOLE1* and *RiOLE1-LIKE* expression on acyl-CoA composition was determined in *N benthamiana* leaves and in yeast cultures. Acyl-CoA measurement with Q-TOF LC-MS/MS allowed the separation of acyl-CoA molecular species according to their fatty acid moieties. In *N. benthamiana* leaves, expression of *RiOLE1-LIKE* but not *RiOLE1* led to the occurrence of 16:1-CoA that is otherwise not detectable in leaf tissue. In yeast, 16:1-CoA was also detected in WT (Figure 26a). Quantification of the acyl-CoA molecular species in transgenic *N. benthamiana* additionally revealed an increase in 18:1-CoA when *RiOLE1* was expressed (Figure 26b and c). The occurrence of 16:1-CoA in *N. benthamiana* expressing *RiOLE1-LIKE* was accompanied by a relative decrease in 16:0-CoA (Figure 26c).

Heterologous expression of *RiOLE1* and *RiOLE1-LIKE* had an impact on the yeast acyl-CoA pool as well (Figure 26d and e). In yeast WT expressing *RiOLE1*, 18:1-CoA was increased and in the Sc*Δole1* background, this 18:1-CoA increase was also seen (Figure 26e). When *RiOLE1-LIKE* was expressed, the alterations of the acyl-CoA pool were strongest in the Sc*Δole1* background, where 16:1-CoA accumulated while 16:0-CoA was decreased. Additionally, 18:1-CoA was increased in relation to EV-*ScΔole1* but not to *RiOLE1-ScΔole1*. As the most abundant acyl-CoA was 16:1-CoA in yeast WT, expression in the WT background likely caused *R. irregularis* desaturases to compete with the endogenous yeast acyl-CoA desaturase OLE1, masking the CoA substrate preference in the case of *RiOLE1-LIKE*.

The described influence on the acyl-CoA molecular species in *N. benthamiana* and yeast leads to the suggestion that *Ri*OLE1 and *Ri*OLE1-LIKE are acyl-CoA desaturases, as is their homolog in yeast, *Sc*OLE1. However, as phospholipids, especially PC, rapidly exchange acyl groups
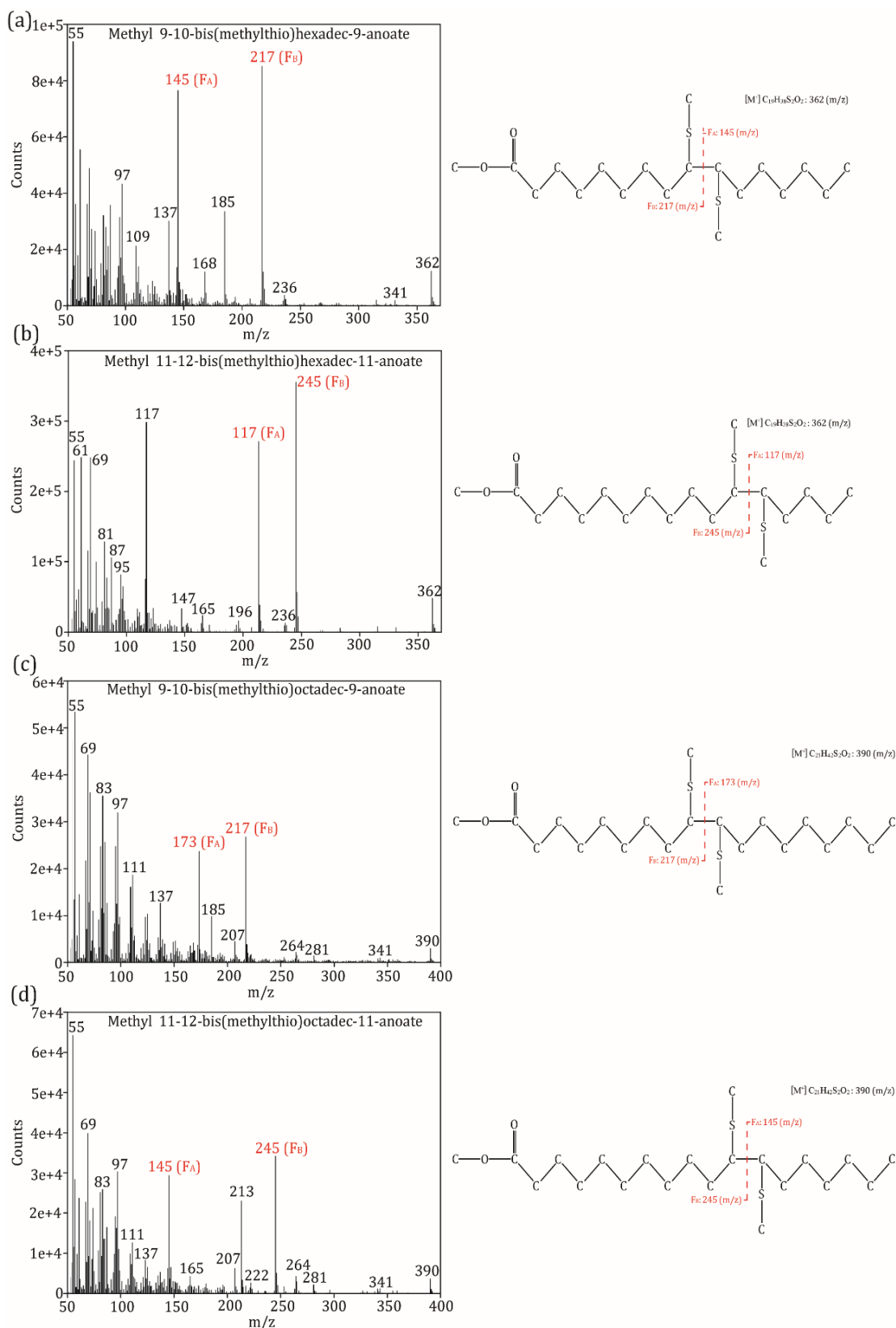
Figure 25: GC-MS Mass Spectra and Structures of Methyl-bis(methylthio) Fatty Acids.
a—d) Mass spectra and the corresponding structures of monoeonic fatty acids obtained after DMDS-deriviatisation of total fatty acid methyl esters from *ScΔole1* yeast cultures expressing Rhiozphagus *OLE1* or *OLE1-LIKE* coding sequences. Two major fragments are present in the mass spectra representing fragmentation between the methylthio-derivatised carbon atoms that formed the double bond in the original fatty acids. FA, Fragment A; FB, Fragment B.

with the acyl-CoA pool, thereby equilibrating the acyl composition of the PC and acyl-CoA pool, the observed effects on acyl-CoAs could also be the result from desaturation of e. g. PC and rapid equilibration with the acyl-CoA pool.
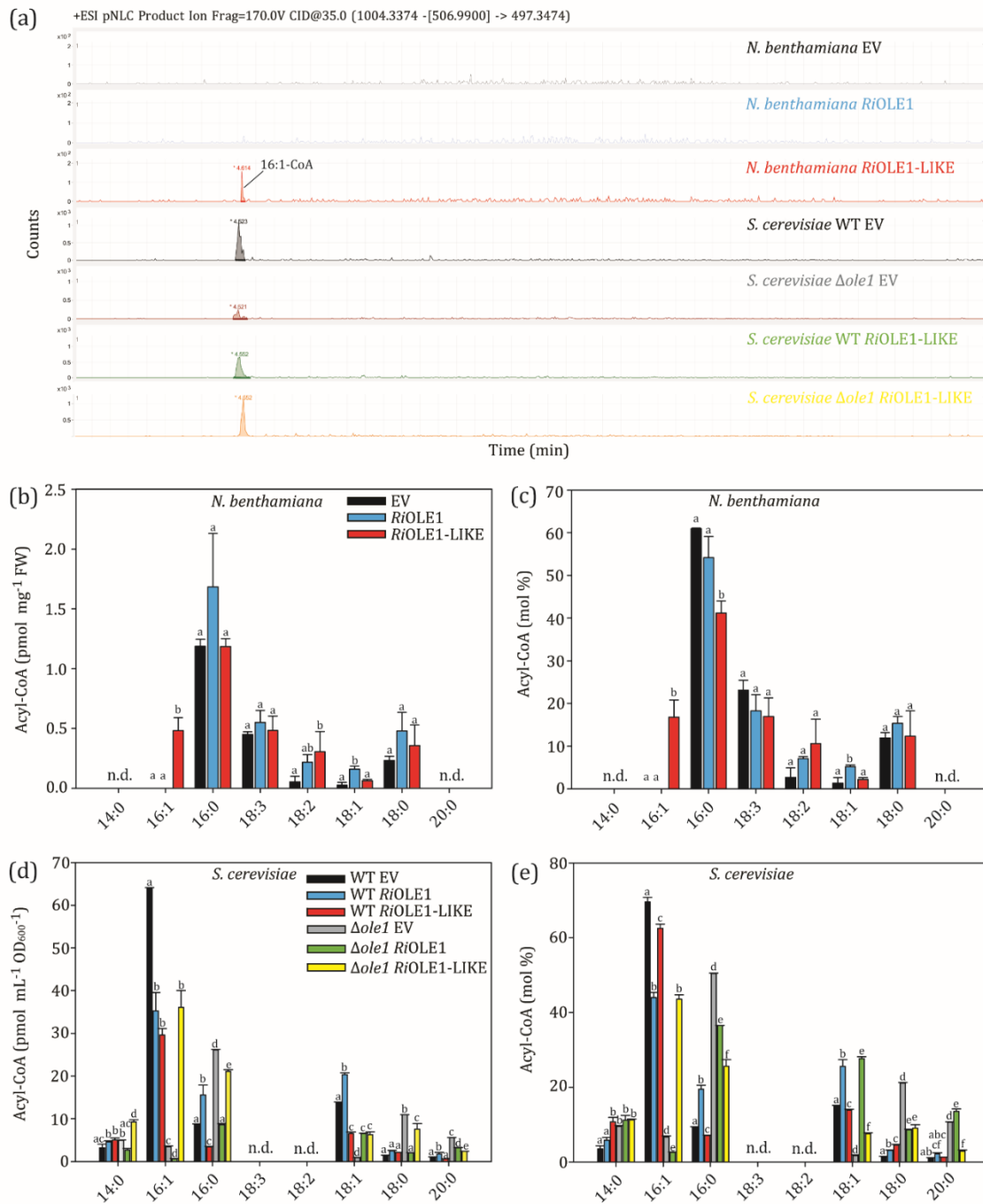
Figure 26: Acyl-CoA Composition in *N. benthamiana* and *S. cerevisiae* expressing *RiOLE1* and *RiOLE1-LIKE*.
a) Q-TOF LC-MS/MS chromatogram of acyl-CoAs extracted for the product ion (497.3474 m/z) obtained after neutral loss of adenosine-3'-phosphate,5'-diphosphate (506.9900 m/z) from the 16:1-CoA precursor (1004.3374 m /z).
b—e) Quantification of acyl-CoAs in relation to internal standard 17:0-CoA and tissue fresh weight or OD. RiOLE1-LIKE prefers 16:0-CoA but can also act on 18:0-CoA while RiOLE1 acts primarily on 18:0-CoA. WT, wild-type; EV, Empty vector control; Ole1, Oleic acid dependent 1; Ri, *R. irregularis.* All graphs represent average values, error bars depict standard deviation. One-way ANOVA with post-hoc Tukey, different letters indicate significant differences ($P < 0.05$).

4 Discussion

4.1 The *L. japonicus* Acyl-ACP Thioesterase FatM is required for the Synthesis of Palmitic Acid for Feeding of the Mycorrhiza Fungi

4.1.1 Arbuscular Mycorrhiza Host Plant Species contain an evolutionary conserved Set of Genes for Lipid Synthesis during Symbiosis

The *FatM* gene is exclusively expressed in roots that are infected with mycorrhiza (Gomez *et al.*, 2009; Wewer *et al.*, 2014), while the other acyl-ACP thioesterases *FatA*, *FatB* and *FatC* show ubiquitous expression patterns (Figure 29). *FatM* and *FatC* are only present in the genomes of plant species that engage in mycorrhiza symbiosis. FatM and FatC form seperate clades because the FatM sequences are more similar to FatB acyl-ACP thioesterases and are more distant to the FatA-type (Figure 4). This phylogenetic relationship is consistent with previously published phylogenetic analyses for *FatM* and other genes coding for proteins involved in lipid biosynthesis as well as symbiotic nutrient exchange, signal transduction and other metabolic processes (Bravo *et al.*, 2016; Favre *et al.*, 2014). *FatM* and these other AM-specific genes were lost during evolution in non-AM host families i. e. the Brassicales (Delaux *et al.*, 2014). *FatM* is therefore probably indispensable for AM symbiosis, and the phylogenetic distribution of *FatM* in hosts and non-hosts highlights the impact of AMF symbiosis on evolution of host genomes. However, FatM does not comprise a novel molecular function, but rather is involved in expansion and regulation of a pre-existing function (synthesis of palmitic acid) to orchestrate AM symbiosis. Taking a pre-existing molecular function and coordinating it for AM-symbiosis in AM-hosts, has been hypothesized for multiple molecular functions before, such as redox metabolism, signaling, transcription, membrane transport, lipid metabolism (including *FatM* and *RAM2*), defense, exocytosis, secondary metabolism and stress responses (Bravo *et al.*, 2016).

Reliance on host fatty acids was most likely acquired along with the establishment of the endomycorrhizal fungi, but is likely not a feature of the ectomycorrhizal fungi, because the genome of the ectomycorrhizal fungus *Laccaria bicolor* does contain a vertebrate-type I *FAS* (Reich *et al.*, 2009) and therefore presumably can produce its own fatty acids. The absence of *FAS* genes was reported as well for the fungal human skin pathogen *Malassezia sp.* that contains secreted lipases to scavenge host lipids (Triana *et al.*, 2017; xu *et al.*, 2007). Also, the maize pathogenic fungus *Ustilago maydis* induces host lipid metabolism to feed, among other metabolites, on the accumulating lipids at the infection sites, even though *U. maydis* still contains *FAS* genes (Doehlemann *et al.*, 2008; Lanver *et al.*, 2018). Thus, outsourcing of lipid synthesis is a feature observed in pathogenic and symbiotic interactions.

4.1.2   *FatM* is required for unimpeded Mycorrhiza Colonization

4.1.2.1 The *FatM* Mutation affects Mycorrhzia Marker Gene Expression

Using a reverse genetic approach with LORE1 transposon insertional mutants of *FatM* (Figure 5 a, b), mutant lines were identified with reduced *FatM* gene expression (Figure 5 c, d). Two independent alleles, designated *fatm-1* and *fatm-2*, were identified in which *FatM* gene expression was absent at 4 wpi (corresponding to ~30—40% total root colonization) (Figure 9c) but was present to some extent under extensive colonization at 7 wpi (50—90% total root colonization) (Figure 9d). However, *FatM* expression compared to WT remained strongly reduced. In both mutant alleles, the LORE1-transposon insertions are located upstream of the start codon of *FatM* at-218 bp in *fatm*-1 and -248 bp in *fatm*-2 and therefore might be promoter insertions or in the 5´UTR. Thus, these mutant lines do not represent null mutations, but show severely decreased *FatM* expression.

In both mutant alleles, the expression of *PT4*, a plant gene that is exclusively induced in arbuscocytes was reduced at 4 wpi but recovered to WT levels at 7 wpi (Figure 5d). The same expression pattern was observed for the fungal α-*TUBULIN* gene. The PT4 transporter locates to the PAM in juxtaposition to the hyphal fine-branches and its expression is therefore indicative of fully-branched, functional arbuscules (Pimprikar and Gutjahr, 2018) (see 4.2.2.2). α-*TUBULIN* is a fungal housekeeping gene expressed in hyphae and spores (Corradi *et al.*, 2004). Thus, at 4 wpi, mycorrhiza marker gene expression corresponds to reduced root colonization in the two *fatm* mutant alleles (Figure 5a and Figure 6a). At 7 wpi, reduced total root colonization and reduced colonization with arbuscules and hyphae in *fatm*-1 (Figure 6a) was not reflected by the level of *PT4* and α-*TUBULIN* gene expression, which was similar to WT. Therefore, mycorrhiza marker gene expression measured by RT-PCR can be recovered by increased colonization at 7 wpi in *fatm*-1 and *fatm*-2, even though the actual degree of colonization in *fatm*-1, investigated via staining and microscopy, remained decreased.

4.1.2.2 The Mutation of *FatM* Leads to Defective Fungal Fine Branching during the Formation of Functional Arbuscules and compromises Symbiotic Phosphate Transfer

Arbuscules are dynamic structures, and a fully functional arbuscule is characterized by extensive hyphal branching. Two types of branches are present on healthy WT arbuscules: large and fine branches. The phosphate transporter PT4 localizes to the PAM at the hyphal fine branches, indicating that these structures are active in symbiotic nutrient exchange. A GFP fusion protein of *M. truncatula* FatM was shown to be localized to stromulated plastids surrounding the fine branches of fully-branched arbuscules (Bravo *et al.*, 2017). In Medicago and Lotus *fatm* mutants, arbuscule branching was distorted and led to the occurrence of stunted arbuscules that lacked

extensive branching, which caused them also to be smaller (Figure 6) (Bravo *et al.*, 2017). As branching of hyphae causes the surface area of the symbiotic interface to increase (Alexander *et al.*, 1989), less extensive branching of *R. irregularis* hyphae in *fatm* probably leads to compromised metabolite exchange and ineffective arbuscules. This is reflected by decreased shoot inorganic phosphate (Figure 5e), although this could also be explained by the overall decreased colonization in *fatm* (Figure 5a).

Aborted arbuscule branching in *fatm* could be a result of the lack of symbiotic lipid transfer, mediated by *FatM*, leading to a shortage of membrane synthesizing capacity in *R. irregularis*. Alternatively, the decrease in symbiotic phosphate transfer (and probably other nutrients) might initiate a negative feedback response from the plant host. Accommodation of the fungus is controlled by the plant, and inefficient arbuscules are actively aborted by the host to prevent underperformance of the fungus (Choi *et al.*, 2018; Floss *et al.*, 2017; Gutjahr and Parniske, 2017; Toth and Miller, 1984). The stunted arbuscule phenotype of Lotus and Medicago *fatm* mutants resembles those of *pt4* and *str* transporter mutants (Breuillin-Sessoms *et al.*, 2015; MacLean *et al.*, 2017; Zhang *et al.*, 2010), therefore suggesting that symbiotic mineral nutrient exchange and symbiotic lipid exchange are connected, resulting in the same arrest of arbuscule development that ultimately leads to an inefficient symbiosis.

4.1.2.3 Lipid Storage in *R. irregularis* is compromised by the *fatm* Mutation

Spores and hyphae of AMF mainly contain neutral storage lipids, predominantly TAGs with fatty acids 16:0 and 16:1 (Beilby, 1980; Beilby and Kidby, 1980) that circulate as lipid droplets in between the fungal IRM and ERM (Bago *et al.*, 2002) and accumulate either in spores or in intraradical vesicles. In *fatm* mutants, vesicles occur less frequent and are smaller (Figure 6), indicating that intraradical lipid storage is compromised due to the *fatm* mutation. This is also reflected by the severe reduction in TAG, especially TAG containing the fatty acids 16:0 and 16:1 (Figure 9, 10). In agreement, 16:1 fatty acid accumulation was positively correlated with vesicle frequency in *R. irregularis* colonizing citrus roots (Graham *et al.*, 1995). In *R. irregularis*, vesicles consist of 58.2% lipids relative to their dry weight. Of these, 16.7% are neutral lipids, 28.32% glycolipids and sphingolipids and 15.91% phospholipids. Remarkably, 16:1 and 18:1 fatty acids predominate in neutral lipids as well as in glycolipids and sphingolipids but are less abundant in the phospholipids (Jabaji-Hare *et al.*, 1984). After initial root colonization and establishment of a functional AM symbiosis, the content of neutral lipids, foremost acylated with 16:0 and 16:1, drastically increases in colonized roots and ERM of *R. irregularis*, while phospholipids are only marginally increased by comparison (Olsson and Johansen, 2000). The strong reduction in 16:1ω5 (Figure 9), which is mostly due to decrease in 16:1ω5-NLFA (Figure 10a, b) in colonized *fatm* roots, therefore is indicative of a specific reduction in storage lipid accumulation. Fungal membrane (phospho)lipids probably are less affected by the reduction of symbiotic fatty acid

transfer because 16:1ω5-PLFA is present in drastically lower absolute amounts, even though 16:1ω5-PLFA was reduced by the same factor as 16:1ω5-NLFA in *fatm*-1 mutants (Figure 10).

As discussed above, decreased fungal lipid accumulation in colonized *fatm* roots could be the direct consequence of compromised fatty acid transfer from the plant to the fungus. With regard to the cumulative evidence for symbiotic fatty acid transfer presented here and in other studies (for review, see Keymer and Gutjahr (2018)), this is the most likely explanation for the observed vesicle and lipid phenotype. Eventhough in theory, reduced lipid accumulation could merely be the consequence of reduced fungal colonization and not specifically reduced fatty acid transfer, which then would be only an indirect side-effect of reduced colonization. Most mutations that negatively affect mycorrhiza colonization probably lead to a decrease in fungal membranes and consequently reduced marker lipids. Even when these genes might not directly be involved in host lipid reprogramming and lipid transfer to the fungus. Nonetheless, hyphae morphology was regular in *fatm* mutants and hyphae colonization was not as severely affected as vesicle formation, especially at 7 wpi (Figure 6), when symbiotic lipid transfer supposedly has been going on for 5—6 weeks. Specifically in *fatm*-2 at 7 wpi, hyphae and arbuscule colonization was restored to WT levels, but vesicles remained markedly reduced. Taken together, these observations favor a specific role for *FatM* in lipid accumulation in vesicles that becomes visible especially at later stages of AM symbiosis. Consistently, vesicle formation is common in orders of the Glomeromycotina except for the Gigasporales (Smith and Read, 2008) but not in ectomycorrhiza, which do not accumulate excessive amounts of lipids and contain *FAS* genes for synthesis of fatty acids (Reich *et al.*, 2009). The physiology and role of vesicles is largely unknown (Montero *et al.*, 2019). The first vesicles are formed early after root colonization and occur more frequently at later stages of the AM symbiosis. They could therefore fulfill a function that is vital for the fatty acid-auxotrophic lifestyle of AMF fungi, i. e. as temporary lipid storages until lipids are translocated to spores during sporulation.

4.1.3 Lipid Accumulation in AMF and use of Lipids as Biomarkers for Mycorrhiza Colonization

R. irregularis contains different unsaturated fatty acids that are absent from the plant host and therefore are employed as fatty acid biomarkers for estimation of mycorrhiza biomass. The most abundant one, 16:1ω5 (palmitvaccenic acid) occurs in many acyl-glycerolipids, mostly in the neutral storage lipid TAG (Figure 9) (Olsson and Johansen, 2000; Wewer *et al.*, 2014). Palmitvaccenic acid and other fatty acids of mycorrhiza origin as well as sterol lipids were used as lipid biomarkers for AMF under laboratory conditions and in the field (Bentivenga and Morton, 1996; Graham *et al.*, 1995, Lehman *et al.*, 2019; Nordby *et al.*, 1981). There is a correlation between the rate of colonization with *R. irregularis* and accumulation of marker fatty acids or sterol lipids in colonized roots (Figure 6 and 9) (Olsson *et al.*, 1995; Schliemann *et al.*, 2008;

Stumpe *et al.*, 2005). Fatty acid analysis in the colonized *fatm* mutant revealed that the mycorrhiza-marker fatty acids were differently reduced in the *fatm* mutants. While 16:1ω5 showed the most prominent reduction, 20:3 was less affected (Figure 9, 10). This was true for fatty acids in the neutral lipid fraction and the polar lipid fraction (Figure 10). Also, the free sterol lipid 24-methylcholesterol only showed a minor decrease, compared to 16:1ω5 in colonized *fatm* mutants (Figure 11). Therefore, even though all these compounds are restricted to *R. irregularis* tissue, their suitability as mycorrhiza lipid marker differs. In WT, 16:1ω5 quantification reveals mainly lipid storage in vesicles as well as spore formation, mostly due to accumulation of neutral lipids. Still, 16:1ω5 is also present to some degree in membrane-forming polar lipids, although in a considerable lower concentration (~14-fold less) (Figure 10a). In contrast, fungal 20:3 fatty acid accumulates approximately to a similar amount in the neutral lipid fraction (0.133 nmol.mg FW^1) and the polar lipid fraction (0.164 nmol.mg FW^{-1}). Different to 16:1ω5, 20:3 therefore is less valuable as marker for storage lipid accumulation, but provides insight into fungal membranes and storage lipids alike. The sterol lipid 24-methylcholesterol provides only information on AMF membrane abundance, but not of storage lipid accumulation as it is absent from the neutral lipid fraction.

Mycorrhiza signature fatty acids can also be detected in polar and neutral lipids of ectomycorrhizal fungi albeit their concentrations are very low in comparison to saturated fatty acids. In contrast to AMF the ecotmycorrhiza fungi *Pichia tinctorius* and *P. sylvestris* do not accumulate excessive amounts of lipids (Lackzo *et al.*, 2004). This confirms that especially monunsaturated 16:1ω5-NLFA is a suitable marker for *R. irregularis* lipid accumulation and likely also for other oleaginous AMF fungi, albeit there is less knowledge about the lipid accumulation in other AMF besides *R. irregularis*.

4.1.4 *FatM* dictates symbiotic Fatty Acid Supply for *R. irregularis*

4.1.4.1 Reprogramming of Plastidial Fatty Acid Synthesis by AMF

Heterologous expression in *E. coli* followed by fatty acid measurements or enzyme assays with recombinant protein demonstrate that FatM preferentially hydrolyses 16:0-ACP (Figure 14). The massive induction of *FatM* expression upon colonization with AMF (see appendix 7.3 and (Gomez *et al.*, 2009; Wewer *et al.*, 2014)) and the localization to plastids close to the fine branches of arbuscules (Bravo *et al.*, 2017) indicate that the colonization with AMF and the resulting arbuscule formation leads to a reprogramming of host plastidial fatty acid synthesis towards *de novo* synthesis of 16:0. This is in accordance with the finding that the most abundant fatty acids in *R. irregularis* ERM are 16:0 and its direct desaturation product 16:1ω5 (Figure 9 and (Wewer *et al.*, 2014)). The enzyme assay revealed that FatM is also able to hydrolyze considerable amounts of 18:0-ACP and 18:1Δ9cis-ACP *in vitro* when only these substrates were offered (Figure 14). In

arbuscocytes *in vivo*, FatM will however likely hydrolyze much less 18:0 and 18:1, as most of the elongated acyl-ACP will be scavenged as 16:0-ACP already and exported as 16:0 fatty acid from the plastid, due to the highest preference for 16:0-ACP.

In Arabidopsis *fatb* mutants, it was demonstrated how the different substrate specificities of the Fat enzymes influence *de novo* fatty acid synthesis. Arabidopsis *fatb* mutants reveal decreased 16:0 fatty acid content and a concomitant increase in 18:1Δ9, the main product of *At*FatA, in extraplastidial, eukaryotic lipids (Bonaventure *et al.*, 2003). The similarities in amino acid sequences of Lotus *Lj*FatM and Arabidopsis *At*FatB reveals the close relationship between these two enzymes (Figure 4). In addition, the functional relationship of FatM and *At*FatB was confirmed through complementation of the Arabidopsis *fatb* mutant using *FatM* from *M. truncatula* (Jiang *et al.*, 2018). Similar to *Lj*FatM, Arabidopsis FatB also prefers 16:0-ACP as substrate (Salas and Ohlrogge, 2002). However, while Arabidopsis FatB showed the second most activity with 18:1-ACP, the second most preferred substrate for *Lj*FatM was 18:0-ACP, while 18:1-ACP was only the third most preferred substrate (Figure 14c). This reveals that *Lj*FatM has a strong tendency to act on saturated acyl-ACPs (16:0-ACP>18:0-ACP>18:1-ACP) which is not strictly conserved in Arabidopsis FatB (16:0-ACP>18:1-ACP>18:0-ACP), even though the most preferred substrate also is saturated 16:0-ACP. Another important difference between *Lj*FatM and *At*FatB is the enzyme activity on 14:0-ACP. 14:0-ACP was hydrolyzed by *Lj*FatM at 0.092 pmol^{-1} min^{-1} μg protein^{-1}, which corresponds to 3.5-times less enzyme activity than on 16:0-ACP (0.33 pmol^{-1} min^{-1} μg protein^{-1}). In contrast, enzyme activity of *At*FatB on 14:0-ACP was ~22-fold less than for 16:0-ACP (Salas and Ohlrogge, 2002), which shows that *Lj*FatM has a broader substrate range by accepting also shorter chain lengths (14:0-ACP), contrary to *At*FatB.

The bay laurel acyl-ACP thioesterase *Uc*FatB1 also has enzyme activity on shorter chain, saturated acyl-ACPs (12:0-ACP>14:0-ACP) (Voelker *et al.*, 1992) and was accordingly placed in the phylogenetic analysis in between Arabidopsis FatB and *Lj*FatM (Figure 4). Similar to *Lj*FatM, the preference for 16:0-ACP is also conserved in the acyl-ACP thioesterase from *Cuphea hookeriana*, *Ch*FatB1. Similar to Arabidopsis FatB and contrary to *Lj*FatM, *Ch*FatB1 accepts 18:1 as second most preferred substrate (Jones *et al.*, 1995). *C. hookeriana* contains a second acyl-ACP thioesterase, *Ch*FatB2 for shorter chain fatty acids (10:0-ACP>8:0-ACP). In comparison, *Lj*FatM cannot hydrolyze these shorter chain acyl-ACPs (Figure 14c).

In conclusion, the substrate specificities of acyl-ACP thioesterases from multiple plant species have been shown to reflect the demand of fatty acids for subsequent lipid synthesis (Aznar-Moreno *et al.*, 2018; Dehesh *et al.*, 1996; El Tahchy *et al.*, 2017; Jones *et al.*, 1995; Rodríguez-Rodríguez *et al.*, 2014; Salas and Ohlrogge, 2002; Voelker *et al.*, 1992). Thus, the substrate specificity of *Lj*FatM reflects the importance of the different fatty acids induced by AMF colonization. They can therefore be ranked by their importance for AMF: 16:0 18:0>18:1>14:0,

even though subsequent modifications at the ER (elongation, desaturation) could have an influence as well.

Contrary to *LjFatM, LjFatA* and *LjFatB* gene expression is not affected by mycorrhiza colonization (see appendix 7.3). They show acyl-ACP substrate specificities related to their orthologs in Arabidopsis (Figure 15). Thus, they are likely to act as housekeeping thioesterases ensuring plant fatty acid supply independent from mycorrhiza fatty acid demand. Yet, their expression levels in colonized roots are low compared to *FatM* and thus their enzyme activities will likely be exceeded by the massively induced FatM, which causes a temporal increase in 16:0 fatty acids and consequently a decrease in plant 18:0 and 18:1 fatty acids in arbuscocytes.

The fungal demand for molecules synthesized in the plastids of the host cell is also revealed by the finding that in arbuscocytes, plastids were shown to proliferate and stromulate around the branching arbuscule (Fester *et al.*, 2001; Lohse *et al.*, 2005). Cytoplasmic rearrangement of host organelles and the endomembrane system is commonly observed around haustoria formed by pathogenic infection, and is the consequence of manipulation of the host metabolism (Kwaaitaal *et al.*, 2017). Therefore, induction of plastidial activity, i. e. 16:0 fatty acid synthesis via *FatM*, is in agreement with re-organisation of the host metabolism by AMF.

4.1.4.2 Transfer of Symbiotic Fatty Acids after Labeling with $^{13}C_2$-Acetate

In plant plastids, acetyl-coenzyme A synthetase (ACS) converts imported cytosolic acetate and coenzyme A into acetyl-coenzyme A (acetyl-CoA) (Behal *et al.*, 2002). The carboxylation of acetyl-CoA to malonyl-CoA is the committed step in fatty acid *de novo* synthesis. It is catalyzed by acetyl-CoA carboxylase (ACC). In the next reaction, two carbons from malonyl-ACP are added per reaction cycle to the growing fatty acid chain. Therefore, exogenously applied $^{13}C_2$-acetate is relocated to the plastid and the two ^{13}C-atoms are used to synthesize fatty acids *de novo* via elongation by addition of two carbons per cycle. Consequently, mutants of *acs* in Arabidopsis show strongly reduced labeling of fatty acids by exogenous application of acetate, highlighting the importance of this enzyme for acetate-labeling of fatty acids (Lin and Oliver, 2008).

In Lotus colonized and non-colonized roots subjected to exogenous $^{13}C_2$-acetate, the ^{13}C-label could be quantified in all major fatty acids (Figure 16, 17, 18). The amount of ^{13}C introduced via $^{13}C_2$-acetate was corrected for the abundance of naturally occurring isotopologs, giving rise to the ^{13}C over-excess label. When comparing colonized and mock-inoculated WT roots, the abundance of ^{13}C over-excess label in all fatty acids was increased by colonization with *R. irregularis* (Figure 16b). This finding was previously reported by labeling of *Glomus mosseae*-inoculated onion roots with $^{14}C_2$-acetate (Lösel and Cooper, 1979). In the Lotus experiment described here, the colonized roots were placed in $^{13}C_2$-acetate containing buffer ON (~12 h labeling period). The $^{13}C_2$-acetate is taken up into the root cell apoplast. From there, it could be accessed by the plant and the fungal hyphae alike. In hyphae, it could be used for

elongation of fatty acids (Calonne *et al.*, 2014; Trepanier *et al.*, 2005). Accordingly, *R. irregularis* extraradical hyphae, growing asymbiotically from germinating spores, or in symbiosis *with D. carota*, were able to take up and metabolize labeled glycerol, glucose,xylose and acetate. This shows that AM hyphae have the mechanisms for uptake and acquisition of these carbon compounds independent of transfer via arbuscules (Bücking *et al.*, 2008; Helber *et al.*, 2011; Lammers *et al.*, 2001; Pfeffer *et al.*, 1999). As AMF lack cytosolic type-I *FAS* (Ropars *et al.*, 2016; Sedzielewska Toro and Brachmann, 2016; Tang *et al.*, 2016; Tisserant *et al.*, 2013; Wewer *et al.*, 2014), 16:0 fatty acids are very likely not synthesized in *R. irregularis.* This was brought forward as hypothesis from earlier labeling experiments using a split-petri dish system where the ^{14}C-label from ^{14}C-acetate accumulated in 16:0 and 16:1 fatty acid in ERM only if the plant was also able to access the acetate (Trepanier *et al.*, 2005). Therefore*,* despite of being available to the plant roots and the fungal intraradical hyphae alike*,* a considerable portion of the ^{13}C$_2$-acetate applied to colonized Lotus roots was likely acquired by the plant and used for *de novo* synthesis of fatty acids. This is also emphasized by the abundance of ^{13}C over-excess label in 16:0 fatty acid in colonized WT. The isotopolog labeling pattern of 16:0 congruently showed the typical ^{13}C$_2$-pattern indicative of incorporation via malonyl-ACP during *de novo* synthesis, because the isotopologs with even number of ^{13}C carbon atoms were abundantly labeled (Figure 16a). In the fungus, 16:0 fatty acid is desaturated to the mycorrhiza-signature fatty acid 16:1ω5 (see 3.2). In colonized WT, the ^{13}C-label was highest in 16:1ω5 (Figure 16b). Together, these results indicate that a high proportion of the applied ^{13}C$_2$-acetate was acquired by the plant to synthesize 16:0 that then was transferred to the fungus for desaturation to 16:1ω5.

In the colonized *fatm*-1 mutant, ^{13}C over-excess in 16:1ω5 was reduced compared to colonized WT and the same was observed for 20:3 fatty acid, albeit the latter was of lower abundance (Figure 16). This reduction was independent of the reduced total root colonization in *fatm*-1 mutants (Figure 9a), as was demonstrated by relative ^{13}C over-excess incorporation in % to total fatty acid abundance (Figure 17). Reduced ^{13}C over-excess in mycorrhiza-signature fatty acids in colonized *fatm*-1 therefore reveals that FatM is required for unimpaired symbiotic fatty acid supply. In colonized *fatm*-1, the ^{13}C label increased almost two-fold in 18:2 and 18:0 fatty acids, compared to colonized WT (Figure 16b) and this was also independent of reduced fungal biomass in colonized *fatm*-1 (Figure 17b). Therefore, this suggests that due to reduced gene expression of *FatM* in colonized *fatm*-1, the ^{13}C over-excess is re-directed from mycorrhiza marker fatty acids (16:1 ω5 and 20:3) into other fatty acids (18:2 and 18:0). 18:2 and 18:0 fatty acids occur in both symbiotic partners. Thus, re-direction of ^{13}C over-excess in colonized *fatm*-1 is either due to increased uptake of ^{13}C$_2$-acetate and elongation of fatty acids by fungal mycelium or due to increased labeling of plant 18:2 and 18:0.

Despite of the imminent importance of FatM for accumulation of ^{13}C over-excess label in mycorrhiza fatty acids from ^{13}C$_2$-acetate labeling, residual ^{13}C over-excess label is still observed in

16:1ω5 in colonized *fatm*-1 (Figure 16, 17, 18). One explanation could be the residual gene expression of *FatM* in colonized *fatm*-1 (Figure 5). Even though these colonized *fatm*-1 roots were enriched in stunted arbuscules that were arrested in hyphal fine branching, there were also normal, fully branched arbuscules (see 3.14). These could likely still function in symbiotic nutrient (i. e. fatty acid) transfer. Therefore, symbiotic fatty acid transfer is severely reduced, but not fully abolished in colonized *fatm*-1 mutants.

The ^{13}C over-excess in 16:0 fatty acid was increased two-fold by AMF-colonization in WT, compared to mock-inoculated roots (Figure 16b). As discussed above, ^{13}C over-excess in 16:0 in colonized roots very likely exclusively originates from *de novo* synthesis of 16:0 fatty acid in the plant. Therefore, colonization with *R. irregularis* increased the rate of 16:0 fatty acid *de novo* synthesis. This is in agreement with the requirement of the *DIS* gene for mycorrhiza development and symbiotic fatty acid transfer (Keymer *et al.*, 2017). *DIS* encodes a β-ketoacyl-ACP synthase (KAS), a component of the FAS complex. Figure 27 summarizes lipid synthesis during symbiosis and specifically highlights the movement of acyl-groups containing ^{13}C-labeled carbon from ^{13}C$_2$-acetate feeding.

4.1.4.2.1 Estimation of the Rate of Symbiotic Fatty Acid Transfer

As discussed above, the ^{13}C$_2$-acetate labeling experiment suggested that a substantial portion of ^{13}C over-excess was transferred as 16:0 fatty acid. As an estimate, this was at least ~38.5% of the total ^{13}C over-excess signal, because 38.5% ^{13}C over-excess label was found in 16:1ω5 at 4 wpi in WT roots (Figure 18). In other experiments, seven days of labeling with ^{13}C-glucose of *D. carota* inoculated with *R. irregularis* revealed an enrichment of ^{13}C in the 16:1ω5-NLFA signature fatty acids by 2.2% of total root carbon in IRM and 1.1% in ERM (Olsson *et al.*, 2005). These results indicate that next to the fatty acid transfer indicated by ^{13}C$_2$-acetate labeling in figures 16—18, glucose is transferred as well. How the transfer of these carbon compounds compares to each other and whether the fungus prefers one over the other remains unknown. However, comparison of labeling rates from glucose versus acetate fedding suffer from the fact that the glucose taken up by the plant might not be transferred to the fungus directly but broken down in plant glycolysis. The resulting acetate could be used to synthesis fatty acids that might eventually be transferred to the fungus.

At 4 wpi in colonized WT, 4.9% of ^{13}C over-excess label was found in fungal 20:3 fatty acid (Figure 18a, first column). As opposed to the ^{13}C over-excess label in 16:1ω5, which likely exclusively originates from labeled ^{13}C-16:0 obtained from the plant, the ^{13}C over-excess label in 20:3 can have two origins (Figure 27). Firstly, ^{13}C-labeled fatty acids acquired from the plant (i. e. ^{13}C-16:0 fatty acid) that are then elongated and desaturated to 20:3 within the fungus using unlabeled acetate from fungal metabolism. And, secondly, unlabeled fungal fatty acids that were elongated with ^{13}C-acetate scavenged by the fungus from the apoplast or the labeling buffer.
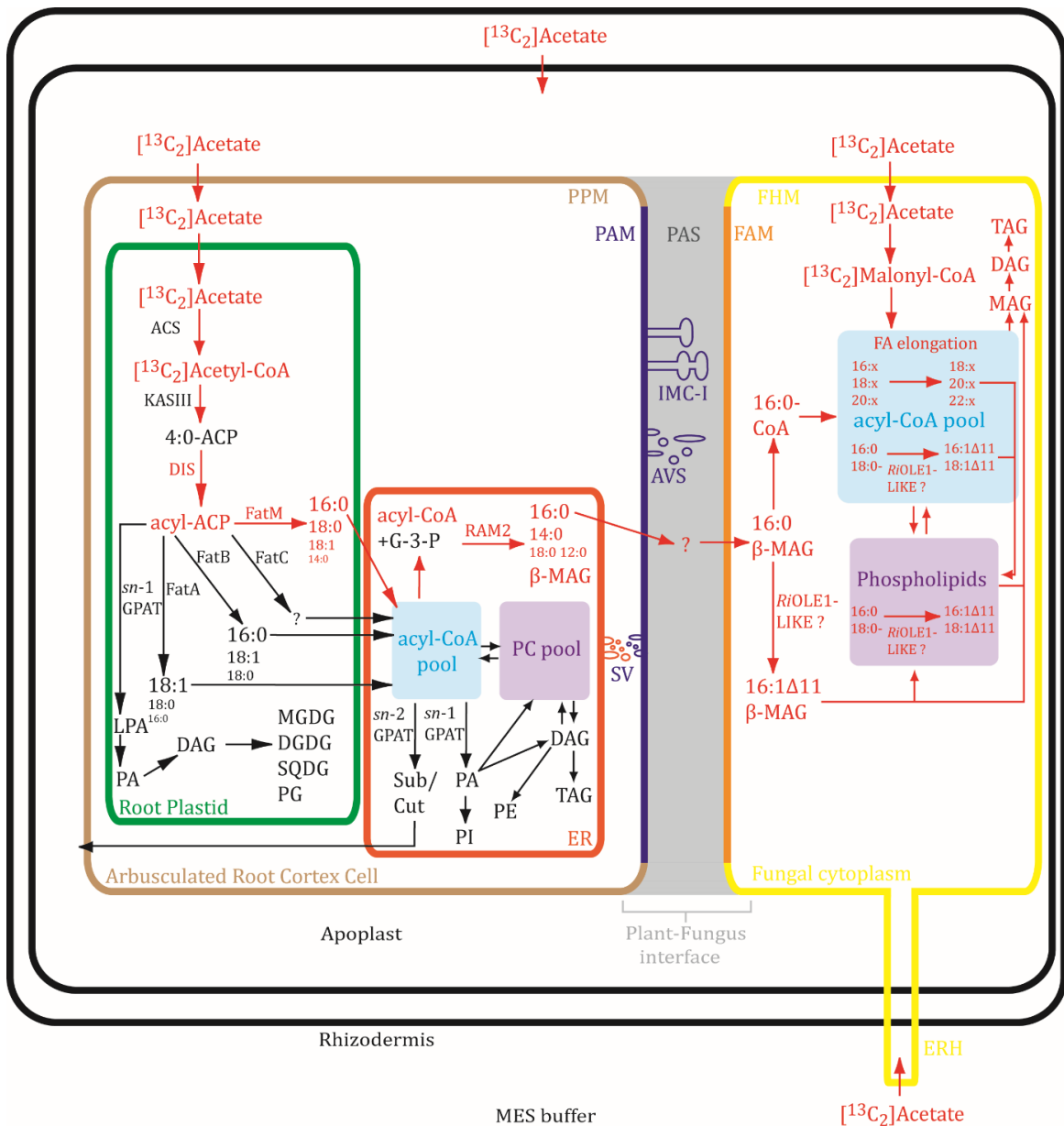
Figure 27: Metabolism of ¹³C-Acyl Groups after ¹³C₂-Acetate Labeling during AM symbiosis

In arbuscocytes, genes encoding plastidial *de novo* fatty acids synthesis genes (*DIS*, *FatM*) and lipid synthesis genes at the ER (*RAM2*) are essential for fungal development. 16:0 fatty acid from the plastid might be incorporated into 16:0-β MAG hypothetically for secretion to the fungus. At the ER-Golgi network, the plant secretory pathway is active for synthesis of the PAM via membrane fusion of secretory vesicles (SV). In the apoplastic interface between plant cell and fungal arbuscule, evaginations of the PAM (Intramatrix compartment I, IMC-I; Ivanov et al, 2019) and discrete, apoplastic extracellular vesicles (AVS; Roth et al, 2019) are present. Regular plant lipid synthesis that is likely not responsive to mycorrhiza colonization is depicted in black. The mycorrhiza-induced lipid synthesis pathway and the possible fate of ¹³C-labeled carbon from ¹³C₂-acetate are highlighted in red. Due to the lack of type-I *FAS* genes in *R. irregularis*, ¹³C in fungal 16:x fatty acids are most likely derived from *de novo* synthesized plant fatty acids, while label in 18:x and 20:x fatty acids could also have arisen by fatty acid elongation at the ER with ¹³C₂-acetate taken up by fungal ERH from the medium or via IRH from the apoplast. The mycorrhiza signature fatty acid 16:1ω5/Δ11 is synthesized by *Ri*OLE1-LIKE. The substrate specificities of plant Fat and RAM2 enzymes are depicted with the most preferred substrate in large letter size.

ACS, ACETYL-COA SYNTHASE; KASIII, β-KETOACYL SYNTHASE; G-3-P, Glycerol-3-Phosphate; Sub/Cut, Suberin/Cutin; SV, Secretory vesicles; IMC-I, Intramatrix compartment I; AVS, Apoplastic vesicular structure; PPM, Plant plasma membrane; PAM, Periarbuscular membrane; PAS, Periarbuscular space; FAM, Fungal arbuscule membrane; FHM, Fungal hyphae membrane; ERH, Extraradical hyphae.

To provide a more accurate estimation of the rate of symbiotic fatty acid transfer, it is therefore important to distinguish these two routes for ^{13}C enrichment of 20:3 fatty acid. In the colonized *fatm*-1 mutant, the relative ^{13}C over-excess label in fungal 20:3 fatty acid was decreased to 10.05% as compared to 14.3% in WT (in% of ^{12}C + ^{13}C fatty acids) (Figure 17). Because FatM provides an entry point for ^{13}C-labeled fatty acids to the fungus, this suggests that in the present experiment at least one third of the ^{13}C over-excess label in fungal 20:3 was retrieved from the plant as fatty acid. Thus, of the 4.9% ^{13}C over-excess label in 20:3, at least 1.6% were probably retrieved as fatty acid from the plant. As the origin of the other fatty acids that were labeled by ^{13}C$_2$-acetate (14:0, 16:1Δ9, 18:0, 18:1, 18:2 and 18:3) are present in plant and fungus, the rate of labeling in these fatty acids cannot be seperately estimated in the plant and the fungus, but only as the sum of both.

Other labeling experiments with ^{13}C-glucose of Lotus roots in a two-compartment system focused on the ^{13}C-isotopolog pattern in 16:0 and 16:1ω5 fatty acids in fungal ERM and the colonized roots. In the ERM from *dis* and *ram2* mutants, the ^{13}C-isotopolog pattern did not resemble the one from colonized roots and the total ^{13}C label in these fatty acids was reduced. In addition to the labeling experiments presented here, these observations provide evidence that next to FatM, symbiotic fatty acid transfer also requires β-keto-acyl ACP synthesis by DIS and lipid modification at the ER by RAM2 (Keymer *et al.*, 2017; Keymer and Gutjahr, 2018).

4.1.5 RAM2 might synthesize β-Monoacylglycerols for AMF from Fatty Acids released by FatM

The mycorrhiza-specific *RAM2* gene encodes a glycerol-3-phosphate acyltransferase with phosphatase domain, that produces predominantly 16:0 β-MAG from 16:0-CoA and glycerol-3-phosphate (Luginbuehl *et al.*, 2017). 16:0 β-MAG showed a mycorrhiza-signature pattern and failed to accumulate to the same extent in *fatm*-1 colonized roots as in colonized WT (Figure 12 and Figure 13). The latter was previously also reported for Medicago *fatm* (Bravo *et al.*, 2017). 16:0 β-MAG also fails to accumulate in the colonized lipid synthesis mutants *ram2* and *dis* of Lotus as well as in a mutant for the hypothetic lipid transporter *str* (Keymer *et al.*, 2017). These results suggest that FatM is responsible for a shift in plant fatty acid export from the plastids towards 16:0, which is converted into 16:0-CoA and transferred to 16:0 β-MAG at the ER by RAM2. 16:0 β-MAG might subsequently be secreted to the periarbuscular space for uptake by the fungus. 16:0 β-MAG was present in profound amounts in the ERM of *R. irregularis* and was less abundant in ERM with less spores and even less in colonized roots (Figure 12). This is to some extent counter-intuitive, because if 16:0 β-MAG is the lipid that is transported to the fungus, one would expect the highest concentration in colonized roots, as this is where the nutrient exchange takes place. One explanation for this discrepancy could be that not all of the transferred 16:0 β-MAG is directly incorporated into fungal glycerolipids but stored and transported as β-MAG to the spores.
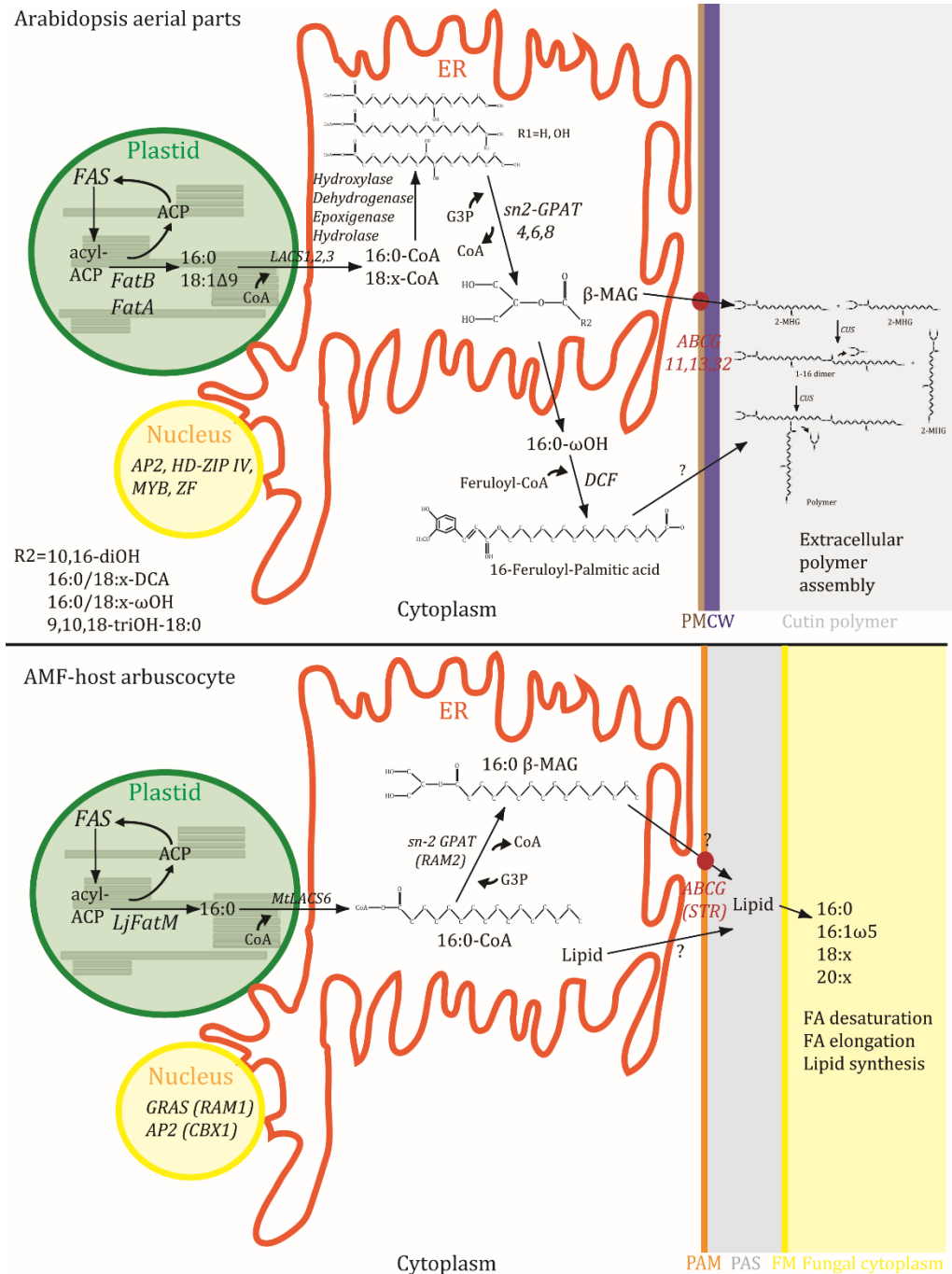
Figure 28: Cutin Biosynthesis in Arabidopsis Aerial Parts compared to hypothetical extracellular Lipid Secretion stimulated by Mycorrhiza Colonization in AMF-host Roots.

In Arabidopsis (upper panel), synthesis of cutin is depicted. Acyl-CoAs are modified by cytochrome P450 (CYP450) monoyxgenases to generate cutin precursors that are used by *sn2*-GPAT to generate *sn2*-MAG (β-MAG), which serves as cutin monomer. PM-resident ABCG transporters are inferred in secretion of monomers into the apoplast for subsequent polymerization of β-MAG cutin monomers (2-MHG) by CUTIN SYNTHASE (CUS) (Yeats *et al.*, 2012; Yeats *et al.*, 2014). In AMF-host arbuscocytes (lower panel), the massive induction of *FatM* might lead to a surplus of 16:0-CoA at the ER that could be used by the RAM2 GPAT to synthesize 16:0 β-MAG, which is subsequently secreted to the PAS via the ABCG transporter STR and taken up by the fungus. The pathway is depicted for 16:0 fatty acid, because it is the primary product of DIS (KASI), FatM and RAM2. As there is no direct evidence for the 16:0 β-MAG secretion-route, lipids could be taken up by the fungus via alternative mechanisms.

FAS, *FATTY ACID SYNTHASE*; *LACS*, *LONG-CHAIN ACYL-COA SYNTHASE*; G3P, Glycerol-3-Phosphate; *DCF*, *DEFICIENT IN CUTIN FERULATE*; *GPAT*, *GLYCEROL-3-PHOSPHATE ACYLTRANSFERASE*; 2-MHG, 2-mono(10,16-dihydroxyhexadecanoyl)glycerol; *CUS, CUTIN SYNTHASE*; *RAM2*, *REDUCED ARBUSCULAR MYCORRHIZA*; *STR*, *STUNTED ARBUSCULES*; PM, Plasma membrane; CW, Polysaccharide cell wall; PAM, Periarbuscular membrane; PAS, Periarbscular space; FM, Fungal membrane.

The mycorrhiza-marker fatty acid 16:1ω5 is produced by desaturation of 16:0 by the fungal desaturase *RiOLE1-LIKE* (see 3.2)*. Even though the exact substrate of *RiOLE1-LIKE* is unknown, fungal fatty acid desaturases either use acyl-CoA or acyl-lipids as substrate (Los and Murata, 1998). As *Ri*OLE1-LIKE is a homolog of the yeast acyl-CoA desaturase *Sc*OLE1 (Figure 20), it likely also acts on acyl-CoA. If 16:0 fatty acids are transferred as β-MAG, they could be involved in a fungal acyl-CoA synthesis reaction to generate e. g. 16:0-CoA, which is then desaturated by *Ri*OLE1-LIKE and then enters fungal glycerolipid (phospholipids and TAG) synthesis via the acyl-CoA pool (Figure 27). Alternatively, *Ri*OLE1-LIKE could act directly on glycerolipids, such as phospholipids or MAGs, to generate the desaturated fatty acid that could then be used for TAG synthesis, even though there is no experimental evidence that *Ri*OLE1-LIKE act on acyl-lipids and not on acyl-CoA.

Regardless of the substrate of *Ri*OLE1-LIKE, the relatively high abundance of 16:1ω5 α-MAG and β-MAG species could also reflect that these are intermediates in TAG synthesis in *R. irregularis*. Consistently, 16:1ω5 β-MAG and 16:0 β-MAG were also present in colonized *D. carota*, confirming that some TAG synthesis also occurs in the IRM and not exclusively in the ERM during spore formation. Upon sporulation in the AMF *Glomus versiforme*, TAG is hydrolyzed by lipases to yield energy and fatty acids for membrane synthesis (Gaspar *et al.*, 1994). In the AMF *Glomus caledonius*, MAGs acylated to 16:0 and 16:1 increased upon spore germination and hyphae growth (Beilby and Kidby, 1980). In isolated spores and vesicles from *R. irregularis* and *Glomus vesiculiferum*, MAGs were the third most abundant lipid species, next to TAGs and free fatty acids (Jabaji-Hare, 1988). These findings together with the results presented here show that MAGs can be substrates of fungal lipid catabolism and may therefore also serve in anabolism during TAG synthesis. However, more research targeting storage lipid synthesis in AMF is required to answer the question how 16:0 fatty acids are transferred and integrated in the fungal lipid metabolism.

RAM2 was initially proposed to function in the synthesis of cutin monomers that have a signaling function for pathogens and AMF (Murray *et al.*, 2013; Wang *et al.*, 2012). GPATs are localized to the ER-membrane and. In Arabidopsis, they have been organized by the presence of a phosphatase domain and by their involvement in subern, cutin or membrane and storage lipid synthesis (Beisson *et al.*, 2012; Shockey *et al.*, 2016). Figure 28 compares cutin biosynthesis in Arabidopsis aerial parts and mycorrhiza-colonized roots of AMF-host plants. Three cutin-specific GPATs exist in Arabidopsis that transfer an acyl group from acyl-CoA to the *sn-2* position of glycerol-3-phosphate: *AtGPAT4*, *AtGPAT6* and *AtGPAT8* (Jayawardhane *et al.*, 2018). These enzymes produce *sn-2* lysophosphatidic acid as intermediate product and finally produce *sn-2* MAG (β-MAG) by cleavage of the phosphate via the phosphatase domain. *AtGPAT6* has the most sequence similarity to *RAM2* from AMF-host plants (Wang *et al.*, 2012). *In vitro* enzyme assays with *At*GPAT6 showed that the most preferred acyl donor is 16:0 ω-OH-CoA, but that it can also

use 18:1 ω-OH-CoA and 18:1 DCA-CoA as well as 10,16-diOH 16:0-CoA (Yang *et al.*, 2012). The ω-hydroxylated and α,ω-dicarboxylic fatty acids are typical aliphatic monomers found after depolymerization of cutin in the shoots and suberin in the roots (Nawrath *et al.*, 2013). *Atgpat6* mutant flower cutin is deficient in 16:0 ω-OH and 16:0 DCA (Li-Beisson *et al.*, 2009), while stem cutin in *Atgpat4/Atgpat8* double mutants is deficient in all (16:0/18:x) ω-OH and DCA cutin monomers (Li *et al.*, 2007). Similar to *At*GPAT6, RAM2 preferentially uses a 16 carbon fatty acid, albeit 16:0 non-hydroxylated fatty acid (Luginbuehl *et al.*, 2017). Therefore, the RAM2 enzyme might have evolved from cutin-specific GPATs. However, contrary to biosynthesis of cutin precursors, the hypothetical AMF-induced MAG synthesis does likely not involve further fatty acid modifications at the ER, as no MAG species (α or β) with hydroxylated fatty acids or dicarboxylic fatty acids could be detected. Taken together, this indicates that the β-MAG species produced by RAM2 function in fungal nutrition rather than signaling, in accordance with the current scientific consensus (Bravo *et al.*, 2017; Choi *et al.*, 2018; Jiang *et al.*, 2017; Keymer *et al.*, 2017; Keymer and Gutjahr, 2018; Luginbuehl *et al.*, 2017; Luginbuehl and Oldroyd, 2017; MacLean *et al.*, 2017; Rich *et al.*, 2017; Roth and Paszkowski, 2017). How does the putative lipid (i. e. 16:0 β-MAG) reaches the fungus? During extracellular cutin assembly, PM-resident ABCG transporters (*AtABCG11*, *AtABCG13*, *AtABCG23*) have been described that have been inferred to be involved in secretion of cutin monomers to the apoplast for subsequent extracellular polymerization (Fich *et al.*, 2016). In addition, β-MAGs with C22 and C24 fatty acids were shown to be present as components of extracellular root waxes (Li *et al.*, 2007), showing that after intracellular synthesis, MAGs can be exported from the cell. Therefore, a similar trans-membrane lipid transport mechanism might exist in AM symbiosis (see 4.1.5.1).

4.1.5.1 Lipid Secretion across the Symbiotic Interface

Fatty acids and lipids are water-insoluble and therefore insoluble in the plant cytoplasm, the periarbuscular space and the fungal cytoplasm. Furthermore, they need to traverse the periarbuscular membrane and the fungal plasma membrane to reach the fungal cytoplasm and finally the ER, where they can be incorporated into fungal lipids. Recently, electron microscopy and tomography have revealed electron-dense fungal tubular structures close to the fungal plasma membrane, located in the fine and thick branches of the arbuscules (Ivanov *et al.*, 2019). In the same study, intramatrix compartments (IMC-I, see figure 27), which are tubular and vesicular extensions of the PAM into the PAS around the arbuscule thick branches, were reported. It has also been described that in functional arbuscules close to the PAM, the plant cytoplasm is enriched in ER, golgi bodies, plastids and mitochondria.

In a second study using the same approach, similar PAM evaginations, called memtubes, were described, which also are continuous with the plant cytoplasm and are close to the fungal membrane around the arbuscule fine branches. Additionally, discrete vesicles were described that

were present in the PAS in the vicinity of the arbuscule fine and thick branches. These were termed apoplastic vesicular structures (AVS, see figure 27) and might resemble secretory, extracellular vesicles directed by the plant to the fungus for symbiotic nutrient (lipid) transfer (Roth *et al.*, 2019).

Taken together, the plant might set up a secretory machinery to enable export of molecules from the ER, such as lipids (i. e. 16:0 β-MAG), and an interconnected network of membrane evaginations and extracellular vesicles to enable transfer across the plant-fungus interface. Earlier results have shown that the PAM adjacent to the fine branches is targeted by polar localization of exocytosis (Ivanov *et al.*, 2012; Zhang *et al.*, 2015) and is thus the place of arbuscule growth by hyphal extension and branching. Additionally, the symbiotic phosphate transporter PT4, which engages in symbiotic mineral nutrient transfer, is targeted to the PAM at these fine branches (Breuillin-Sessoms *et al.*, 2015; Harrison *et al.*, 2002; Pumplin *et al.*, 2012). The fine branches are thus very active in symbiotic mineral exchange and therefore could very well be the place for the suggested symbiotic lipid transfer. Even though the thick branches and the arbuscule trunk do also contain close contact sites with the plant cytoplasm and might therefore also engage in metabolic exchange.

The half-size ABC transporters STR1 and STR2 are expressed in the PAM in the arbuscule branch domain, similar to PT4 (Gutjahr *et al.*, 2012; Zhang *et al.*, 2010). In Arabidopsis, different ABCG transporter have been characterized that exhibit defects in root and pollen suberin (Yadav *et al.*, 2014), and in the cuticle of Arabidopsis aerial organs (Bessire *et al.*, 2011; Bird *et al.*, 2007; Panikashvili *et al.*, 2011). The suberin and cutin chemical composition of these mutants is furthermore characterized by a decrease in aliphatic and aromatic components. Therefore, ABCG transporters have been concluded to be involved in cutin and suberin monomer export across the plasma membrane for extracellular polymer assembly. However, no direct transport experiments were conducted and the nature of the transported lipid substrate was not investigated for any ABCG transporter involved in cutin and suberin assembly. For cutin, β-MAG export was inferred for these ABCG transporters, because the recombinant, cuticle-localized CUS1 (CUTIN SYNTHASE) enzyme from tomato catalyzes polymerization of β-MAG monomers with 10,16-dihydroxy fatty acids (2-mono(10,16-dihydroxyhexadecnoyl)glycerol) (Fich *et al.*, 2016; Yeats *et al.*, 2012; Yeats *et al.*, 2014). Consequently, STR1 and STR2 might be involved in symbiotic fatty acid export during AM-symbiosis by transporting 16:0 β-MAG into the PAS. Currently, there is no direct experimental evidence for this hypothesis, but 16:0 β-MAG in colonized *str* mutants of Medicago was not as severely reduced as 16:0 β-MAG in colonized *ram2* and *fatm* mutants. Although it still remained reduced in comparison to colonized WT, this finding could indicate that in colonized Medicago *str* mutants, 16:0 β-MAG export is blocked and therefore accumulates to a certain degree in the plant (Bravo *et al.*, 2017; MacLean *et al.*, 2017).

4.1.6 Possible alternative Mechanisms for AMF to obtain Fatty Acids and Lipids

Next to the data presented here, multiple other lines of evidence suggest that AMF obtain their fatty acids by inducing fatty acid and lipid synthesis in plants via DIS, FatM and RAM2. As discussed above (see 4.1.5), lipids or fatty acids might then be exported from plants to mycorrhiza fungi via a plant lipid export mechanism involving secreted extracellular vesicles or membrane-transport via STR (Jiang *et al.*, 2017; Keymer *et al.*, 2017; Luginbuehl *et al.*, 2017; Rich *et al.*, 2017). Even though this is the most likely mechanism of how AMF obtain fatty acids, alternatives to this AM-induced plant lipid synthesis and export pathway are discussed below. These could provide alternatives of how AMF obtain fatty acids and lipids, if they are not directly fed to the fungus by the plant.

During arbuscule senescence, lipid droplets that contain lipids from the PAM accumulate around the collapsing arbuscule branches (Kobae *et al.*, 2014). These lipids could be incorporated by the fungus and therefore could be a source of lipids to AMF. Alluringly, *R. irregularis* contains 36 putatively secreted lipases that could be employed for hydrolysis of the PAM-lipids and subsequent uptake of fatty acids into the fungus (Kamel *et al.*, 2017). In theory, *FatM* could be involved in synthesis of fatty acids directed towards the PAM, rather than direct feeding of fatty acids to the fungus. However, *FatM* expression is highest in arbuscocytes when the hyphae form fine branches and therefore already represent fully-branched, functional arbuscules (Bravo *et al.*, 2017). As a pre-requisite, this requires extensive PAM synthesis beforehand. The timely expression of *FatM* in the vicinity of functional arbuscules therefore argues against a function in synthesis of the PAM.

As a second alternative mechanism how AMF could obtain fatty acids, they could have evolved a yet uncharacterized way to synthesize the bulk amount of fatty acids. Mitochondria are capable of fatty acid synthesis and even though AMF lack the genes coding for cytosolic type-I *FAS*, AMF still contain mitochondrial type II *FAS* genes. Three genes from *Rhizophagus* with homology to mitochondrial FAS II enzymes are upregulated in a low-phosphate dependent manner in colonized roots (Vijayakumar *et al.*, 2016). In eukaryotes, mitochondrial FAS (mtFASII) produces octanoyl-ACP as a precursor for lipoic acid (Witkowski *et al.*, 2007). Alterations in mtFASII activity affected the amounts of lysophospholipids and sphingolipids but not the fatty acid composition of mitochondria, although it remained unclear whether these effects are caused by alterations in lipoic acid metabolism or respiration (Clay *et al.*, 2016). It has been suggested that long-chain fatty acids can be produced by mtFASII for mitochondrial phospholipid remodeling and protein acylation, but this has not been experimentally demonstrated (Hiltunen *et al.*, 2010). These findings indicate that mtFASII produces mainly lipoic acid as a cofactor for enzymes of oxidative decarboxylation rather than serving as source for the bulk-supply of fatty acids for extra mitochondrial lipids of AMF.

In the sleeping sickness parasite *Trypanosoma spp.* a third way of synthesizing fatty acids apart from type-I and type-II FAS complexes has evolved. *Trypanosoma* employs microsomal elongase enzymes (ELO) to elongate butyryl-CoA (C4) with repetitive incorporation of acetate units from malonyl-CoA to yield myristic acid (C14). Myristic acid serves as acyl-chain of GPI-anchors or can be elongated to C16—C20 via other ELO enzymes (ELO3) for incorporation into phospholipids. *Trypanosoma* can also scavenge fatty acids from the host environment to supply the ELO3-elongation pathway and it has been speculated that it switches to *de novo* synthesis from butyryl-CoA when it enters the cerebrospinal fluid, where fatty acid concentrations are lower than in the blood (Lee *et al.*, 2007). Thus, depending on the environmental conditions, *Trypanosoma* is able to synthesize fatty acids from acetate (after conversion into acetyl-CoA and malonyl-CoA) independent of the cytosolic type I *FAS* genes.

Taken together, the uptake of lipids from the receding PAM via lipid droplets by the fungus might be an indirect way of how plant-derived lipids reach the fungus. However, the timed expression of *FatM* argues against a function in PAM synthesis and rather favors a function in 16:0 fatty acid production for direct feeding of fatty acids to the fungus. Due to the lack of evidence that mitochondrial fatty acid synthesis can supply the bulk amount of fatty acids, it is also rather unlikely that mitochondrial type II *FAS* genes have evolved to take over the function of cytosolic type I *FAS* in AMF. Whether AMF have evolved an alternative yet uncharacterized way of synthesizing fatty acids *de novo*, comparable to *Trypanosoma*, remains speculative.

4.2 Fatty Acid Desaturation in *R. irregularis*

4.2.1 *R. irregularis* contains two Functional Homologs of *ScOLE1*

The *R. irregularis* genome contains two that are orthologos of the *acyl-CoA desaturase* gene *OLE1* from *S. cerevisiae*. These two sequences were termed *RiOLE1* and *RiOLE1-LIKE* (Figure 20). As *S. cerevisiae* contains only a single copy of *OLE1* and the *Ri*OLE1 amino acid sequence is more similar to *Sc*OLE1 (56% amino acid sequence identity) than *Ri*OLE1-LIKE (54.2% amino acid sequence identity), *RiOLE1-LIKE* could have occurred via gene duplication of *OLE1* in *R. irregularis*, making *RiOLE1* and *RiOLE1-LIKE* paralogs.

Transformation of yeast WT and yeast ScΔ*ole1* mutant with *RiOLE1* and *RiOLE1-LIKE* both led to partial complementation of the fatty acid auxotrophy of *Sc*Δ*ole1* when grown in the absence of monounsaturated fatty acids at 28°C (Figure 21). Thus, *Ri*OLE1 and *Ri*OLE1-LIKE are functionally related to *Sc*OLE1 and therefore represent functional homologs of *Sc*OLE1. Acyl-CoA desaturases are ubiquitously present in many organisms, and in previous experiments, the function of genes similar to yeast *OLE1* from various organisms was studied by functional replacement of the disrupted *ScOLE1* in the Δ*ole1* mutant (Anamnart *et al.*, 1997; Miyazaki *et al.*, 2006; Shanklin *et al.*, 1994; Stukey *et al.*, 1990; Tsai *et al.*, 2019; Wongwathanarat *et al.*, 1999), similar to the experiment presented in figure 18. In this experiment, *RiOLE1* did complement the

growth deficiency of Δ*ole1* better than *RiOLE1-LIKE* (Figure 21), which shows that the closer sequence similarity of *Sc*OLE1 to *Ri*OLE1 is also reflected on a functional level. *Sc*OLE1 is active with palmitoyl-CoA and stearoyl-CoA, producing palmitoleoyl-CoA and oleoyl-CoA, respectively (Tsai *et al.*, 2019). Due to the closer sequence similarity, *Ri*OLE1 likely shares this activity, while *RiOLE1-LIKE* might have a more specialized function.

4.2.2 *Ri*OLE1-LIKE is specialized for Mycorrhiza-Signature Fatty Acids

In yeast WT and Δ*ole1* expressing *RiOLE1-LIKE*, the mycorrhiza-signature fatty acids 16:1ω5 and 18:1ω7 were detected that are normally only observed in AMF-colonized roots and extraradical mycelium (Figure 22a, b). Transient expression in *N. benthamiana* confirmed the occurrence of 16:1ω5 when *RiOLE1-LIKE*, but not *RiOLE1,* was expressed (Figure 22c, d). From these results it can be deduced that *Ri*OLE1-LIKE is responsible for insertion of the mycorrhiza-signature double bond at position ω5(Δ11).

The *ScΔole1* mutant is a suitable model system to study fatty acid desaturation as it has a low background desaturation activity (Stukey *et al.*, 1989). However, in *ScΔole1* harboring an empty vector control, residual Δ9-desaturation activity was revealed by the presence of 16:1 Δ9 and 18:1 Δ9, even though the latter was present in smaller amounts (Figure 22e, f). In comparison to *ScΔole1* EV, the amount of the two Δ9 monounsaturated fatty acids decreased in *ScΔole1* when *RiOLE1-LIKE* was expressed, while 18:1Δ9 was lower in comparison to *ScΔole1* expressing *RiOLE1*. Upon expression of *RiOLE1* in *ScΔole1*, mainly 18:1Δ9 accumulated and the amount of 16:1Δ9 was reduced in comparison to *ScΔole1* EV (Figure 22e, f). In addition, 16:1ω5 was the most abundant fatty acid in *ScΔole1* expressing *RiOLE1-LIKE* and therefore, *Ri*OLE1-LIKE likely prefers 16:0 fatty acid as a substrate but can also act to some degree on 18:0 fatty acid, synthesizing only the ω5/Δ11 double bond and not ω9/Δ9. In contrast, *Ri*OLE1 likely acts primarily on 18:0 and to a lesser extent on 16:0, introducing a double bond at the position Δ9.

As mentioned for heterologous expression of plant acyl-ACP thioesterase in *E. coli* (see 3.18 and 3.19), the endogenous substrate availability in the organism used for expression also has an impact on the rate of reaction product formation. Yeast WT-EV and *ScΔole1*-EV contain by default approximately three-times more 16:0 fatty acid than 18:0 fatty acid (Figure 22e), which probably already shifts the activity of heterologously expressed *Ri*OLE1 and *Ri*OLE1-LIKE towards 16:0, just because it is more abundant. Nevertheless, the suggested substrate specificities of *Ri*OLE1-LIKE (16:0>18:0) and *Ri*OLE1 (18:0>16:0) are reflected by the accumulation of desaturated products in *R. irregularis* ERM, which contains substantially more 16:1ω5 than 18:1ω7 and more 18:1Δ9 than 16:1Δ9 (Olsson and Johansen, 2000). Functional differentiation of desaturases has been reported before. In mice, four *OLE1* isoforms are present, called *STEAROYL-COA DESATURASES* (*SCD*), of which three act on 16:0-CoA and 18:0-CoA and one only

on acyl-CoAs with acyl chains < 16:0, producing Δ9 monounsaturated fatty acids (Miyazaki *et al.*, 2006).

4.2.3 *Ri*OLE1-LIKE and *Ri*OLE1 are Front-End Desaturases

Detailed analysis of 16:1 and 18:1 DMDS-adducts via mass spectrometry confirmed the specific position of the double bonds at either Δ9 or Δ11 (ω5 in 16:1 and ω7 in 18:1, respectively), depending on which Rhizophagus desaturase was expressed (Figure 22). Fatty acid desaturases recognize the position for insertion of the double bond by counting carbon atoms from the methyl or the carboxyl end (Meesapyodsuk and Qiu, 2012). In *RiOLE1-LIKE*-expressing *ScΔole1*, 18:1ω5 was not detected, but only 18:1ω7. The presence of 18:1ω5 would have indicated that 18:1 in *R. irregularis* arises from elongation of 16:1ω5 or by recognition of the ω5-carbon by the desaturase. Instead, the majority of monoeonic fatty acids in *RiOLE1-LIKE*-expressing *ScΔole1* were derived from desaturation of 16:0 and 18:0, respectively, and not by elongation. Hence, both desaturases recognize the position for insertion of the double bond with respect to the carboxyl end and are thus front-end desaturases. The resulting fatty acids therefore should be called 16:1Δ11 and 18:1Δ11.

Next to unsaturated 16 and 18 carbon fatty acids, polyunsaturated fatty acids with chain lengths >20 occur in *R. irregularis* (Jabaji-Hare, 1988; Wewer *et al.*, 2014). The most abundant one, 20:3, was also employed as lipid marker in this study (Figure 9, 10, 16, 17, 18). How *R. irregularis* produces these fatty acids is unknown, but the occurrence of 20:1-CoA in *R. irregularis* colonized roots that was absent from colonized *fatm*-1 and mock-inoculated WT roots (Figure 19) suggests that the 20:3 synthesis could involve a stepwise desaturation of 20:0, or elongation of 16:1, 18:1 and then further desaturation. *R. irregularis* also contains 18:2 fatty acid, and in the AMF *Glomus caledonius*, a second 18:3 isomer (n-6) was reported (Beilby and Kidby, 1980) that is also present in *R. irregularis* (Jabaji-Hare, 1988). This could represent the 20:3 precursor. The enzymes responsible for desaturation of 20:x fatty acids are unknown and could involve yet uncharacterized desaturases. As an alternative hypothesis, *Ri*OLE1 and *Ri*OLE1-LIKE could also accept 20:x fatty acids for further desaturation and might even insert multiple double bonds into 18:x and 20:x fatty acids, but not 16:1, as there is no 16:2 or 16:3 fatty acids in *R. irregularis*.

4.2.4 Acyl-CoA Accumulation during Symbiosis with *R. irregularis*

Expression of *RiOLE1* and *RiOLE1-LIKE* in yeast and *N. benthamiana* led to changes in the composition of acyl-CoAs (Figure 26). In *N. benthamiana*, the most prominent change was the occurrence of 16:1-CoA when *RiOLE1-LIKE* was expressed (Figure 26 b, c). In *ScΔole1*, where 16:1-CoA can also be detected in EV controls, *RiOLE1-LIKE* expression greatly increased 16:1-CoA content. 18:1-CoA was increased by *RiOLE1* expression (Figure 26 d, e). Desaturases have been

classified based on their substrates, which can be acyl-ACPs, acyl-lipids or acyl-CoAs (Los and Murata, 1998). Acyl-ACP desaturases have only been described in plants (Cahoon *et al.*, 1992; Cahoon *et al.*, 1994). Therefore, *Ri*OLE1 and *Ri*OLE1-LIKE either act on acyl-CoAs or acyl-lipids. The observed changes in acyl-CoAs in yeast and *N. benthamiana* could be the consequence of direct desaturation of acyl-CoAs or could be due to equilibration of acyl-groups from acyl-lipids with the acyl-CoA pool.

Nevertheless, acyl-CoAs play a role in lipid metabolism in *R. irregularis* as revealed by the changes in acyl-CoA composition in colonized and non-colonized *L. japonicus* roots (Figure 19). 16:1-CoA and 20:1-CoA were not detected in mock-inoculated roots, which indicates that at least some of the acyl groups in *R. irregularis* are shuttled into TAG and membrane lipid synthesis via acyl-CoA. In *Mortierella alpina*, another oleaginous fungus, desaturation of 18:1Δ9, other 18:x and 20:x fatty acids was shown to be catalyzed by two distinct desaturases that act on acyl-CoA as substrates (Wang *et al.*, 2018), and this could therefore also apply to the *R. irregualris* desaturases.

4.2.5 Importance of desaturated Fatty Acids in *R. irregularis*

The accumulating fatty acids in *R. irregularis* spores are most likely broken down to acetyl-CoA via β-oxidation upon spore germination to subsequently yield reducing energy via follow-up reaction. In theory, saturated fatty acids would be best suited for carbon and energy storage, and there is no need to produce desaturated fatty acids. Why does *R. irregularis* invests additional resources to desaturate 16:0 into 16:1Δ11 monounsaturated fatty acids? As 16:1Δ11 and other mono and poly unsaturated fatty acids also occur in membrane lipids, one purpose of having desaturated fatty acids could be to adapt membrane fluidity under stressful environmental conditions, as has been shown for other fungi (Rodríguez-Vargas *et al.*, 2007; Tan *et al.*, 2017).

Alternatively, mycorrhiza signature fatty acids in hyphal membranes could serve for recognition by the host. Surface-associated molecules are important for recognition of colonizing fungi. For example, chitin in the fungal cell wall is recognized by hosts of pathogenic and mycorrhiza fungi alike and either triggers plant defense reactions or the nuclear calcium-spiking that precedes mycorrhiza accommodation, depending on the type of fungus (Bonfante and Genre, 2015). Modification of chitin in fungal cell walls was observed for the pathogenic fungi *Puccinia graminis* f. sp. *Tritici* and *Uromyces fabae*, which modified surface-exposed chitin to chitosane by de-N-acetylation to avoid host recognition (El Gueddari *et al.*, 2002). Therefore, the fatty acid desaturation signature of mycorrhiza hyphal membranes might be used to differentiate them from pathogenic fungi.

The mycorrhiza signature fatty acid 16:1Δ11 is not only present in *R. irregularis* membranes but also the most abundant fatty acid in the storage lipid TAG. Mycorrhiza fungi are hosts to endophytic bacteria (Salvioli *et al.*, 2016). The Δ11-desaturation signature on storage lipids could therefore be a way to regulate lipid synthesis in response to the bacterial symbiont.

In the symbiosis between the endosymbiotic bacterium *Spiroplasma poulsonii* and *Drosophila melanogaster, D. melanogaster* prevents over-proliferation of the symbiont by controlling the availability of DAG that serves as carbon source for the symbiont. Interestingly, two DAG molecular species containing one saturated and a monounsaturated fatty acid (32:1, 16:0-16:1Δ9 and 34:1, 16:0-18:1Δ9) are the primary source of fatty acids (Herren *et al.*, 2014). An analogous mechanism might be present in *R. irregularis* as well.

Having unusual fatty acids could also serve as obstruction to potential pathogens that could try to scavenge lipids from the spores in the soil. A double bond does require more energy investment for release of reducing energy in β-oxidation and the subsequent reactions. Thus, the Δ11fatty acids would be less attractive for other organisms, or might even be completely useless because they lack the appropriate enzymes to metabolize these unusual fatty acids, or might even not recognized them. This would provide an advantage for *R. irregularis* spores to increase the chances of survival in the soil.

5 Summary

Arbuscular mycorrhiza colonization of roots is an ancient symbiosis that presumably was involved in the conquest of the land by early plants. Its main benefit for plants is the increased access to soil mineral nutrients beyond the root depletion zone. Arbuscular mycorrhiza fungi follow an obligate biotrophic lifestyle. Metabolites derived from photosynthesis of the host plant represent the sole source of reduced carbon for AMF. During symbiotic growth, AMF colonize the root and penetrate the cortex cells where the highly branched hyphae form arbuscules and where metabolites are exchanged between host and symbiont. During post-symbiotic growth, the fungus forms lipid-storage structures called vesicles and eventually grows out of the root into the soil where it forms spores again that are filled with neutral storage lipids. Lipids in *R. irregularis* contain fatty acids with unusual double bond positions, i. e. 16:1 Δ11/ω5 that are specific for AMF and primarily accumulate in neutral lipids but also in membrane lipids. The genomes of multiple AMF, such as the model fungus *Rhziophagus irregularis,* lack type-I cytosolic fatty acid synthase genes (FAS) that are required for the synthesis of fatty acids. The absence of *de novo* fatty acid synthesis from AMF therefore led to the hypothesis that next to hexoses, fatty acids serve as an additional source of reduced carbon.

AMF-host co-evolution has shaped host plant genomes to contain conserved genes exclusively dedicated to AMF symbiosis. One of these genes is the *acyl-ACP Thioesterase M* (*FatM*). Fat enzymes terminate fatty acid elongation during *de novo* synthesis by hydrolysis of the thioester and thereby liberate free fatty acids for lipid metabolism. The importance of *FatM* for AMF symbiosis was investigated in the host plant *Lotus japonicus* during symbiosis with *R. irregularis*. For this purpose, mycorrhiza-colonization of *fatm* transposon-insertion mutants was characterized, ^{13}C-labeling of fatty acids during symbiosis was conducted and the recombinant FatM enzyme was studied *in vitro*.

Consistent with an essential role in AMF symbiosis, *FatM* gene expression was only detectable in colonized roots. Reduction of *FatM* gene expression in *fatm* mutants led to impaired mycorrhiza symbiosis. Fungal root colonization was reduced and *R. irregularis* exhibited a defect in storage lipid accumulation. Furthermore, arbuscule branching was affected in *fatm* mutants and as a consequence, symbiotic phosphate supply was decreased. The fatty acids 16:0, 18:0 and 18:1Δ9 are the three main products of plant fatty acid *de novo* synthesis and *R. irregularis* mainly accumulates 16:0 and 16:1ω5. Recombinant expression and *in vitro* enzyme assays of FatM revealed that 16:0-ACP is the preferred substrate. Therefore, plastids in arbuscocytes are reprogrammed by induction of *FatM* to increase 16:0 fatty acid synthesis, which subsequently accumulate in *R. irregularis*. Quantification of β-monoacylglycerols (MAG) revealed that 16:0 β-MAG shows a mycorrhiza-dependent profile, i. e. it accumulated upon colonization in the WT as

well as in ERM (hyphae and spores) but failed to accumulate to the same extent in colonized *fatm* mutants. 16:0 β-MAG synthesis and secretion to the PAS might therefore represent the major mechanism for 16:0 fatty acid transfer to the fungus. Labeling of fatty acids during symbiosis with $^{13}C_2$-acetate demonstrated that *FatM* is essential for accumulation of the mycorrhiza-signature fatty acids 16:1ω5 and 20:3, as a decrease of ^{13}C over-excess label was observed in colonized *fatm* mutants, which was independent of decreased fungal biomass.

Similar to other oleaginous fungi, AMF contain multiple unsaturated long-chain fatty acids. The enzymes responsible for desaturation of these mycorrhiza-marker fatty acids were previously unknown. Two genes with homology to the yeast acyl-CoA desaturase *OLE1* are present in *R. irregularis*, termed *RiOLE1* and *RiOLE1-LIKE*. Both can act on 16:0 and 18:0 fatty acids to produce a Δ9 (*RiOLE1*) or the mycorrhiza-specific ω5/Δ11 (*RiOLE1-LIKE*) double bond, as revealed by heterologous expression in yeast and *N. benthamiana*. Expression also changed the acyl-CoA pool composition, which was enriched in 18:1 or 16:1, depending on the heterologous expression of *Ri*OLE1 or *Ri*OLE1-LIKE, respectively. Based on the high sequence similarity with *Sc*OLE1, *Ri*OLE1 and *Ri*OLE1-LIKE are most likely acyl-CoA desaturases.

The experiments presented here show that AMF reprogram fatty acid and lipid synthesis towards the production of 16:0 fatty acids via *FatM* that are then transferred to the fungus for desaturation and incorporation into lipids. In future, knowledge on symbiotic nutrient exchange can help to understand and improve the benefits of mycorrhiza symbiosis for crop plant nutrition and plant breeding.

6 References

Ait Lahmidi, N., Courty, P.-E., Brulé, D., Chatagnier, O., Arnould, C., Doidy, J., Berta, G., Lingua, G., Wipf, D. and Bonneau, L. (2016) Sugar exchanges in arbuscular mycorrhiza: RiMST5 and RiMST6, two novel Rhizophagus irregularis monosaccharide transporters, are involved in both sugar uptake from the soil and from the plant partner. *Plant Physiol. Biochem.*, 107, 354–363.

Akiyama, K., Matsuzaki, K.-i. and Hayashi, H. (2005) Plant sesquiterpenes induce hyphal branching in arbuscular mycorrhizal fungi. *Nature*, 435, 824–827.

Alexander, T., Toth, R., Meier, R. and Weber, H.C. (1989) Dynamics of arbuscule development and degeneration in onion, bean, and tomato with reference to vesicular–arbuscular mycorrhizae in grasses. *Can. J. Bot.*, 67, 2505–2513.

Anamnart, S., Tomita, T., Fukui, F., Fujimori, K., Harashima, S., Yamada, Y. and Oshima, Y. (1997) The P-OLE1 gene of Pichia angusta encodes a Δ9-fatty acid desaturase and complements the ole1 mutation of Saccharomyces cerevisiae. *Gene*, 184, 299–306.

Andre, C., Haslam, R.P. and Shanklin, J. (2012) Feedback regulation of plastidic acetyl-coa carboxylase by 18:1-acyl carrier protein in *Brassica napus. Proc. Natl. Acad. Sci. USA*, 109, 10107–10112.

Aznar-Moreno, J.A., Sánchez, R., Gidda, S.K., Martínez-Force, E., Moreno-Pérez, A.J., Venegas Calerón, M., Garcés, R., Mullen, R.T. and Salas, J.J. (2018) New insights into sunflower (Helianthus annuus L.) FatA and FatB thioesterases, their regulation, structure and distribution. *Front. Plant Sci.*, 9, 1496.

Bago, B., Pfeffer, P.E., Abubaker, J., Jun, J., Allen, J.W., Brouillette, J., Douds, D.D., Lammers, P.J. and Shachar-Hill, Y. (2003) Carbon export from arbuscular mycorrhizal roots involves the translocation of carbohydrate as well as lipid. *Plant Physiol.*, 131, 1496–1507.

Bago, B., Pfeffer, P.E., Douds, D.D., Brouillette, J., Bécard, G. and Shachar-Hill, Y. (1999) Carbon metabolism in spores of the arbuscular mycorrhizal fungus Glomus intraradices as revealed by nuclear magnetic resonance spectroscopy. *Plant Physiol.*, 121, 263–272.

Bago, B., Pfeffer, P.E. and Shachar-Hill, Y. (2000) Carbon metabolism and transport in arbuscular mycorrhizas. *Plant Physiol.*, 124, 949–958.

Bago, B., Pfeffer, P.E., Zipfel, W., Lammers, P. and Shachar-Hill, Y. (2002 a) Tracking metabolism and imaging transport in arbuscular mycorrhizal fungi. Metabolism and transport in AM fungi. *Plant Soil*, 244, 189–197.

Bago, B., Zipfel, W., Williams, R.M., Jun, J., Arreola, R., Lammers, P.J., Pfeffer, P.E. and Shachar-Hill, Y. (2002 b) Translocation and utilization of fungal storage lipid in the arbuscular mycorrhizal symbiosis. *Plant Physiol.*, 128, 108–124.

Baier, M.C., Keck, M., Gödde, V., Niehaus, K., Küster, H. and Hohnjec, N. (2010) Knockdown of the symbiotic sucrose synthase MtSucS1 affects arbuscule maturation and maintenance in mycorrhizal roots of Medicago truncatula. *Plant Physiol.*, 152, 1000–1014.

Bárzana, G., Aroca, R. and Ruiz-Lozano, J.M. (2015) Localized and non-localized effects of arbuscular mycorrhizal symbiosis on accumulation of osmolytes and aquaporins and on antioxidant systems in maize plants subjected to total or partial root drying. *Plant Cell Environ.*, 38, 1613–1627.

Bates, P.D., Johnson, S.R., Cao, X., Li, J., Nam, J.-W., Jaworski, J.G., Ohlrogge, J.B. and Browse, J. (2014) Fatty acid synthesis is inhibited by inefficient utilization of unusual fatty acids for glycerolipid assembly. *Proc. Natl. Acad. Sci. USA*, 111, 1204–1209.

Bates, P.D., Stymne, S. and Ohlrogge, J. (2013) Biochemical pathways in seed oil synthesis. *Curr. Opin. Plant Biol.*, 16, 358–364.

Behal, R.H., Lin, M., Back, S. and Oliver, D.J. (2002) Role of acetyl-coenzyme A synthetase in leaves of Arabidopsis thaliana. *Arch. Biochem. Biophys.*, 402, 259–267.

Beilby, J.P. (1980) Fatty acid and sterol composition of ungerminated spores of the vesicular-arbuscular mycorrhizal fungus, Acaulospora laevis. *Lipids*, 15, 949–952.

Beilby, J.P. and Kidby, D.K. (1980) Biochemistry of ungerminated and germinated spores of the vesicular-arbuscular mycorrhizal fungus, *Glomus caledonius.* Changes in neutral and polar lipids. *J. Lipid Res.,* 21, 739–750.

Beisson, F., Li-Beisson, Y. and Pollard, M. (2012) Solving the puzzles of cutin and suberin polymer biosynthesis. *Curr. Opin. Plant Biol.,* 15, 329–337.

Benning, C. and Ohta, H. (2005) Three enzyme systems for galactoglycerolipid biosynthesis are coordinately regulated in plants. *J. Biol. Chem.,* 280, 2397–2400.

Bentivenga, S.P. and Morton, J.B. (1996) Congruence of fatty acid methyl ester profiles and morphological characters of arbuscular mycorrhizal fungi in Gigasporaceae. *Proc. Natl. Acad. Sci. USA,* 93, 5659–5662.

Bernardo, L., Carletti, P., Badeck, F.W., Rizza, F., Morcia, C., Ghizzoni, R., Rouphael, Y., Colla, G., Terzi, V. and Lucini, L. (2019) Metabolomic responses triggered by arbuscular mycorrhiza enhance tolerance to water stress in wheat cultivars. *Plant Physiol. Biochem.,* 137, 203–212.

Besserer, A., Bécard, G., Jauneau, A., Roux, C. and Séjalon-Delmas, N. (2008) GR24, a synthetic analog of strigolactones, stimulates the mitosis and growth of the arbuscular mycorrhizal fungus *Gigaspora rosea* by boosting its energy metabolism. *Plant Physiol.,* 148, 402–413.

Besserer, A., Puech-Pagès, V., Kiefer, P., Gomez-Roldan, V., Jauneau, A., Roy, S., Portais, J.-C., Roux, C., Bécard, G. and Séjalon-Delmas, N. (2006) Strigolactones stimulate arbuscular mycorrhizal fungi by activating mitochondria. *PLoS Biol.,* 4, e226.

Bessire, M., Borel, S., Fabre, G., Carraça, L., Efremova, N., Yephremov, A., Cao, Y., Jetter, R., Jacquat, A.-C., Métraux, J.-P. and Nawrath, C. (2011) A Member of the pleiotropic drug resistance family of atp binding cassette transporters is required for the formation of a functional cuticle in arabidopsis. *Plant Cell,* 23, 1958–1970.

Binder, A., Lambert, J., Morbitzer, R., Popp, C., Ott, T., Lahaye, T. and Parniske, M. (2014) A modular plasmid assembly kit for multigene expression, gene silencing and silencing rescue in plants. *PLoS One,* 9, e88218.

Bird, D., Beisson, F., Brigham, A., Shin, J., Greer, S., Jetter, R., Kunst, L., Wu, X., Yephremov, A. and Samuels, L. (2007) Characterization of Arabidopsis ABCG11/WBC11, an ATP binding cassette (ABC) transporter that is required for cuticular lipid secretion. *Plant J.,* 52, 485–498.

Bitterlich, M., Krügel, U., Boldt-Burisch, K., Franken, P. and Kühn, C. (2014) The sucrose transporter SlSUT2 from tomato interacts with brassinosteroid functioning and affects arbuscular mycorrhiza formation. *Plant J.,* 78, 877–889.

Blee, K.A. and Anderson, A.J. (2002) Transcripts for genes encoding soluble acid invertase and sucrose synthase accumulate in root tip and cortical cells containing mycorrhizal arbuscules. *Plant Mol. Biol.,* 50, 197–211.

Bligh, E.G. and Dyer, W.J. (1959) A rapid method of total lipid extraction and purification. *Can. J. Biochem. Physiol.,* 37, 911–917.

Blilou, I., Ocampo, J.A. and García-Garrido, J.M. (2000) Induction of Ltp (lipid transfer protein) and Pal (phenylalanine ammonia-lyase) gene expression in rice roots colonized by the arbuscular mycorrhizal fungus Glomus mosseae. *J. Exp. Bot.,* 51, 1969–1977.

Block, M.A. and Jouhet, J. (2015) Lipid trafficking at endoplasmic reticulum-chloroplast membrane contact sites. *Curr. Opin. Cell Biol.,* 35, 21–29.

Boldt, K., Pörs, Y., Haupt, B., Bitterlich, M., Kühn, C., Grimm, B. and Franken, P. (2011) Photochemical processes, carbon assimilation and RNA accumulation of sucrose transporter genes in tomato arbuscular mycorrhiza. *J. Plant Physiol.,* 168, 1256–1263.

Bonaventure, G., Salas, J.J., Pollard, M.R. and Ohlrogge, J.B. (2003) Disruption of the FATB gene in Arabidopsis demonstrates an essential role of saturated fatty acids in plant growth. *Plant Cell,* 15, 1020–1033.

Bonfante, P. (2018) The future has roots in the past: the ideas and scientists that shaped mycorrhizal research. *New Phytol.,* 220, 982–995.

Bonfante, P. and Genre, A. (2015) Arbuscular mycorrhizal dialogues: do you speak 'plantish' or 'fungish'? *Trends Plant Sci.,* 20, 150–154.

Bradford, M.M. (1976) A rapid and sensitive method for the quantitation of microgram quantities of protein utilizing the principle of protein-dye binding. *Anal. Biochem.*, 72, 248–254.

Brands, M., Wewer, V., Keymer, A., Gutjahr, C. and Dörmann, P. (2018) The Lotus japonicus acyl-acyl carrier protein thioesterase FatM is required for mycorrhiza formation and lipid accumulation of Rhizophagus irregularis. *Plant J.*, 95, 219–232.

Bravo, A., Brands, M., Wewer, V., Dörmann, P. and Harrison, M.J. (2017) Arbuscular mycorrhiza-specific enzymes FatM and RAM2 fine-tune lipid biosynthesis to promote development of arbuscular mycorrhiza. *New Phytol.*, 214, 1631-1645.

Bravo, A., York, T., Pumplin, N., Mueller, L.A. and Harrison, M.J. (2016) Genes conserved for arbuscular mycorrhizal symbiosis identified through phylogenomics. *Nat. Plants*, 2, 15208.

Breuillin-Sessoms, F., Floss, D.S., Gomez, S.K., Pumplin, N., Ding, Y., Levesque-Tremblay, V., Noar, R.D., Daniels, D.A., Bravo, A., Eaglesham, J.B., Benedito, V.A., Udvardi, M.K. and Harrison, M.J. (2015) Suppression of arbuscule degeneration in Medicago truncatula phosphate transporter mutants is dependent on the ammonium transporter 2 family protein AMT2;3. *Plant Cell*, 27, 1352–1366.

Brown, A.P., Affleck, V., Fawcett, T. and Slabas, A.R. (2006) Tandem affinity purification tagging of fatty acid biosynthetic enzymes in Synechocystis sp. PCC6803 and Arabidopsis thaliana. *J. Exp. Bot.*, 57, 1563–1571.

Brundrett, M. (1996) *Working with mycorrhizas in forestry.* Canberra: Australian Centre for International Agricultural Research.

Brundrett, M.C. (2002) Coevolution of roots and mycorrhizas of land plants. *New Phytol.*, 154, 275–304.

Brundrett, M.C. and Tedersoo, L. (2018) Evolutionary history of mycorrhizal symbioses and global host plant diversity. *New Phytol.*, 220, 1108–1115.

Bücking, H., Abubaker, J., Govindarajulu, M., Tala, M., Pfeffer, P.E., Nagahashi, G., Lammers, P. and Shachar-Hill, Y. (2008) Root exudates stimulate the uptake and metabolism of organic carbon in germinating spores of Glomus intraradices. *New Phytol.*, 180, 684–695.

Cahoon, E.B., Cranmer, A.M., Shanklin, J. and Ohlrogge, J.B. (1994) delta 6 Hexadecenoic acid is synthesized by the activity of a soluble delta 6 palmitoyl-acyl carrier protein desaturase in Thunbergia alata endosperm. *J. Biol.Chem.*, 269, 27519–27526.

Cahoon, E.B., Shanklin, J. and Ohlrogge, J.B. (1992) Expression of a coriander desaturase results in petroselinic acid production in transgenic tobacco. *Proc. Natl. Acad. Sci. USA*, 89, 11184–11188.

Calonne, M., Fontaine, J., Debiane, D., Laruelle, F., Grandmougin-Ferjani, A. and Lounes-Hadj Sahraoui, A. (2014) The arbuscular mycorrhizal *Rhizophagus irregularis* activates storage lipid biosynthesis to cope with the benzoapyrene oxidative stress. *Phytochemistry*, 97, 30–37.

Campagnac, E., Fontaine, J., Lounès-Hadj Sahraoui, A., Laruelle, F., Durand, R. and Grandmougin-Ferjani, A. (2009) Fenpropimorph slows down the sterol pathway and the development of the arbuscular mycorrhizal fungus Glomus intraradices. *Mycorrhiza*, 19, 365–374.

Campopiano, D.J. (2014) ACP-AasS you like it. *Chem. Biol.*, 21, 1257–1259.

Campos, P., Borie, F., Cornejo, P., López-Ráez, J.A., López-García, Á. and Seguel, A. (2018) Phosphorus acquisition efficiency related to root traits: is mycorrhizal symbiosis a key factor to wheat and barley cropping? *Front. Plant Sci.*, 9, 1-21.

Chan, D.I. and Vogel, H.J. (2010) Current understanding of fatty acid biosynthesis and the acyl carrier protein. *Biochem. J.*, 430, 1–19.

Chapin, F.S. and Bieleski, R.L. (1982) Mild phosphorus stress in barley and a related low-phosphorus-adapted barleygrass: Phosphorus fractions and phosphate absorption in relation to growth. *Physiol. Plant.*, 54, 309–317.

Chen, E.C., Mathieu, S., Hoffrichter, A., Sedzielewska-Toro, K., Peart, M., Pelin, A., Ndikumana, S., Ropars, J., Dreissig, S., Fuchs, J., Brachmann, A. and Corradi, N. (2018) Single nucleus sequencing reveals evidence of inter-nucleus recombination in arbuscular mycorrhizal fungi. *Elife*, 7:e39813.

Chen, L.-Q., Hou, B.-H., Lalonde, S., Takanaga, H., Hartung, M.L., Qu, X.-Q., Guo, W.-J., Kim, J.-G., Underwood, W., Chaudhuri, B., Chermak, D., Antony, G., White, F.F., Somerville, S.C., Mudgett, M.B. and Frommer, W.B. (2010) Sugar transporters for intercellular exchange and nutrition of pathogens. *Nature*, 468, 527–532.

Chen, M., Arato, M., Borghi, L., Nouri, E. and Reinhardt, D. (2018) Beneficial services of arbuscular mycorrhizal fungi - from ecology to application. *Front. Plant Sci.*, 9, 1270.

Chiu, C.H. and Paszkowski, U. (2019) Mechanisms and impact of symbiotic phosphate acquisition. *Cold Spring Harb. Perspect. Biol.*, 11, 1-32.

Choi, J., Summers, W. and Paszkowski, U. (2018) Mechanisms underlying establishment of arbuscular mycorrhizal symbioses. *Annu. Rev. Phytopathol.*, 56, 135–160.

Clay, H.B., Parl, A.K., Mitchell, S.L., Singh, L., Bell, L.N. and Murdock, D.G. (2016) Altering the mitochondrial fatty acid synthesis (mtFASII) pathway modulates cellular metabolic states and bioactive lipid profiles as revealed by metabolomic profiling. *PLoS One*, 11, e0151171.

Cooper, K.M. and Lösel, D.M. (1978) Lipid physiology of vesicular-abuscular mycorrhiza. Composition of lipids in roots of onion, clover and ryegrass infected with *Glomus mosseae*. *New Phytol.*, 80, 143–151.

Corradi, N., Hijri, M., Fumagalli, L. and Sanders, I.R. (2004) Arbuscular mycorrhizal fungi (Glomeromycota) harbour ancient fungal tubulin genes that resemble those of the chytrids (Chytridiomycota). *Fung. Genet. Biol.*, 41, 1037–1045.

Cranenbrouck, S., Voets, L., Bivort, C., Renard, L., Strullu, D.-G. and Declerck, S. (2005) Methodologies for in vitro cultivation of arbuscular mycorrhizal fungi with root organs. In *In Vitro Culture of Mycorrhizas* (Declerck, S., Fortin, J.A. and Strullu, D.-G., eds). Berlin, Heidelberg: Springer Berlin Heidelberg, 341–375.

Cronan, J.E. and Klages, A.L. (1981) Chemical synthesis of acyl thioesters of acyl carrier protein with native structure. *Proc. Natl. Acad. Sci. USA*, 78, 5440–5444.

Dalpé, Y., Trépanier, M., Sahraoui, A.L.-H., Fontaine, J. and Sancholle, M. (2012) 8 lipids of mycorrhizas. In *Fungal Associations.* 2nd edn. (Hock, B., ed): Springer Berlin Heidelberg, 137–169.

Debiane, D., Calonne, M., Fontaine, J., Laruelle, F., Grandmougin-Ferjani, A. and Lounes-Hadj Sahraoui, A. (2011) Lipid content disturbance in the arbuscular mycorrhizal, *Glomus irregulare* grown in monoxenic conditions under PAHs pollution. *Fungal Biol.*, 115, 782–792.

Dehesh, K., Jones, A., Knutzon, D.S. and Voelker, T.A. (1996) Production of high levels of 8:0 and 10:0 fatty acids in transgenic canola by overexpression of Ch FatB2, a thioesterase cDNA from Cuphea hookeriana. *Plant J.*, 9, 167–172.

Delaux, P.-M., Varala, K., Edger, P.P., Coruzzi, G.M., Pires, J.C. and Ané, J.-M. (2014) Comparative phylogenomics uncovers the impact of symbiotic associations on host genome evolution. *PLoS Genet.*, 10, e1004487.

Destaillats, F., Cruz-Hernandez, C., Nagy, K. and Dionisi, F. (2010) Identification of monoacylglycerol regio-isomers by gas chromatography-mass spectrometry. *J. Chromat. B*, 1217, 1543–1548.

Diezel, W., Kopperschläger, G. and Hofmann, E. (1972) An improved procedure for protein staining in polyacrylamide gels with a new type of coomassie brilliant blue. *Anal. Biochem.*, 48, 617–620.

Doehlemann, G., Wahl, R., Horst, R.J., Voll, L.M., Usadel, B., Poree, F., Stitt, M., Pons-Kühnemann, J., Sonnewald, U., Kahmann, R. and Kämper, J. (2008) Reprogramming a maize plant: transcriptional and metabolic changes induced by the fungal biotroph Ustilago maydis. *Plant J.*, 56, 181–195.

Doidy, J., van Tuinen, D., Lamotte, O., Corneillat, M., Alcaraz, G. and Wipf, D. (2012) The *Medicago truncatula* sucrose transporter family: characterization and implication of key members in carbon partitioning towards arbuscular mycorrhizal fungi. *Mol. Plant*, 5, 1346–1358.

Domergue, F., Abbadi, A., Zähringer, U., Moreau, H. and Heinz, E. (2005) In vivo characterization of the first acyl-CoA Δ6-desaturase from a member of the plant kingdom, the microalga *Ostreococcus tauri*. *Biochem. J.*, 389, 483–490.

Dörmann, P., Voelker, T.A. and Ohlrogge, J.B. (1995) Cloning and expression in *Escherichia coli* of a novel thioesterase from *Arabidopsis thaliana* specific for long-chain acyl-acyl carrier proteins. *Arch. Biochem. Biophys.*, 316, 612–618.

Douds, D.D. (1994) Relationship between hyphal and arbuscular colonization and sporulation in a mycorrhiza of Paspalum notatum Flugge. *New Phytol.*, 126, 233–237.

Douds, D.D. and Schenk, N.C. (1990) Relationship of colonization and sporulation by VA mycorrhizal fungi to plant nutrient and carbohydrate contents. *New Phytol.*, 116, 621–627.

Dreher, D., Yadav, H., Zander, S. and Hause, B. (2017) Is there genetic variation in mycorrhization of Medicago truncatula? *PeerJ*, 5, e3713.

Ecclestone, V.S. and Ohlrogge, J.B. (1998) Expression of lauroyl-acyl carrier protein thioesterase in Brassica napus seeds induces pathways for both fatty acid oxidation and biosynthesis and implies a set point for triacylglycerol accumulation. *Plant Cell*, 10, 613–622.

Ejsing, C.S., Duchoslav, E., Sampaio, J., Simons, K., Bonner, R., Thiele, C., Ekroos, K. and Shevchenko, A. (2006) Automated identification and quantification of glycerophospholipid molecular species by multiple precursor ion scanning. *Anal. Chem.*, 78, 6202–6214.

El Gueddari, N.E., Rauchhaus, U., Moerschbacher, B.M. and Deising, H.B. (2002) Developmentally regulated conversion of surface-exposed chitin to chitosan in cell walls of plant pathogenic fungi. *New Phytol.*, 156, 103–112.

El Tahchy, A., Reynolds, K.B., Petrie, J.R., Singh, S.P. and Vanhercke, T. (2017) Thioesterase overexpression in Nicotiana benthamiana leaf increases the fatty acid flux into triacylgycerol. *FEBS Lett.*, 591, 448–456.

Endre, G., Kereszt, A., Kevei, Z., Mihacea, S., Kaló, P. and Kiss, G.B. (2002) A receptor kinase gene regulating symbiotic nodule development. *Nature*, 417, 962–966.

Favre, P., Bapaume, L., Bossolini, E., Delorenzi, M., Falquet, L. and Reinhardt, D. (2014) A novel bioinformatics pipeline to discover genes related to arbuscular mycorrhizal symbiosis based on their evolutionary conservation pattern among higher plants. *BMC Plant Biol.*, 14, 333.

Fester, T. (2002) Occurrence and localization of apocarotenoids in arbuscular mycorrhizal plant roots. *Plant Cell Physiol.*, 43, 256–265.

Fester, T., Strack, D. and Hause, B. (2001) Reorganization of tobacco root plastids during arbuscule development. *Planta*, 213, 864–868.

Fich, E.A., Segerson, N.A. and Rose, J.K.C. (2016) The plant polyester cutin: biosynthesis, structure, and biological roles. *Annu. Rev. Plant. Biol.*, 67, 207–233.

Flores, C.-L. and Gancedo, C. (2015) The gene YALI0E20207g from Yarrowia lipolytica encodes an N-acetylglucosamine kinase implicated in the regulated expression of the genes from the N-acetylglucosamine assimilatory pathway. *PLoS One*, 10, 1-21.

Floss, D.S., Gomez, S.K., Park, H.-J., MacLean, A.M., Müller, L.M., Bhattarai, K.K., Lévesque-Tremblay, V., Maldonado-Mendoza, I.E. and Harrison, M.J. (2017) A transcriptional program for arbuscule degeneration during AM symbiosis is regulated by MYB1. *Curr. Biol.*, 27, 1206–1212.

Floss, D.S., Levy, J.G., Lévesque-Tremblay, V., Pumplin, N. and Harrison, M.J. (2013) DELLA proteins regulate arbuscule formation in arbuscular mycorrhizal symbiosis. *Proc. Natl. Acad. Sci. USA*, 110, E5025-34.

Fontaine, J., Grandmougin-Ferjani, A., Glorian, V. and Durand, R. (2004) 24-methyl/methylene sterols increase in monoxenic roots after colonization by arbuscular mycorrhizal fungi. *New Phytol.*, 163, 159–167.

Fontaine, J., Grandmougin-Ferjani, A., Hartmann, M.A. and Sancholle, M. (2001a) Sterol biosynthesis by the arbuscular mycorrhizal fungus Glomus intraradices. *Lipids*, 36, 1357–1363.

Fontaine, J., Grandmougin-Ferjani, A. and Sancholle, M. (2001b) Lipid metabolism of the endomycorrhizal fungus. *Glomus intraradices. C. R. Acad. Sci. III*, 324, 847–853.

Francis, G.W. (1981) Alkylthiolation for the determination of double-bond position in unsaturated fatty acid esters. *Chem. Phys. Lipids*, 29, 369–374.

Fulda, M., Schnurr, J., Abbadi, A., Heinz, E. and Browse, J. (2004) Peroxisomal Acyl-CoA synthetase activity is essential for seedling development in Arabidopsis thaliana. *Plant cell*, 16, 394–405.

Garabagi, F., Gilbert, E., Loos, A., McLean, M.D. and Hall, J.C. (2012) Utility of the P19 suppressor of gene-silencing protein for production of therapeutic antibodies in Nicotiana expression hosts. *Plant Biotechnol. J.*, 10, 1118–1128.

Gaspar, L., Pollero, R. and Cabello, M. (1997) Variations in the lipid composition of alfalfa roots during colonization with the arbuscular mycorrhizal fungus Glomus versiforme. *Mycologia*, 89, 37–42.

Gaspar, L., Pollero, R. and Cabello, M. (2001) Biosynthesis and degradation of glycerides in external mycelium of Glomus mosseae. *Mycorrhiza*, 11, 257–261.

Gaspar, M.L., Pollero, R. and Cabello, M. (1997) Partial purification and characterization of a lipolytic enzyme from spores of the arbuscular mycorrhizal fungus Glomus versiforme. *Mycologia*, 89, 610–614.

Gaspar, M.L., Pollero, R.J. and Cabello, M.N. (1994) Triacylglycerol consumption during spore germination of vesicular-arbuscular mycorrhizal fungi. *J. Am. Oil Chem. Soc.*, 71, 449–452.

Gasulla, F., vom Dorp, K., Dombrink, I., Zähringer, U., Gisch, N., Dormann, P. and Bartels, D. (2013) The role of lipid metabolism in the acquisition of desiccation tolerance in *Craterostigma plantagineum*: A comparative approach. *Plant J.*, 75, 726–741.

Gaude, N., Bortfeld, S., Duensing, N., Lohse, M. and Krajinski, F. (2012) Arbuscule-containing and non-colonized cortical cells of mycorrhizal roots undergo extensive and specific reprogramming during arbuscular mycorrhizal development. *Plant J.*, 69, 510–528.

Genre, A., Chabaud, M., Balzergue, C., Puech-Pagès, V., Novero, M., Rey, T., Fournier, J., Rochange, S., Bécard, G., Bonfante, P. and Barker, D.G. (2013) Short-chain chitin oligomers from arbuscular mycorrhizal fungi trigger nuclear Ca^{2+} spiking in *Medicago truncatula* roots and their production is enhanced by strigolactone. *New Phytol.*, 198, 190–202.

Genre, A., Chabaud, M., Faccio, A., Barker, D.G. and Bonfante, P. (2008) Prepenetration apparatus assembly precedes and predicts the colonization patterns of arbuscular mycorrhizal fungi within the root cortex of both Medicago truncatula and Daucus carota. *Plant Cell*, 20, 1407–1420.

Genre, A., Chabaud, M., Timmers, T., Bonfante, P. and Barker, D.G. (2005) Arbuscular mycorrhizal fungi elicit a novel intracellular apparatus in *Medicago truncatula* root epidermal cells before infection. *Plant Cell*, 17, 3489–3499.

Genre, A. and Russo, G. (2016) Does a common pathway transduce symbiotic signals in plant-microbe interactions? *Front. Plant Sci.*, 7, 96.

Gibert, A., Tozer, W. and Westoby, M. (2019) Plant performance response to eight different types of symbiosis. *New Phytol.*, 222, 526–542.

Gidda, S.K., Shockey, J.M., Rothstein, S.J., Dyer, J.M. and Mullen, R.T. (2009) *Arabidopsis thaliana* GPAT8 and GPAT9 are localized to the ER and possess distinct ER retrieval signals: Functional divergence of the dilysine ER retrieval motif in plant cells. *Plant Physiol. Biochem.*, 47, 867–879.

Gietz, R.D., Schiestl, R.H., Willems, A.R. and Woods, R.A. (1995) Studies on the transformation of intact yeast cells by the LiAc/SS-DNA/PEG procedure. *Yeast*, 11, 355–360.

Giovannetti, M., Tolosano, M., Volpe, V., Kopriva, S. and Bonfante, P. (2014) Identification and functional characterization of a sulfate transporter induced by both sulfur starvation and mycorrhiza formation in Lotus japonicus. *New Phytol.*, 204, 609–619.

Gomez, S.K., Javot, H., Deewatthanawong, P., Torres-Jerez, I., Tang, Y., Blancaflor, E.B., Udvardi, M.K. and Harrison, M.J. (2009) *Medicago truncatula* and *Glomus intraradices* gene expression in cortical cells harboring arbuscules in the arbuscular mycorrhizal symbiosis. *BMC Plant Biol.*, 9, 10.

Govindarajulu, M., Pfeffer, P.E., Jin, H., Abubaker, J., Douds, D.D., Allen, J.W., Bucking, H., Lammers, P.J. and Shachar-Hill, Y. (2005) Nitrogen transfer in the arbuscular mycorrhizal symbiosis. *Nature*, 435, 819–823.

Graham, J.H., Hodge, N.C. and Morton, J.B. (1995) Fatty acid methyl ester profiles for characterization of glomalean fungi and their endomycorrhizae. *Appl. Environm. Microbiol.*, 61, 58–64.

Grandmougin-Ferjani, A., Dalpé, Y., Hartmann, M.-A., Laruelle, F. and Sancholle, M. (1999) Sterol distribution in arbuscular mycorrhizal fungi. *Phytochemistry*, 50, 1027–1031.

Gutjahr, C., Gobbato, E., Choi, J., Riemann, M., Johnston, M.G., Summers, W., Carbonnel, S., Mansfield, C., Yang, S.-Y., Nadal, M., Acosta, I., Takano, M., Jiao, W.-B., Schneeberger, K., Kelly, K.A. and Paszkowski, U. (2015) Rice perception of symbiotic arbuscular mycorrhizal fungi requires the karrikin receptor complex. *Science*, 350, 1521–1524.

Gutjahr, C. and Parniske, M. (2013) Cell and developmental biology of arbuscular mycorrhiza symbiosis. *Annu. Rev. Cell Dev. Biol.*, 29, 593–617.

Gutjahr, C. and Parniske, M. (2017) Cell biology: control of partner lifetime in a plant-fungus relationship. *Curr. Biol.*, 27, 420-423.

Gutjahr, C., Radovanovic, D., Geoffroy, J., Zhang, Q., Siegler, H., Chiapello, M., Casieri, L., An, K., An, G., Guiderdoni, E., Kumar, C.S., Sundaresan, V., Harrison, M.J. and Paszkowski, U. (2012) The half-size ABC transporters STR1 and STR2 are indispensable for mycorrhizal arbuscule formation in rice. *Plant J.*, 69, 906–920.

Hammer, E.C., Pallon, J., Wallander, H. and Olsson, P.A. (2011) Tit for tat? A mycorrhizal fungus accumulates phosphorus under low plant carbon availability. *FEMS Microbiol. Ecol.*, 76, 236–244.

Handa, Y., Nishide, H., Takeda, N., Suzuki, Y., Kawaguchi, M. and Saito, K. (2015) RNA-seq transcriptional profiling of an arbuscular mycorrhiza provides insights into regulated and coordinated gene expression in Lotus japonicus and Rhizophagus irregularis. *Plant Cell Physiol.*, 56, 1490–1511.

Harrison, M.J. (1993) Isoflavonoid accumulation and expression of defense gene transcripts during the establishment of vesicular-arbuscular mycorrhizal associations in roots of Medicago truncatula. *Mol. Plant Micr. Interact.*, 6, 643.

Harrison, M.J. (1996) A sugar transporter from Medicago truncatula: altered expression pattern in roots during vesicular-arbuscular (VA) mycorrhizal associations. *Plant J.*, 9, 491–503.

Harrison, M.J., Dewbre, G.R. and Liu, J. (2002) A phosphate transporter from *Medicago truncatula i*nvolved in the acquisition of phosphate released by arbuscular mycorrhizal fungi. *Plant Cell*, 14, 2413–2429.

Harrison, M.J. and van Buuren, M.L. (1995) A phosphate transporter from the mycorrhizal fungus *Glomus versiforme. Nature*, 378, 626–629.

Hause, B., Maier, W., Miersch, O., Kramell, R. and Strack, D. (2002) Induction of jasmonate biosynthesis in arbuscular mycorrhizal barley roots. *Plant Physiol.*, 130, 1213–1220.

Helber, N., Wippel, K., Sauer, N., Schaarschmidt, S., Hause, B. and Requena, N. (2011) A versatile monosaccharide transporter that operates in the arbuscular mycorrhizal fungus Glomus sp is crucial for the symbiotic relationship with plants. *Plant Cell*, 23, 3812–3823.

Herren, J.K., Paredes, J.C., Schüpfer, F., Arafah, K., Bulet, P. and Lemaitre, B. (2014) Insect endosymbiont proliferation is limited by lipid availability. *Elife*, 3, e02964.

Hiltunen, J.K., Autio, K.J., Schonauer, M.S., Kursu, V.A.S., Dieckmann, C.L. and Kastaniotis, A.J. (2010) Mitochondrial fatty acid synthesis and respiration. *Biochem. Biophys. Acta*, 1797, 1195–1202.

Ho, I. and Trappe, J.M. (1973) Translocation of 14C from festuca plants to their endomycorrhizal fungi. *Nat. New Biol.*, 244, 30–31.

Hohnjec, N., Perlick, A.M., Pühler, A. and Küster, H. (2003) The Medicago truncatula sucrose synthase gene MtSucS1 is activated both in the infected region of root nodules and in the cortex of roots colonized by arbuscular mycorrhizal fungi. *Mol. Plant Micr. Interact.*, 16, 903–915.

Huisman, R., Hontelez, J., Mysore, K.S., Wen, J., Bisseling, T. and Limpens, E. (2016) A symbiosis-dedicated SYNTAXIN OF PLANTS 13II isoform controls the formation of a stable host-microbe interface in symbiosis. *New Phytol.*, 211, 1338–1351.

Itaya, K. and Ui, M. (1966) A new micromethod for the colorimetric determination of inorganic phosphate. *Clin. Chim. Acta*, 14, 361–366.

Ivanov, S., Austin, J., Berg, R.H. and Harrison, M.J. (2019) Extensive membrane systems at the host–arbuscular mycorrhizal fungus interface. *Nat. Plants*, 5, 194–203.

Ivanov, S., Fedorova, E.E., Limpens, E., Mita, S. de, **Genre, A., Bonfante, P. and Bisseling, T.** (2012) Rhizobium-legume symbiosis shares an exocytotic pathway required for arbuscule formation. *Proc. Natl. Acad. Sci. USA*, 109, 8316–8321.

Jabaji-Hare, S. (1988) Lipid and fatty acid profiles of some vesicular-arbuscular mycorrhizal fungi: contribution to taxonomy. *Mycologia*, 80, 622.

Jabaji-Hare, S., Deschene, A. and Kendrick, B. (1984) Lipid content and composition of vesicles of a vesicular-arbuscular mycorrhizal fungus. *Mycologia*, 76, 1024–1030.

Javot, H., Penmetsa, R.V., Terzaghi, N., Cook, D.R. and Harrison, M.J. (2007) A Medicago truncatula phosphate transporter indispensable for the arbuscular mycorrhizal symbiosis. *Proc. Natl. Acad. Sci. USA*, 104, 1720–1725.

Jayawardhane, K.N., Singer, S.D., Weselake, R.J. and Chen, G. (2018) Plant sn-glycerol-3-phosphate acyltransferases: biocatalysts involved in the biosynthesis of intracellular and extracellular lipids. *Lipids,* 53, 469–480.

Jenni, S., Leibundgut, M., Boehringer, D., Frick, C., Mikolásek, B. and Ban, N. (2007) Structure of fungal fatty acid synthase and implications for iterative substrate shuttling. *Science*, 316, 254–261.

Jiang, Y., Wang, W., Xie, Q., Liu, N., Liu, L., Wang, D., Zhang, X., Yang, C., Chen, X., Tang, D. and Wang, E. (2017) Plants transfer lipids to sustain colonization by mutualistic mycorrhizal and parasitic fungi. *Science*, 356, 1172–1175.

Jiang, Y., Xie, Q., Wang, W., Yang, J., Zhang, X., Yu, N., Zhou, Y. and Wang, E. (2018) Medicago AP2-domain transcription factor WRI5a is a master regulator of lipid biosynthesis and transfer during mycorrhizal symbiosis. *Mol. Plant*, 11, 1344–1359.

Jing, F., Cantu, D.C., Tvaruzkova, J., Chipman, J.P., Nikolau, B.J., Yandeau-Nelson, M.D. and Reilly, P.J. (2011) Phylogenetic and experimental characterization of an acyl-ACP thioesterase family reveals significant diversity in enzymatic specificity and activity. *BMC Biochem.*, 12, 44.

Jing, F., Zhao,L., Yandeau-Nelson, M.D. and Nikolau, B.J. (2018) Two distinct domains contribute to the substrate acyl chain length selectivity of plant acyl-ACP thioesterase. *Nat. Commun.*, 9, 860.

Johansen, A., Finlay, R.D. and Olsson, P.A. (1996) Nitrogen metabolism of external hyphae of the arbuscular mycorrhizal fungus *Glomus intraradices*. *New Phytol.*, 133, 705–712.

Johnston, M.L., Luethy, M.H., Miernyk, J.A. and Randall, D.D. (1997) Cloning and molecular analyses of the Arabidopsis thaliana plastid pyruvate dehydrogenase subunits. *Biochem. Biophys. Acta*, 1321, 200–206.

Jones, A., Davies, H.M. and Voelker, T.A. (1995) Palmitoyl-acyl carrier protein (ACP) thioesterase and the evolutionary origin of plant acyl-ACP thioesterases. *Plant Cell*, 7, 359–371.

Kamel, L., Keller-Pearson, M., Roux, C. and Ané, J.-M. (2017) Biology and evolution of arbuscular mycorrhizal symbiosis in the light of genomics. *New Phytol.*, 213, 531–536.

Keymer, A. and Gutjahr, C. (2018) Cross-kingdom lipid transfer in arbuscular mycorrhiza symbiosis and beyond. *Curr. Opin. Plant Biol.*, 44, 137–144.

Keymer, A., Pimprikar, P., Wewer, V., Huber, C., Brands, M., Bucerius, S.L., Delaux, P.-M., Klingl, V., Röpenack-Lahaye, E.v., Wang, T.L., Eisenreich, W., Dörmann, P., Parniske, M. and Gutjahr, C. (2017) Lipid transfer from plants to arbuscular mycorrhiza fungi. *Elife*, 6, e29107.

Kikuchi, Y., Hijikata, N., Yokoyama, K., Ohtomo, R., Handa, Y., Kawaguchi, M., Saito, K. and Ezawa, T. (2014) Polyphosphate accumulation is driven by transcriptome alterations that lead to near-synchronous and near-equivalent uptake of inorganic cations in an arbuscular mycorrhizal fungus. *New Phytol.*, 204, 638–649.

Kim, H.J., Silva, J.E., Vu, H.S., Mockaitis, K., Nam, J.-W. and Cahoon, E.B. (2015) Toward production of jet fuel functionality in oilseeds: identification of FatB acyl-acyl carrier protein thioesterases and evaluation of combinatorial expression strategies in *Camelina* seeds. *J. Exp. Bot.*, 66, 4251–4265.

Kim, H.U. (2005) Ubiquitous and endoplasmic reticulum-located lysophosphatidyl acyltransferase, LPAT2, is essential for female but not male gametophyte development in *Arabidopsis. Plant Cell*, 17, 1073–1089.

Klemptner, R.L., Sherwood, J.S., Tugizimana, F., Dubery, I.A. and Piater, L.A. (2014) Ergosterol, an orphan fungal microbe-associated molecular pattern (MAMP). *Mol. Plant*, 15, 747–761.

Kloppholz, S., Kuhn, H. and Requena, N. (2011) A secreted fungal effector of Glomus intraradices promotes symbiotic biotrophy. *Curr. Biol.*, 21, 1204–1209.

Kobae, Y. (2019) Dynamic phosphate uptake in arbuscular mycorrhizal roots under field conditions. *Front. Environ. Sci.*, 6, 1216.

Kobae, Y., Gutjahr, C., Paszkowski, U., Kojima, T., Fujiwara, T. and Hata, S. (2014) Lipid droplets of arbuscular mycorrhizal fungi emerge in concert with arbuscule collapse. *Plant Cell Physiol.*, 55, 1945–1953.

Kobae, Y. and Hata, S. (2010) Dynamics of periarbuscular membranes visualized with a fluorescent phosphate transporter in arbuscular mycorrhizal roots of rice. *Plant Cell Physiol.*, 51, 341–353.

Kobae, Y., Kawachi, M., Saito, K., Kikuchi, Y., Ezawa, T., Maeshima, M., Hata, S. and Fujiwara, T. (2015) Up-regulation of genes involved in N-acetylglucosamine uptake and metabolism suggests a recycling mode of chitin in intraradical mycelium of arbuscular mycorrhizal fungi. *Mycorrhiza*, 25, 411–417.

Kobayashi, Y., Maeda, T., Yamaguchi, K., Kameoka, H., Tanaka, S., Ezawa, T., Shigenobu, S. and Kawaguchi, M. (2018) The genome of Rhizophagus clarus HR1 reveals a common genetic basis for auxotrophy among arbuscular mycorrhizal fungi. *BMC Genomics*, 19, 465.

Koncz, C. and Schell, J. (1986) The promoter of T_L-DNA gene *5* controls the tissue-specific expression of chimaeric genes carried by a novel type of *Agrobacterium* binary vector. *Mol. Gen. Genet.*, 204, 383–396.

Konishi, T., Shinohara, K., Yamada, K. and Sasaki, Y. (1996) Acetyl-CoA carboxylase in higher plants: most plants other than gramineae have both the prokaryotic and the eukaryotic forms of this enzyme. *Plant Cell Physiol.*, 37, 117–122.

Kortz, L., Dorow, J., Becker, S., Thiery, J. and Ceglarek, U. (2013) Fast liquid chromatography-quadrupole linear ion trap-mass spectrometry analysis of polyunsaturated fatty acids and eicosanoids in human plasma. *J. Chromat. B*, 927, 209–213.

Krajinski, F., Courty, P.-E., Sieh, D., Franken, P., Zhang, H., Bucher, M., Gerlach, N., Kryvoruchko, I., Zoeller, D., Udvardi, M. and Hause, B. (2014) The H+-ATPase HA1 of Medicago truncatula is essential for ohosphate transport and plant growth during arbuscular mycorrhizal symbiosis. *Plant Cell*, 26, 1808–1817.

Kretzschmar, T., Kohlen, W., Sasse, J., Borghi, L., Schlegel, M., Bachelier, J.B., Reinhardt, D., Bours, R., Bouwmeester, H.J. and Martinoia, E. (2012) A petunia ABC protein controls strigolactone-dependent symbiotic signalling and branching. *Nature*, 483, 341–344.

Kumar, M., Prasad, R., Kumar, V., Tuteja, N. and Varma, A. (2017) Mycorrhizal fungi under biotic and abiotic stress. In *Mycorrhiza - Eco-Physiology, Secondary Metabolites, Nanomaterials.* 4th edn. (Varma, A., Prasad, R. and Tuteja, N., eds). Cham: Springer International Publishing, pp. 57–69.

Kwaaitaal, M., Nielsen, M.E., Böhlenius, H. and Thordal-Christensen, H. (2017) The plant membrane surrounding powdery mildew haustoria shares properties with the endoplasmic reticulum membrane. *J. Exp. Bot.*, 68, 5731–5743.

Lackzo, E., Boller, T. and WIEMKEN, V. (2004) Lipids in roots of Pinus sylvestris seedlings and in mycelia of Pisolithus tinctorius during ectomycorrhiza formation: changes in fatty acid and sterol composition. *Plant Cell Environm.*, 27, 27–40.

Laemmli, U.K. (1970) Cleavage of structural proteins during the assembly of the head of bacteriophage T4. *Nature*, 227, 680–685.

Lammers, P.J., Jun, J., Abubaker, J., Arreola, R., Gopalan, A., Bago, B., Hernandez-Sebastia, C., Allen, J.W., Douds, D.D., Pfeffer, P.E. and Shachar-Hill, Y. (2001) The glyoxylate cycle in an arbuscular mycorrhizal fungus. Carbon flux and gene expression. *Plant Physiol.*, 127, 1287–1298.

Lanfranco, L., Fiorilli, V. and Gutjahr, C. (2018) Partner communication and role of nutrients in the arbuscular mycorrhizal symbiosis. *New Phytol.*, 220, 1031–1046.

Lanver, D., Müller, A.N., Happel, P., Schweizer, G., Haas, F.B., Franitza, M., Pellegrin, C., Reissmann, S., Altmüller, J., Rensing, S.A. and Kahmann, R. (2018) The biotrophic development of Ustilago maydis studied by RNA-Seq analysis. *Plant Cell*, 30, 300–323.

Lardizabal, K.D., Mai, J.T., Wagner, N.W., Wyrick, A., Voelker, T. and Hawkins, D.J. (2001) DGAT2 is a new diacylglycerol acyltransferase gene family. purification, cloning, and expression in insect cells of two polypeptides from *Mortierella ramanniana* with diacylglycerol acyltransferase activity. *J. Biol. Chem.*, 276, 38862–38869.

Larose, G., Chênevert, R., Moutoglis, P., Gagné, S., Piché, Y. and Vierheilig, H. (2002) Flavonoid levels in roots ofMedicago sativa are modulated by the developmental stage of the symbiosis and the root colonizing arbuscular mycorrhizal fungus. *J. Plant Physiol.*, 159, 1329–1339.

Larson, T.R., Edgell, T., Byrne, J., Dehesh, K. and Graham, I.A. (2002) Acyl CoA profiles of transgenic plants that accumulate medium-chain fatty acids indicate inefficient storage lipid synthesis in developing oilseeds. *Plant J.*, 32, 519–527.

Larson, T.R. and Graham, I.A. (2001) Technical Advance. A novel technique for the sensitive quantification of acyl CoA esters from plant tissues. *Plant J.*, 25, 115–125.

Lauciello, L., Lack, G., Scapozza, L. and Perozzo, R. (2016) A high yield optimized method for the production of acylated ACPs enabling the analysis of enzymes involved in P. falciparum fatty acid biosynthesis. *Biochem. Biophys. Rep.*, 8, 310–317.

Lee, S.H., Stephens, J.L. and Englund, P.T. (2007) A fatty-acid synthesis mechanism specialized for parasitism. *Nat. Rev. Microbiol.*, 5, 287–297.

Lehman, R.M., Osborne, S.L., Taheri, W.I., Buyer, J.S. and Chim, B.K. (2019) Comparative measurements of arbuscular mycorrhizal fungal responses to agricultural management practices. *Mycorrhiza*, 29, 227–235.

Lenoir, I., Fontaine, J. and Lounès-Hadj Sahraoui, A. (2016) Arbuscular mycorrhizal fungal responses to abiotic stresses: A review. *Phytochemistry*, 123, 4–15.

Li, N., Gügel, I.L., Giavalisco, P., Zeisler, V., Schreiber, L., Soll, J. and Philippar, K. (2015) FAX1, a novel membrane protein mediating plastid fatty acid export. *PLoS Biol.*, 13, e1002053.

Li, Y., Beisson, F., Koo, A.J.K., Molina, I., Pollard, M. and Ohlrogge, J. (2007) Identification of acyltransferases required for cutin biosynthesis and production of cutin with suberin-like monomers. *Proc. Natl. Acad. Sci. USA*, 104, 18339–18344.

Li, Y., Beisson, F., Ohlrogge, J. and Pollard, M. (2007) Monoacylglycerols are components of root waxes and can be produced in the aerial cuticle by ectopic expression of a suberin-associated acyltransferase. *Plant Physiol.*, 144, 1267–1277.

Li-Beisson, Y., Pollard, M., Sauveplane, V., Pinot, F., Ohlrogge, J. and Beisson, F. (2009) Nanoridges that characterize the surface morphology of flowers require the synthesis of cutin polyester. *Proc. Natl. Acad. Sci. USA*, 106, 22008–22013.

Li-Beisson, Y., Shorrosh, B., Beisson, F., Andersson, M.X., Arondel, V., Bates, P.D., Baud, S., Bird, D., DeBono, A., Durrett, T.P., Franke, R.B., Graham, I.A., Katayama, K., Kelly, A.A., Larson, T., Markham, J.E., Miquel, M., Molina, I., Nishida, I., Rowland, O., Samuels, L., Schmid, K.M., Wada, H., Welti, R., Xu, C., Zallot, R. and Ohlrogge, J. (2013) Acyl-Lipid Metabolism. In *The Arabidopsis Book, No. 12*, pp. e0161.

Lin, K., Limpens, E., Zhang, Z., Ivanov, S., Saunders, D.G.O., Mu, D., Pang, E., Cao, H., Cha, H., Lin, T., Zhou, Q., Shang, Y., Li, Y., Sharma, T., van Velzen, R., Ruijter, N. de, **Aanen, D.K., Win, J., Kamoun, S., Bisseling, T., Geurts, R. and Huang, S.** (2014) Single nucleus genome sequencing reveals high similarity among nuclei of an endomycorrhizal fungus. *PLoS Gen.*, 10, e1004078.

Lin, M. and Oliver, D.J. (2008) The role of acetyl-coenzyme a synthetase in Arabidopsis. *Plant Physiol.*, 147, 1822–1829.

Lohse, S., Schliemann, W., Ammer, C., Kopka, J., Strack, D. and Fester, T. (2005) Organization and metabolism of plastids and mitochondria in arbuscular mycorrhizal roots of *Medicago truncatula*. *Plant Physiol.*, 139, 329–340.

López-Ráez, J.A., Fernández, I., García, J.M., Berrio, E., Bonfante, P., Walter, M.H. and Pozo, M.J. (2015) Differential spatio-temporal expression of carotenoid cleavage dioxygenases regulates apocarotenoid fluxes during AM symbiosis. *Plant Sci.*, 230, 59–69.

Los, D.A. and Murata, N. (1998) Structure and expression of fatty acid desaturases. *Biochim. Biophys. Acta*, 1394, 3–15.

Lösel, D.M. and Cooper, K.M. (1979) Incorporation of 14 C-labeled substrates by uninfected and VA mycorrhizal roots of onion. *New Phytol.*, 83, 415–426.

Lota, F., Wegmüller, S., Buer, B., Sato, S., Bräutigam, A., Hanf, B. and Bucher, M. (2013) The cis-acting CTTC-P1BS module is indicative for gene function of LjVTI12, a Qb-SNARE protein gene that is required for arbuscule formation in Lotus japonicus. *Plant J.*, 74, 280–293.

Luginbuehl, L.H., Menard, G.N., Kurup, S., van Erp, H., Radhakrishnan, G.V., Breakspear, A., Oldroyd, G.E.D. and Eastmond, P.J. (2017) Fatty acids in arbuscular mycorrhizal fungi are synthesized by the host plant. *Science*, 356, 1175–1178.

Luginbuehl, L.H. and Oldroyd, G.E.D. (2017) Understanding the Arbuscule at the Heart of Endomycorrhizal Symbioses in Plants. *Curr. Biol.*, 27, R952-R963.

MacLean, A.M., Bravo, A. and Harrison, M.J. (2017) Plant signaling and metabolic pathways enabling arbuscular mycorrhizal symbiosis. *Plant Cell*, 29, 2319–2335.

Maillet, F., Poinsot, V., Andre, O., Puech-Pagès, V., Haouy, A., Gueunier, M., Cromer, L., Giraudet, D., Formey, D., Niebel, A., Martinez, E.A., Driguez, H., Becard, G. and Denarie, J. (2011) Fungal lipochitooligosaccharide symbiotic signals in arbuscular mycorrhiza. *Nature*, 469, 58–63.

Majerus, P.W., Alberts, A.W. and Vagelos, R. (1965) The acyl carrier protein of fatty acid synthesis: Purification, physical properties and substrate binding site. *Proc. Natl. Acad. Sci. USA*, 51, 1231–1238.

Maldonado-Mendoza, I.E., Dewbre, G.R. and Harrison, M.J. (2001) A phosphate transporter gene from the extra-radical mycelium of an arbuscular mycorrhizal fungus Glomus intraradices is regulated in response to phosphate in the environment. *Mol. Plant Micr. Interact.*, 14, 1140–1148.

Malolepszy, A., Mun, T., Sandal, N., Gupta, V., Dubin, M., Urbanski, D., Shah, N., Bachmann, A., Fukai, E., Hirakawa, H., Tabata, S., Nadzieja, M., Markmann, K., Su, J., Umehara, Y., Soyano, T., Miyahara, A., Sato, S., Hayashi, M., Stougaard, J. and Andersen, S.U. (2016) The LORE1 insertion mutant resource. *Plant J.*, 88, 306–317.

Manck-Götzenberger, J. and Requena, N. (2016) Arbuscular mycorrhiza symbiosis induces a major transcriptional reprogramming of the potato SWEET sugar transporter family. *Front. Plant Sci.*, 7, 487.

Martin, F., Kohler, A., Murat, C., Veneault-Fourrey, C. and Hibbett, D.S. (2016) Unearthing the roots of ectomycorrhizal symbioses. *Nat. Rev. Microbiol.*, 14, 760–773.

Mathieu, S., Cusant, L., Roux, C. and Corradi, N. (2018) Arbuscular mycorrhizal fungi: intraspecific diversity and pangenomes. *New Phytol.*, 220, 1129–1134.

McGonigle, T.P., Miller, M.H., Evans, D.G., Fairchild, G.L. and Swan, J.A. (1990) A new method which gives an objective measure of colonization of roots by vesicular-arbuscular mycorrhizal fungi. *New Phytol.*, 115, 495–501.

Meesapyodsuk, D. and Qiu, X. (2012) The front-end desaturase: structure, function, evolution and biotechnological use. *Lipids*, 47, 227–237.

Miyata, K., Kozaki, T., Kouzai, Y., Ozawa, K., Ishii, K., Asamizu, E., Okabe, Y., Umehara, Y., Miyamoto, A., Kobae, Y., Akiyama, K., Kaku, H., Nishizawa, Y., Shibuya, N. and Nakagawa, T. (2014) The bifunctional plant receptor, OsCERK1, regulates both chitin-triggered immunity and arbuscular mycorrhizal symbiosis in rice. *Plant Cell Physiol.*, 55, 1864–1872.

Miyazaki, M., Bruggink, S.M. and Ntambi, J.M. (2006) Identification of mouse palmitoyl-coenzyme A Delta9-desaturase. *J. Lipid Res.*, 47, 700–704.

Montero, H., Choi, J. and Paszkowski, U. (2019) Arbuscular mycorrhizal phenotyping: the dos and don'ts. *New Phytol.*, 221, 1182–1186.

Mori, N., Nishiuma, K., Sugiyama, T., Hayashi, H. and Akiyama, K. (2016) Carlactone-type strigolactones and their synthetic analogues as inducers of hyphal branching in arbuscular mycorrhizal fungi. *Phytochemistry*, 130, 90–98.

Murray, J.D., Cousins, D.R., Jackson, K.J. and Liu, C. (2013) Signaling at the root surface: The role of cutin monomers in mycorrhization. *Mol. Plant*, 6, 1381–1383.

Nadal, M., Sawers, R., Naseem, S., Bassin, B., Kulicke, C., Sharman, A., An, G., An, K., Ahern, K.R., Romag, A., Brutnell, T.P., Gutjahr, C., Geldner, N., Roux, C., Martinoia, E., Konopka, J.B. and Paszkowski, U. (2017) An N-acetylglucosamine transporter required for arbuscular mycorrhizal symbioses in rice and maize. *Nat. Plants*, 3, 17073.

Nagahashi, G. and Douds, D.D. (2011) The effects of hydroxy fatty acids on the hyphal branching of germinated spores of AM fungi. *Fung. Biol.*, 115, 351–358.

Nakamura, Y. (2017) Plant phospholipid diversity: emerging functions in metabolism and protein-lipid Interactions. *Trends Plant Sci.*, 22, 1027–1040.

Nawrath, C., Schreiber, L., Franke, R.B., Geldner, N., Reina-Pinto, J.J. and Kunst, L. (2013) Apoplastic diffusion barriers in Arabidopsis. *Arabidopsis Book*, 11, e0167.

Nordby, H.E., Nemec, S. and Nagy, S. (1981) Fatty acids and sterols associated with citrus root mycorrhizae. *J. Agricult. Food Chem.*, 29, 396–401.

Nouri, E., Breuillin-Sessoms, F., Feller, U. and Reinhardt, D. (2015) Phosphorus and Nitrogen Regulate Arbuscular Mycorrhizal Symbiosis in Petunia hybrida. *PloS one*, 10, e0127472.

Ocón, A., Hampp, R. and Requena, N. (2007) Trehalose turnover during abiotic stress in arbuscular mycorrhizal fungi. *New Phytol.*, 174, 879–891.

Ogasawara, Y., Kira, S., Mukai, Y., Noda, T. and Yamamoto, A. (2017) Ole1, fatty acid desaturase, is required for Atg9 delivery and isolation membrane expansion during autophagy in Saccharomyces cerevisiae. *Biol. Open*, 6, 35–40.

Ohlrogge, J. and Browse, J. (1995) Lipid biosynthesis. *Plant Cell*, 7, 957–970.

Olsson, P.A., Bååth, E., Jakobsen, I. and Söderström, B. (1995) The use of phospholipid and neutral lipid fatty acids to estimate biomass of arbuscular mycorrhizal fungi in soil. *Mycol. Res.*, 99, 623–629.

Olsson, P.A., Burleigh, S.H. and van Aarle, I.M. (2005) The influence of external nitrogen on carbon allocation to *Glomus intraradices* in monoxenic arbuscular mycorrhiza. *New Phytol.*, 168, 677–686.

Olsson, P.A. and Johansen, A. (2000) Lipid and fatty acid composition of hyphae and spores of arbuscular mycorrhizal fungi at different growth stages. *Mycol. Res.*, 104, 429–434.

Olsson, P.A. and Johnson, N.C. (2005) Tracking carbon from the atmosphere to the rhizosphere. *Ecol. Lett.*, 8, 1264–1270.

Olsson, P.A., Larsson, L., Bago, B., Wallander, H. and van Aarle, I.M. (2003) Ergosterol and fatty acids for biomass estimation of mycorrhizal fungi. *New Phytol.*, 159, 7–10.

Olsson, P.A., van Aarle, I.M., Gavito, M.E., Bengtson, P. and Bengtsson, G. (2005) 13C incorporation into signature fatty acids as an assay for carbon allocation in arbuscular mycorrhiza. *Appl. Environm. Microbiol.*, 71, 2592–2599.

Overath, P., Pauli, G. and Schairer, H.U. (1969) Fatty acid degradation in *Escherichia coli*. *Eur. J. Biochem.*, 7, 559–574.

Pan, H., Oztas, O., Zhang, X., Wu, X., Stonoha, C., Wang, E., Wang, B. and Wang, D. (2016) A symbiotic SNARE protein generated by alternative termination of transcription. *Nat. Plants*, 2, 15197.

Panchuk-Voloshina, N., Haugland, R.P., Bishop-Stewart, J., Bhalgat, M.K., Millard, P.J., Mao, F. and Leung, W.Y. (1999) Alexa dyes, a series of new fluorescent dyes that yield exceptionally bright, photostable conjugates. *J. Histochem. Cytochem.*, 47, 1179–1188.

Panikashvili, D., Shi, J.X., Schreiber, L. and Aharoni, A. (2011) The Arabidopsis ABCG13 transporter is required for flower cuticle secretion and patterning of the petal epidermis. *New Phytol.*, 190, 113–124.

Park, H.-J., Floss, D.S., Levesque-Tremblay, V., Bravo, A. and Harrison, M.J. (2015) Hyphal branching during arbuscule development requires reduced arbuscular mycorrhiza1. *Plant Physiol.*, 169, 2774–2788.

Parniske, M. (2008) Arbuscular mycorrhiza. the mother of plant root endosymbioses. *Nat. Rev. Microbiol.*, 6, 763–775.

Paszkowski, U., Kroken, S., Roux, C. and Briggs, S.P. (2002) Rice phosphate transporters include an evolutionarily divergent gene specifically activated in arbuscular mycorrhizal symbiosis. *Proc. Natl. Acad. Sci. USA,* 99, 13324–13329.

Pfeffer, P.E., Douds, D.D., Becard, G. and Shachar-Hill, Y. (1999) Carbon uptake and the metabolism and transport of lipids in an arbuscular mycorrhiza. *Plant Physiol.,* 120, 587–598.

Pimprikar, P., Carbonnel, S., Paries, M., Katzer, K., Klingl, V., Bohmer, M.J., Karl, L., Floss, D.S., Harrison, M.J., Parniske, M. and Gutjahr, C. (2016) A CCaMK-CYCLOPS-DELLA complex activates transcription of RAM1 to regulate arbuscule branching. *Curr. Biol.,* 26, 987–998.

Pimprikar, P. and Gutjahr, C. (2018) Transcriptional regulation of arbuscular mycorrhiza development. *Plant Cell Physiol.,* 59, 673–690.

Post-Beittenmiller, D., Roughan, G. and Ohlrogge, J.B. (1992) Regulation of plant fatty acid biosynthesis. Analysis of acyl-coenzymeA and acyl-acyl carrier protein substrate pools in spinach and pea chloroplasts. *Plant Physiol.,* 100, 923–930.

Pozo, M.J., López-Ráez, J.A., Azcón-Aguilar, C. and García-Garrido, J.M. (2015) Phytohormones as integrators of environmental signals in the regulation of mycorrhizal symbioses. *New Phytol.,* 205, 1431–1436.

Pumplin, N. and Harrison, M.J. (2009) Live-cell imaging reveals periarbuscular membrane domains and organelle location in *Medicago truncatula* roots during arbuscular mycorrhizal symbiosis. *Plant Physiol.,* 151, 809–819.

Pumplin, N., Zhang, X., Noar, R.D. and Harrison, M.J. (2012) Polar localization of a symbiosis-specific phosphate transporter is mediated by a transient reorientation of secretion. *Proc. Natl. Acad. Sci. USA,* 109, 72.

Rapparini, F. and Peñuelas, J. (2014) Mycorrhizal Fungi to Alleviate Drought Stress on Plant Growth. In *Use of Microbes for the Alleviation of Soil Stresses*, 1, 21–42.

Rausch, C., Daram, P., Brunner, S., Jansa, J., Laloi, M., Leggewie, G., Amrhein, N. and Bucher, M. (2001) A phosphate transporter expressed in arbuscule-containing cells in potato. *Nature,* 414, 462–470.

Reich, M., Göbel, C., Kohler, A., Buée, M., Martin, F., Feussner, I. and Polle, A. (2009) Fatty acid metabolism in the ectomycorrhizal fungus *Laccaria bicolor*. *New Phytol.,* 182, 950–964.

Rentsch, D., Laloi, M., Rouhara, I., Schmelzer, E., Delrot, S. and Frommer, W.B. (1995) NTR1 encodes a high affinity oligopeptide transporter in *Arabidopsis*. *FEBS Lett.,* 370, 264–268.

Rich, M.K., Nouri, E., Courty, P.-E. and Reinhardt, D. (2017) Diet of arbuscular mycorrhizal fungi: bread and butter? *Trends Plant Sci.,* 22, 652–660.

Rich, M.K., Schorderet, M., Bapaume, L., Falquet, L., Morel, P., Vandenbussche, M. and Reinhardt, D. (2015) The petunia GRAS transcription factor ATA/RAM1 regulates symbiotic gene expression and fungal morphogenesis in arbuscular mycorrhiza. *Plant Physiol.,* 168, 788–797.

Rivero, J., Álvarez, D., Flors, V., Azcón-Aguilar, C. and Pozo, M.J. (2018) Root metabolic plasticity underlies functional diversity in mycorrhiza-enhanced stress tolerance in tomato. *New Phytol.,* 220, 1322–1336.

Rock, C.O. and Garwin, J.L. (1979) Preparative enzymatic synthesis and hydrophobic chromatography of acyl-acyl carrier protein. *J. Biol. Chem.,* 254, 7123–7128.

Rodríguez-Rodríguez, M.F., Salas, J.J., Garcés, R. and Martínez-Force, E. (2014) Acyl-ACP thioesterases from Camelina sativa: cloning, enzymatic characterization and implication in seed oil fatty acid composition. *Phytochemistry,* 107, 7–15.

Rodríguez-Vargas, S., Sánchez-García, A., Martínez-Rivas, J.M., Prieto, J.A. and Randez-Gil, F. (2007) Fluidization of membrane lipids enhances the tolerance of Saccharomyces cerevisiae to freezing and salt stress. *Appl. Environm. Microbiol.,* 73, 110–116.

Ropars, J., Toro, K.S., Noel, J., Pelin, A., Charron, P., Farinelli, L., Marton, T., Kruger, M., Fuchs, J., Brachmann, A. and Corradi, N. (2016) Evidence for the sexual origin of heterokaryosis in arbuscular mycorrhizal fungi. *Nat. Microbiol.,* 1, 16033.

Rosewarne, G., M., Barker, S., J., Smith, S.E., Smith, F.A. and Schachtman, D., P. (1999) A Lycopersicon esculentum phosphate transporter (LePT1) involved in phosphorus uptake from a vesicular-arbuscular mycorrhizal fungus. *New Phytol.,* 144, 507–516.

Roth, R., Hillmer, S., Funaya, C., Chiapello, M., Schumacher, K., Lo Presti, L., Kahmann, R. and Paszkowski, U. (2019) Arbuscular cell invasion coincides with extracellular vesicles and membrane tubules. *Nat. Plants*, 5, 204–211.

Roth, R. and Paszkowski, U. (2017) Plant carbon nourishment of arbuscular mycorrhizal fungi. *Curr. Opin. Plant Biol.*, 39, 50–56.

Ruiz-Lozano, J.M., Aroca, R., Zamarreño, Á.M., Molina, S., Andreo-Jiménez, B., Porcel, R., García-Mina, J.M., Ruyter-Spira, C. and López-Ráez, J.A. (2015) Arbuscular mycorrhizal symbiosis induces strigolactone biosynthesis under drought and improves drought tolerance in lettuce and tomato. *Plant Cell Environm.*, 39, 441–452.

Salas, J.J. and Ohlrogge, J.B. (2002) Characterization of substrate specificity of plant FatA and FatB acyl-ACP thioesterases. *Arch. Biochem. Biophys.*, 403, 25–34.

Salvioli, A., Ghignone, S., Novero, M., Navazio, L., Venice, F., Bagnaresi, P. and Bonfante, P. (2016) Symbiosis with an endobacterium increases the fitness of a mycorrhizal fungus, raising its bioenergetic potential. *ISME J.*, 10, 130–144.

Sambrook, J. and Russell, D.W. (2001) *Molecular cloning. A laboratory manual.* 3rd edn. Cold Spring Harbor, N.Y: Cold Spring Harbor Laboratory Press.

Sawers, R.J.H., Svane, S.F., Quan, C., Grønlund, M., Wozniak, B., Gebreselassie, M.-N., González-Muñoz, E., Chávez Montes, R.A., Baxter, I., Goudet, J., Jakobsen, I. and Paszkowski, U. (2017) Phosphorus acquisition efficiency in arbuscular mycorrhizal maize is correlated with the abundance of root-external hyphae and the accumulation of transcripts encoding PHT1 phosphate transporters. *New Phytol.*, 214, 632–643.

Schaarschmidt, S., Gonzalez, M.-C., Roitsch, T., Strack, D., Sonnewald, U. and Hause, B. (2007) Regulation of arbuscular mycorrhization by carbon. The symbiotic interaction cannot be improved by increased carbon availability accomplished by root-specifically enhanced invertase activity. *Plant Physiol.*, 143, 1827–1840.

Schaarschmidt, S., Roitsch, T. and Hause, B. (2006) Arbuscular mycorrhiza induces gene expression of the apoplastic invertase LIN6 in tomato (*Lycopersicon esculentum*) roots. *J. Exp. Bot.*, 57, 4015–4023.

Schaeffer, A., Bronner, R., Benveniste, P. and Schaller, H. (2001) The ratio of campesterol to sitosterol that modulates growth in Arabidopsis is controlled by sterol methyltransferase 2;1. *Plant J.*, 25, 605–615.

Schliemann, W., Ammer, C. and Strack, D. (2008) Metabolite profiling of mycorrhizal roots of *Medicago truncatula. Phytochemistry*, 69, 112–146.

Schüssler, A., Martin, H., Cohen, D., Fitz, M. and Wipf, D. (2006) Characterization of a carbohydrate transporter from symbiotic glomeromycotan fungi. *Nature*, 444, 933–936.

Schüßler, A., Martin, H., Cohen, D., Fitz, M. and Wipf, D. (2007) Arbuscular Mycorrhiza. *Plant Signal. Behav.*, 2, 431–434.

Sedzielewska Toro, K. and Brachmann, A. (2016) The effector candidate repertoire of the arbuscular mycorrhizal fungus *Rhizophagus clarus. BMC Genom.*, 17, 101.

Shachar-Hill, Y., Pfeffer, P.E., Douds, D., Osman, S.F., Doner, L.W. and Ratcliffe, R.G. (1995) Partitioning of intermediary carbon metabolism in vesicular-arbuscular mycorrhizal leek. *Plant Physiol.*, 108, 7–15.

Shanklin, J. (2000) Overexpression and purification of the *Escherichia coli* inner membrane enzyme acyl-acyl carrier protein synthase in an active form. *Protein Expr. Purif.*, 18, 355–360.

Shanklin, J. and Somerville, C. (1991) Stearoyl-acyl-carrier-protein desaturase from higher plants is structurally unrelated to the animal and fungal homologs. *Proc. Natl. Acad. Sci. USA*, 88, 2510–2514.

Shanklin, J., Whittle, E. and Fox, B.G. (1994) Eight histidine residues are catalytically essential in a membrane-associated iron enzyme, stearoyl-CoA desaturase, and are conserved in alkane hydroxylase and xylene monooxygenase. *Biochemistry*, 33, 12787–12794.

Shimada, T.L., Hayashi, M. and Hara-Nishimura, I. (2018) Membrane Dynamics and Multiple Functions of Oil Bodies in Seeds and Leaves. *Plant Physiol.*, 176, 199–207.

Shockey, J., Regmi, A., Cotton, K., Adhikari, N., Browse, J. and Bates, P.D. (2016) Identification of Arabidopsis GPAT9 (At5g60620) as an essential gene involved in triacylglycerol biosynthesis. *Plant Physiol.*, 170, 163–179.

Siebers, M., Brands, M., Wewer, V., Duan, Y., Hölzl, G. and Dörmann, P. (2016) Lipids in plant-microbe interactions. *Biochim. Biophys. Acta*, 1861, 1379–1395.

Smet, C.H. de, Vittone, E., Scherer, M., Houweling, M., Liebisch, G., Brouwers, J.F. and Kroon, A.I.P.M. de (2012) The yeast acyltransferase Sct1p regulates fatty acid desaturation by competing with the desaturase Ole1p. *Mol. Biol. Cell*, 23, 1146–1156.

Smith, S.E. and Read, D.J. (2008) *Mycorrhizal symbiosis.* 3rd edn. Amsterdam, London: Academic.

Solaiman, M.D.Z. and Saito, M. (1997) Use of sugars by intraradical hyphae of arbuscular mycorrhizal fungi revealed by radiorespirometry. *New Phytol.*, 533–538.

Solaiman, M.Z., Ezawa, T., Kojima, T. and Saito, M. (1999) Polyphosphates in intraradical and extraradical hyphae of an arbuscular mycorrhizal fungus, Gigaspora margarita. *Appl. Environ. Microbiol.*, 65, 5604–5606.

Sparkes, I.A., Runions, J., Kearns, A. and Hawes, C. (2006) Rapid, transient expression of fluorescent fusion proteins in tobacco plants and generation of stably transformed plants. *Nat. Protoc.*, 1, 2019–2025.

Steinkellner, S., Lendzemo, V., Langer, I., Schweiger, P., Khaosaad, T., Toussaint, J.-P. and Vierheilig, H. (2007) Flavonoids and strigolactones in root exudates as signals in symbiotic and pathogenic plant-fungus interactions. *Molecules*, 12, 1290–1306.

Stracke, S., Kistner, C., Yoshida, S., Mulder, L., Sato, S., Kaneko, T., Tabata, S., Sandal, N., Stougaard, J., Szczyglowski, K. and Parniske, M. (2002) A plant receptor-like kinase required for both bacterial and fungal symbiosis. *Nature*, 417, 959–962.

Strullu, Chamel, A., Eloy, J.F. and Gourret, J., P. (1983) Ultrastructure and analysis by laser probe mass spectrography of the mineral composition of the vesicles of Trifolium pratense endomycorrhizas. *New Phytol.*, 94, 81–88.

Stukey, J.E., McDonough, V.M. and Martin, C.E. (1989) Isolation and characterization of OLE1, a gene affecting fatty acid desaturation from Saccharomyces cerevisiae. *J. Biol. Chem.*, 264, 16537–16544.

Stukey, J.E., McDonough, V.M. and Martin, C.E. (1990) The OLE1 gene of Saccharomyces cerevisiae encodes the delta 9 fatty acid desaturase and can be functionally replaced by the rat stearoyl-CoA desaturase gene. *J. Biol. Chem.*, 265, 20144–20149.

Stumpe, M., Carsjens, J.-G., Stenzel, I., Gobel, C., Lang, I., Pawlowski, K., Hause, B. and Feussner, I. (2005) Lipid metabolism in arbuscular mycorrhizal roots of *Medicago truncatula*. *Phytochemistry*, 66, 781–791.

Sun, X., Chen, W., Ivanov, S., MacLean, A.M., Wight, H., Ramaraj, T., Mudge, J., Harrison, M.J. and Fei, Z. (2019) Genome and evolution of the arbuscular mycorrhizal fungus Diversispora epigaea (formerly Glomus versiforme) and its bacterial endosymbionts. *New Phytol.*, 221, 1556–1573.

Sun, X.-G., Bonfante, P. and Tang, M. (2015) Effect of volatiles versus exudates released by germinating spores of Gigaspora margarita on lateral root formation. *Plant Phys. Biochem.*, 97, 1–10.

Symanczik, S., Lehmann, M.F., Wiemken, A., Boller, T. and Courty, P.-E. (2018) Effects of two contrasted arbuscular mycorrhizal fungal isolates on nutrient uptake by Sorghum bicolor under drought. *Mycorrhiza*, 28, 779–785.

Tan, L., Zhuo, R., Li, S., Ma, F. and Zhang, X. (2017) Differential expression of desaturase genes and changes in fatty acid composition of Mortierella sp. AGED in response to environmental factors. *J. Sci. Food Agric.*, 97, 1876–1884.

Tang, N., San Clemente, H., Roy, S., Becard, G., Zhao, B. and Roux, C. (2016) A survey of the gene repertoire of *Gigaspora rosea* unravels conserved features among Glomeromycota for obligate biotrophy. *Front. Microbiol.*, 7, 233.

Tehlivets, O., Scheuringer, K. and Kohlwein, S.D. (2007) Fatty acid synthesis and elongation in yeast. *Biochim. Biophys. Acta*, 1771, 255–270.

Tisserant, E., Kohler, A., Dozolme-Seddas, P., Balestrini, R., Benabdellah, K., Colard, A., Croll, D., da Silva, C., Gomez, S.K., Koul, R., Ferrol, N., Fiorilli, V., Formey, D., Franken, P., Helber, N., Hijri, M., Lanfranco, L., Lindquist, E., Liu, Y., Malbreil, M., Morin, E., Poulain, J., Shapiro, H., van Tuinen, D., Waschke, A., Azcon-Aguilar, C., Becard, G., Bonfante, P.,

Harrison, M.J., Kuster, H., Lammers, P., Paszkowski, U., Requena, N., Rensing, S.A., Roux, C., Sanders, I.R., Shachar-Hill, Y., Tuskan, G., Young, J.P., Gianinazzi-Pearson, V. and Martin, F. (2012) The transcriptome of the arbuscular mycorrhizal fungus *Glomus intraradices* (DAOM 197198) reveals functional tradeoffs in an obligate symbiont. *New Phytol.*, 193, 755–769.

Tisserant, E., Malbreil, M., Kuo, A., Kohler, A., Symeonidi, A., Balestrini, R., Charron, P., Duensing, N., Frei dit Frey, N., Gianinazzi-Pearson, V., Gilbert, L.B., Handa, Y., Herr, J.R., Hijri, M., Koul, R., Kawaguchi, M., Krajinski, F., Lammers, P.J., Masclaux, F.G., Murat, C., Morin, E., Ndikumana, S., Pagni, M., Petitpierre, D., Requena, N., Rosikiewicz, P., Riley, R., Saito, K., San Clemente, H., Shapiro, H., van Tuinen, D., Becard, G., Bonfante, P., Paszkowski, U., Shachar-Hill, Y.Y., Tuskan, G.A., Young, J.P.W., Sanders, I.R., Henrissat, B., Rensing, S.A., Grigoriev, I.V., Corradi, N., Roux, C. and Martin, F. (2013) Genome of an arbuscular mycorrhizal fungus provides insight into the oldest plant symbiosis. *Proc. Natl. Acad. Sci. USA*, 110, 20117–20122.

Tjellström, H., Andersson, M.X., Larsson, K.E. and Sandelius, A.S. (2008) Membrane phospholipids as a phosphate reserve. the dynamic nature of phospholipid-to-digalactosyl diacylglycerol exchange in higher plants. *Plant Cell Environ.*, 31, 1388–1398.

Toth, R. and Miller, R.M. (1984) Dynamics of arbuscule development and degeneration in a Zea mays mycorrhiza. *Am. J. Bot.*, 71, 449.

Towbin, H., Staehelin, T. and Gordon, J. (1979) Electrophoretic transfer of proteins from polyacrylamide gels to nitrocellulose sheets: procedure and some applications. *Proc. Natl. Acad. Sci. USA*, 76, 4350–4354.

Trepanier, M., Becard, G., Moutoglis, P., Willemot, C., Gagne, S., Avis, T.J. and Rioux, J.-A. (2005) Dependence of arbuscular-mycorrhizal fungi on their plant host for palmitic acid synthesis. *Appl. Environm. Microbiol.*, 71, 5341–5347.

Triana, S., Cock, H. de, Ohm, R.A., Danies, G., Wösten, H.A.B., Restrepo, S., González Barrios, A.F. and Celis, A. (2017) Lipid metabolic versatility in Malassezia spp. yeasts studied through metabolic modeling. *Front. Microbiol.*, 8, 1772.

Tsai, Y.-Y., Ohashi, T., Wu, C.-C., Bataa, D., Misaki, R., Limtong, S. and Fujiyama, K. (2019) Delta-9 fatty acid desaturase overexpression enhanced lipid production and oleic acid content in Rhodosporidium toruloides for preferable yeast lipid production. *J. Biosci. Bioeng.*, 127, 430–440.

Tsuzuki, S., Handa, Y., Takeda, N. and Kawaguchi, M. (2016) Strigolactone-induced putative secreted protein 1 is required for the establishment of symbiosis by the arbuscular mycorrhizal fungus Rhizophagus irregularis. *Mol. Plant. Microbe Interact.*, 29, 277–286.

van Dam, N.M. and Bouwmeester, H.J. (2016) Metabolomics in the Rhizosphere: tapping into belowground chemical communication. *Trends Plant Sci.*, 21, 256–265.

Venkateshwaran, M., Jayaraman, D., Chabaud, M., Genre, A., Balloon, A.J., Maeda, J., Forshey, K., den Os, D., Kwiecien, N.W., Coon, J.J., Barker, D.G. and Ané, J.-M. (2015) A role for the mevalonate pathway in early plant symbiotic signaling. *Proc. Natl. Acad. Sci. USA*, 112, 9781–9786.

Vierheilig, H., Coughlan, A.P., Wyss, U. and Piché, Y. (1998) Ink and vinegar, a simple staining technique for arbuscular-mycorrhizal fungi. *Appl. Environm. Microbiol.*, 64, 5004–5007.

Vijayakumar, V., Liebisch, G., Buer, B., Xue, L., Gerlach, N., Blau, S., Schmitz, J. and Bucher, M. (2016) Integrated multi-omics analysis supports role of lysophosphatidylcholine and related glycerophospholipids in the *Lotus japonicus-Glomus intraradices* mycorrhizal symbiosis. *Plant Cell Environm.*, 39, 393–415.

Vodala, S., Abruzzi, K.C. and Rosbash, M. (2008) The nuclear exosome and adenylation regulate posttranscriptional tethering of yeast GAL genes to the nuclear periphery. *Mol. Cell*, 31, 104–113.

Voelker, T.A., Worrell, A.C., Anderson, L., Bleibaum, J., Fan, C., Hawkins, D.J., Radke, S.E. and Davies, H.M. (1992) Fatty acid biosynthesis redirected to medium chains in transgenic oilseed plants. *Science*, 257, 72–74.

vom Dorp, K., Dombrink, I. and Dormann, P. (2013) Quantification of diacylglycerol by mass spectrometry. *Meth. Mol. Biol.*, 1009, 43–54.

Vos, C., Claerhout, S., Mkandawire, R., Panis, B., Waele, D. de and **Elsen, A.** (2012) Arbuscular mycorrhizal fungi reduce root-knot nematode penetration through altered root exudation of their host. *Plant Soil*, 354, 335–345.

Walter, M.H. Role of carotenoid metabolism in the arbuscular mycorrhizal symbiosis. In *Molecular Microbial Ecology of the Rhizosphere 1&2*, pp. 513–524.

Wang, E., Schornack, S., Marsh, J.F., Gobbato, E., Schwessinger, B., Eastmond, P., Schultze, M., Kamoun, S. and Oldroyd, G.E.D. (2012) A common signaling process that promotes mycorrhizal and oomycete colonization of plants. *Curr. Biol.*, 22, 2242–2246.

Wang, E., Yu, N., Bano, S.A., Liu, C., Miller, A.J., Cousins, D., Zhang, X., Ratet, P., Tadege, M., Mysore, K.S., Downie, J.A., Murray, J.D., Oldroyd, G.E.D. and Schultze, M. (2014) A H+-ATPase that energizes nutrient uptake during mycorrhizal symbioses in rice and Medicago truncatula. *Plant Cell*, 26, 1818–1830.

Wang, M., Chen, H., Ailati, A., Chen, W., Chilton, F.H., Todd Lowther, W. and Chen, Y.Q. (2018) Substrate specificity and membrane topologies of the iron-containing ω3 and ω6 desaturases from Mortierella alpina. *Appl. Microbiol. Biotechnol.*, 102, 211–223.

Wewer, V., Brands, M. and Dörmann, P. (2014) Fatty acid synthesis and lipid metabolism in the obligate biotrophic fungus *Rhizophagus irregularis* during mycorrhization of *Lotus japonicus. Plant J.*, 79, 398–412.

Wewer, V., Dombrink, I., vom Dorp, K. and Dörmann, P. (2011) Quantification of sterol lipids in plants by quadrupole time-of-flight mass spectrometry. *J. Lipid Res.*, 52, 1039–1054.

Wewer, V. and Dörmann, P. (2014) Determination of sterol lipids in plant tissues by gas chromatography and Q-TOF mass spectrometry. In *Plant Isoprenoids, Methods and Protocols. Methods in Molecular Biology (vol. 1153) (*Rodrígues-Concepción, M., ed). New York: Humana Press, New York, pp. 115–133.

Witkowski, A., Joshi, A.K. and Smith, S. (2007) Coupling of the *de novo* fatty acid biosynthesis and lipoylation pathways in mammalian mitochondria. *J. Biol. Chem.*, 282, 14178–14185.

Wongwathanarat, P., Michaelson, L.V., Carter, A.T., Lazarus, C.M., Griffiths, G., Stobart, A.K., Archer, D.B. and MacKenzie, D.A. (1999) Two fatty acid delta9-desaturase genes, ole1 and ole2, from Mortierella alpina complement the yeast ole1 mutation. *Microbiol.*, 145 (Pt 10), 2939–2946.

Xie, X., Lin, H., Peng, X., Xu, C., Sun, Z., Jiang, K., Huang, A., Wu, X., Tang, N., Salvioli, A., Bonfante, P. and Zhao, B. (2016) Arbuscular Mycorrhizal Symbiosis Requires a Phosphate Transceptor in the Gigaspora margarita Fungal Symbiont. *Mol. Plant*, 9, 1583–1608.

Xu, J., Saunders, C.W., Hu, P., Grant, R.A., Boekhout, T., Kuramae, E.E., Kronstad, J.W., DeAngelis, Y.M., Reeder, N.L., Johnstone, K.R., Leland, M., Fieno, A.M., Begley, W.M., Sun, Y., Lacey, M.P., Chaudhary, T., Keough, T., Chu, L., Sears, R., Yuan, B. and Dawson, T.L. (2007) Dandruff-associated *Malassezia* genomes reveal convergent and divergent virulence traits shared with plant and human fungal pathogens. *Proc. Natl. Acad. Sci. USA*, 104, 18730–18735.

Xu, P., Gu, Q., Wang, W., Wong, L., Bower, A.G.W., Collins, C.H. and Koffas, M.A.G. (2013) Modular optimization of multi-gene pathways for fatty acids production in *E. coli. Nat. Commun.*, 4, 1409.

Xue, L., Cui, H., Buer, B., Vijayakumar, V., Delaux, P.-M., Junkermann, S. and Bucher, M. (2015) Network of GRAS transcription factors involved in the control of arbuscle development in *Lotus japonicus. Plant Physiol.*, 167, 854–871.

Yadav, V., Molina, I., Ranathunge, K., Castillo, I.Q., Rothstein, S.J. and Reed, J.W. (2014) ABCG transporters are required for suberin and pollen wall extracellular barriers in *Arabidopsis. Plant Cell*, 26, 3569–3588.

Yamamoto, K., Shibahara, A., Nakayama, T. and Kajimoto, G. (1991) Determination of double-bond positions in methylene-interrupted dienoic fatty acids by GC-MS as their dimethyl disulfide adducts. *Chem. Phys. Lipids*, 60, 39–50.

Yang, S.-Y., Grønlund, M., Jakobsen, I., Grotemeyer, M.S., Rentsch, D., Miyao, A., Hirochika, H., Kumar, C.S., Sundaresan, V., Salamin, N., Catausan, S., Mattes, N., Heuer, S. and Paszkowski, U. (2012) Nonredundant regulation of rice arbuscular mycorrhizal symbiosis by two members of the phosphate transporter1 gene family. *Plant Cell*, 24, 4236–4251.

Yang, W., Pollard, M., Li-Beisson, Y., Beisson, F., Feig, M. and Ohlrogge, J. (2010) A distinct type of glycerol-3-phosphate acyltransferase with sn-2 preference and phosphatase activity producing 2-monoacylglycerol. *Proc. Natl. Acad. Sci. USA*, 107, 12040–12045.

Yang, W., Simpson, J.P., Li-Beisson, Y., Beisson, F., Pollard, M. and Ohlrogge, J.B. (2012) A land-plant-specific glycerol-3-phosphate acyltransferase family in Arabidopsis. Substrate specificity, *sn*-2 preference, and evolution. *Plant Physiol.*, 160, 638–652.

Yeats, T.H., Huang, W., Chatterjee, S., Viart, H.M.-F., Clausen, M.H., Stark, R.E. and Rose, J.K.C. (2014) Tomato cutin deficient 1 (CD1) and putative orthologs comprise an ancient family of cutin synthase-like (CUS) proteins that are conserved among land plants. *Plant J.*, 77, 667–675.

Yeats, T.H., Martin, L.B.B., Viart, H.M.-F., Isaacson, T., He, Y., Zhao, L., Matas, A.J., Buda, G.J., Domozych, D.S., Clausen, M.H. and Rose, J.K.C. (2012) The identification of cutin synthase: formation of the plant polyester cutin. *Nat. Chem. Biol.*, 8, 609–611.

Yen, C.-L.E., Monetti, M., Burri, B.J. and Farese, R.V. (2005) The triacylglycerol synthesis enzyme DGAT1 also catalyzes the synthesis of diacylglycerols, waxes, and retinyl esters. *J. Lipid Res.*, 46, 1502–1511.

Zeng, T., Holmer, R., Hontelez, J., Te Lintel-Hekkert, B., Marufu, L., Zeeuw, T. de, **Wu, F., Schijlen, E., Bisseling, T. and Limpens, E.** (2018) Host- and stage-dependent secretome of the arbuscular mycorrhizal fungus Rhizophagus irregularis. *Plant J.*, 94, 411–425.

Zhang, C., Cahoon, R.E., Hunter, S.C., Chen, M., Han, J. and Cahoon, E.B. (2013) Genetic and biochemical basis for alternative routes of tocotrienol biosynthesis for enhanced vitamin E antioxidant production. *Plant J.*, 73, 628–639.

Zhang, L., Feng, G. and Declerck, S. (2018) Signal beyond nutrient, fructose, exuded by an arbuscular mycorrhizal fungus triggers phytate mineralization by a phosphate solubilizing bacterium. *ISME J.*, 12, 2339–2351.

Zhang, Q., Blaylock, L.A. and Harrison, M.J. (2010) Two *Medicago truncatula* half-ABC transporters are essential for arbuscule development in arbuscular mycorrhizal symbiosis. *Plant Cell*, 22, 1483–1497.

Zhang, S., Lehmann, A., Zheng, W., You, Z. and Rillig, M.C. (2019) Arbuscular mycorrhizal fungi increase grain yields: a meta-analysis. *New Phytol.*, 222, 543–555.

Zhang, X., Pumplin, N., Ivanov, S. and Harrison, M.J. (2015) EXO70I is required for development of a sub-domain of the periarbuscular membrane during arbuscular mycorrhizal symbiosis. *Curr. Biol.*, 25, 2189–2195.

Zipfel, C. and Oldroyd, G.E.D. (2017) Plant signalling in symbiosis and immunity. *Nature*, 543, 328–336.

7 Appendix

7.1 Synthetic Oligonucleotides and PCR Reaction Conditions

Oligonucleotide	Sequence (5'-3')[1]	PCR, Target DNA	PCR Reaction conditions
RT-PCR			
FW (bn2221)	GAAGGACTCTTGCGGATTAC	RT-PCR, *Lotus UBI*	95°C-120 s, 30 cycles: (94°C-30 s, 60°C-40 s, 72°C-40 s), 72°C-10 min
RW (bn2222)	GAGGCCACAACAAACGATAC		
FW (bn2508)	GAAGAGCATCCCGTTCTGTT	RT-PCR, *Lotus ACT*	95°C-120 s, 30 cycles: (94°C-30 s, 62°C -40 s, 72°C-40 s), 72°C-10 min
RW (bn2509)	TCTGCTGAAGTGGTAAACGAG		
FW (bn2027)	ACAAGACGCCTCTCCAAAC	RT-PCR, *Lotus FatM*	95°C-120 s, 30 cycles: (94°C-30 s, 58°C -40 s, 72°C- 40 s), 72°C-10 min
RW (bn2028)	GTTCCCAATGGCTACTACTTCC		
FW (bn2456)	GGACTTGTGCCTAGAAGAGCA	RT-PCR, *Lotus FatA*	95°C-120s , 30 cycles: (94°C-30 s, 60°C-40 s, 72°C-40 s), 72°C-10 min
RW (bn2457)	GCGGTTGATCTCAAGTCCTT		
FW (bn2500)	GGGTGGATTCTGGAGAGTGC	RT-PCR, *Lotus FatB*	95°C-120 s, 30 cycles: (94°C-30 s, 60°C -40 s, 72°C- 40 s), 72°C-10 min
RW (bn2501)	TGGAACTCGATTCAAAGCATCA		
FW (bn2502)	ATCTGGGTTGGCTCCAAGG	RT-PCR, *Lotus FatC*	95°C-120 s, 30 cycles: (94°C-30 s, 60°C -40 s, 72°C- 40 s), 72°C-10 min
RW (bn2503)	AGTGTGTGTATTGCAGGTCAG		
FW (bn2454)	CACTCGTCGGAACGTTATCC	RT-PCR, *Lotus PT4*	95°C-120 s, 30 cycles: (94°C-30 s, 58°C -40 s, 72°C-40 s), 72°C-10 min
RW (bn2455)	AGGATGCCTTGAAACCTGCT		
FW (bn1942)	TGTCCAACCGGTTTTAAAGT	RT-PCR, *Rhizophagus α-TUB*	95°C-120 s, 30 cycles: (94°C-30 s, 56°C-40 s, 72°C-30 s), 72°C-10 min
RW (bn1943)	AAAGCACGTTTGGCGTACAT		
Genotyping of LORE1 insertion			
FW (bn 2306)	CGGCTCGAACAAGATTGACTCAGTGGA	Genotyping of insertion in *FatM*-1	95°C-180 s, 5 cycles: (95°C-30 s, 72°C-75 s), 10 cycles: (95°C-30 s, 72°C to 68°C with -0.5°C per cycle, 72°C-45 s), 20 cycles: (95°C-30 s, 68°C-30 s, 72°C-45 s), 72°C-10 min
RW (bn 2307)	AGCCCTTGGCGATGAGGATCAACC		
FW (bn 2300)	CGGCTCGAACAAGATTGACTCAGTGGA	Genotyping of insertion in *FatM*-2	95°C-180 s, 5 cycles: (95°C-30 s, 72°C-75 s), 10 cycles: (95°C-30 s, 72°C to 68°C with -0.5°C per cycle, 72°C-45 s), 20 cycles: (95°C-30 s, 68°C-30 s, 72°C-45 s), 72°C-10 min
RW (bn 2301)	AGCCCTTGGCGATGAGGATCAACC		

Cloning by PCR-introduced RE-overhang

FW (bn2363)	TATGGATCCATGGCTGCTAC TTTCACATT	Expression of *LjFatM* in *E. coli* (pQE-80L)	98°C-30 s, 35 cycles: (98°C-10 s, 60°C-30 s, 72°C- 35 s), 72°C- 120 sec)
RW (bn2418)	ATAAAGCTTCTAGGTGGAA AATGGAATTG		
FW (bn2340)	GCGGGATCCGAGACACTTAG CCACA	Expression of *LjFatM^Δtp* in *E. col* (pQE-80L)	98°C-30 s, 15 cycles: (98°C-10 s, 57°C-20 s, 7°C- 35 s), 98°C- 30 s, 20 cycles: (98°C-10 sec, 72°C -25 sec, 72°C-120 sec)
RW (bn2335)	CGCAAGCTTTAGGTGGAAA ATGGAA		
FW (bn2354)	TATGGATCCGCAGAAACTGT GAAGCGTGA	Expression of *LjFatB^Δtp* in *E. coli* (pQE-80L)	98°C-30 s, 35 cycles: (98°C-10 s, 63°C-30 s, 72°C- 35 s), 72°C- 120 sec)
RW (bn2356)	ATAAAGCTTTTACCTGGCAC TTTCTCCTG		
FW (bn3075)	TATCCCGGGATGGTGGCACA GGCAACATT	Expression of *RiOLE1* in yeast (pDR196)	98°C-30 s, 10 cycles: (98°C-7 s, 58°C-20 s, 72°C- 32 s), 25 cycles: (98°C-7 sec, 68°C -20 sec, 72°C- 32 s)₂₅ₓ, 72°C- 120 sec
RW (bn3083)	ATACTCGAGTTATTTGGTTT TCCTATGTT		
FW (bn3077)	TATCCCGGGATGGCTGCTGC GCCAGTAAA	Expression of *RiOLE1-LIKE* in yeast (pDR196)	98°C-30 s, 10 cycles: (98°C-7 s, 63°C-20 s, 72°C- 32 s), 25 cycles: (98°C-7 sec, 72°C -20 sec, 72°C- 32 s), 72°C- 120 sec
RW (bn3084)	ATACTCGAGCTATTCTTCCT TCTGACTCT		
FW (bn3079)	TATAAGCTTATGGTGGCACA GGCAACATT	Expression of *RiOLE1* in yeast (pYES2)	98°C-30 s, 10 cycles: (98°C-7 s, 58°C-20 s, 72°C- 32 s), 25 cycles: (98°C-7 sec, 67°C -20 sec, 72°C- 32 s), 72°C- 120 sec
RW (bn3080)	ATAGGATCCTTATTTGGTTT TCCTATGTT		
FW (bn3081)	TATAAGCTTATGGCTGCTG CGCCAGTAAA	Expression of *RiOLE1-LIKE* in yeast (pYES2)	98°C-30 s, 10 cycles: (98°C-7 s, 63°C-20 s, 72°C- 32 s), 25 cycles: (98°C-7 sec, 72°C -20 sec, 72°C- 32 s), 72°C- 120 sec
RW (bn3082)	ATAGAGCTCCTATTCTTCCT TCTGACTCT		
FW (bn3214)	TATGGATCCATGGTGGCACA GGCAACATT	Expression of *RiOLE1* in *N. benthamiana* (p917RFPUBQExpr)	98°C-30 s, 10 cycles: (98°C-7 s, 58°C-20 s, 72°C- 32 s), 25 cycles: (98°C-7 sec, 68°C -20 sec, 72°C- 32 s), 72°C- 120 sec
RW (bn3076)	ATAAAGCTTTTATTTGGTTT TCCTATGTT		
FW (bn3212)	TATACGCGTATGGCTGCTGC GCCAGTAAA	Expression of *RiOLE1-LIKE* in *N. benthamiana* (pBin35S)	98°C-30 s, 10 cycles: (98°C-7 s, 63°C-20 s, 72°C- 32 s), 25 cycles: (98°C-7 sec, 72°C -20 sec, 72°C- 32 s), 72°C- 120 sec
RW (bn3213)	ATACTCGAGCTATTCTTCCT TCTGACTCT		

Golden Gate Cloning

FW (bn 3016)	ATGAAGACTTTACGGGTCTC AGCGGGAATGATCATTATG CCAACA	p*FatM* cloning for p*FatM*:*gFatM*	98°C-30 s, 10 cycles: (98°C-7 s, 52°C-20 s, 72°C- 50 s), 25 cycles: (98°C-7 s, 72°C-20 s, 72°C- 50 s),72°C-2 min

RW (bn 3017)	ATGAAGACTTCAGAGGTCTC TCAGATCTTTTTTCTATTTT TTTGG		
FW (bn 3018)	ATGAAGACTTTACGGGTCTC ACACCATGGCTGCTACTTTC ACATT	g*FatM* fragment 1 cloning for p*FatM*:*gFatM*	98°C-30 s, 10 cycles: (98°C-7 s, 55°C-20 s, 72°C- 20 s), 25 cycles: (98°C-7 s, 66°C-20 s, 72°C- 20 s),
RW (bn 3021)	TAGAAGACAAAGATCACTT ATAAATAGGGTATCC		72°C-2 min
FW (bn 3020)	TAGAAGACAAATCTTCAAT GAACGGATCCAGCAT	g*FatM* fragment 2 cloning for p*FatM*:*gFatM*	98°C-30 s, 10 cycles: (98°C-7 s, 54°C-20 s, 72°C- 17 s), 25 cycles: (98°C-7 s, 66°C-20 s, 72°C- 17 s),
RW (bn 3023)	TAGAAGACAAGACTTTCTCA TGAAGTAGTTAAAT		72°C-2 min
FW (bn 3022)	TAGAAGACAAAGTCTCATG GGCTTCAGTGTTTTG	g*FatM* fragment 3 cloning for p*FatM*:*gFatM*	98°C-30 s, 10 cycles: (98°C-7 s, 62°C-20 s, 72°C- 50 s), 25 cycles: (98°C-7 s, 72°C-20 s, 72°C- 50 s),
RW (bn 3019)	ATGAAGACTTCAGAGGTCTC TCCTTCTTCCACACTTATTG CTAGG		72°C-2 min

7.2 Glycostocks

Construct	Insert with Restriction Sites or PCR primer used	Plasmid	Organism/Strain	Glycostock Number
pJ-*LjFatA^Δtp*	*LjFatA* cDNA, PCR bn2403-bn2405	pJET1.2	*E.coli*/ElectroSHOX	bn 1139
pJ-*LjFatB^Δtp*	*LjFatB* cDNA, PCR bn2354-bn2356	pJET1.2	*E.coli*/ElectroSHOX	bn 1140
pJ-*LjFatM^Δtp*	*LjFatM* cDNA, PCR bn2340-bn2335	pJET1.2	*E.coli*/ElectroSHOX	bn 849
pJ-*LjFatM^TE*	*LjFatM* cDNA, PCR bn2342-bn2335	pJET1.2	*E.coli*/ElectroSHOX	bn 850
pJ-*LjFatM*	*LjFatM* cDNA, PCR bn2334-bn2418	pJET1.2	*E.coli*/ElectroSHOX	bn 1016
pQE-*LjFatA^Δtp*	*LjFatA* cDNA, *BamH*I-*Hind*III (989 bp)	pQE-80L	*E.coli*/ElectroSHOX	bn 1160, bn 1161
pQE-*LjFatB^Δtp*	*LjFatB* cDNA, *BamH*I-*Hind*III (1101 bp)	pQE-80L	*E.coli*/ElectroSHOX	bn 1162, bn 1163
pQE-*LjFatM^Δtp*	*LjFatM* cDNA, *BamH*I-*Hind*III (1070 bp)	pQE-80L	*E.coli*/ElectroSHOX	bn 881
pJ-*RiOLE1*	*RiOLE1* cDNA, PCR bn3214-bn3076	pJET1.2	*E.coli*/ElectroSHOX	bn 1244
pJ-*RiOLE1-LIKE*	*RiOLE1-LIKE* cDNA, PCR bn3211-bn3213	pJET1.2	*E.coli*/ElectroSHOX	bn 1243
pDR196-*RiOLE1*	*RiOLE1* cDNA, *Sma*I-*Xho*I (1226 bp)	pDR196	*E.coli*/ElectroSHOX	bn 1215
pDR196-*RiOLE1-LIKE*	*RiOLE1-LIKE* cDNA, *Sma*I-*Xho*I (1262 bp)	pDR196	*E.coli*/ElectroSHOX	bn 1216
pYES2-*RiOLE1-LIKE*	*RiOLE1-LIKE* cDNA, *Hind*III-*Sac*I (1262 bp)	pYES2	*E.coli*/ElectroSHOX	bn 1217
pJ-*RiOLE1*	*RiOLE1* cDNA, PCR bn3214-bn3076	pJET1.2	*E.coli*/ElectroSHOX	bn 1249
p917UBQ3-*RiOLE1*	*RiOLE1* cDNA, *BamH*I-*Hind*III (1226 bp)	p917RFP UBQ Expr	*E.coli*/ElectroSHOX	bn 1250
pJ-*RiOLE1-LIKE*	*RiOLE1-LIKE* cDNA, PCR bn3212-bn3213	pJET1.2	*E.coli*/ElectroSHOX	bn 1243

pBin35S-*RiOLE1-LIKE*	*RiOLE1*cDNA, *Mlu*I-*Xho*I (1262 bp)	pBin35S	*E.coli*/ ElectroSHOX	bn 1246
p917UBQ3-*RiOLE1*	*RiOLE1*cDNA, *BamH*I-*Hin*dIII (1226 bp)	p917RFP UBQ Expr	*A. tumefaciens*/ GV3101 (pMP90)	bn 1265
pDR196-EV	-	pDR196	*S. cerevisae*/ BY4741 (WT)	bn 1231
pDR196-*RiOLE1*	*RiOLE1*cDNA, *Sma*I-*Xho*I (1226 bp)	pDR196	*S. cerevisae*/ BY4741 (WT)	bn 1232
pDR196-*RiOLE1-LIKE*	*RiOLE1-LIKE* cDNA, *Sma*I-*Xho*I (1262 bp)	pDR196	*S. cerevisae*/ BY4741 (WT)	bn 1233
pDR196-EV	-	pDR196	*S. cerevisae*/ *ole1*-Δ	bn 1234
pDR196-*RiOLE1*	*RiOLE1*cDNA, *Sma*I-*Xho*I (1226 bp)	pDR196	*S. cerevisae*/ *ole1*-Δ	bn 1235
pDR196-*RiOLE1-LIKE*	*RiOLE1-LIKE* cDNA, *Sma*I-*Xho*I (1262 bp)	pDR196	*S. cerevisae*/ *ole1*-Δ	bn 1236
LI-pUC57(BB03)-p*FatM*	*LjFatM* promoter (1.8 kb) without mutagenesis, *Bpi*I (1824 bp)	L1pUC57+BpiI (Gent)	*E.coli*/ ElectroSHOX	bn 1198
LI-pUC57(BB03)-g*FatM*	*LjFatM* gene with mutagenesis, *Bpi*I (3200 bp)	L1pUC57+BpiI (Gent)	*E.coli*/ ElectroSHOX	bn 1199
LI-pUC57(BB03)-g*FatM*	*LjFatM* gene with mutagenesis, *Bpi*I (3200 bp)	L1pUC57+BpiI (Gent)	*E.coli*/ TOP10	bn 1200

7.3 Transcriptomics of *L. japonicus Fat* genes
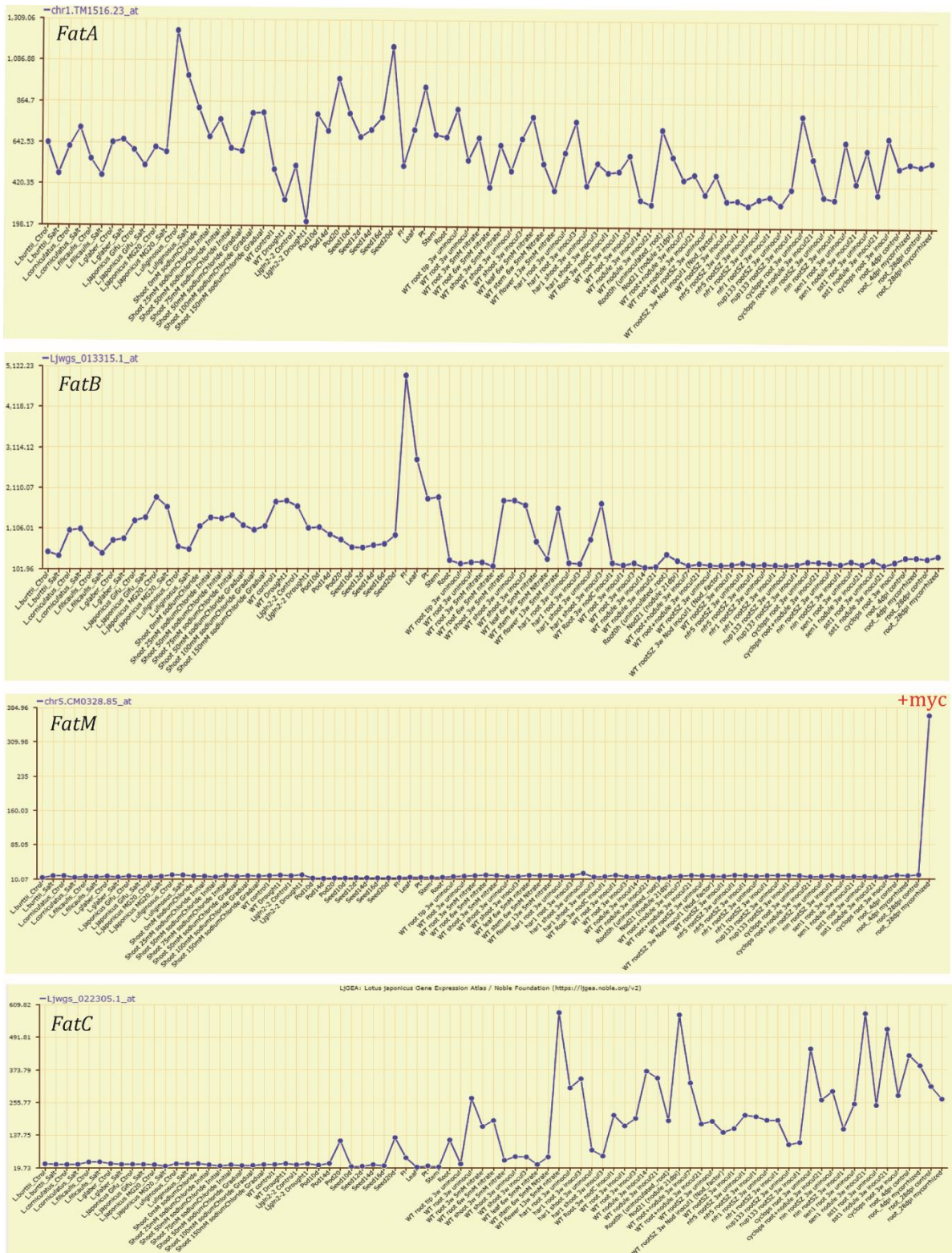
Figure 29: Gene Expression of *L. japonicus Fat* Genes during differential Treatments.
The *L. japonicus* Gene Expression Atlas (LjGEA; https://ljgea.noble.org/v2/) was used for a BLAST search using the coding sequence of *FatM* (chr5.CM0328.70.r2.d) as query. Gene expression levels of *FatM* and homologous genes *LjFatA*, *LjFatB* and *LJFatC* is depicted on the y-axis and different treatment conditions on thex-axis. *FatM* is extensively and exclusively expressed in mycorrhiza-inoculated roots (+myc), where the other *Fat* genes show a differential expression pattern and are also expressed in e. g. developing seeds, flowers, shoots and leaves.

7.4 Cloning of *RiOLE1* and *RiOLE1-like* into the Yeast Expression Vector pDR196

The *RiOLE1* (Gloin1|344273) cDNA (1226 bp) and *RiOLE1-like* (Gloin1|340272) cDNA (1262 bp) cDNAs were obtained by RT-PCR using wild type *R. irregularis* ERM RNA with primers bn3075 + bn3083 and bn3077 + bn3084, respectively, using Q5 polymerase with proofreading ability to incorporate 5′ overhangs suitable for restriction digestion. The PCR products were isolated, ligated into the linearized vector pJET1.2 and transformed into *E. coli* electroSHOX. Recombinant clones were selected with carbenicillin (100 μg mL $^{-1}$) and plasmid DNA was purified. The constructs were digested with restriction enzymes or PCR was performed to confirm the successful cloning of *RiOLE1* and *RiOLE1-like* into pJET 1.2. The appropariate fragments were then cloned into pDR196 expression vector (Table 15). To confirm correct sequences, plasmids were sequenced at Eurofins Genomics, Ebersberg (D). The sequences obtained were aligned with the *RiOLE1* sequence (Gloin1|344273) and *RiOLE1-LIKE* (Gloin1|340272) from EnsemblFungi database.

Table 15: Cloning of *RiOLE1* and *RiOLE1-LIKE* for Expression in Yeast.

Construct	Restriction Endonucleases	Fragments obtained for Orientation A	Fragments obtained for Orientation B	Primer used for Sequencing or Colony PCR
pJ-*RiOLE1*	*Sma*I,*xho*I	25, **1231**[a], 2963	23, 1235, 2961	bn2444 + bn2445
pJ-*RiOLE1-LIKE*	*Sma*I,*xho*I	25, **1267**[a], 2963	23, 1271, 2961	bn2444 + bn2445
pDR196 (EV[b])	*Sma*I,*xho*I	**6363**[a], 43	-	-
pDR196-*RiOLE1*	*Bam*HI, *Hin*dIII	1292, 5519, 783	-	bn3075 + bn3083
pDR196-*RiOLE1-LIKE*	*Bam*HI, *Hin*dIII	354, 494, 480, 5519, 783	-	bn3077 + bn3084

[a]Underlined, bold fragments were eluted from the gel and used in subsequent ligation reactions.
[b]EV= Empty vector.
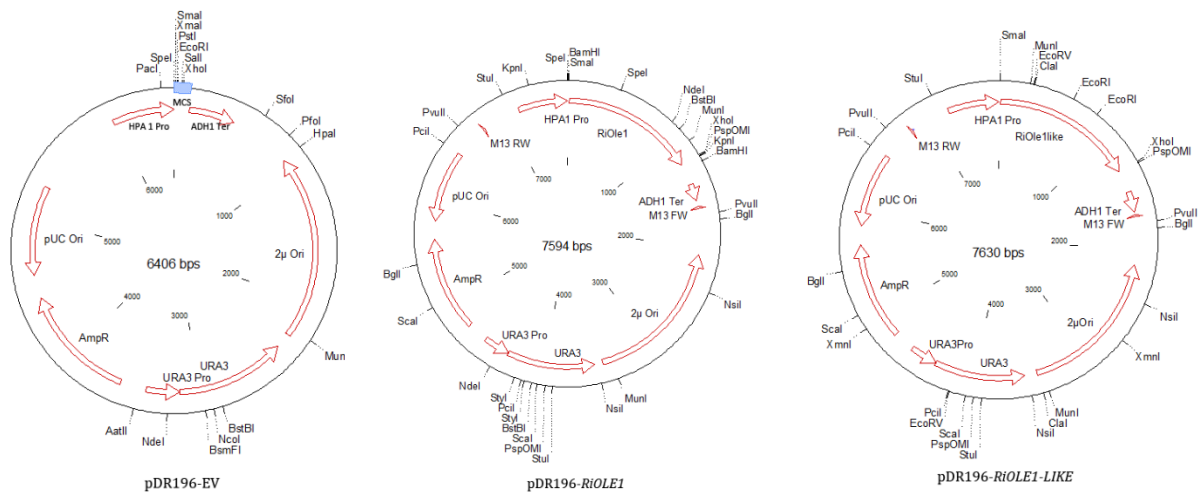
Figure 30: Vector for constitutive Expression of *RiOLE1* and *RiOLE1-LIKE* in *S. cerevisiae*.
RiOLE11 and *RiOLE1-LIKE* cDNAs were cloned into the pDR196. HPA Pro, Plasma membrane H^+-ATPase promoter; MCS, multiple cloning site; ADH1 Ter, alcohol dehydrogenase 1 terminator; 2μ Ori= yeast 2μ origin of replication, URA3= yeast orotidine-5-phosphate decarboxylase, URA3 Pro= yeast orotidine-5-phosphate decarboxylase promoter, AmpR= Ampicillin/carbenicillin resistance gene ß-lactamase (bla), pUC Ori= pUC bacterial origin of replication.

7.5 **Cloning of *RiOLE1* and *RiOLE1-LIKE* into Expression Vectors for *N. benthamiana***

RiOLE1 (Gloin1|344273) cDNA (1226 bp) and *RiOLE1-like* (Gloin1|340272) cDNA (1262 bp) were obtained by RT-PCR using wild type *R. irregularis* ERM cDNA with primers bn3214 + bn3076 and bn3212 + bn3213, respectively, using Q5 polymerase with proofreading ability to incorporate 5´ overhangs suitable for restriction digestion. The PCR products were isolated, ligated into the linearized vector pJET1.2 and transformed into *E. coli* electroSHOX. Recombinant clones were selected with carbenicillin (100 µg mL^{-1}) and plasmid DNA was purified. The constructs were digested with restriction enzymes or PCR was performed to confirm the successful cloning of *RiOLE1* and *RiOLE1-like* into pJET 1.2 (Table 16). The appropriate fragments were then cloned into p917RFPUBQExpr (*RiOLE1*) or pBin35S-AtWSD1 (*RiOLE-LIKE*) expression vector (Table 16). p917UBQ3-*RiOLE1* was selected with streptomycin (300 µg mL^{-1}) and spectinomycin (100 µg mL^{-1}) and pBin35S-*RiOLE1-LIKE* with Kanamycin (50 µg mL^{-1}). To confirm that the sequences were correct, plasmids were sequenced at Eurofins Genomics, Ebersberg (D). The sequences obtained were aligned with the *RiOLE1* sequence (Gloin1|344273) and *RiOLE1-LIKE* (Gloin1|340272) from EnsemblFungi database.

Table 16: Cloning of *RiOLE1* and *RiOLE1-LIKE* for Expression in *N. benthamiana*.

Construct	Restriction Endonucleases	Fragments obtained for Orientation A	Fragments obtained for Orientation B	Primer used for Sequencing and Colony PCR
pJ-*RiOLE1*	*Hin*dIII	261, 3958	1494, 2725	bn2444 + bn2445
	*Bam*HI, *Hin*dIII	261, **1233**[a], 2725	261, **1233**[a], 2725	-
pJ-*RiOLE1-LIKE*	*Xba*I, *Kpn*I	456, 3799	833, 3422	bn2444 + bn2445
	*Xba*I, *Eco*RV	1022, 3233	271, 3984	-
	*Mlu*I,*xho*I	23, **1269**[a], 2963	23, **1269**[a], 2963	-
p917RFPUBQExpr (EV[b])	*Bam*HI, *Hin*dIII	24, **13522** [a]	-	-
p917UBQ3-*RiOLE1*	*Bam*HI, *Hin*dIII,*xho*I	5275, 1233, 8247	-	bn3214+ bn3076
	*Bam*HI, *Hin*dIII	1233, 13522		-
	*Xba*I	2495, 738, 2781, 8741		
pBin35S-*AtWSD1*[c]	*Xho*I, *Mlu*I	1452, **10334**[a]	-	-
pBin35S-*RiOLE1-LIKE*	*Xho*I, *Hin*dIII	11145, 458	-	bn3212 + bn3213

[a]Underlined, bold fragments were eluted from the gel and used in subsequent ligation reactions; *RiOLE1*+p917RFPUBQExpr and *RiOLE1-LIKE* + pBin35S.
[b]EV= Empty vector.
[c]*AtWSD1* (glycostock bn1173) was removed from pBin35S-*AtWSD1* and the pBin35S backbone used for expression of *RiOLE1-LIKE*.
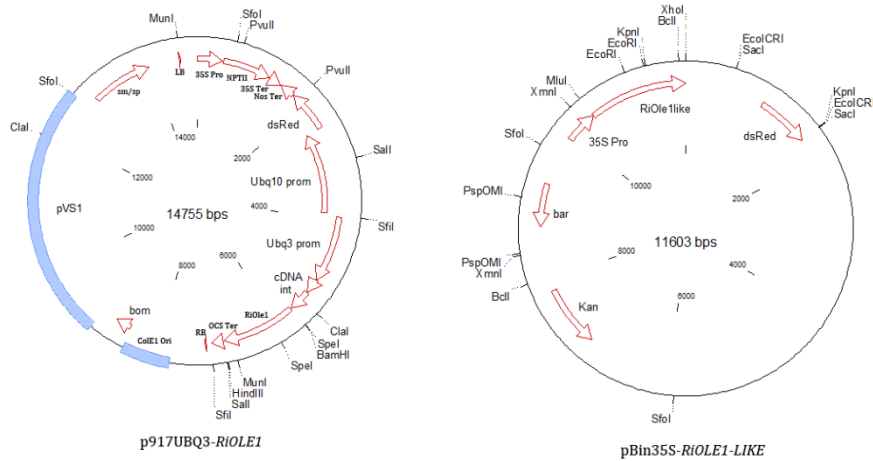
Figure 31: Vectors for transient Expression of *RiOLE1* and *RiOLE1-LIKE* in *N. benthamiana*.
RiOLE1 and *RiOLE1-LIKE* cDNAs were cloned into expression vectors p917RFPUBQExpr and pBIN35S. 35S. Pro, 35S Promoter from Cauliflower Mosaic Virus; NPTII, Neomycin Phosphotransferase for Kanamycin resistance; 35 S Ter, 35S Terminator; Nos Ter, Nopaline Synthase (Nos) Terminator; dsRed, *Discosoma* (ds) Red Fluorescence Protein; Ubq10 prom, *UBIQUITIN10* Promoter; Ubq3 prom, *UBIQUITIN3* Promoter; cDNA int, *UBQ3* Intron for enhanced expression; RiOle1, *R. irregularis OLE1* cDNA; OCS Ter, Octopine Synthase Terminator; RB, Right border; ColE1 Ori, Colicin E1 Origin of Replication for replication of Plasmid in *E. coli*; pVS1, backbone from predecessor plasmid; sm/sp, Spectinomycin/Streptomycin Resistance genes; LB, Left border.

7.6 Cloning of *LjFatA*, *LjFatB* and L*jFatM* into pQE80L for Expression in *E. coli*

cDNA from *L. japonicus* roots colonized with *R. irregularis* was used to amplify *Fat* genes without the predeceding N-terminal transit peptides generating the fragments *LjFatA*$^{\Delta tp}$ (972 bp) with primers bn2403 + bn2405, *LjFatB*$^{\Delta tp}$ (1120 bp) with bn2354 + bn2356 and *LjFatM*$^{\Delta tp}$ (1089 bp) with bn2340 + bn2335. Additionally, for *LjFatM*, the full coding sequence (*LjFatM*) was amplified with bn2363 + bn2418 (1214 bp) and the thioesterase domain (*LjFatM*^{TE}) with bn 2432 + bn 2335 (942 bp). All RT-PCRs were done with Q5 polymerase (NEB) with proofreading ability. The PCR products were seperated by DNA gel electrophoresis. The PCR products were isolated, ligated into the linearized vector pJET1.2 and transformed into *E. coli* electroSHOX. Recombinant clones were selected with carbenicillin (100 µg mL^{-1}) and plasmid DNA was purified. The constructs were digested with restriction enzymes or PCR was performed to confirm the successful cloning of *LjFat* sequences into pJET 1.2 (Table 17). The appropariate fragments were then cloned into pQE80-L expression vector. To confirm correct sequences, plasmids were sequenced at Eurofins Genomics, Ebersberg (D).

Table 17: Cloning of *L. japonicus Fat* coding sequences for expression in *E. coli*.

Construct	Restriction Endonucleases	Fragments obtained for Orientation A	Fragments obtained for Orientation B	Primer used for Sequencing and Colony PCR
pJ-*FatA*$^{\Delta tp}$	*Bam*HI, *Hin*dIII	261, 2725, **960**[a]	261, 2725, **960**[a]	bn2444 + bn2445
pJ-*FatB*$^{\Delta tp}$	*Bam*HI, *Hin*dIII	**1109**[a], 261, 2725	**1109**[a], 261, 2725	bn2444 + bn2445
pJ-*FatM*$^{\Delta tp}$	*Bam*HI, *Hin*dIII	**1077**[a], 261, 2725	**1077**[a], 261, 2725	bn2444 + bn2445
pJ-*FatM*	*Bam*HI, *Hin*dIII	**1202**[a], 261, 2725	**1202**[a], 261, 2725	bn2444 + bn2445
pJ-*FatM*^{TE}	*Bam*HI, *Hin*dIII	**930**[a], 261, 2725	**930**[a], 261, 2725	bn2444 + bn2445
pQE-80L (EV[b])	*Bam*HI, *Hin*dIII	**4709**[a], 42	-	-
pQE-*LjFatA*$^{\Delta tp}$	-	-	-	bn2638 + bn2639
pQE-*LjFatB*$^{\Delta tp}$	-	-	-	bn2638 + bn2639
pQE-*LjFatM*$^{\Delta tp}$	-	-	-	bn2638 + bn2639

[a]Underlined, bold fragments were eluted from the gel and used in subsequent ligation reactions; *RiOLE1*+p917RFPUBQExpr and *RiOLE1-LIKE* + pBin35S.
[b]EV= Empty vector.
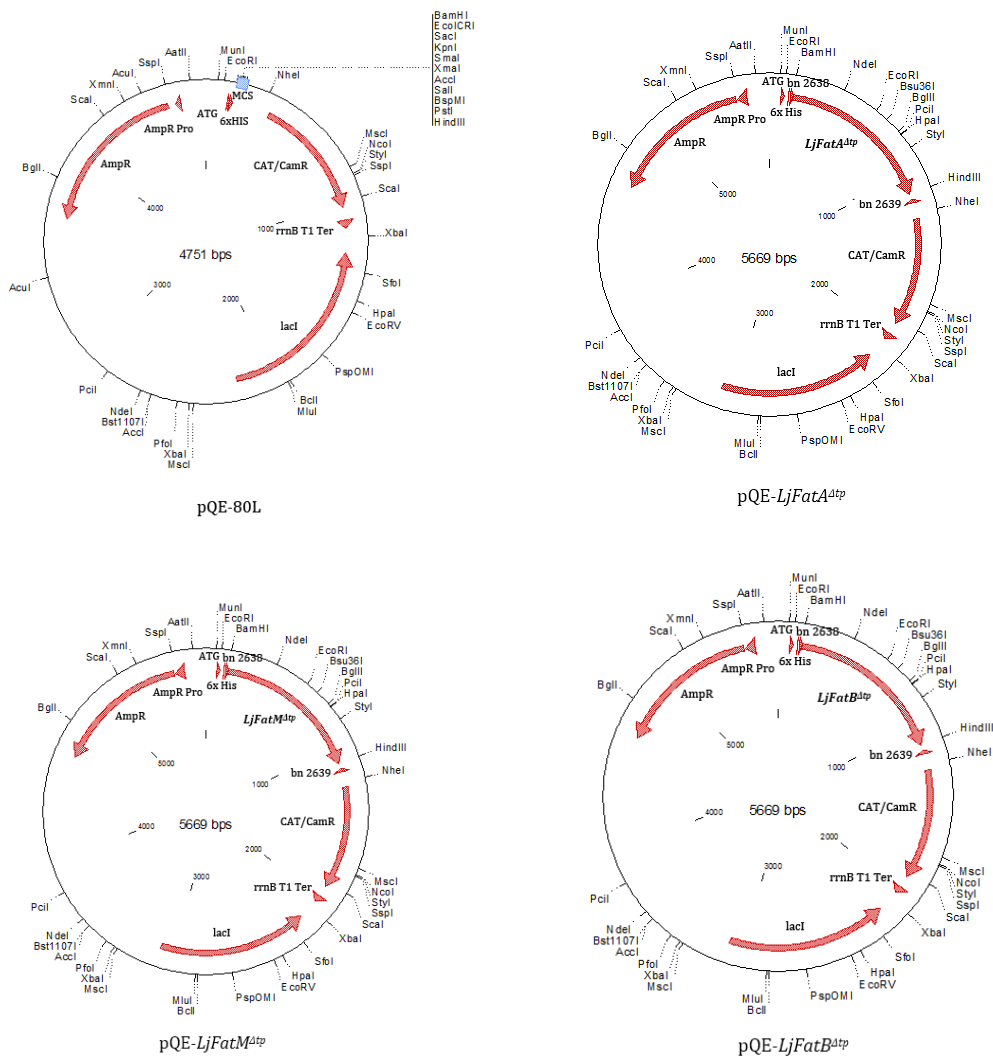
Figure 32: Expression Vectors for heterologous Expression of *L. japonicus* Acyl-ACP Thioesterases in *E. coli*.

LjFat cDNAs were cloned into pQE-80L. ATG, Start Codon for in-Frame cloning of Gene of interest (GOI); 6x His, 6x His nucleotide triplet for N-terminal addition of His-tag; bn 2638, Forward sequencing primer; *LjFatA/B/M^Δtp*, Coding sequences of *L. japonicus* acyl-ACP thioesterases without the N-terminal transit peptide; CAT/CamR, Chloramphenicol acetyltransferase/chloramphenicol resistance; rrnB1 T1 Ter, *E. coli* ribosomal RNA gene T1 terminator; lacI, Lac operon repressor gene; AmpR, Ampicilline resistance gene; AmpR pro, Ampicillin resistance gene promoter.

7.7 Golden Gate Cloning of the *LjFatM* Gene and Promoter and Genetic Complementation of *fatm*-1

Level II and Level III cloning was performed by Andreas Keymer at the Ludwigs Maximilian University, München, in the group of Caroline Gutjahr in 2018. As template for the *FatM* gene and promoter, DNA from *L. japonicus* roots colonized with *R. irregularis* was used.

In golden gate cloning, the type IIS restriction enzymes *Bbs*I (*Bpi*I) and *Bsa*I that cut outside the recognition sequence are used. Level I sublconing constructs are assembled from level 0 plasmids using *Bbs*I, Level II constructs are generated with *Bsa*I and for assembly of Level III plant expression constructs, *Bbs*I is used again.

Level 0 Subcloning into pUC57 (Amp)

The genomic *FatM* sequence (*gFatM*) contains type IIS restriction enzyme recognition sites, therefore mutagenesis PCR is performed to disrupt these. The g*FatM* gene contains one *Bbs*I(*Bpi*I) and one *Bsa*I recognition site. To distrup the recognition sites, single nucleotides were exchanged via mutagenesis PCR by introducing a mismatch at the 5´ overhang of PCR primer. With the same primer, a 5´ *Bpi*I-recognition site was added to ensure the correct orientation of the gene sequence after the three fragments from mutagenesis PCR are assembled again. The three fragments were produced using primer bn 3018 + bn 3021 (643 bp), bn 3020 + bn 3023 (388 bp), and bn 3022+ bn3019 (2244 bp).

The 1.8 kb sequence upstream of the g*FatM* start codon was designated as the putative promoter region (p*FatM*) and amplified with primers bn 3016 + bn 3017 (1850 bp) without mutagenesis as it did not contain type IIS recognition sites.

The correct PCR products were excised from the agarose gel, purified, used for blunt-end ligation into linearized subcloning vector pJET1.2 and transformed into *E. coli* ElectroSHOX. Selection of recombinant clones was done on LB agar containing carbenicilin (100 µg mL $^{-1}$) and plasmid DNA was purified from ON cultures.

To verify the correct insertion into the subcloning vector, the constructs were digested with the following enzymes or PCR was performed with the following primers to confirm the successful cloning of pJ-L0g*FatM*1, pJ-L0g*FatM*2, pJ-L0g*FatM*3 and pJ-L0p*FatM* into pJET 1.2.

Construct	Restriction Endonucleases	Fragments obtained for Orientation A	Fragments obtained for Orientation B	Primer used for Sequencing and Colony PCR
pJ-L0g*FatM*1	*Bbs*I (*Bpi*I)	330, 619, 2668	330, 619, 2668	bn2444 + bn2445
pJ-L0g*FatM*2	*Bbs*I (*Bpi*I)	330, 364, 2668	330, 364, 2668	bn2444 + bn2445
pJ-L0g*FatM*3	*Bbs*I (*Bpi*I)	330, 2220, 2668	330, 2220, 2668	bn2444 + bn2445
pJ-L0p*FatM*	*Bbs*I (*Bpi*I)	330, 1820, 2668	330, 1820, 2668	bn2444 + bn2445

Level I Subcloning into LI-pUC57+*Bpi*I (BB03)

To obtain the level I vectors, the level 0 vectors were digested with *Bbs*I (*Bpi*I) and ligated into *Bbs*I (*Bpi*I)-digested level I vector LI-pUC57+*Bpi*I. This was done in a single cut-ligation reaction containing 62.5 fmol DNA per fragment.

Cut-ligation LI-g*FatM*
1 µL LI-pUC57+*Bpi*I (BB03) (100 ng *µL $^{-1}$)
0.7 µL pJ-L0g*FatM*1 (208 ng *µL $^{-1}$)
1.9 µL pJ-L0g*FatM*2 (70 ng *µL $^{-1}$)
1.22 µL pJ-L0g*FatM*3 (72.8 ng *µL $^{-1}$)

Cut-ligation LI-p*FatM*
1 µL LI-pUC57+*Bpi*I (BB03) (100 ng *µL $^{-1}$)
1.45 µL pJ-L0p*FatM* (51 ng *µL $^{-1}$)
0.75 µL T4 DNA Ligase M0202S (400.000 U.mL^{-1})

0.75 µL T4 DNA Ligase M0202S (400.000 U.mL^{-1})	1.5 µLx T4 DNA Ligase buffer
1.5 µLx T4 DNA Ligase buffer	0.5 µL *Bbs*I-HF (20.000 U.mL^{-1})
0.5 µL *Bbs*I-HF (20.000 U.mL^{-1})	Add nuclease-free ddH$_2$O to a final volume of 15 µL.
Add nuclease-free ddH$_2$O to a final volume of 15 µL.	

The reactions were mixed, spinned down and incubated in a PCR cycler with the following settings: (37°C-2 min, 25°C-5 min)$_{35x}$—50°C-5 min, 80°C–5min. The cut-ligation mixture was desalted and transformed into *E. coli* ElectroSHOX and and *E. coli* TOP10 (Thermo Fisher Scientific) selection of recombinant clones was done on LB agar containg gentamycin (20 µg mL^{-1}) and plasmid DNA was purified from ON cultures.

To verify the correct insertion into the Level I subcloning vector, the constructs were digested with the following enzymes or PCR was performed with the following primers to confirm the successful cloning of LI-pUC57(BB03)-g*FatM* and LI-pUC57(BB03)-p*FatM*.

Construct	Restriction Endonucleases	Fragments obtained (bp)	Primer used for Colony PCR and Fragments obtained (bp)	Primer used for Sequencing
LI-pUC57(BB03)-g*FatM*	*Bsa*I	3181, 2483	bn 2027 + bn 2632 (1109 bp)	bn2301/bn2303 + bn2632
LI-pUC57(BB03)-p*FatM*	*Bsa*I	1804, 2483	-	bn2310/bn2311 + bn2632

Level II and III Cloning

In Level II, *Bsa*I sites flanking the desired inserts in the Level I constructs were used to assemble these in the correct orientation (promoter fragment in front of the gene fragment and Nos terminator after gene sequence) in the Level II plasmid. In Level III cloning, *Bpi*I was used to transfer the assembled fragments (p*FatM*:g*FatM* and p*FatM*:EV) into an expression vector suitable for plant transformation containing a resistance gene (kanamycin) and a *mCherry* fluorescence marker (p35s:*mCherry*).

Overview of Golden Gate Cloning

In the table below, all constructs used for the assembly of *L. japonicus FatM* promoter upstream of the *FatM* gene sequence for complementation of the *FatM* mutation, are summarized (Brands *et al.*, 2018).

Purpose	Construct	Description
Golden Gate level 0 and I (L0, LI) elements		
L0 subcloning of p*FatM* without mutagenesis	L0 pJET1.2 p*LjFatM*	PCR amplification from genomic DNA of *L. japonicus* Gifu wild type. *FatM* 1.8 kb promoter fragment (p*FatM*) with bn 3016 + bn 3017 (1850 bp) and assembly by blunt-end ligation into L0 pJET1.2.
L0 subcloning of g*FatM* with mutagenesis	L0 pJET1.2 g*FatM*-Fragment1	Assembled by blunt-end ligation of g*FatM* PCR fragment 1, 2 and 3 into L0 pJET1.2 plasmid

	L0 pJET1.2 *gFatM*-Fragment2 L0 pJET1.2 *gFatM*-Fragment3	amplified from genomic DNA of *L. japonicus* Gifu wild type. Primers: Fragment 1: bn 3018 + bn 3021 (643 bp) Fragment 2: bn 3020 + bn2023 (388 bp) Fragment 3: bn 3022 + bn2019 (2244 bp)
LI p*FatM* module generation	LI p*LjFatM*	Assembled 1 fragment from L0 pJET1.2 p*LjFatM* by *BpiI* cut-ligation into LI-pUC57+BpiI plasmid (BB03)
LI *gFatM* module generation	LI *gFatM*	Assembled 3 fragments from L0 pJET1.2 *gFatM* 1,2,3 by BpiI cut ligation into LI-pUC57+BpiI plasmid (BB03)
Golden Gate level II (LII) plasmids		
LII construct generation	LIIc 1_2 p*FatM:gFatM* (pAK44)	Assembled by BsaI cut ligation from: LI A-B p*LjFatM* + LI B-C dy (BB06) + LI *gFatM* + LI D-E dy (BB08) + LI E-F NosT (G006) + LI F-G dy (BB09) + LIIc F 1_2 (BB30)
LII construct generation	LIIc 1_2 p*FatM:EV* (pAK45)	Assembled by BsaI cut ligation from: LI A-B p*LjFatM* + LI B-C dy (BB06) + LI C-D dy (BB07) + LI D-E dy (BB08) + LI E-F NosT (G006) + LI F-G dy (BB09) + LIIc F 1_2 (BB30)
	LIIc 3_4 p35s:*mCherry* (pAK18)	Assembled by BsaI cut ligation from: LI A-B p*35s* (G005) + LI B-C dy (BB06) + LI C-D *mCherry* (G057) + LI D-E dy (BB08) + LI E-F 35sT (G059) + LI F-G dy (BB09) + LIIc R 3_4 (BB34)
Golden Gate level III (LIII) plasmids for plant transformation		
Genetic complementation of *FatM-1*	LIIIβ F A-B p*FatM:gFatM* (pAK46)	Assembled by BpiI cut ligation from: LIIc 1_2 p*FatM:gFatM* + LII 2-3 ins (BB43) + LIIc R 3-4 p*35s:mCherry* + LII 4-6 dy (BB41) + LIIIβ F A-B (BB53)
Genetic complementation of *FatM-1*	LIIIβ F A-B p*FatM:EV* (pAK47)	Assembled by BpiI cut ligation from: LIIc 1_2 p*FatM:EV* + LII 2-3 ins (BB43) + LIIc R 3-4 p*35s:mCherry* + LII 4-6 dy (BB41) + LIIIβ F A-B (BB53)

7.8 Mass-over-charge Values for the Quantification of Lipids

Lipids were quantified via Q-TOF MS/MS Nanoflow Direct Infusion with Chip Cube Technology (Wewer *et al.*, 2014).

Table 18: Calculated masses of ion adducts (targeted list) for Phospholipids, Galactolipids, Sufolipid and Neutral Lipids

Molecular Species	Calculated Molecular Mass of ion adduct (m/z)[a]	Molecular Species	Calculated Molecular Mass of ion adduct (m/z)[a]
34:6 MGDG	764.5307	28:0 PS (IS)[b]	680.4503
34:5 MGDG	766.5463	34:4 PS	756.4810
34:4 MGDG	768.5620	34:3 PS	758.4967
34:3 MGDG	770.5776	34:2 PS	760.5123
34:2 MGDG	772.5933	34:1 PS	762.5280
34:1 MGDG	774.6089	36:6 PS	780.4810
34:0 MGDG (IS)[b]	776.6246	36:5 PS	782.4967
36:6 MGDG	792.5620	36:4 PS	784.5123
36:5 MGDG	794.5776	36:3 PS	786.5280
36:4 MGDG	796.5933	36:2 PS	788.5436
36:3 MGDG	798.6089	36:1 PS	790.5593
36:2 MGDG	800.6246	38:6 PS	808.5123
36:1 MGDG	802.6402	38:5 PS	810.5280
36:0 MGDG (IS)[b]	804.6559	38:4 PS	812.5436
38:6 MGDG	820.5933	38:3 PS	814.5593
38:5 MGDG	822.6089	38:2 PS	816.5749
38:4 MGDG	824.6246	38:1 PS	818.5906
38:3 MGDG	826.6402	40:4 PS	840.5749
34:6 DGDG	926.5835	40:3 PS	842.5906
34:5 DGDG	928.5992	40:2 PS	844.6062
34:4 DGDG	930.6148	40:1 PS	846.6219
34:3 DGDG	932.6305	40:0 PS (IS)[b]	848.6375
34:2 DGDG	934.6461	42:4 PS	868.6062
34:1 DGDG	936.6618	42:3 PS	870.6219
34:0 DGDG (IS)[b]	938.6775	42:2 PS	872.6375
36:6 DGDG	954.6148	42:1 PS	874.6532
36:5 DGDG	956.6305	34:4 PI	848.5283
36:4 DGDG	958.6461	34:3 PI 3	850.5440
36:3 DGDG	960.6618	34:2 PI 3	852.5597
36:2 DGDG	962.6774	34:1 PI 3	854.5753
36:1 DGDG	964.6931	34:0 PI 3 (IS)[b]	856.5910
36:0 DGDG (IS)[b]	966.7087	36:6 PI 3	872.5283
38:6 DGDG	982.6461	36:5 PI 3	874.5440
38:5 DGDG	984.6618	36:4 PI 3	876.5596
38:4 DGDG	986.6774	36:3 PI 3	878.5753
38:3 DGDG	988.6931	36:2 PI 3	880.5909
34:6 SGDG	828.4926	36:1 PI 3	882.6066
34:5 SGDG	830.5082	36:0 PI (IS)[b]	884.6223
34:4 SGDG	832.5239	28:0 PE (IS)[b]	636.4604
34:3 SGDG	834.5395	34:4 PE	712.4912
34:2 SGDG	836.5552	34:3 PE	714.5069
34:1 SGDG	838.5708	34:2 PE	716.5225
34:0 SQDG (IS)[b]	840.5865	34:1 PE	718.5382
36:6 SGDG	856.5239	36:6 PE	736.4912

**Table 18
(continued)**

36:5 SGDG	858.5395	36:5 PE	738.5069
36:4 SGDG	860.5552	36:4 PE	740.5225
36:3 SGDG	862.5708	36:3 PE	742.5382
36:2 SGDG	864.5865	36:2 PE	744.5538
36:1 SGDG	866.6022	36:1 PE	746.5695
36:0 SQDG (IS)[b]	868.6178	38:6 PE	764.5225
28:0 PA (IS)[b]	610.4448	38:5 PE	766.5382
34:6 PA	682.4442	38:4 PE	768.5538
34:5 PA	684.4462	38:3 PE	770.5695
34:4 PA	686.4755	38:2 PE	772.5851
34:3 PA	688.4912	40:3 PE	798.6008
34:2 PA	690.5068	40:2 PE	800.6164
34:1 PA	692.5225	40:0 PE (IS)[b]	804.6477
36:6 PA	710.4755	42:4 PE	824.6169
36:5 PA	712.4912	42:3 PE	826.6321
36:4 PA	714.5068	42:2 PE	828.6477
36:3 PA	716.5225	28:0 PG (IS)[b]	684.4816
36:2 PA	718.5381	32:1 PG	738.5279
40:0 PA (IS)[b]	778.6326	32:0 PG	740.5436
28:0 PS (IS)[b]	680.4503	34:4 PG	760.5123
34:4 PS	756.4810	34:3 PG	762.5279
34:3 PS	758.4967	34:2 PG	764.5436
34:2 PS	760.5123	34:1 PG	766.5592
34:1 PS	762.5280	34:0 PG	768.5749
36:6 PS	780.4810	40:0 PG (IS)[b]	852.6694
36:5 PS	782.4967	28:0 PC (IS)[b]	678.5074
36:4 PS	784.5123	32:0 PC	734.5695
36:3 PS	786.5280	34:4 PC	754.5382
36:2 PS	788.5436	34:3 PC	756.5538
36:1 PS	790.5593	34:2 PC	758.5695
38:6 PS	808.5123	34:1 PC	760.5851
38:5 PS	810.5280	36:6 PC	778.5382
38:4 PS	812.5436	36:5 PC	780.5538
38:3 PS	814.5593	36:4 PC	782.5695
38:2 PS	816.5749	36:3 PC	784.5851
38:1 PS	818.5906	36:2 PC	786.6008
40:4 PS	840.5749	36:1 PC	788.6164
40:3 PS	842.5906	38:6 PC	806.5695
40:2 PS	844.6062	38:5 PC	808.5851
40:1 PS	846.6219	38:4 PC	810.6008
40:0 PS (IS)[b]	848.6375	38:3 PC	812.6164
42:4 PS	868.6062	38:2 PC	814.6321
42:3 PS	870.6219	40:5 PC	836.6164
42:2 PS	872.6375	40:4 PC	838.6321
42:1 PS	874.6532	40:3 PC	840.6477
30:0 TAG (IS)[b]	572.4885	40:2 PC	842.6634
33:3 TAG (IS)[b]	608.4885	40:0 PC (IS)[b]	846.6952
48:9 TAG	806.6297	28:2 DAG (IS)[b]	526.4466
48:8 TAG	808.6453	28:0 DAG (IS)[b]	530.4784
48:7 TAG	810.6609	32:3 DAG[k]	580.4937
48:6 TAG	812.6765	32:2 DAG	582.5093
48:5 TAG	814.6921	32:1 DAG	584.5249
48:4 TAG	816.7077	32:0 DAG	586.5405

Table 18
(continued)

48:3 TAG	818.7233	34:6 DAG	602.478
48:2 TAG	820.7389	34:5 DAG[l]	604.4936
48:1 TAG	822.7545	34:4 DAG[m]	606.5092
48:0 TAG	824.7702	34:3 DAG[n]	608.5249
50:9 TAG	834.6608	34:2 DAG[o]	610.5405
50:8 TAG[c]	836.6764	34:1 DAG[p]	612.5562
50:7 TAG	838.6920	34:0 DAG	614.5718
50:6 TAG	840.7076	36:6 DAG[q]	630.5092
50:5 TAG	842.7232	36:5 DAG[r]	632.5248
50:4 TAG	844.7389	36:4 DAG[s]	634.5405
50:3 TAG	846.7545	36:3 DAG[t]	636.5562
50:2 TAG	848.7702	36:2 DAG[u]	638.5718
50:1 TAG	850.7858	36:1 DAG	640.5875
50:0 TAG	852.8015	36:0 DAG	642.6031
52:9 TAG	862.6921	38:6 DAG	658.5405
52:8 TAG	864.7077	38:5 DAG	660.5561
52:7 TAG	866.7233	38:4 DAG[v]	662.5718
52:6 TAG	868.7389	38:3 DAG	664.5874
52:5 TAG	870.7545	40:10 DAG	678.5092
52:4 TAG[d]	872.7702	40:9 DAG	680.5248
52:3 TAG	874.7858	40:8 DAG	682.5405
52:2 TAG	876.8015	40:7 DAG	684.5561
52:1 TAG	878.8171	40:6 DAG	686.5718
52:0 TAG	880.8328	40:5 DAG	688.5875
54:9 TAG	890.7233	40:2 DAG	694.6344
54:8 TAG	892.7389	40:1 DAG	696.6500
54:7 TAG[e]	894.7545	42:2 DAG	722.6657
54:6 TAG[f]	896.7702	42:1 DAG	724.6813
54:5 TAG[g]	898.7858	44:6 DAG	742.6344
54:4 TAG[h]	900.8015	44:5 DAG	744.6500
54:3 TAG[i]	902.8171	44:4 DAG	746.6657

[a] Exact molecular masses corresponds to $[M+NH_4]^+$ adducts (MGDG, DGDG, SQDG, PA, PI, PG, TAG, DAG) and $[M+H]^+$ adducts (PS, PE, PC).

[b] IS= Internal standard.

[c] Representing 16:2-16:3-18:3 and 16:3-16:3-18:2

[d] Representing 16:0-18:1-18:3 and 16:0-18:2-18:2

[e] Representing 18:2-18:2-18:3 and 18:1-18:3-18:3

[f] Representing 18:0-18:3-18:3, 18:1-18:2-18:3 and 18:2-18:2-18:2

[g] Representing 18:0-18:2-18:3, 18:1-18:1-18:3 and 18:1-18:2-18:2

[h] Representing 18:0-18:1-18:3, 18:1-18:1-18:2 and 18:0-18:2-18:2

[i] Representing 18:0-18:0-18:2 and 18:0-18:1-18:1

[k] Representing 16:0-16:3 and 16:1-16:2

[l] Representing 16:2-18:3 and 16:3-18:2

[m] Representing f 16:1-18:3, 16:2-18:2 and 16:3-18:1

[n] Representing 16:0-18:3, 16:1-18:2 and 16:3-18:0

[o] Representing 16:0-18:2, 16:1-18:1 and 16:2-18:0

[p] Representing 16:0-18:1 and 16:1-18:0

[q] Representing 18:3-18:3 and 16:1-20:5

[r] Representing 16:1-20:4, 16:0-20:5 and 18:2-18:3

[s] Representing 18:2-18:2, 18:1-18:3, 16:1-20:3 and 16:0-20:4

[t] Representing 16:0-20:3, 18:0-18:3 and 18:1-18:2

[u] Representing 18:0-18:2 and 18:1-18:1;

[v] Representing 18:1-20:3 and 18:0-20:4

For the quantification of lipids with liquid chromatography electorspray ionization Q-TOF MS/MS (Q-TOF LC-MS/MS) and Q-TOF LC-MS, the following m/z values were used.

Table 19: Caclulated Molecular Masses of Acyl-CoA, Acyl-ACP and Fatty Acids adduct ions

Molecular Species	Calculated Molecular Mass of Ion Adduct (m/z)	Ion
14:0-CoA	1028.3374	$[M+H]^+$
16:1-CoA	1004.3374	$[M+H]^+$
16:0-CoA	1006.3530	$[M+H]^+$
17:0-CoA (IS)[a]	1020.3678	$[M+H]^+$
18:3-CoA	1028.3374	$[M+H]^+$
18:2-CoA	1030.3530	$[M+H]^+$
18:1-CoA	1032.3687	$[M+H]^+$
18:0-CoA	1034.3840	$[M+H]^+$
20:1-CoA	1060.3996	$[M+H]^+$
20:0-CoA	1062.4156	$[M+H]^+$
13:0-ACP	870.4532	$[M+NH_4]^+$
14:0-ACP	884.4688	$[M+NH_4]^+$
16:3-ACP	906.4532	$[M+NH_4]^+$
16:2-ACP	908.4688	$[M+NH_4]^+$
16:1-ACP	910.4845	$[M+NH_4]^+$
16:0-ACP	912.5001	$[M+NH_4]^+$
18:3-ACP	934.4845	$[M+NH_4]^+$
18:2-ACP	936.5001	$[M+NH_4]^+$
18:1-ACP	938.5158	$[M+NH_4]^+$
18:0-ACP	940.5314	$[M+NH_4]^+$
14:0-FA	227.2011	$[M-H]^-$
15:0-FA (IS)[a]	241.2168	$[M-H]^-$
16:1-FA	253.2168	$[M-H]^-$
16:0-FA	255.2324	$[M-H]^-$
18:3-FA	277.2168	$[M-H]^-$
18:2-FA	279.2324	$[M-H]^-$
18:1-FA	281.2481	$[M-H]^-$
18:0-FA	283.2637	$[M-H]^-$
20:5-FA	301.2168	$[M-H]^-$
20:4-FA	303.2324	$[M-H]^-$
20:3-FA	305.2481	$[M-H]^-$
20:2-FA	307.2637	$[M-H]^-$
20:1-FA	309.2794	$[M-H]^-$
20:0-FA	311.2950	$[M-H]^-$

[a]IS, Internal standard.

Table 20: Molecular masses of MAG ions and respective product ions used for the identifaction and quantification by GC-MS

Molecular Species	Calculated Molecular Mass of $[M^{+\cdot}15]$ ion (m/z)	Characteristic Product Ion for α-MAG $[M^{+}15]-88$ (m/z)	Characteristic Product Ion for β-MAG $[M^{+}15]-146$ (m/z)
14:0-MAG	431	343	285
15:0-MAG (IS)[a]	445	357	299
16:1-MAG	457	369	311
16:0-MAG	459	371	313
18:3-MAG	481	393	335
18:2-MAG	483	395	337
18:1-MAG	485	397	339
18:0-MAG	487	399	341
20:5-MAG	505	417	359
20:4-MAG	507	419	361
20:3-MAG	509	421	363
20:1-MAG	513	425	367
20:0-MAG	515	427	369
22:0-MAG	543	455	397

[a]IS, Internal standard.

Table 21: Molecular masses, parental ions and product ions used for the identification and quantification of free sterols by GC-MS

Sterol	Caclulated Molecular Mass of M^+(m/z)	Characteristic Product Ion (m/z)
Cholestanol (IS)[a]	460	355
Cholesterol	458	368
Campesterol (24-Methylcholesterol)	472	382
Stigmasterol (24-Ethylcholesta-5,22-dienol)	484	394
Lanosterol	498	393
ß-Sitosterol (24-Ethyl-cholesterol)	486	396

[a]IS, Internal standard.

7.9 Glycerolipid molecular Species Distribution during Mycorrhiza Symbiosis in *fatm* Mutants and WT
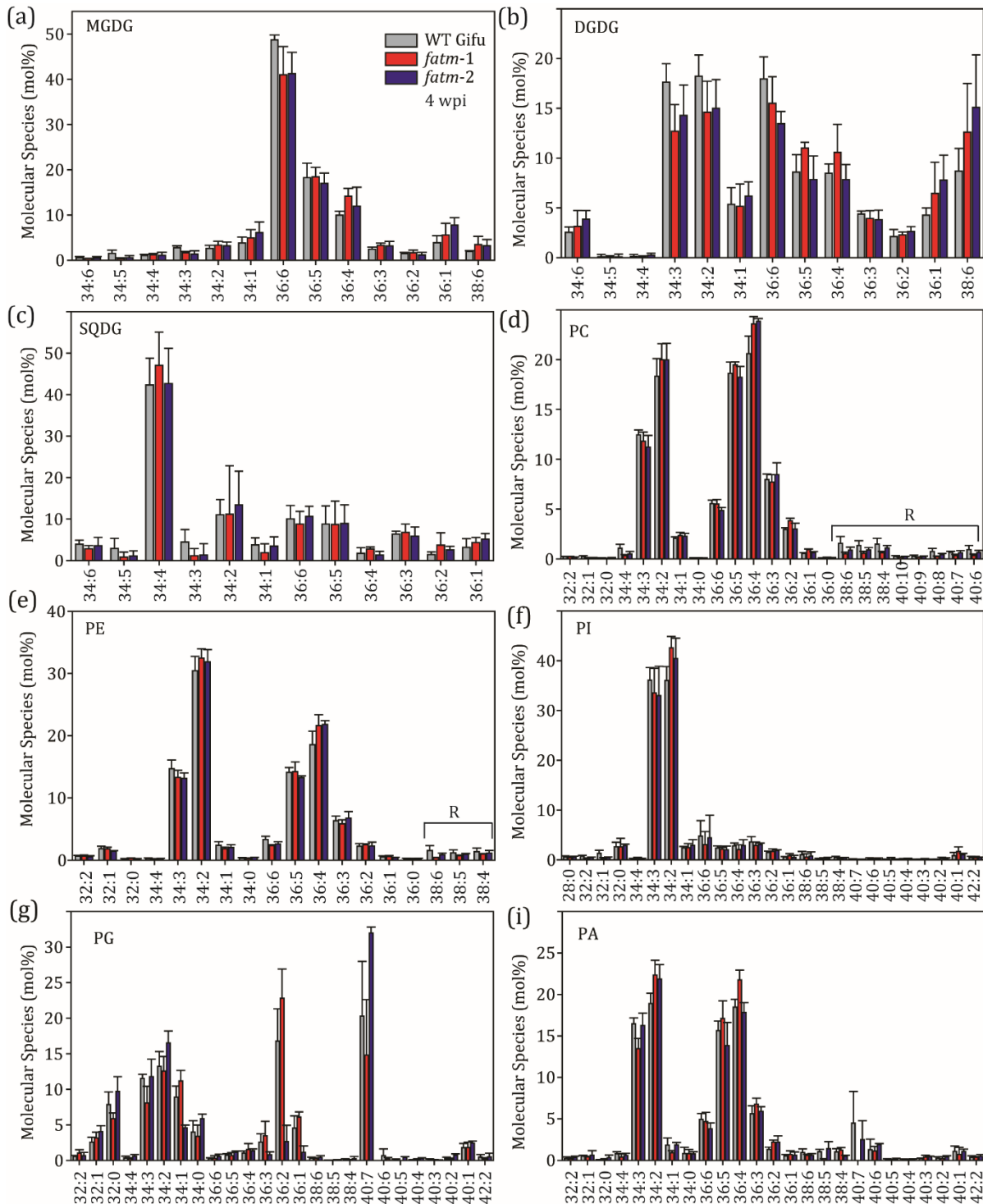
Figure 33: Molecular Species Composition of Membrane Galactolipids and Phospholipids in colonized WT and *fatm* Mutants at 4 wpi.
Molecular species composition of **a)** MGDG, **b)** DGDG, **c)** SQDG, **d)** PC, **e)** PE, **f)** PI, **g)** PG and **i)** PA. Glycerolipids were measured by Q-TOF MS/MS. Lipid species that contain the Rhiozphagus signature fatty acids 16:1, 20:3, 20:4 and 20:5, as well as 16:0, accumulate under colonization to a lesser extend in mutants than in WT. Combination of carbon chain length and fatty acids are indicated on the x-Axis. Values are means and error bars are SD of three measurements. R, Molecular species specifically accumulating in *R. irregularis*.
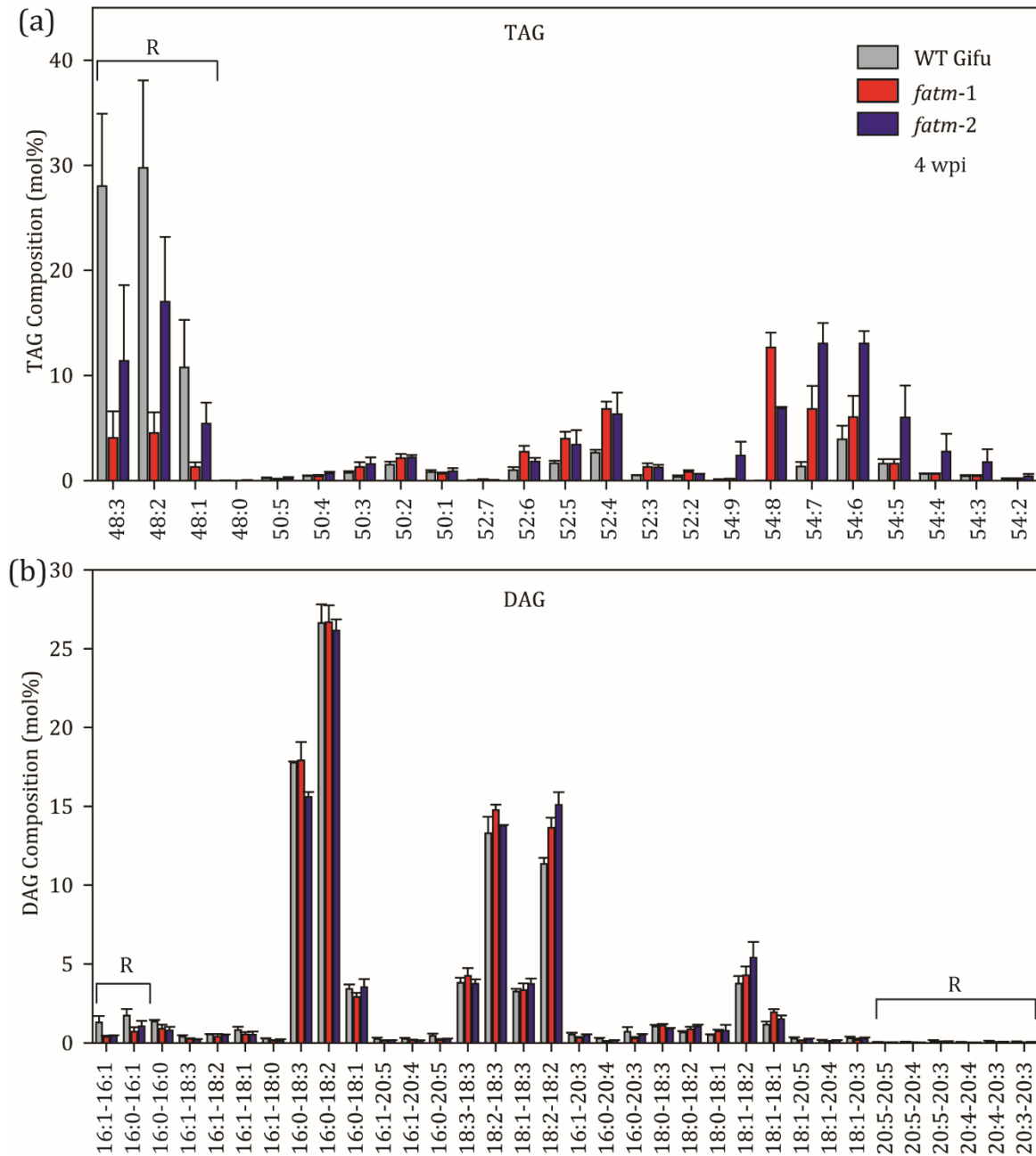
Figure 34: Molecular Species Composition of non-Membrane Neutral Glycerolipids in colonized WT and *fatm* Mutants at 4 wpi.

Molecular species composition of **a)** TAG and **b)** DAG. Neutral glycerolipids were measured by Q-TOF MS/MS. Lipid species that contain the *Rhiozphagus* signature fatty acids 16:1, 20:3, 20:4 and 20:5, as well as 16:0, accumulate under colonization to a lesser extend in mutants than in WT. The most abundant mycorrhiza-specific lipid is TAG with the molecular species 48:3 and 48:2. Combination of carbon chain length and fatty acids are indicated on thex-Axis.

Values are means and error bars are SD of three measurements. R, Molecular species specifically accumulating in *R. irregularis.*

7.10 Preparation of acyl-ACP Substrates
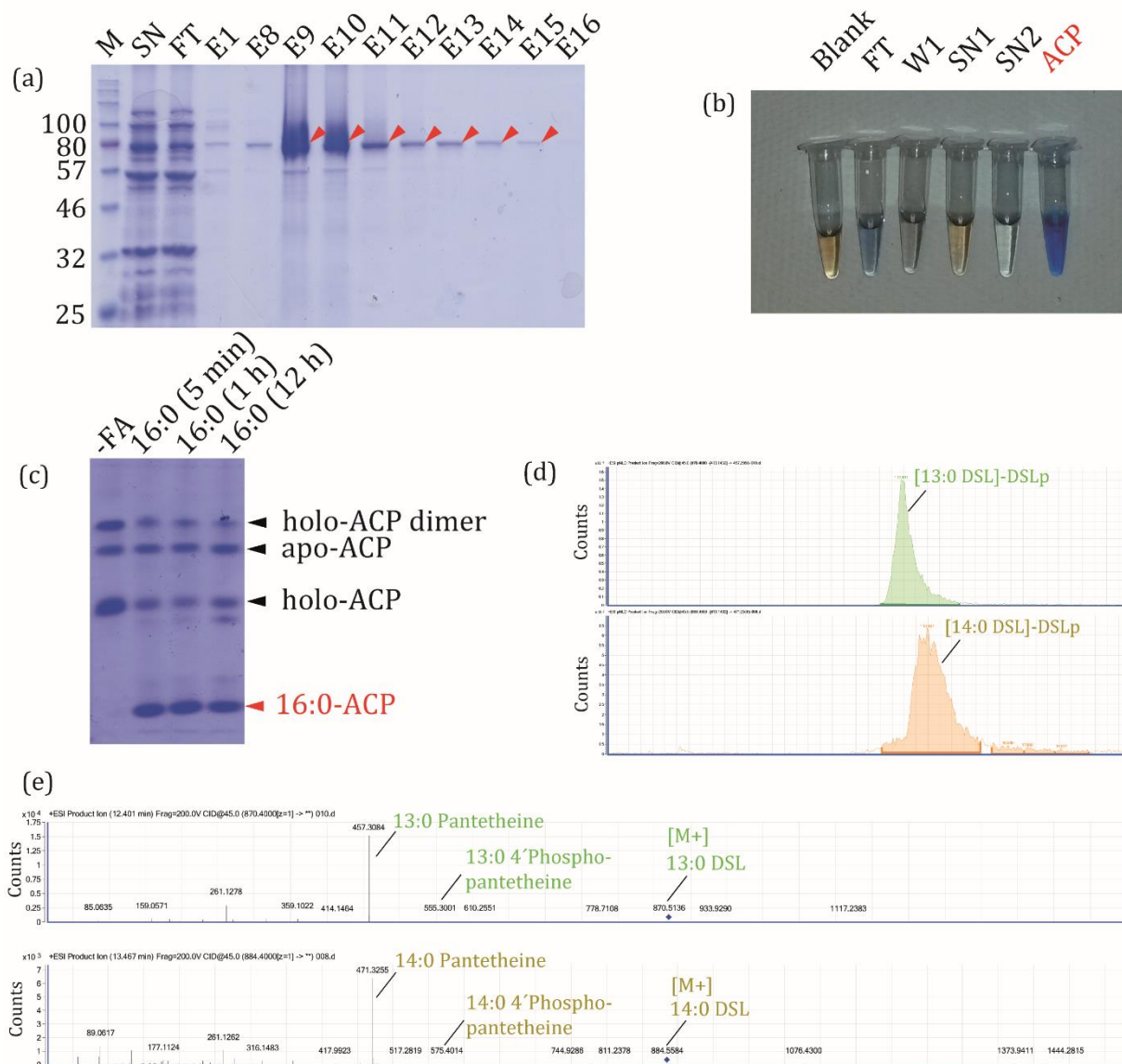
Figure 35: Preparation of acyl-ACP Substrates.
a) Ni-NTA purification of *E. coli* acyl-ACP synthetase (Aas). Different elution fractions from the preparation and the protein chromatography were compared by SDS-PAGE. Elution fractions containing recombinant Aas protein (80.6 kDA, red arrowhead) were kept.
b) ACP preparation from *E. coli* WT. Samples were kept from different steps during the ACP preparation and anion-exchange chromatography. Samples were mixed with Bradford color reagent that gives a blue color for proteins showing the successful isolation of ACP.
c) Acylation reaction of palmitic acid with *E. coli* ACP using *E. coli* Aas. As a control, the fatty acid was omitted (-FA). The reaction products were seperated using urea-PAGE. ACP dimerisation products and ACP apo and holo isoforms are seperated from acyl-ACP (16:0-ACP). During acylation, holo-ACP is converted into acyl-ACP, which can be seen by reduction of holo-ACP and the occurrence of acyl-ACP in the three reactions containing palmitic acid. Increasing the reaction time from 5 min to 1h and 12 h did not lead to increased acyl-ACP abundance.
d) Q-TOF LC MS/MS measurement of Asp-N endoproteinase digested acyl-ACP limbs. Acyl-ACP limbs were seperated on a RP8 column and identified based on the neutral loss of DSLp.
e) Mass spectra of 13:0 and 14:0-ACP limbs. The most abundant fragment ion is the fatty acid with pantetheine. Minor fragments for the fatty acid containing the 4´-phosphopantetheine group and the unfragmented acyl-ACP limb ([M+], blue diamond) are detected.
M, Marker, SN, Supernatant, FT, Flow-through, E1—E16, Elution fractions 1—16, W, Wash step, ACP, Acyl-carrier protein, DSLp, Aspartic acid-Serine-Leucine with 4´-phopshopantetheine group.

List of Publications

Parts of this thesis were published in:

Brands, M., Wewer, V., Keymer, A., Gutjahr, C. and Dörmann, P. (2018) The Lotus japonicus acyl-acyl carrier protein thioesterase FatM is required for mycorrhiza formation and lipid accumulation of R. irregularis. *Plant J.,* 95, 219–232.

During the doctoral studies the following manuscripts derived from collaborations were published:

Bravo, A., Brands, M., Wewer, V., Dörmann, P. and Harrison, M.J. (2017) Arbuscular mycorrhiza-specific enzymes FatM and RAM2 fine-tune lipid biosynthesis to promote development of arbuscular mycorrhiza. *New Phytol.*, 214, 1631-1645.

Keymer, A., Pimprikar, P., Wewer, V., Huber, C., Brands, M., Bucerius, S.L., Delaux, P.-M., Klingl, V., Röpenack-Lahaye, E.v., Wang, T.L., Eisenreich, W., Dörmann, P., Parniske, M. and Gutjahr, C. (2017) Lipid transfer from plants to arbuscular mycorrhiza fungi. *Elife*, 6, e29107.

Xue, L., Klinnawee, L., Zhou, Y., Saridis, G., Vijayakumar, V., Brands, M., Dörmann, P., Gigolashvili, T., Turck, F. and Bucher, M. (2018) AP2 transcription factor CBX1 with a specific function in symbiotic exchange of nutrients in mycorrhizal Lotus japonicus. *Proc. Natl. Acad. Sci USA.* 115, 9239–9246.

Additional publications:

Wewer, V., Brands, M. and Dörmann, P. (2014) Fatty acid synthesis and lipid metabolism in the obligate biotrophic fungus *R. irregularis* during mycorrhization of *Lotus japonicus*. *Plant J.*, 79, 398–412.

Siebers, M., Brands, M., Wewer, V., Duan, Y., Hölzl, G. and Dörmann, P. (2016) Lipids in plant-microbe interactions. *Biochim. Biophys. Acta*, 1861, 1379–1395.

Acknowledgments

Im Folgenden habe ich mal probiert, aufzuschreiben, wofür ich besonders dankbar bin und welche Personen besonderen Anteil am Gelingen der Doktorarbeit und am Nicht-Verzweifeln des Doktoranden haben. Das Ganze ist quasi eine Belohnung für den genigten Leser, dass er bis zum Schluss durchgehalten halt. Aber nich schummeln und einfach bis hierhin vorblättern… Hab ich dich erwischt!?

Da diese Seite mir gehört, würde ich in dieser Danksagung gerne persönliche Sachen nennen und außerdem die Dinge und Personen auflisten, die im wissenschaftlichen Sinne Dank verdienen. Das Ganze soll allerdings keine Rangliste sein, mein Dank ist also genauso herzlich gemeint, wenn ihr erst weiter unten erwähnt werdet.

Wo fängt man an? Meine Lust auf wissenschaftliches Arbeiten, die hoffentlich in dieser Arbeit einigermaßen ansprechend zum Ausdruck kommt, hat sich erst so richtig entwickelt, als ich im September 2011 ins IMBIO in Peters AG gekommen bin, um von Vera bei Projekt- und Bachelorarbeit betreut zu werden. Danke also an dich, vor allem dafür, dass du herzlich, fair und ehrlich warst. Im Laufe der Zeit hat man ja auch den einen oder anderen Studenten betreut und mit einigen geredet und da ist mir klar geworden, wie wichtig ein motivierender und freundlicher Begleiter für mich war. Wer weiß, wenn die Zeit nicht so toll gewesen wäre, ob ich in Bonn und im IMBIO geblieben wäre? Sowieso die Leute ausm IMBIO: Mittlerweile sind aus den meisten Kollegen von damals ja sowieso Freunde geworden – beste acknowledgment!

Natürlich auch danke an Peter für die Unterstützung, die Chanchen und Möglichkeiten, die er mir geboten hat und bietet. Für fachlich exzellente Betreuung und für Verfügbarkeit sowieso. Ich kenne Doktoranden, die sehen ihren Prof. alle paar Wochen mal. Das war hier ganz anders und in der Anfangszeit waren die sehr regelmäßigen und manchmal ausufernden Besprechungen zwar anstrengend, haben aber garantiert zum Erfolg des Projektes geführt.

Die Zeit in Bonn war für mich bisher fachlich und auch persönlich ein Reifeprozess. Von der Bachelorarbeit übern Master bis zum Doktoranden. Da mir auch während der Masterarbeit bei Benni Franke und Lukas Schreiber hier in Bonn viel Vertrauen und Support entgegengebracht worden ist, möchte ich den beiden hier auch danken. Diese Zeit war auch super positiv, sodass für mich klar war, eine Doktorandenstelle anzutreten und mein Glück in der Wissenschaft zu suchen. Danke an alle Kollaborationspartner: Andreas Keymer und Caroline Gutjahr für die Konfokalmikroskopie und die Komplementation von *fatm* Mutanten, die Methoden zum Färben und die Untersützung beim Manuskript. Außerdem an Armando Bravo und Maria Harrison für die produktive Zusammenarbeit bei ihrem Lipid-Mykorrhiza Projekt.

Noch mal explizit ein Lob und Danke an alle aktuellen Kollegen und Kolleginnen aus dem IMBIO: an Helga, Katha und Vera für die Betreuung der Massenspektrometrie und darüber hinaus für das Messen von etlichen Proben und die essentielle Hilfe beim Auswerten von allem Möglichen. Extra Dank noch mal für diverse Male Hilfe und Unterstützung auch bei anderen wissenschaftlichen Problemen und Themen. Das Gleiche gilt für Philipp, der immer positiv eingestellt ist und mit dem man immer science talk machen kann. Liebe auch an Meike als langjährige Kollegin, Sportlerin und als weise ältere Freundin (harhar). Danke für Tipps, Hinweise, Begleitung und Untersützung zu allem. Dank gilt außerdem Marlies fürs Genotypisieren und für den Unterhalt der Mykorrhiza-Karrottenwurzel Sterilkultur sowie alle weiteren Arbeiten, bei denen du mir geholfen hast. Danke an Barbara, die mir gezeigt hat, wie man rekombinante Proteine aufreinigt. Danke auch an Jill, die meine neue Büronachbarin ist und tatsächlich auch mal kurz Stundentin bei mir war. Vielen Dank an Regina als ehemalige Labor- und Büronachbarin, sowie an Mina für seine Tipps mit Hefe und seine friedliche Art. Lieben Dank und einen freundlichen Klaps an alle Studenten, die ich betreut habe, an vorderster Front diejenigen, die ihre Abschlussarbeiten bei mir gemacht haben: Johanna, Steven und Cornelia. Danke an Andreas für die technische Unterstützung beim Parieren. Danke auch an Georg, Biggi, Ellen und EPJ.

Ganz am Schluss Liebe an meine Familie: Anne, Wolfgang, Flip und Flo und am allermeisten an dich, Lea. Peace out and praise the sun!